Faculty of Engineering Science and Technology (IVT)
Department of Industrial Engineering

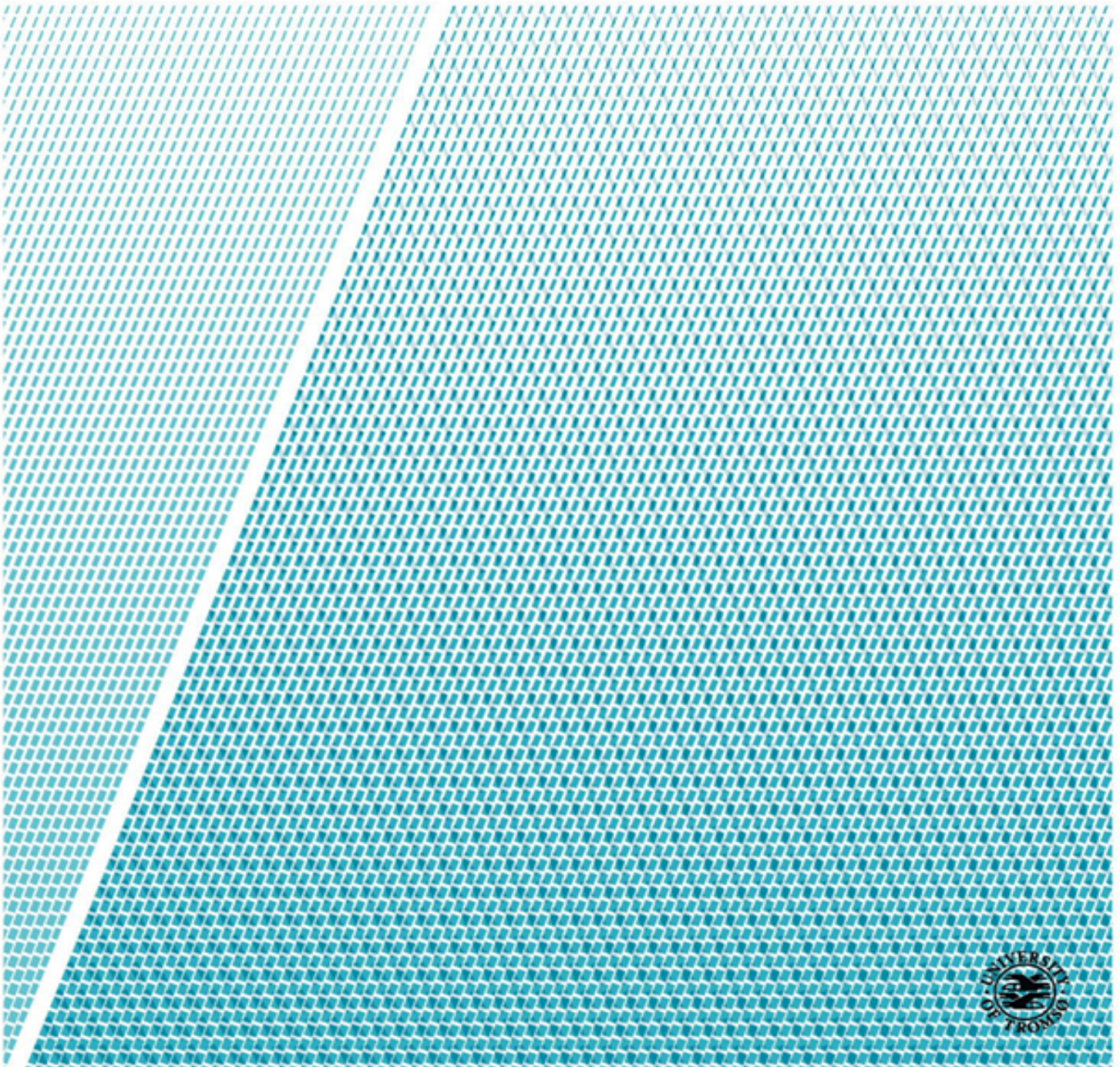# Thin Wall Structure by Welding

Stud. Techn. Hans Ivar Arumairasa

Table of Contents

List of Figures

List of Tables

Terms and Abbreviations

PWHT - Post Weld Heat Treatment
HIC - Hydrogen Induced Cracking
WPQR = Welding procedure qualification record
TWS = Thin Wall Structure
BP = Baseplate
RS = Residual stresses
FEM = Fenite Element Method
VP = Vision Component
H = Horizontal
V = Vertical

ACKNOWLEDGEMENT

I would first like to thank my Norwegian thesis advisors Gabor Sziebig and Magnus Aangstad of Industrial Engineering at The Artic University of Norway (UiT). The door to Prof. Sziebig office was always open whenever I ran into a trouble spot or had a question about my research or writing. He was consistently available during my welding operation at campus Narvik and always replied me in short time. I want to further gratitude my thanks to my two Chinese supervisors Zhiping Xiong of Material Science and Jing XIE of Mechanical Science at Beijing Institute of Technology (BiT). They have always helped me with their best interests and made arrangement and meetings for my behalf. Without their passionate participation and input, my dissertation could not have been successfully conducted.

I would also like to thank the experts Professor Shiyuan Zhou who were involved in the ultrasound measurement test for this research project and made this experiment happened.

I want to give my sincerely gratitude to Hao You for helping me with arranging the exchange trip to China and always be available with fast response overseas.

I would also like to acknowledge lector Øyvind Sørås and Assosciate Professor Mikhail Khadyko of the University of Tromsø (UiT) at Narvik Campus, their input has contributed an huge impact at my first experiment of investigating residual stress test by calculating residual stresses by deformation. I am gratefully indebted to their valuable comments on this thesis.

Finally, I must express my very profound gratitude to my co-student Halldor Arnarson for providing me with technical support during my welding experiment.

This accomplishment would not have been possible without the advice, input and comment from all these people. Thank you.

Author

Hans Ivar Arumairasa

1 Abstract

Manufacturing of thin wall structure by wire arc additive manufacturing (WAAM) is on the main application of additive manufacturing. 3D-printing technology has significant advantages over traditional milling and machining techniques or welded analogs. Thin wall structure constitutes an essential and growing proportion of engineering construction, within common areas as in structural aerospace and large scale-components. The dissertation utilized a layer-wise production technique known as gas arc tungsten arc welding (GTAW), performed by a programmed KUKA-30 robot. The thesis aspect of welded structures is the degree of how disposable the product is after manufactured, due to the different set of welding parameters. Therefore are an investigation of residual stresses and deformation implemented by different structure geometries. The research includes two practical and analytical experiment tests in addition to an FEA-simulation. The experiments involve; ultrasound measurement by a self-programmed measuring device developed by BiT, calculation due to measured deformation along the welding length and simulation performed in ANSYS. Findings of the methods implicate an estimated value of residual stresses and distortion in the thin wall structure and substrate. Through ten tests of the welding process can the technique of this technology state as slow with frequently sources of error, using the KUKA-30 robot welding system for a certain height. The level of residual stresses depends on the severity of the manufacturing process, which this research confirmed a generally low value along the length of the structural components and base plate due to the parameters developed in this study.

2 Keywords

Additive Manufacturing, Robotic welding, Residual stresses, welding process, Gas Tugten Arc Welding,

3   Introduction

3.1   Introduction

Manufacture thin wall structure by welding, is a more economical, flexible, and faster way of production than conventional subtractive manufacturing technologies, such as machining and milling. It generates growth concerning the engineering industry like aerospace, marine, aircraft, bridges, ships, and general complex and large structures. The thin wall structure is an arc-based deposition process of a thin wall structure in a layer upon layer manner, which is conducted by a technique of Additive Manufacturing [AM [1]. AM are commonly known as 3D-printing technology with a waste specter of different methods. The method chosen for the research is Wire Arc Additive Manufacturing (WAAM). It is a lesser-known branch within AM, which is a large-scale metal technology that uses an arc welding process to manufacture metal structure additively. However, this study utilizes gas tungsten arc welding (GTAW)-Based Wire Arc Additive Manufacturing System to weld the thin wall structure by a KUKA-30 robot, the welding process is illustrated in the figure below [2].
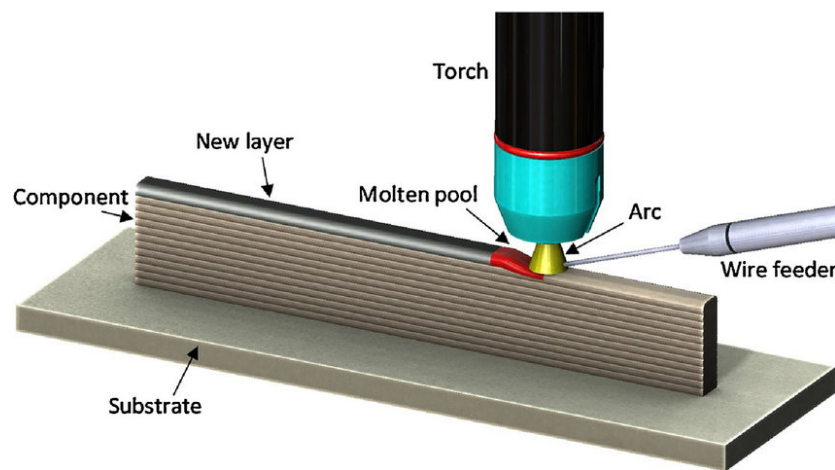
Figure 1: GTAW-Based Wire Arc Additive Manufacturing System. Source [**vladimir**]

This study of welding technology (3D-printing) aim for utilizing GTAW-based wire arc additive manufacturing, which is conducted by a KUKA-KR30-3 robot to produce an optimal thin structure. In figure 1 the welding process of the thin wall structure is illustrated. The welding operation includes a process where a wire of a given material is fed beneath the arc tungsten electrode to melt under the molten pool, which generates the layer of deposition. The welding process deposits the layers upon each other until a certain height is achieved. Investigation of residual stresses (RS) is performed after production for the purpose to investigate the degree of disposable the welded structure are. It is achieved by two methods, calculation by deformation and ultrasound measurement. Findings in those methods are then compared with the result of a finite elemental simulation to provide a digital analytic overview. Furthermore, the welding process is documented by a welding procedure qualification record (WPQR), which elaborates the details of the thin wall structure (TWS) production process.

The master thesis is divided into two parts. Part one is a literature review where information and research of the topic are gathered to gain a platform of basic knowledge within welding, robotic welding, additive manufacturing, residual stress test an experimental setup for the welding process. During the next part of the thesis, the actual empirical work is conducted and documented which the results are built upon.

3.2 Background

Reason for choosing the thesis subject, Thin Wall Structure by Welding, is because of my interest within welding and robotics. Welding has from earlier job context been an exciting theme for me, as robotics from previous subjects woke my interest in automation technology.

The thesis was handed out from the University of Tromsø campus Narvik, who wanted to achieve further result and documentation of robotic welding. Previously researcher "Tania" and master thesis of "Tomas Maske" has in the past worked out research and master thesis regarding welding with the KUKA-30 robot. Their studies aimed to find the optimal weld by manipulating the parameters by testing and calculation. This theme was therefore interesting, especially when the topic of thin walls structure is a low documented subject, which has not been accomplished at this institute in the past. Additional it has increasing popularity at a global level within the additive manufacturing technology [3].

Finite Element Method by simulation in ANSYS has from previous experience at school project and job context remained a past skill from my bachelor degree. The combination of the subjects, welding, robotics, and simulation matched my interest and experiences, which is the main reason for choosing this master thesis.

3.3 Problem statement and result goals

For replacing the existing production technology like milling and machining, additive manufacturing needs to achieve a faster way of production as well as strong results in the structure's property. The 3D-technology of robotic welding, therefore, need to achieve a good weld by finding the right parameters.

At the end of the project will the thin wall structure be analyzed through practical tests and digital simulations which will answer these tasks:

- Conduct a welding experiment with a mixture and manipulation of parameters, the design of weld and thermal and mechanical process techniques to produce thin wall structures.

- Study, analyze and identify residual stresses and distortion in the weld.

- Develop an optimal procedure process which contains all documentation of the thin wall structures.

- Document carried out work in written form.

- Conduct a tensile strength, hardness, and notch impact- test.

4   Literature review

During the research in thin wall structure by welding by layer additive manufacturing, an elaboration of working principals of TIG welding, description of the basic material, process of additive manufacturing and its experimental setup are presented to understand current challenges of today's method/process which will be used in the practical experiments. Research section addresses:

- History of welding

- TIG/GTAW (Gas Tungsten Arc Welding)

- Robotic welding

- Additive manufacturing

- Thin wall structures

- Experimental setup (testing)

4.1   Brief history of welding

Welding is an old art which originates during the bronze-iron ages and still being perfected today. Early on, blacksmiths heated two peace of metals and hammered them together [4]. Processes of iron ore created to crafts are found as far as 3000 BC in Egypt were welding or "solid-phase" was first recorded [5]. Metal surfaces in the open air are covered in oxide layer which old blacksmiths needed to pin out with the skill of the hammer. Today we can remove the layer with heating in vacuum or reduced atmospheric circumstances. Today this method as frictional- and resistance welding where the end of the surfaces is pieced together, so the oxide layer are squeezed out of the joint. In the old days, they knew that heating up and solidification would result in a joint between two pieces of the same material. The main issue was the hold the melting blade together because the process is dependent on holding the heating source at one local spot, which was not possible before the last century.

After electricity became available in workshops like the carbon arc, it was experienced that sparks and electric-overload could melt metallic conductors. Auguste De Meritens was first to succeed fusion lead plates from the electrical arc in 1881. However, he was not able to add fillers to combine a bond between the two plates. This was the start of a revolution from developing blacksmithing towards welding [6]. Later in 1885 did the Russian inventor Barnados form an arc between a workpiece and a carbon electrode which result in a small metal rod in the arc and filled the gap between the workpieces. To generate electricity, a steam-engine was used since the battery at that time did not last long because of the short-circuiting involved. This was the first electric arc weld accomplished. He did a similar process later with TIG welding. He was afterword known as "father of welding" in Russia for he's work [4].

Some years later came the innovation "blowpipe" or "torch," were the gases acetylene oxygen was used to block the air from the melting bath, which increased the quality in the joint. This

method was conducted to weld and cut several types of metal. In the years 1903-07 O. Kjellberg developed covered metal electrodes which we know today as arc welding. The layer that melts from the electrode in the welding pin emits both gas and slag that protect against oxidation and nitration in the air. Welding with covered metal electrodes has been the dominated method in steel for until 20 years ago. When other method emerged in arc welding proved to be more productive and suitable for automation and mechanization [4].

Generally, welding is a method of repairing or creating metal structures by a fusion process. Due to operational simplicity, welding has become the most important industrial process in the manufacturing of metal parts. Considering the process of joining two metals composition into an integrated part, it additionally has the ability of deposition of material on a surface to coat with special characteristics or to recover parts. Basic welding equipment can emerge from open flame, electric arc, or laser light [7].

4.2 TIG/GTAW (Gas Tungsten Arc Welding)

4.2.1 Fundamentals for TIG/GTAW welding process

Regarding daily challenges by additive manufacturing produced by TIG, we need to understand the fundamentals, how the welding works and operates during the process. Gas Tungsten Arc Welding (GTAW), also known as Tungsten Inert Gas (TIG) welding, became a success in the 1940's for non-ferrous welding materials as magnesium and aluminum. It's a versatile process that utilizes non-consumable tungsten electrode to produce the weld. TIG/GTAW is routinely used for welding thin base metal, edge – and flange joints were filler metals are not used. For thicker dimensional metals an external TIG filler rod is normally used as seen in figure 2.

Figure 2: TIG welding process. Source: [8].

The gas added creates an electrical shield at the weld pool to protect the oxygen in the atmosphere, before it was used slag [9]. Purpose of the shield is to protect the welding pool until the iron solidifies, thus decrease the possibility to oxidize. It is a crucial process because the liquid iron bonds with the oxygen in the air and make it highly reactive. Additional the gas increases the conductivity between the work peace and the electrode of tungsten, which make a strike an electric arc. The gas used is normally argon (sometimes are hydrogen blended with

argon up to around 30%). The reason of those considerations of the argon-hydrogen mixture is because of that argon give arc stability were hydrogen, on the other hand, ensure better thermal efficiency, which again performs a deeper penetration [9], sees 1.3.5 for further details of the parameter. Type of gas shield regarding which kind of current are used is further explained in 1.2.2.

The electrode material is made from a tungsten alloy. It has a melting point of 3422 [8] degree Celsius, the strength of the material makes it possible to remain solid during the weld. Thus, resulting in a process with precise control of the electric arc and welding heat. The process is also known as TIG/GTAW. The system consists of a constant power source, generally between 3 and 300 A, and 10 to 35 V [10]. It can be performed manually or semiautomatic and are used in production in addition to repair welding. It means that the filler metal can be directly fed by hand into the arc during the welding. Manually operating require highly skilled worker, where the operator has one hand on the torch, the other on the filler and the foot to control the current. The method referred to as "three arm welding". Since the welding will be executed by a robot will manual operation not be relevant for this thesis.

4.2.2   Type of welding current used in TIG:

The power source from the torch is less compare to other systems. It contains a small nuzzle, tungsten electrode, TIG filler Rod and power switch, where the actual weight arrives from the power switch. Different factors are therefore taken into account when choosing the amount of current that is used in TIG. Amount of electric electrode in the process varies. Type of material and dimension of the metal determines the amount and type of current that again also decide which type of gas shield should be used. We distinguish between three types of welding current for TIG, which emits different heat distribution between the tungsten electrode and the workpiece:

1. **DCSP** – Direct Current Straight Polarity- Direct current with a negative electrode (DCSP) gives deeper penetration, and faster welding speed, with helium gas, is used as a shield and provide a large amount of current. This type of connection is mostly used in the DC type welding current connections. With the connection of tungsten to the negative terminal, it will receive 30% of the welding energy (heat). In other words, the tungsten runs a lot cooler than DCRP. The welding results will achieve good penetration and a narrow profile, see figure 2 [11].

2. **DCRP**- Direct Current Reverse Polarity- Direct current with a positive electrode on the other hand offer less penetration but instead remove surface oxides from metal which produce a shallow wide profile and are for the most part used on light material at a lower amount of current. This type of connection is rarely used because most heat is on the tungsten, which can easily result in overheat and burn away, see figure 2 [11].

3. **AC**- Alternative current- Removes oxides from surfaces which creates an amount of sputtering allowing for good quality welds results where a moderate amount of current are used. It is mainly the preferred welding current for white metals like aluminum and magnesium. In this case, when using argon as a shielding gas, AC is selected instead

of helium because helium does not sputter. Commonly are argon "the-go-to" -choice as shield gas regardless of direct or alternative current. The heat input to the tungsten is average distributed as the AC wave passes from the one side of the wave to the other [11].
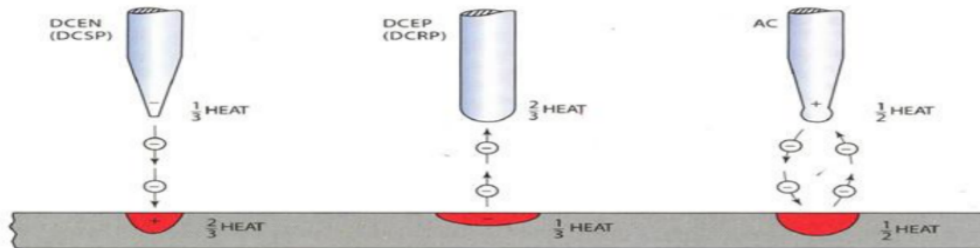
Figure 3: Heat distributions between the tungsten electrode and the work with each of welding current. Source: [11].

4.2.3 Advantages and Disadvantages of GTAW

	Advantages	Disadvantage
1	Makes high quality welds in mainly all alloys.	Does not provide a high production or high deposit-rate welding process.
2	Low post weld clean up required.	Requires a highly skilled operator.
3	Clearly visible arc and weld pool for the welder.	Produce pollution due to unclean work area.
4	The arc carries no filler, which eliminate splatter.	Hard to weld in difficult operator positions.
5	GTAW consumes almost 1/3 of the gas compered to GMAW.	-
6	Produce no slag which potentially can be trapped in the weld.	-
7	Welding can be performed in all positions.	-

Table 1: Advantages and disadvantages of GTAW

4.2.4 Preweld Operation

Preweld operation is a crucial routine when it comes to preparing the weld before using robotic welding during the experiments in the thesis. Several steps must be completed to secure the quality of the weld, as preparation of electrode and the weld joint, fixture the weldment, set the variables (speed, feeding, etc.) and preheat the ground material if necessary. The quantity of preparation depends on the type of material, size of the welding operation, and quality requirements [9].

Electrode Preparation: Electrode preparation depends on the type of electrode and welding operation. When welding with AC, the tip can have a ground point or a ball end. Electrode with a point requires the ground mark to run parallel to the electrode. Preparation of a ball on the end of the tungsten requires first to switch the power supply to DCEP (reverse polarity). Afterward following up with starting the arc between the electrode and a piece of material, which must be maintained at a moderate current level. The tip of the ball should now be clean and have a mirror-like look.

Preparing the Weld Joint: Several different methods can be used to prepare the weld joint. This includes oxyfuel and- plasma cutting, shearing, machining, air carbon arc gouging, grinding or chipping. Importance of preparing the weld joint thorough will achieve a sound weldment and meet the requirement of quality standard of welding.

Cleaning: Cleaning the welding area on the material is crucial because GTAW is normally exposed to contamination like oil, grease, paint, dirt, oxides, and foreign material during welding. Especially aluminum has an oxide coating that will contaminate the weld area if not removed. The solution of methods that can remove the contamination is wire brushes, grinders and abrasive blasting (normally with sand).

Fixturing: and Positioning: Fixture and positioning affect the welding property such as size, shape, and uniformity. Fixtures have a function to locate and hold the position of the working part during the weldment, so no distortion occurs, thus decrease the welding time. After fixturing can positioning of the weldment be achieved. It helps welder to maneuver into a flat position for producing a better weld. For preventing burn-through in the material during welding can heat sinks, backing bars or chill blocks be used to reduce distortion and overheat temperature at base material.

Preheating: Preheating has the potential to be useful, which further depends on the property of the alloy at the base material, thickness, and the configuration of the joint. The various method can be used to control the temperature, which includes: furnace heating, electric induction coils, oxyfuel torches, and resistance heating blankets. The necessary preheat the material needs are normally obtained from the welding procedure. Measurement of the heat is normally conducted with sticks, temperature indicators, thermistors, crayon pellets, thermocouples or infrared thermometers.

The fundamentals about GTAW process will provide wiser choices when it comes to welding process in the thesis, and selection of equipment based on the welding application for the elemental material.

4.3   Primary GTAW Process Parameters

Toughness and the resistance of the weld, that work to failure are dependent on different factors such as welding parameters (current, voltage, welding speed, etc.), geometric shape, the design of the weld piece, method of welding and nature of applied stress among other things. Based on the prime parameters for welding [12], an overview of the most common factors will be defined, which are crucial for the experimental part of the thesis.

4.3.1   Welding Current

As mentioned in 1.2.2, there are three different types of welding current: DCSP, DCRP, and AC. Welding current is the parameter that has the most important variable in the arc welding process. It controls the electrode burn-off rate, the depth of fusion, and geometry of the weldments. Current influence directly the weld bead shape, welding speed, and quality of the weld. Again, while higher current setting in GTAW can cause splatter and damage the workpiece, leads lower current on the other hand to sticking of the filler wire. Occasionally larger heat affected area can be found with lower welding current, as high temperature are applied for longer periods to deposit the same amount of filling materials. Fixed current mode need a variation of the voltage to maintain a constant arc current [12].

4.3.2   Welding Voltage

Welding Voltage is the electric potential difference in the gap between the tip of the welding wire and the surface of the molten weld pool. Depending on the GTAW equipment can welding voltage differs from adjustable to fixed, to determines the shape of the fusion zone and weld reinforcement. A high start voltage allows for easy arc initiation and a greater range of working tip distance. Although it produces wider, flatter and less deeply penetration welds than low welding voltage, depth of penetration is maximal at ideal arc voltage. Because too high voltage leads to a larger variable in welding quality (unstable welding) [13].

4.3.3   Welding Speed

Welding speed is defined as the rate of travel of the electrode across/under the seam [14]. Thus, Travel speed = Travel of electrode/arc time [mm/min] [15]. The welding speed is an important parameter for GTAW because the effect of increasing the welding speed at the same level of current and voltage reduces the heat input. The welding speed has no impact on the electromagnetic force and the arc pressure since they are dependent on the current type. When the welding speed increase, the weld section area decreases, which impacts a reduction at the consequent penetration depth (D) and the weld with (W). This tells us that the ratio of D/W has a fragile dependence on the travel speed, and it does not influence the mechanisms to involve in the weld pool formation. Welding speed rather impact the volume of melted material, normally does the travel speed vary between 100 to 500 [mm/min] which depends on the current, type of material and thickness of the plate [16].

4.3.4   Heat Input

Heat input is a measurement of energy transferred per unit length of the weld. Higher the heat input, the slower the cooling rate. Contra, the lower the heat input, the faster the cooling rate. Thus, like preheat, heat input is an essential characteristic that impacts the cooling rate that again affects the mechanical properties, metallurgical structure, and HAZ [33]. As earlier mentioned are the energy of arc welding transferred from the welding electrode to the base metal by an electric arc (like WAAM). Heat input is typically calculated as the ratio of the power (voltage multiplied with the current) to the velocity of the heat source (the arc) [17]. The equation of heat input is generally calculated by:

$$H = \frac{x * I * X * V}{v} \tag{1}$$

Where,

H= Heat input [KJ/mm]

η = efficiency = 0.60 for GTAW,

V= voltage [V]

I=current [A]

v= welding speed [mm/sec]

4.3.5   Shield Gases

Shielding gas used in GTAW has two functions, to protect the welding pool against atmospheric contamination and to cool down the weld material. The gases feature of cooling down the material decides which property the material obtain based on the mixture of gases (example Argon and helium). The contamination can cause porosity, weld cracking, scaling, and even change in the chemical composition of the welded metal. Additionally, has the shield gas also a large effect on the stability of the electric arc. Gases with low ionization potential promote the ignition of the electric arc, and those with low thermal conductivity tend to increase the arc stability.

Argon is most common in GTAW shielding gas and has low ionization potential. Because it's heavier than air, it provides a perfect layer of shielding of the molten weld pool. Argon is far less expensive than helium and is used in the welding process with metals like carbon, stainless steel, and thin aluminum alloy components. Helium is recommended for welding operation with thicker aluminum components (plates) and other high-conductive materials as copper. Because of Helium's high ionization potential, it needs higher voltage start-up and maintenance but producing higher heat-input [18].

As previous stated does the gas impact the property of the material, which also leads to variation in welding speed, voltage inflicted weld penetration and heat input during the process. Some examples of mixtures and its advantages regarding other parameters in the welding process:

– Helium/Argon (30%-80% He) mixture allows increased welding speed and better process tolerance (commonly used for low alloy steel, as aluminum and copper).

– Combinations of Argon with up to 5% hydrogen are regularly used in the welding of authentic stainless steels. The hydrogen, in this case, increases arc-voltage and hence the heat input, addition to the weld penetration and weld travel speed it furthermore improves weld appearance [18]. Argon/hydrogen blending are also common in welding of copper-nickel alloys.

Shielding gas is measured in a flow rate on [l/min] during the welding operation. The quantity of the flow rate depends on the weld thickness. Generally, examples, rule of thumb:

- Argon: 4-10 [l/min]

- Helium: 10-15 [l/min] (More flow because it's lighter than Argon and is thus less effective in shielding purposes [19]).

Gases with most purity (99.995%) are mainly used in welding metals, like titanium, which has a level less than 50 ppm. Choice of shield gas depends on the factors as working metals, the effect on the welding cost, weld temperature, arc stability, weld speed, splatter, and electrode life. In this study with welding at stainless steel, Argon is used in the welding process. Argon generally provides an arc that operates more smoothly and quietly, which contribute a less penetration than if helium is used. Thus, for these reasons, Argon is preferred for most of the applications in general.

4.3.6   Filler Metal

Filler metal is in general used for plate thickness above 2 [mm], where chemical composition similar to the parent metal is added. The diameter from the filler metal varies from 1.6 to 3.2 [mm] wherein automated system is added cold from the roll or a coil. The majority of the super austenitic alloys require the use of filler metal to acquire proper corrosion resistance of the weld. Because not all of the austenitic stainless steel can be welded without filler metal and heat treatment. Normally, the welding created by the filler metal can meet the minimum requirements at yielding-stress and strength of the annealed base material. Because if the created weld is to strong compared to the base material, it will cause fracture on the side, and if the weld is too weak, it causes a fracture in the middle. This is because of the stress generated by the heat during the welding operation. Low carbon grades of filler metals contribute better corrosion resistant in the material.

Conversely, high carbon grades provide better high-temperature strength. During the solidification in the welding process, an amount of ferrite is desirable to prevent hot cracking. It allows for higher heat inputs and thus, higher welding speeds. For a particular application, a low amount of ferrite is made for a specific purpose, but most common filler metal used has a nominal match of ferrite in the filler metal [19].

4.3.7   Cup Size

Cups or gas nozzle is made of various type of heat resistant materials in different shapes, diameter and lengths. The cups are either screwed within the torch head or pushed into place. The material of the cups can be made of ceramic, metal, metal-jacketed ceramic, glass, among other types. The most common one is ceramic since the material is very porous it can easily break. The gas cup/nozzle should by the rule of thumb be at least three times the tungsten diameter to provide adequate shielding gas coverage to the weld pool and welding area. Because a given size will allow only a given amount of gas to flow before the flow becomes turbulent. The type of cup that is used during the welding process depends on the torch, current, and kind of alloy. The cup that is normally chosen in GTAW is with AC, which also is used during the welding test in this thesis [20].

4.4   Additive Manufacturing (AM)

Additive Manufacturing (AM) is a technique where structures are manufactured by adding and depositing material in a layer upon layer manner. AM production method has major advantages over traditional milling, machining techniques, and welded analogs. For large-scale component or complex component structure, layer deposition strategy provides advantages as reducing waste and improving manufacturing costs with almost no limitation withing creating the structures geometry. The metal deposition in additive manufacturing has several techniques achieve layer-wise build ups, which occur in different arc welding processes (MIG, TIG and plasma), Electron Beam Melting (EBM), Sective Laser Melting (SLM), among others [3]. This section will convey mainly about arc wire additive manufacturing technique with gas tungsten and the daily challenges with the current method/process.

4.4.1   What is Additive Manufacturing?

The technological evolution has from the mid-'70s brought new: machining tools, design methodologies, guidelines for the development of projects focused to manufacturing, assembly among other innovations that have allowed systematization and optimization for machine tools development. Additive manufacturing was innovated in 1987, where the process was initially named as Rapid Prototyping to try to improve the method of producing products. Natural defects during the melting of metal alloy and the geometric aspects of the located layers give us knowledge and certainty of the manufacturing process by layers [3].

Additive manufacturing (AM) is commonly known as 3D-technology, 3D objects are produced by adding layer-upon-layer of material. Type of the material depends on the usage and purpose of the product, it varies from metal to plastic, and maybe one day even human tissue. Common factors for AM-technology is to use 3D software (CAD), machine equipment, and layering material. The general process starts with a modulated product produced in a 3D-software which the AM-equipment reads and finally generate the object by creating the layer upon layers. [21].

4.4.2   GTAW-Based Wire Arc Additive Manufacturing system (WAAM)

Wire Arc Additive Manufacturing (WAAM) is a technology which has been under the scope for the last 30 years, although the first patent of the technology dates from almost 100 years ago. The technology became interesting for scientists and manufacturer due to its ability to produce completely dense metal parts and large near-net-shape products. The method utilizes the power source of electric arc using welding wire as feedstock. Because of this, it is more economical than other AM technologies, which need specific equipment and materials [22].

Additive manufacturing contains a wide specter of 3D-printing technology. Selecting the right application can be challenging because each type offers variation as material processed, dimensional accuracy, surface finish, and post-processing requirements. Industry companies have an increasing demand for manufactured parts size component of medium geometric complexity. Extensive processes such as Selective Laser Melting (SLM) or Laser Metal Deposition (LMD) can in comparison not provide the same highly deposition rates and quality

without size limitation as Wire-Arc Additive Manufacture (WAAM). There are mainly three welding processes used in WAAM [23]:

- Plasma Arc Welding (PAW)

- Gas Tungsten Arc Welding (GTAW or TIG)

- Gas Metal Arc Welding (GMAW or MIG)

This study aims towards GTAW-based WAAM process which is performed during the welding operations. Further challenges are to be presented regarding the welding method, applications, and the execution of the process. GTAW is conducting the process with a non-consumable tungsten electrode in combination with a separated wire feeder that produces the weld deposit.
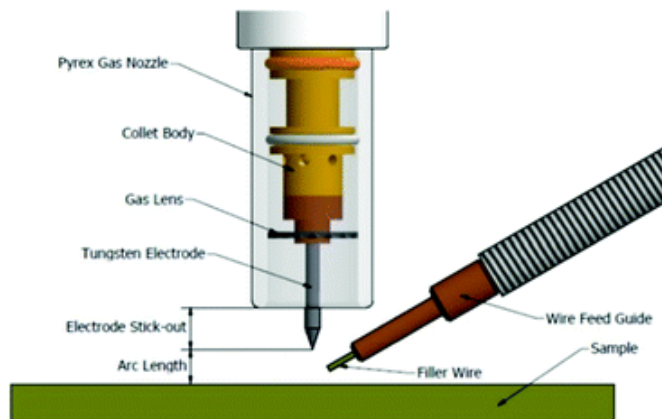
Figure 4: WAAM process. Source [24]

During the deposition process, the wire feed location affects the material transfer and quality of the deposit. Different orientation of feeding (back, front, side) is also possible to gain a better result, the best direction can depend on the alloy. For improving deposition accuracy, a mathematic model is developed which optimize the direction and position of the wire feed. Increasing the arc length occur with a corresponding increase at a distance between the shielding nozzle and workpiece. A gas lens is used to generate a continuous flow of shielding gas to reduce oxidation during the process. Typically are trailing shield device used to prevent oxidation during the welding process at titanium alloy in the open air.

4.4.3 Comparison of WAAM with Powder alloys

WAAM has some distinct advantages concerning conventional technologies. Some of them are mentioned below [25]:

- Flexible in terms of output performance, parameters, feed, and feeding speed.

- Produces near networking (NNS) - parts with a little material loss

- Conventional processing time is reduced to a minimum

- Reduced lead times

- Good structural integrity

Comparison between WAAM and powder base system, which is an other popular additive manufacturing method can be summarized in table 2. One of the main reason why WAAM stands out as one of the most optimal methods it's the ability to work in an open atmosphere with shielding gas that protects the weld-pool. However, it's known that the degree of complexity of the parts that can be manufactured is lower by using WAAM due to the greater width of the melting bath, higher roughness, and appearance.

	Powder alloy	WAAM
Cost	Høy	Medium
Availability for materials	Few available as standards (more under development)	Many such as: Ti, Fe, Ni, Al
Material Efficiency	Typical: 40-60%	100%
Recycling	Possible	Possible
Process in several positions [not onlt in PA]	No	Yes
Rotationproblems	Coaxial-No, Sidemate-Yes	Coaxial-No, Sidemate-Yes
Provision Rate per hour (depending on process parameters)	**2.0 kg/h**	**3.5 kg/h = 70% more**

Table 2: Comparison between Powder-system and WAAM. Source: [25]

4.4.4   Function by solid wire for WAAM

Comparison between welding and other processes to merge materials relates to the challenges in the additive material (filler wire). The reasons are related to the more demanding metallurgical and process requirements. Pure metallurgical leads to the use of high heat input and lower cooling velocity due to the subsequent welding strings, and therefore, the physical and mechanical properties of the additives must be adapted to such conditions. In addition, the additive material must be designed to take several heat/tempering cycles of multiple layers and be able to perform heat treatment when and if necessary.

The chemical preparation of the filler material also influences the arc stability and flow behavior, which can be destructive to the subsequent layers of the process. Because stable arc and wire feed are critical to the process, perfect spooling with controlled wire surface makes a huge difference to minimize the number of downtimes. Thus provides profitability and quality for the final product. An example of this is Bohler-Welding, which has developed their filler metal called "3DPrint AM" it is customized to their productive Wire-Arc Additive Manufacturing. As for this thesis the filler metal: Bohler CN 13/4-IG are utilized to be welded on the materials: Stainless steel 304L and X3CrNiMo13-4 in regards to gain optimal productivity, material integrity, chemical, and mechanic property [25].

4.4.5 Path Planning Strategy for WAAM

There are several types of tool-path planning of WAAM- welding process. However,the tool pattern which will be focused in the GTAW welding process are the "raster" path which is one of the most used path during 2D-planning of thin wall structure. The "raster" path are illustrated in the table below:
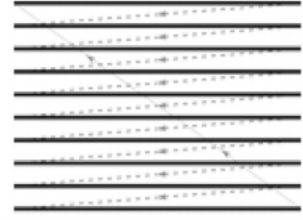
References	Tool Path Pattern	Examples:
[26]	Raster	

Table 3: Path Planning Strategies for WAAM

4.5 Thin Wall Structure Made by Layer Additive Manufacturing

Manufacturing of thin walls structure is one of the major application of AM, where it has huge advantages over conventional milling, machining manufacturing or welded analogs. Manufacturing techniques as thin wall structure are commonly in structural aerospace components, aircraft parts, and other complex structures, typically made in titanium alloys. Layer deposition is the best strategy when it comes to such large-scale components due to the demand for high productivity and size requirement. In this thesis is thin wall structure conducted by adding a layer of deposition with GTAW based WAAM [2].

4.5.1 Thin wall structure by welding

Thin wall structure by welding is achieved in this study by the WAAM-method, an arc-based deposition process which is conducted by gas tungsten arc welding (GTAW). The process by building a structure based on a 3D-model is done by adding material with layer upon layer manner. A welded string is placed as a layer on the base material where the next layer is added upon the previous ones, the binding process is repeated to a wall structure are produced. The process is conducted by adding the filler material beneath the welding pool generated by the torch through the tungsten. The material is then melted to the deposition that creates the layer of the thin wall structure. Generally, CAD-models are sliced to different levels to obtain a tool path and layer information that is used by the Additive Manufacturing equipment [2]. The process utilizes robotic automation that can perform the designs of the different thin-wall structure section.

Daily challenges associated with welding layers in thin wall structures are mainly the heating and cooling cycle that causes shrinkage in both base metal and weld metal. The shrinkage forces tend to create a degree of distortion. As a result of this, the welded product may not be capable of performing its intended purpose and of containing the property of the original material. This is due to the poor fit-up, vibration problems, high reaction stresses, reduced buckling strength, premature cracking, or unacceptable appearance. Control of residual stress

and distortion in the weld is a vital task in the making of thin wall structure by GTAW, which will be further elaborated in 2.6.2.

4.5.2   Thermal and mechanical processes during welding

During this applied research, wire arc welding (WAAM) by GTAW is used in the material-joining process, which is a widely common process in industries around the globe. Due to the welding process, localized heating followed with rapid cooling can contribute stresses and distortion near butt-welded joints. Because of high residual stresses in the region near the weld may develop a brittle fracture, fatigue, or stress corrosion cracking. Therefore, various methods are suggested for reducing residual stress and gain control of distortion in weldments. In this work, three techniques are introduced which have a direct impact on the thermal and mechanical property in the weldment process:

1. Preheating

2. Welding Sequence

3. PWHT (Post Weld Heat Treatment)

The two techniques: the preheating (Figure:5 to the left) and selection of proper welding sequence (Figure:5 to the right) are introduced based on the research note from [27] and the PWHT are further based on the paper [28].
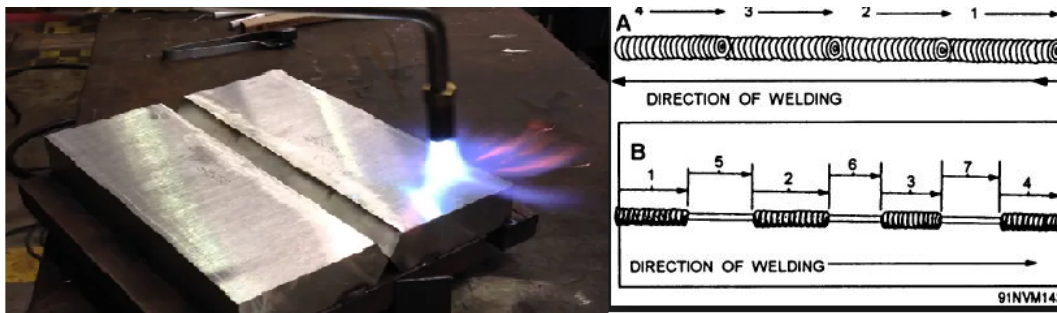
Figure 5: Picture left: Preheating, source: [29]. Picture right: Welding Sequence. source [30]

4.5.2.1   Preheat

Preheat implies raising the temperature of the welded part before welding. It prevents the development of cold cracks by decreasing the cooling rate of weld and heat affected zones (HAZ). Additionally, it also increases the toughness of welds, particularly at low temperature, and restrains shrinkage stress [31]. A crucial criterion to establish the right amount of preheating is the measurement of the hardness, which usually is accomplished by a portable hardness meter.

4.5.2.2   Welding Sequence

Welding sequence can be an effective developed technique and simple approach to decrease residual stress in the weld. An advantage of this method is that it does not require any special equipment, unlike most other heat treatments. As illustrated in figure 5, the welded joint is divided into seven stripes (operations) to distribute the heat from the welding torch. When welding the heat can cause shrinkage of the welded material and high residual stresses when the heat is focused too much at a particular area, which impacts the property of the material. See 2.6.3, for example of the influence of the welding sequence have on residual stress and distortion and where it could be predicted to appear.

The article: [32] "Influence of the welding sequence on residual stress and distortion of fillet welded structures", provide a great example of how meaningful this technique is. The article states an analysis of a T-joint where they investigated the effect of welding sequence on the residual stresses and distortion in T-joint welds by a 3D numerical model. Because the article is based on an experiment of a butt-welded T-joint, it is not a direct comparison of a thin wall structure by WAAM when it comes to the distribution of stresses and deformation. The stresses and deformation are therefore at a lesser amount in tension and compression -stresses as shown in butt welding situation like figure 7. The coordinate system is shown in A-longitudinal stress-distribution and B-transverse stress-distribution.
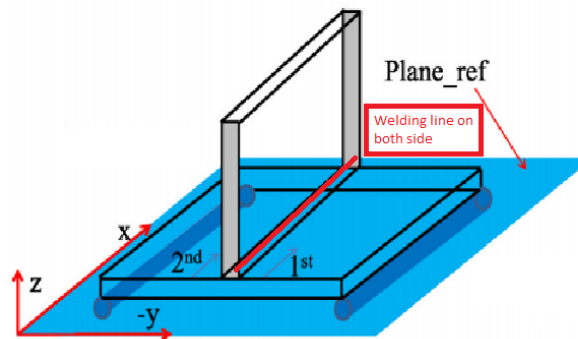
Figure 6: Welding coordinate system and welding lines of the fillet welding used in the article. Source: [32]

Two following conclusion they draw from the [30] article:

- The residual stress distribution, are especially for the transverse stresses (along the y-axis) influenced by welding sequence near the start/end (middle of the y-axis) of the weld, in the middle of the plate, see figure 7. The located concentrated tension-stress is at its peak (along YY) while other regions have no significant influence of the residual stresses.

- The welding deposition sequence significantly influences the magnitude and deformation mode of the deflections. The magnitude of the deflection on both side of the thin plate is smaller than in a single-side weld. The single-side weld sequence causes more distortion than the double-side weld sequence in the T-joint weld.
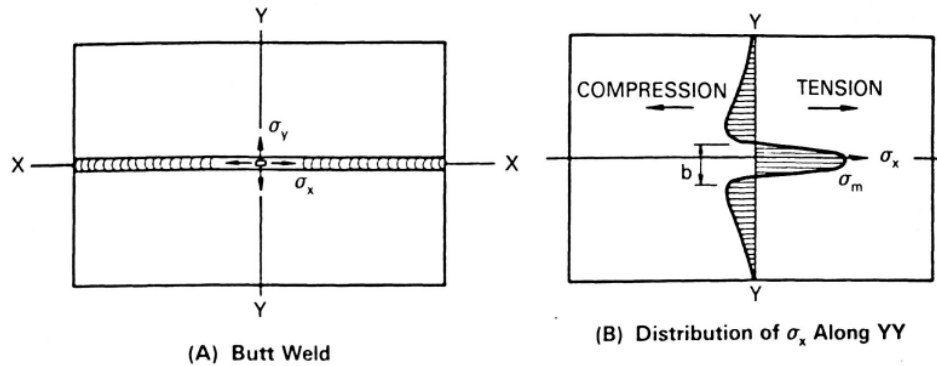
Figure 7: Residual stress distribution at the fillet weld . Source: [33]

4.5.2.3   Post weld heat treatment (PWHT)

Post weld heat treatment (PWHT), defined as any form of treatment after welding, is frequently used to improve the properties of a weldment. The purpose of treatment is to ensure that the material strength is retained after welding. When PWHT is required, it's normally the goal to increase the resistance to brittle fracture and decrease residual stresses. Desires that can also be a result are hardness reduction and even material strength enhancements. PWHT encompasses many different types of a potential treatment, in the case of steel fabrication, the two most common types used are post heating and stress relieving [34]:

- **Post Heating** is used to decrease the potential for hydrogen induced cracking (HIC). HIC occurs when a high level of ambient hydrogen permeate into a material during welding, for this to happen following variables must be present, see figure 8: a sensitive microstructure, a sufficient level of hydrogen, or a high level of stress.
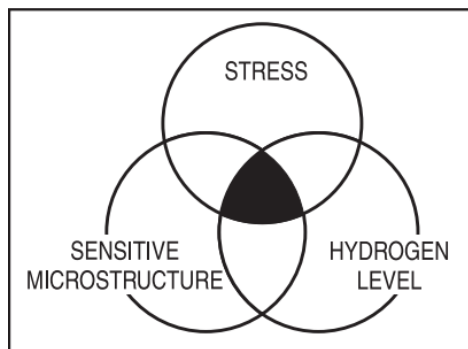
Figure 8: Criteria for hydrogen induced cracking (HIC). Source: [34]

After the welding process is completed, heating is added immediately afterward to diffuse hydrogen from the welded area, hence preventing HIC, which is the process of the post-heating, see figure 9. Instead of allowing the material to cool, it needs to be heated to a certain temperature depending on the type and thickness of the material. It should be held at this temperature for some minimum amount of times, dependent on

the thickness of the material. Code and service requirements can dictate the variety of the temperature, 230°C (450 °F) is a commonly post heat temperature to be maintained for one hour per 25 [mm]. For example, do some chrome molybdenum steels typically need stress relieving at 675-700°C temperature range.
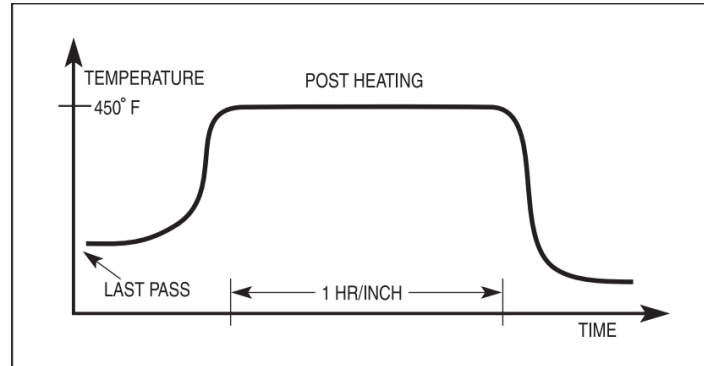
Figure 9: Post heat appplied immediately after weldement. Source: [34]

However, post-heating is not necessary for most applications, some can be damaged by PWHT, while others require it. In the paper published by A.G Olabi and M.S.J Hashmi [35], they present the result of PWHT improves the toughness by about 15% without making any remarkable difference to the tensile strength and the hardness, in addition, it has a huge effect of reducing the residual stress by about 70&. The result of the tests shows tensile stresses near the welding zone, which decrease as the distance from the welding zone increase. They document that after applied PWHT with placing the welded component in the furnace and cool it down with decreasing temperature over time, the residual stress decreases about 330 N/mm^2 to about 90 N/mm^2 in the HAZ.

- **Stress Relieving** heat treatment, on the other hand, is used to reduce the stresses that remain locked in a structure as a consequence of manufacturing processes. After the weldment, a large number of residual stress is inside the material, which can lead to an increased potential for stress corrosion and HIC. PWHT can, therefore, be used to realize these stresses and reduce this potential. This involves a process of heating the material to a specific temperature and then gradually cool it down, see figure 9. If not it is cooled down by the room temperature, either way, does the RS decrease as the temperature after the welding process

Residual stresses that occur during welding have a normal amount of magnitude equal to the yield strength of the base material. Heating a structure to a tolerable high temperature but are adjusted below the lower transformation temperature range, and then uniformly cooling it, can relax these residual stresses. The meaning of uniformly cooling in heat treatment is an equal temperature in the core and surface region of the material. An example of benefits that stress relieving offers can be when a structure

with high residual stresses is machined. The material can move during the metal removal process as the stresses are redistributed. After implied stress relieving, greater dimensional stability is maintained during machining, which again provides increased accuracy [34].

For better control of welding parameters, such as preheating, welding sequence and PWHT. It provides a properly welded joint with minimal detrimental residual stress, which is essential to obtain a safe design. The manufacturer (welder) require time-consuming trial and error methods to develop a right fit for the thermal and mechanic properties as well as the rest of the primary GTAW process parameters.

Analytically method for prediction of stress distribution is precise but are limited by several geometric assumptions. Therefore, numerical modeling, in those cases are expensive options. Despite various advantages of statistical methods, they are complex, and time-consuming, especially for modeling and prediction of occurrence of residual stress in the welded structure. Numerical modeling schemes are conducted as an alternative to the experimental calibration procedure to perform virtual simulation such as the FEA method in ANSYS, see 4.6.

4.6   Prediction of residual stresses and distortion in weld and baseplate

4.6.1   Weld Induced Residual Stresses

Residual stresses (RS) are internal stresses that exist within a material part after external loads and restrains are removed. RS are typically a consequence of the manufacturing of engineering structures. RS is normally generated. In the case of TWS, it gains thermal stresses by welding as a result of local plastic deformations induced by high local temperature consist of rapid heating followed by a cooling phase or PWHT. During the welding process, the welded material is exposed to high heat flow and fused locally. As a result of the high heat, it causes the material to expand, surrounded by a cooler area that restrains the heated zone it gives rise to thermal stresses [36]. Because of thermal stresses slightly exceed the yield limit, which is reduced at elevated temperature, it causes the weld area to be plastically hot-compressed. Subsequently cooling down to quick, narrow or too small comparing to the surrounding area, tensile residual stresses are developed, while the surrounding area is exposed to compressive RS to maintain the self-equilibrium [36].

4.6.2   Prediction of stresses and distortion

The result from the practical experiments and theoretical knowledge of thermal stresses are not only an indicator of prediction for RS and distortion. The FEA method with ANSYS is a general method to predict residual stresses and distortion by many researchers in the past studies. However, during this thesis, the FEA method is implemented after the welding processes to compare the results from the experiments against the theoretical assumptions. According to [37], Z.Feng states that predictions are done by FEA method: "have been reported to be much smaller than the magnitude of the experimentally measured distortion." Reason for this is because of the existence of compressive plastic strains in the weld material made during the heat cycle of the welding process in the FEA model.

Based on practical predictions of stress distribution around filled weld in a T-joint, provide similar transverse and longitudinal stresses as a butt weld, as shown in figure 7 B. The deformation in the plate during welding, will partial be as shown in figure 10.
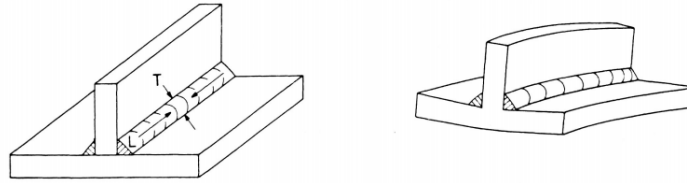
Figure 10: Stresses and deformation in T-joint. Source: [33]

Explained in 4.5.2.2, does the deformation occur at the sides of the baseplate. Additional deformation occurs at the center of the welding stripe to the edge of the plate. As this example covers for fillet weld at a T-joint, it also applies for thin wall structures only with a lower amount of stress and distortion. The reason for this is because of the compression force that emerges from the center of the weld to the end of the plate. In figure 11 illustrate a general indication of stresses in the longitudinal direction at a T-joint. Where the tensile increase in the center and compression increase distance from the center of the weld. The figure gives us a general understanding of predictions of the distributed stresses that occur.
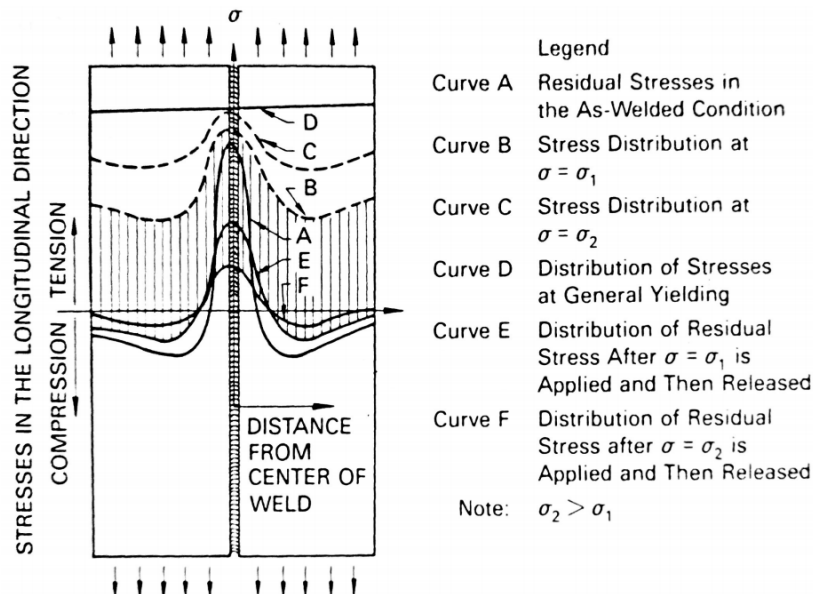
Figure 11: Evenly distributed tensile load overloaded longitudinal residual stress. Source: [33]

During the welding operation, the base plate is normally fixed to the working table with clamps which each of them cover an area of 40x20 [mm] at the BP. Thus exclude the factors as movement and rotation. RS and structural deformation in the form of shrinkage in the welded area are profoundly affected by using of the welding fixtures during the welding operation, the amount of restrains determine the control of distortion and residual stress fields on the

weldment and baseplate. In general, welding RS and strains behave in opposing ways with the degree of restraint, as shown in figure 12. Thus, the fixture-clamps are essential to keep RS low and to reduce residual distortion.
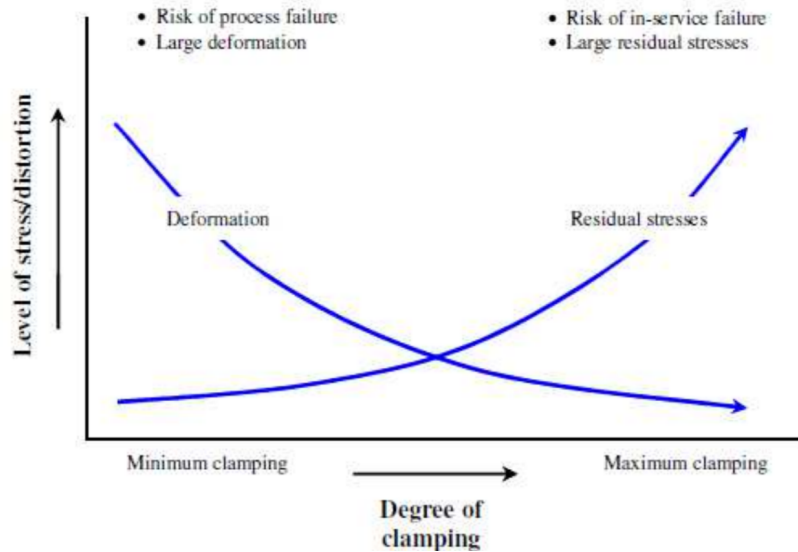
Figure 12: Effect of the degree of clamps-fixture on the level of distortion and RS. Source: [36]

RS and distortion contribute to the problem with machining the structure afterward, where the component itself can move during the machining. It increases the importance of heat treatment after the welding operations and preheating. Also cautions with machining the product afterward is needed in case of residual stresses are too massive in the thin wall structure.

Temperature distribution has a central role because it provides knowledge of where thermal energy is implemented in the material. Additional it gives an insight of where the location of the HAZ, which indicates where the shrinkage occurs. Prediction of the temperature that is distributed in the TWS and BP during and after welding is predicted to occur at a large scale at the fusion zone, and then rapidly decrease down in time if PWHT is not taken into account, like taking the welded part into an industrial heater to slowly decrease the temperature over time. . The HAZ is expected to be half amount lower than the fusion zone, and the base plate, in general, are to be at a low temperature compare to the fusion and HAZ. Illustrated by figure 13 does the temperature of each zone merge during the cooling cycle to and constant temperature, which decreases down to room temperature. This prediction is based on the welding process simulation of article [38] , as they weld a stripe at the baseplate with a similar dimension.
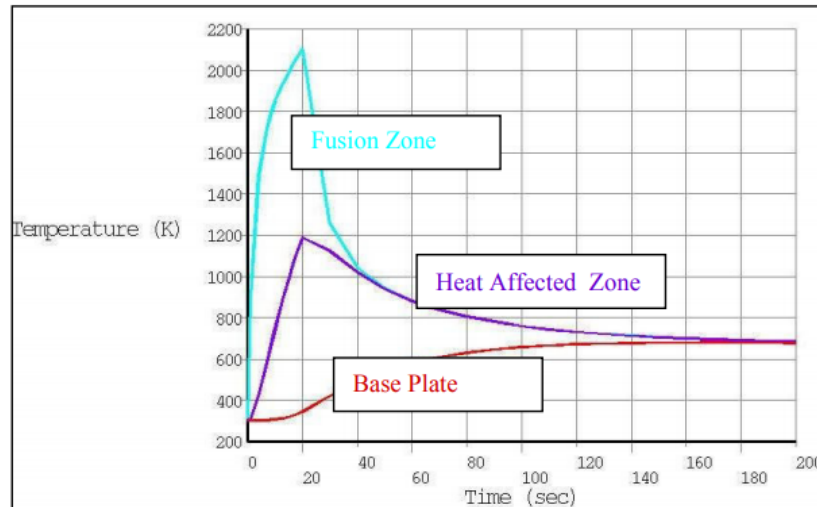
Figure 13: Temperature distribution predictions after weldement . Source [38]

4.7 Vital components regarding robotic welding

A short overview of the critical component used during the experimental setup system performed to controls the parameters, which impact the result of the thin wall structure.

4.7.1 KUKA KR 30-3 Robot

Robotic Wire Arc Additive Manufacturing (WAAM) involves a process that includes building a metal structure that encompasses robotic WAAM by utilizing a KUKA-30 robot that alternatively programs a welding stripe for joining materials one layer at the time for a layer-by-layer structure.
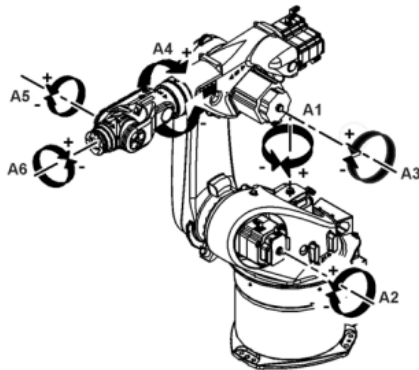
Figure 14: KUKA KR 30-3 axes. Source [39]

The robot used to conduct the GTAW operations is called KUKA KR 30-3 (K), it weighs approximately 635 kg, and it is known as an industrial robot manipulator (IRM). The robot includes six axes IRM and has a working volume of 27.2 m³. The rated payload is 30kg, in addition, it can carry an extra 35kg of weight. Because the robot is a high accuracy (HA) model, it has to pose repeatability (ISO 9283) accuracy on ± 0.06 mm, Additionally it has a maximum reach of 2033 mm from center [40].

Related to the GTAW welding, robotic welding has some advantages and disadvantages which will be briefly mentioned in the purpose of the importance of this equipment.

	Advantages	Disadvantage
1	Decreased production costs. Robot speed impact the profit directly.	The initial cost is high (investment cost).
2	Shorter cycle times (more efficient).	Training is required (new technology need to be learned).
3	Reliability and quality are improved (eliminate human error).	Decision making can be limited (if no data are available the robot will not act).
4	Better floor space utilisation (decrease work area).	Limited functions (specialised robots, as welding for instant can only perform welding).
5	Reduced waste (accurate robots).	-
6	Workplace safety is increased and improved (prevent setting human in hazardous environment).	-

Table 4: Advantages and disadvantages of robotic welding

4.7.2   KD 4000 D-11 Wire Feeder and Wire Feeder material

KD 4000 D-11 is an orbital wire feeder for TIG cold wire welding. The feeder can deliver the filler material at a speed from 0.1 [m/min] to 11[m/min] at a interval on 0.02 [m/min] [42]. The filler material used in the wire feeder is a Böhler CN 13/4 solid wire. It is designed with precisely tuned alloying composition to produce a weld deposition featuring with high ductility. Since the base material in the experimental part of the thesis contains a yield strength at 1100 [MPa] [43], Böhler CN 13/4 solid wire is used as filler material which has an lower yield strength at 400 [MPa] [44].

Figure 15: KD 4000 D-11 Wire Feeder. Source [41]

The chemical composition of Bohler CN 13-4-IG						
Element:	C	Si	Mn	Cr	Ni	Mo
Content in percentage [%]	0.01	0.65	0.7	12.2	4.8	0.5

Table 5: Chemical properties for Bohler Cn 13-4-IG

Böhler EMK 6 solid wire is, in general, the most used wire, which it's a copper-coated wire electrode. Due to the wire's ability to withstand high current, it offers ideal properties for thick sheet welding. Because of the high yield strength of 420 [MPa], the wire can be used in a wide specter of steels [45].

4.7.3 KR C2 - Robot Controller

Robot controller function as the robot's brain with a windows operating system (windows 98), it includes a control PC, power unit, KUKA control panel (KCP) teach pendant and safety logic ESC. It has the ability to control up to eight axes, but in this case, the robot only has six. The KCP is equipped with the control and display functions required to operate and program the robot system. Welding path and speed are programmed through the teach pendant, besides that communicates all other hardware with the controller, which is the hub of this welding system. The figure below shows the details the layout the KR C 2-Robot Controller [46] :

1 Power unit
2 Control PC
3 Safety logic (ESC)
4 Connection panel
5 Servo electronics
6 Mounting plate for customer components
7 Fuses
8 KUKA Control Panel
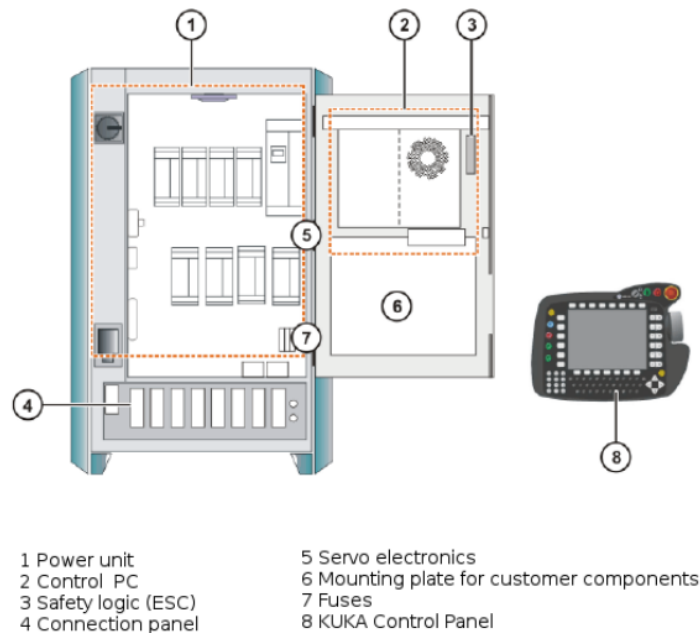
Figure 16: KRC 2 layout. Source: [46]

4.7.4   Power Source: MagicWave 5000

The KUKA robot utilizes the power source Fronius MagicWave 5000. This is a constant current generator which is capable of generating 500 A with an operating voltage between 10,1V - 33V to maintain the arc. The machine has the ability to store over 100 applications, make it easy to change parameters for welding. These settings can be adjusted from the controller- KR C 2.

Figure 17: MagicWave 5000. Source [24]

4.7.5   Welding Electrode

The electrode used in the welding process consists of 98% tungsten and 2% cerium, the diameter of the electrode have a diameter of 3.2 [mm].

4.7.6   AVHC- Automatic Voltage Height Control and RSI log

Due to the constant current from Magicwave 5000, does the voltage increase linearly with the distance from the torch and the substrate material. A software utilizes this correlation of voltage and distance on a separated computer. Further does the software communicate with the controller of the robot which adjusts the z-axis (height) from the zero-point on the substrate. This is a crucial factor due to keeping the efficiency of the arc constant. Thus, higher voltage result in wider and longer arc distance. According to professor Magnus. Aanstad at UiT is the recommended height a product of 1,5 times the electrode diameter:

$$1,5 \times x = 1,5 \times 3.2[mm] = 4.8[mm] \qquad (2)$$

The software of AVHC log-file every weld that has been produced which is named RSI log. The file store information of robots movement directions (X, Y and Z coordinates), and also Z-distance regarding the voltage of the arc. These data can be plotted into a graph which gives an insight into the quality of the weld.

4.7.7   Substrate Materials

The welding process will be conducted on two substrate materials, which is: 304L stainless steel and the steel X3CrNiMo13-4.

4.7.7.1   General Properties of 304L stainless steel

Alloy 304L has a carbon maximum of 0.030, due to its low carbon content, it is resistant to induction hardening or flame hardening. The alloy is the most versatile and widely used steel in the family-tree of stainless steel. Alloy 304L reveals outstanding corrosion resistance, formability, and has high usability of fabrication. The austenitic alloy is considered to be the most weldable high-alloy-steel and can be welded by all welding processes. According to PSP (Penn Stainless Products) has the alloy a welding property that does not require

post-weld annealing to thin sections. Producing weld of the austenitic stainless steel, two consideration bust be taken into account [47]:

1. Preservation of corrosion resistance

2. Avoidance of cracking

The properties of the material are represented by the table below:

Chemical Properties Alloy:304L							
Elements:	C	Mn	Si	P	S	Cr	Ni	N
%-max	0.03	2.0	0.75	0.045	0.03	20	12	0.10

Table 6: Chemical Properties for alloy 304L

Mechanical Properties, Alloy:304L				
Grade	Tensile Strengt [N/mm²]	Yield strengt 0.2% [N/mm²]	Elongation %	Hardness (brinell) Max
304L	483	172	40	201

Table 7: Mechanical properties for alloy 304L

4.7.7.2   General Properties of the steel X3CrNiMo13-4-QT780 (1.4313

The material X3CrNiMo13-4-QT780 is a chromium-nickel martensitic stainless steel with molybdenum addition. Regarding welding procedure, to the steel, the type 1.4313 is used in the process. It can be lightly welded by using arc welding processes, otherwise, the weldment becomes poor. According to "Yaang Industry" [48], they recommend to pre-heating the workpiece to the temperature of 150 °C. This regards especially of thickness larger than 10 [mm] are welded. After welding, the component needs to be hardened/cooled decreasingly down to restore some ductility to the weld zone. Therefore PWHT is important to restore suitable corrosion resistance. MAX HEAT INPUT = 1,5 KJ/mm

Chamical Properties Alloy: X3CrNiMo13-4							
Elements:	C	Si	Mn	P	S	CR	Ni	Mo
%-max	0.05	0.7	1.0	0.04	0.015	14	4.5	1.0

Table 8: Mechanical properies for Steel X3CrNiMo13-4 QT780

Mechanical Properties, Alloy X3CrNiMo13-4				
Grade:	Tensile Strengt [N/mm²]	Yield strengt 0.2% [N/mm²]	Elongation, A5 %	Hardness (HB)
QT780	1100	620	12-17	320

Table 9: Mechanical properies for Steel X3CrNiMo13-4 QT780

4.8 Robotic welding process

4.8.1 Wire Arc Additive Manufacturing System

Figure 18 shows the schematic diagram of a wire arc additive manufacturing by GTAW to produce thin wall structure. It is composed of gas tungsten arc welding (GTAW) equipment's, wire feeder, a computer, argon gas, control cabinet, control panel and a three-dimensional workbench as described in18.
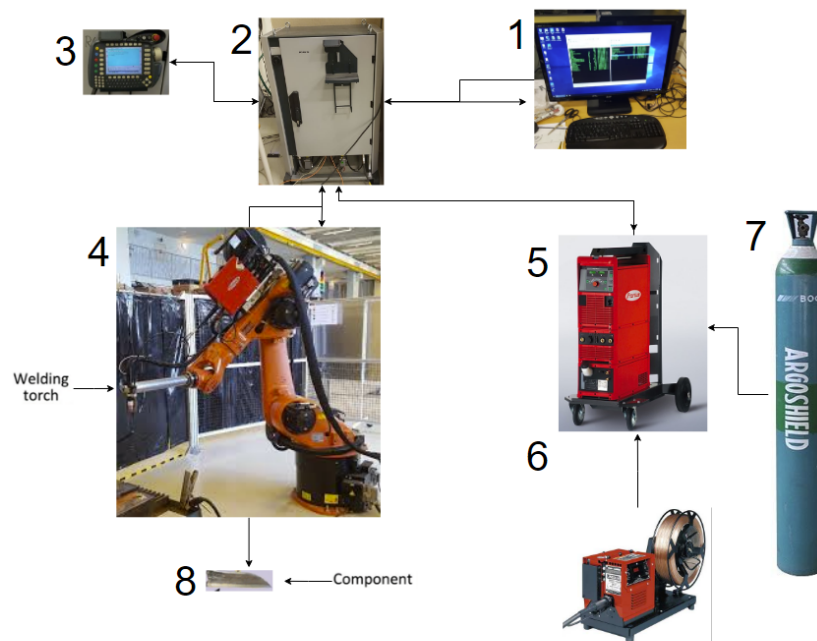
Figure 18: Experiment setup. Source: [49] [41] [39]

The experimental setup has eight parts that represent the welding system. Each element of the experiment are described how they function with each other in eight steps [49] [39]:

1. **Computer**- input of the parameters of the weldment process, which influence the result of the thin wall structure. The computer sends information to the control center (KUKA Robot Controller) which also send feedback of what has been done back to the computer (has two-way connection function).

2. **KUKA Robot Controller** get signal from the computer and control panel. It converts the information of the work assignment and sends the movement to signal it to the

robot with chosen parameters. Since the robot has servo controller, it also sends feed-back back to the controller which store the information of coordinates, which again send back the information to the control panel and computer (has two-way connection function).

3. **Control Panel** It's used to control the robot and create programs (work assignment) which can be executed by control panel by sending a signal to the KUKA Robot controller. The control panel also get information back from the action of the robot (4) through the robot controller (2)

4. **KUKA KR 30-3** Execute the welding operation based on the parameters sett from the computer and the work assignment the control panel(3) gives the KUKA robot controller (2). Since the robot has servo-motors it provide with feedback that goes back, which are a two-way connection function.

5. **Power source: MagicWave 5000** task is to provide with the heat input in the welding process. The signal of parameters set from the computer (1) goes through the controller (2) to the power source (5) which also send information back before the information of settings ends up in the KUKA-robot (4). Thus, this is a two-way connection function. The information the power source (5) provides the voltage and ampere output, which send the amount of power to the robot.

6. **The wire feeder-KD 4000 D-11** task is to feed the amount of wire which is mounted in the robot arm. It collects the data of feeding on the parameters set from the computer (1) through the controller (2) and the power source (5) which decide the right amount of wire feed. Because the wire feeder has a one-way connection to the power source.

7. **Shielding gas** are connected to the power source (5) which again are adjusted with magnitude from the robot controller (2) which provide the protection of the weld in the weldment process. This is a one-way connection function.

8. **Component** is the product of the thin wall structure which is created by the robot (4) and the impact from the other seven elements. This is the results of the WAAM system achieves.

4.8.2   Manufacturing-Standard settings

The feed wire used is an Böhler EMK 6 solid wire with an diameter of 1.0 mm. The substrate used during the experiment where 304L stainless steel and the steel X3CrNiMo13-4 plates with dimensions of 50mm x 100mm x 15mm. The robot (KUKA KR 30-3) utilize GTAW with pure argon as shielding gas. The standard parameters of the process are found in the table below. In the experiment, the design of the thin wall structure varies from a single stripe of additive manufacturing to more complex structures, as shown in the welding procedure qualification record (WPQR). The welding process is conducted based on a procedure shown in the flow diagram [20]. This document provides information about a chronological order to conduct the activity from the unpolished raw material to entirely produced thin wall structure. The flow diagram is based on the literature review of how to perform the process. It

also indicates when to distinguish between an approved weldment sample and not approved sample.

4.8.3   Welding procedure qualification record (WPQR)

Welding operation of the TWS requires specific qualifications to develop a type of structures with different properties. A procedure is therefore initiated to address the process parameters, measurements, temperature, and ductility of the result. WPQR documents every welding sample to the purpose of describing the welding process, it supports the argument of the result which further calculations are based upon (see attachment J). A flow-diagram [??] of the welding operation system is established to ensure the quality of the samples by control-checks, monitoring, and steps during the welding operations.
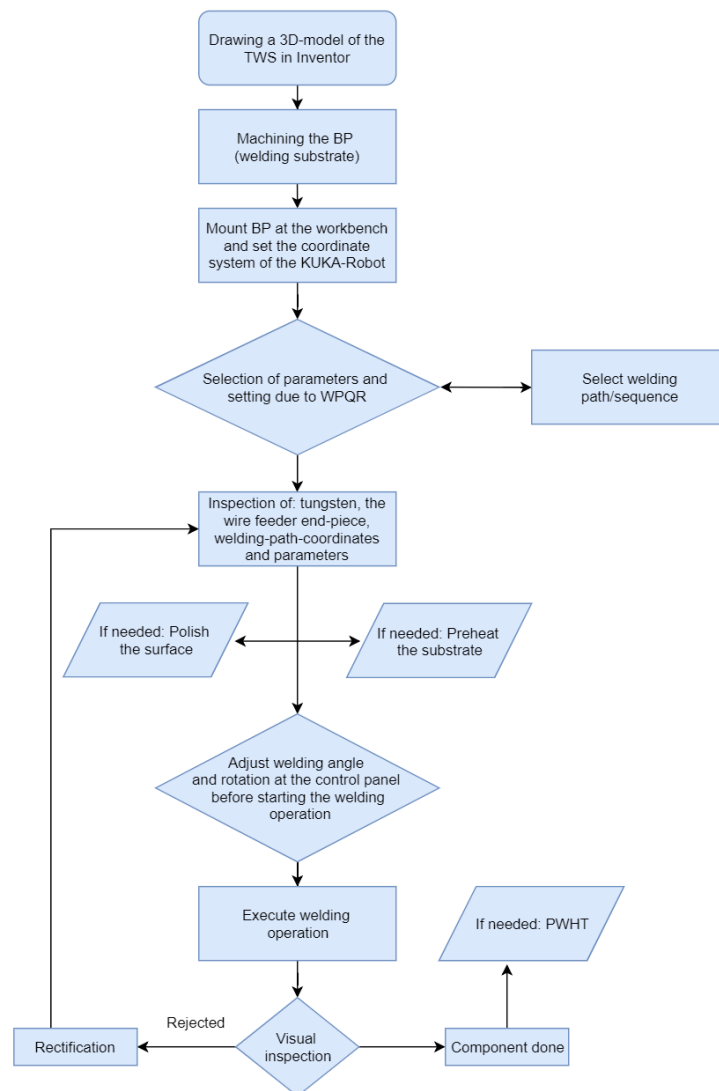
Figure 19: Flow chart of welding procedure operation

4.9 Methods of measuring residual stress in thin wall structure

Residual stresses appear most frequently in manufactured structures and components. GTAW-based WAAM produced thin wall structures is one of the phenomena, which is a new production technology affected by mechanical characteristics. Residual stress in the welded part is an outcome of a variety of parameters like material properties, the geometry of the joints, and the welding process. Over the last few decades, various methods been investigated and developed to measure the residual stresses to provide a reliable assessment of manufactured components. This short review is based on the most popular methods [50] and aim to classify different type of residual stress measurement method to provide a general overview, where two methods, ultrasound measurement, and the practical experiment method are elaborated further to be used in the practical experimental part of the thesis.

4.9.1 Causes of residual stresses

RS are caused by most manufacturing processes including material deformation, heat treatment, machining or processing operations that change the shape or property of the material. They are generated from many different sources and can be presented in the unprocessed raw material, created during manufacturing or arise from in-service loading. RS are represented as tensile and compressive stresses which are opposite forces. Tensile stress appears from elongation caused by stretch forces in the material while compressive forces cause compressive result in shortening of in the material part. For example, the presence of tensile residual stresses in a structural element is often the main caused of fatigue failure stress corrosion cracking. Compressive residual stresses induced by forces in the (sub)surface layer of material are usually beneficial because they prevent origination and propagation of fatigue cracks, and increase wear and corrosion resistance. The forces are created in the structure as the result of differential contractions which occur as the weld metal solidification and cooling to the moving heat source. As a result of the high heat input of welding, non-uniform heat distribution, plastic deformation, and phase transformation occur in the material. These changes cause RS pattern for the weld region and in the heat affected zone (HAZ). RS induced by shrinkage of the molten core are normally tension, transformation occurs at the HAZ where the temperature exceeds the critical level for phase transformation. Along the TWS residual forces are predicted to occur. Therefore a more technical approach is implemented to read out the residual stresses. The measuring techniques are classified in the section below [51].

4.9.2 Classification of residual stress measuring techniques

The basic fundamental for RS test is that they are classified into three categories: destructive, semi-destructive, or non-destructive. The destructive and semi-destructive are known as mechanical methods. It is dependent on derive the original stress from the displacement incurred by completely (destructive) or partially (semi-destructive) relieve the stress by removing material of the specimen. The mechanical method relies on the measurement based on deformation due to the release of residual stresses by removal of material from the component. The most common methods within the different categories of residual stresses are listed in figure **??**: contour, hole-drilling, sectioning, and deep-hole are principals of destructive and semi-destructive techniques. Non-destructive methods which measure residual

stresses by parameters that related to stress include techniques as X-ray, neutron diffraction, ultrasonic or magnetic methods [50].
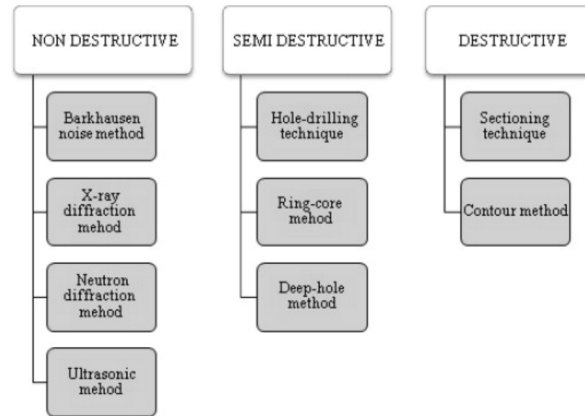
Figure 20: Residual stresses measurement techniques. Source [50]

4.9.3   Ultrasound measurement of residual stress (RS)

Residual stresses caused by thermal processes of weldment are produced as a result of non-uniform thermal expansion and contractions around the heated zone of the material. Welding is known to induce high-level of residual stress (RS), which has a significant effect at the life-time of the welded component used in the mechanical engineering industry. Measurement of RS by ultrasonic waves is a non-destructive test which is easy to use as it is an inexpensive method. However, the measurement is sensitive to a certain level of microstructure effects (grain size, carbon rate, texture) and operation conditions (temperature, couplings, etc). Ultrasound stress measurement is based on a linear relationship between the velocity of ultrasonic waves and the stress in the material. In this relation, within the elastic limits, we find the acoustoelastic effect which tells about the flight time of the ultrasound wave varies with the amount of stress [52]. By the known principle "ultrasonic waves speed is constant for a material" are further used to detect variation in the crystal structure of a material. The measurement method is based on a comparison between a material which is inflicted by forces and material of the same type, which is in zero stress state. The difference from the reference material can then state what the inflicted material obtain. The ultrasonic stress test review is based on the technical notes of Olympus Corporation [53], the study of ultrasound investigation of welding [54] and ultrasonic method to evaluate welding longitudinal residual stress through the thickness in austenitic stainless steel plates [52]

4.9.3.1   Ultrasound - Basic

One of the promising direction towards the development of the non-destructive techniques for residual stresses measurement is the application of ultrasound. Ultrasound has a general sound-frequency from 20kHz and above, depending on the thickness of the material. The ultrasound measurement method is based on the Acoustic-elasticity effect, Acoustic Spectre in figure 21 illustrates three range of frequencies where the ultrasonic range is further broken down to three sub-ranges [53].
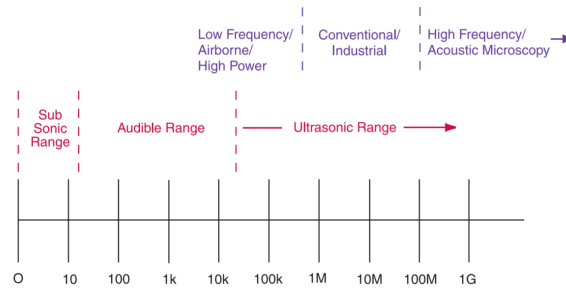
Figure 21: Residual stresses measurement techniques. Source [50]

4.9.3.2 Parameters

Ultrasound waves have travel motion equal to ordinary light waves, while light can travel through vacuum ultrasound waves require elastic media such as liquid or a solid form. Figure 23 shows the parameters of a continuous wave which consist of the wavelength (lambda) and the period (T) of one cycle.
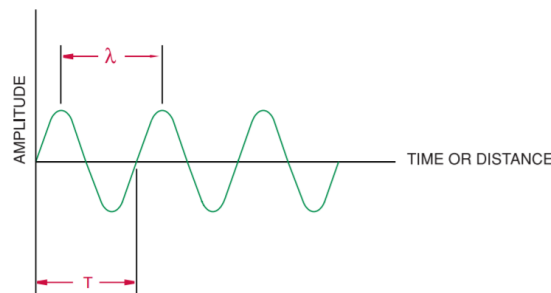
Figure 22: Residual stresses measurement techniques. Source [50]

The period (T) measured in seconds, is the time after one complete cycle. The frequency is based on the relationship of the period (T) and is measured in Hertz, shown in equation 3:

$$f = \frac{1}{T} \tag{3}$$

The velocity of ultrasound (c) in an elastic material with condition of constant pressure and a given temperature, are based on the relation between c,f,lambda and T given by the equations (4) and (5) [[53]]:

$$lambda = \frac{c}{f} \tag{4} \qquad\qquad \lambda = c * T \tag{5}$$

Ultrasonic non-destructive tests generate a sound wave with a high frequency into a test sample, this to obtain information without compromising any damage to the sample. During ultrasound testing two basic quantities are measured; the amount of time the sound used to travel through the sample (t), and the amplitude of the received signal. By the velocity of the sound wave (c) multiplied with the wave time of flight (t) divided by two, the thickness of the material can be calculated:

$$T = \frac{c * t}{2} \tag{6}$$

4.9.3.3 Wave propagation and particle motion

During ultrasound examination are either longitudinal - or share waves most common to utilize. There is other sound propagation as a surface wave or lamb wave, which is not that frequently used. The two common waves [53]:

- A longitudinal wave is a compressional wave which the particle motion is in the same direction as the propagation of the wave.

- A shear wave is a wave motion which particle motion is perpendicular to the direction of the propagation.

- Surface waves have an elliptical particle motion and travel across the surface of the material. The velocity of the shear wave of the material is approximately 90%, and the depth of penetration is almost equal to one wavelength.
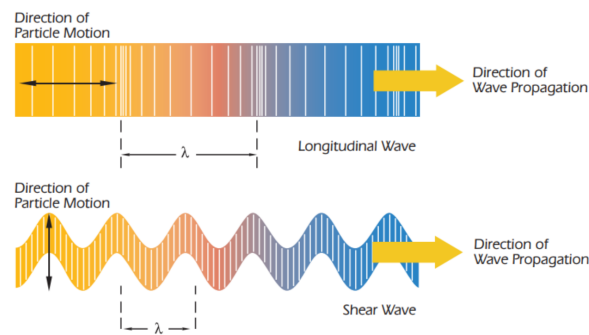
Figure 23: Longitudinal wave and share wave [53]

4.9.3.4 Transducers Signals and types

A critical component within ultrasound measurement is the right application of the transducer. The performance of the system is dependant on the variation in instrument characteristics and settings as well as material properties and coupling condition. Transducers configuration do also has an impact on system performance. Three different series are developed by [53] to counter the need of variety, where each set has its characteristics. The table below provides a general knowledge of the performance characteristics of each transducer series. Each application is unique as their performance are based on electronics, cabling, transducers configuration, frequency, and element diameter [53].
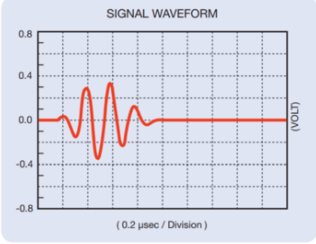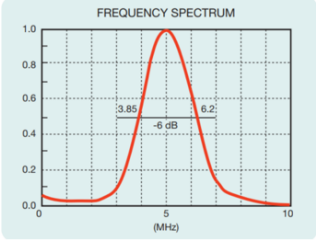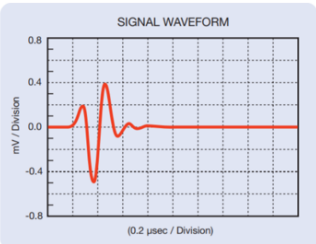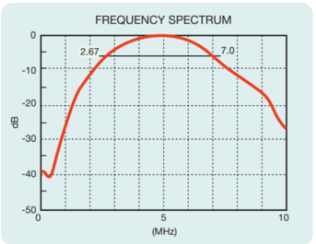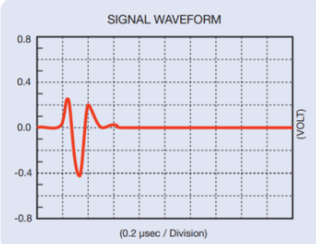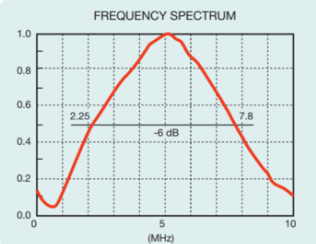
Series of transducers	Signal waveform - graph	Frequency spectrum - graph
Accuscan "S" The accuscan series are designed to provide excellent sensitivity in situations where axial resolution not the primary concern. Typical characteristics for this series is longer wave duration and an relative narrow frequency bandwidth.		
Centrascan The piezocomposite element Centrascan series transducers provide excellent sensitivity with a high signal-to-noise for material that are hard to penetrate. Centrascan have good acoustic matching for low impedance material.		
Videoscan Videoscan transducers are untuned transducers which provide heavily damped broadband performance. They are best intended in application where good axial or distance resolution is necessary or in tests which require improved signal-to-noise in attenuating or scattering materials.		

Figure 24: Active elements in a transducer [53]

Illustrated photo:	Type of transducer:
	Contact Transducer: are a single element transducer which generates the longitudinal wave, the intention is to make direct contact with the test part. Contact transducers are equipped with a WC5 war face that provides superior wear resistance and probe life, additional to offer excellent acoustic impedance match to most metals.

	Dual Element Transducers: A dual element transducer consists of two longitudinal wave crystal elements installed in the same case, one transmitter and one receiver which are isolated by an acoustic barrier inside the component. It has two angled elements that create a V-shape sound path in the test material. Duel element transducer provides a more consistent reading in heavy corroded parts and can be used in a high-temperature environment.
	Angle Beam Transducers: Angle beam transducer is a single element transducer that utilizes a wedge to introduce either longitudinal or share wave sound within apart at a selected angle (45 degrees for steel). Angle beam transducer allows inspection in areas of a material that could not be accessed through the ultrasonic path of a normal contact transducer. This kind of transducer is commonly used in weld inspection was a typical flaw alignment produces strong reflection from the angle beam.
	Delay Line Transducer: Delay line transducers are single element contact transducer specifically designed to insert an epoxy – material in front of the transducer. Reason for choosing a delay line transducer is because of its ability to improve the near surface resolution. The delay allows the element to stop vibrating before a return signal from the reflector can be received. Delay line can be shaped after the surface geometry of the material and an additional be used in higher temperature application.
	Protected Line Transducers: Protected line transducers are single element longitudinal wave transducers that can utilize either a protective membrane, delay line or protective wear cap. Thus, the protected line offers good versatility and ability to cover a wide range of application.
	Immersion Transducers: Immersion transducers are single element longitudinal wave transducers which have a worn face with an impedance matched with water. It has a sealed case that allows them to submerge underwater, where it uses the water as coupling and delay line. Additional it can focus to increase the sound intensity at a specific area and decrease the spot size of the sound beam.
	High-Frequency Transducers: High-frequency lines are either a delay line or focused immersion transducer with a frequency specter between 20-225 [MHz]. The high-frequency delay line can perform measurement on material down to 0,010 [mm] (dependant on transducers, material and settings). High-frequency immersion transducers have a high-performance resolution imaging and flaw detector application on thin, low attenuation material such as silicon microchips.

Table 10: Type of transducers. Source: [53]

4.9.3.5 Configurations for measurement of residual stresses

Ultrasound is a volumetric inspection which utilizes a transmitting transducer to launch wave propagation through a region of a material to a receiving transducer. The signal which goes through the sending - and receiving transducer can further information about the velocity of frequency, which can represent residual stresses in the material. There are three different configurations of ultrasonic equipment for residual measurement; (a) through-thickness pulse-echo (b) through-thickness pitch-catch and (c) surface pitch-catch, illustrated in figure 26 [55]:
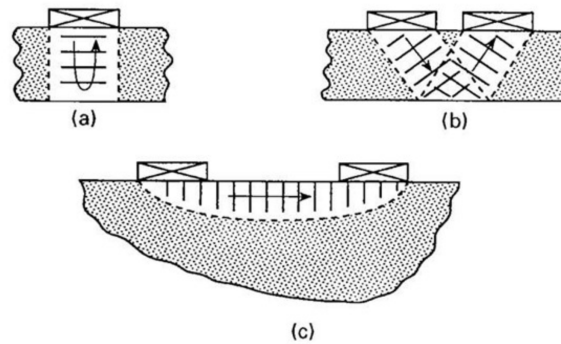
Figure 25: Schematic view of ultrasound measurement configuration [55]

The technique when the same transducer is used for excitation and receiving of ultrasonic waves is often called the pulse-echo method (2a). From configuration 2c, the residual stress in a surface/ subsurface layer is determined.

As proposed in [56] [57] technique, the velocity of longitudinal ultrasonic wave and shear wave of orthogonal polarization (electromagnetic wave which is perpendicular to the direction) are measured at a given point to determine the uni - and biaxial residual stresses. During this approach, the bulk wave is used to determine the average stress over the thickness of the inspected elements. The surface weave is commonly determined by uni - and biaxial stresses at the surface of the scanned material. The proportionality coefficient represents the mechanical properties of the material, that can be calculated or determined experimentally under an external load of a sample of considered material.

4.9.3.6 Theoretical background to evaluate residual stresses from ultrasound measurement

Theoretical description of the acoustoelastic effect refers to a change of velocity of ultrasound wave propagation in strained solids. It applies only to considering the non-linear theory of elasticity. Murnaghan [58] theory addresses third - order terms in strain energy, where Hughe

and Kelly [59] derived the expression for the velocity of elastic wave in a stressed solid. Thus in the case the velocity of the longitudinal wave traveling, the velocity is given by [60]:

$$\rho_0 * [V_1]^2 = \lambda + 2\mu + (2l + \lambda)\theta + (4m + 4\lambda + 10\mu)\alpha \tag{7}$$

Ultrasound measurement of stress are based on the relationship of different direction of wave speed. The figure below illustrates a material under tension with three directions of ultrasound wave propagation. Figure 2a shows the wave propagation parallel to the force and V1 illustrate the velocity of the particle in the same direction (longitudinal wave), while V12 and V13 illustrate velocity in a perpendicular plane (share wave). Waves with particle motion in the direction of the stress field show the greatest sensitivity to stress, and those particle motions perpendicular shows the least sensitive to stress. The largest variation in travel time of the strain is found in the longitudinal waves, where shear waves, on the other hand, vibrated particles in the direction of the load.
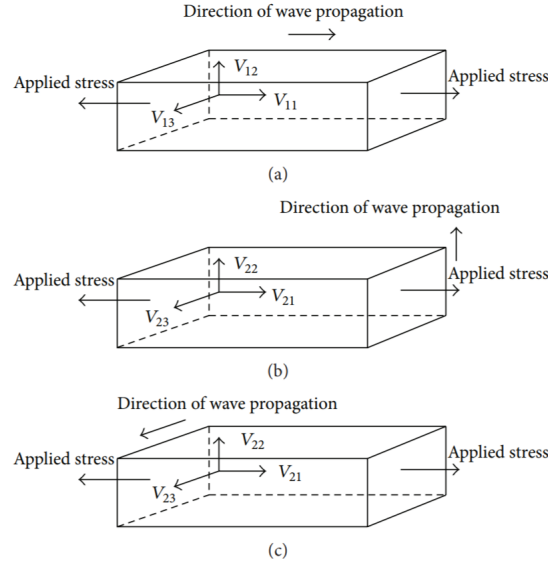
Figure 26: Schematic view of ultrasound measurement configuration [55]

The relative sensitivity is the variation of longitudinal wave velocity with the strain and can be calculated by expression [60]:

$$L_1 = 2 + \frac{(\mu + 2m) + V\mu(1 + 2l/\lambda)}{\lambda + 2\mu} = \frac{dV_1/V_1}{d\epsilon} \tag{8}$$

Before calculating the residual stresses in the component, an evaluation of the acoustoelastic constant need to be known. Normally a uniaxial tensile test is carried out from the tested material to find the constant, the method of finding the constant can also be found from an approach between the relation of thermal stresses and ultrasonic wave velocity. However, the acoustoelastic constant is deduced experimentally from the uniaxial tensile test associated with ultrasound measurement, which is described from the formula:

$$K = -\frac{t - t_o}{\sigma * t_o} \tag{9}$$

Sigma is the applied stress, t and t0 are the time of flight measured between the two receivers for stress and unstressed sample. The acoustoelastic constant (L1) is equal to (-K*E), where the K is from the formula 10 and E is the elasticity modulus.

L1 is the acoustoelastic constant corresponding to the longitudinal mode. Stress can further be calculated by one dimensional application of the stress strain relation in elastic solid. Equation 9 can be reworked to address stress variation in term of time of flight (dt/t0), shown in equation 10, t0 in this case is the time for the wave to go through the stress free material (reference material) [60]:

$$d\sigma = \frac{E(dV_1/V_1)}{L_1} = \frac{E}{L_1 * t_0} * dt \tag{10}$$

4.9.4   X-ray diffraction method

X-ray is a non-destructive technique for measuring residual stresses at the surface of the specimen, due to low penetration depths. Most commonly utilized in this method are Bragg's law, where the diffraction angle 2*theta and the lattice space,d, can be determined for multiple inclination angles of the sample surface, providing the RS measurements. When the material is under stress, applied or residual stress, the deformation in the atomic plane causes elastic strains in the metallic crystal structure to change spacing (d) of the lattice planes [61]. Because of Poisson's ratio effect, when tensile stress applied the lattice spacing will increase for planes perpendicular to the stress direction, and decrease planes parallel to the stress direction. The new spacing (d) is in any similarly oriented planes, concerning the applied stress. Therefore can only the method be applied to crystalline, polycrystalline, and semi-crystalline materials. X-ray diffraction can directly measure those inter-planar atomic spacing, from given quantity the total stress on the metal can be obtained. Because metal is structured in a regular three-dimensional array to form a crystal, most metal components consist of many tiny crystallites (grains) randomly oriented and fused to make a solid. The accuracy of the technique is heavily dependant upon proper surface preparation and grain size/texture. Although the method is classified as a surface measurement technique, the measurement can be done at a depth up to 1 [mm] when combined with layer removal [62].
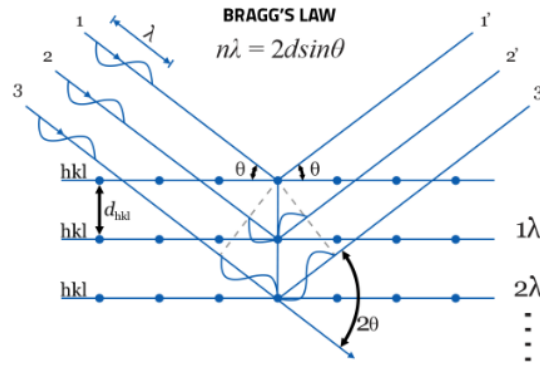
Figure 27: Bragg's Law [61]

4.9.5 Neutron diffraction method

Neutron diffraction method is very similar to the X-ray method as it is also based on elastic deformation within a polycrystalline material that causes changes in the spacing of the lattice planes from their stress-free condition. The main difference is that the neutron can penetrate much deeper into the material due to different scattering properties. Neutron diffraction or elastic neutron scattering is the application of neutron scattering to the determination of the atomic and/or magnetic structure of a material. The investigated sample is placed in the beam of cold or hot neutrons to obtain a diffraction pattern that provides information about the structure of the material. The technique is as mentioned based on X-ray method which uses Bragg's equation, which describes the condition for constructive interference from successive crystallographic planes of the crystalline lattice. Neutron diffraction has four major components; beam source (fixed), sample, detector, and measurement environment, as shown in figure **??**. The method can be categorized into angular variance and wavelength dispersion type. The angular variance uses a single wavelength, and the diffraction pattern obtained depend on the diffraction angle. Within the angular variant type of neutron diffraction, it exists two advanced techniques as "in situ" and "TOF" method. "In situ" includes multi-detectors instead of one to measure the angle dependence of the single beam diffraction. "TOF" on the other hand, can obtain multiple peaks of neutron diffraction simultaneously by utilizing two fixed detectors.

Diffraction methods can be divided into two interactions:

- **Nuclear diffraction** caused by interaction between neutrons and atomic nuclei.

- **Magnetic diffraction** caused by interaction between magnetic moments of neutrons and magnetic moments of atoms.
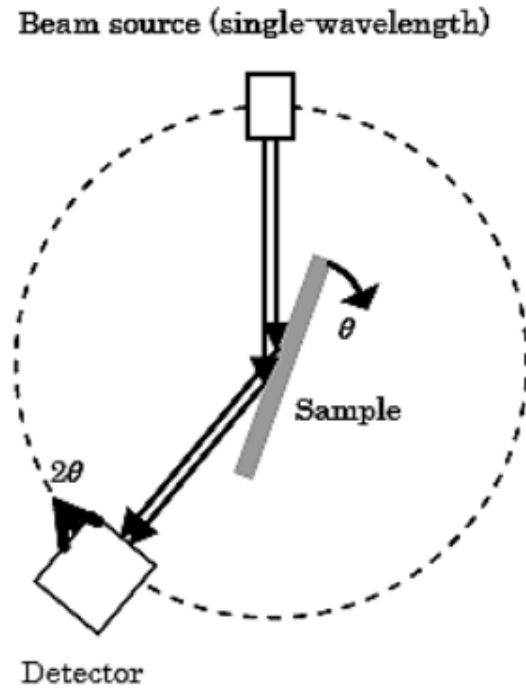
Figure 28: Bragg's Law [61]

4.9.6   Hole drilling method

The hole-drilling method is an easy and quick method, which are one of the most popular semi-destructive methods. It can provide an evaluation of residual stress measurement of distribution across thickness in magnitude, direction, and sense. The method consists of drilling a small local hole in the specimen where the RS is to be measured, which is tolerable or repairable (about 1.8 [mm] diameter and 2 [mm] deep). Due to the drilling of the hole the locked up RS is relieved and suitable strain gauges measure the strains at the surface, these gauges measure the deflection of the surface which is caused by the relived stresses by the drilling which RS-calculation are based upon. Implementation of the method requires a high-speed drill which runs above 200,000 rpm to avoid inducing stresses by machining and thereby modifying the existing stresses. The last element is the strain-gauge rosette, which is based on a deflection in different directions. The hole is drilled in the center of the strain gages where the direction of strain provide the amount of stress. A number of a variant different methodology has been developed to extend the hole-drilling method to more considerable depths, like the ring core method.
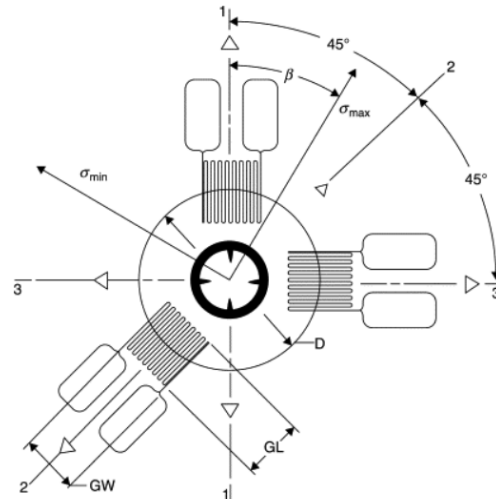
Figure 29: Schematic view illustrating an typical three-element clockwise strain gauge rosette [63]

4.9.7 Sectioning method

Sectioning technique is a destructive method which is based on the deformation due to the release of RS by removal of material from the specimen. The method includes cutting an instrumented plate to release the RS that were present in the cutting line. Due to this, the cutting process should not submit plasticity or heat. The initially RS can be measured without the influence of plasticity effect on the cutting plane's surface. The electrical or mechanical strain gauge is used afterward to measure the released strains after the cutting process.
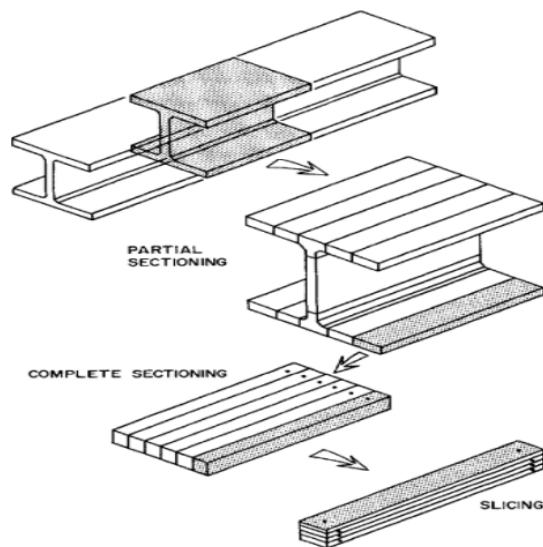
Figure 30: Illustration of the sectioning method [63]

4.9.8 Contour method

Contour is a new technique involves in four steps: cut of the specimen, contour measurement, data reduction, and then stress simulation. The cutting of the sample is a crucial part which is usually done by wire electric discharge machining (EDM) which utilize electrical discharges (sparks) to remove material. The contour measurement is measured on both cut surfaces because the contour of the surface is formed due to the release of the RS. Data reduction is the first step to achieve an average of the measurement to minimize errors in the data, therefore, crucial to get accurate stress evaluation in the contour method. The last step is to perform a finite element modeling and analyze the originally stresses.

4.9.9 Practical experimental method

The practical experiment method is a destructive method, including cutting the specimen from the base plate along the longitudinal direction after welded a thin wall structure with a given height. Due to the relieve of stresses after the cut, deformation of the specimen are measured for further calculation. Thus can the moment be found, which is the force needed to able to bend the specimen in the y-direction (delta-height). The difference in height is the deformation caused by tension or compression of the welding process along the longitudinal direction. Measurement is therefore needed before and after the cut of the weld in the thin wall structure and baseplate to calculate RS. Because this experiment is not a usual method it is dependant on the right measurement of the specimen. Therefore a deviation of the several height-measurement before and after the cut of the weld is crucial to avoid errors. The cut of the welded thin wall structure can be done in several ways, as long two fracture area along the ends of the structure are achieved to place the specimen on for measuring.

4.9.10 Selection of residual stress measurement method

After discussion and evaluation with supervisor Gabor Sziebig and the university-lector Øyvind Sørås, the decision of the measurement method are based on possibilities within resources and time restriction, which has led to the practical experimental method. Because of my further studies would take place in China, at the Beijing Institute of Technology, would possibilities for conduct an ultrasound measurement be possible. Thus are the selection of the residual stress measurement method: Ultrasound and practical experimental method.

5 Experimental lab work

Experimental lab work addresses the design selection of the thin wall structures and the implementation of the welding process. Welding operation involves preparations, parameters settings, and the actual welding process experiment to manufacture the thin wall structure. The produced structure-component lays the groundwork for further experiments as the investigation of residual stresses and deformation is performed in 6. The welding operation is conducted in the laboratory on campus Narvik-UiT.

5.1 Designs of the thin wall structures

The first step by the implementation of the activity robot welding is the design of the thin wall structures. Planning and execution of the welding path are the essential steps of the welding operation. Therefore a conceptual phase is worked out to determine a structure that provides good result during production and within the residual stress test. Six designs were initially sketched where three concepts would be selected by utilizing Nigel Cross Method.

5.1.1 Conceptual phase

The choice of the concepts was decided with the utmost consideration on the weighting of the stated criteria of the student together with supervisor Gabor Sziebig, shown in figure 33. The criteria are judged with a grade from 1-5, how important and usable they are concerning the concept. Each concept is judged from a scale of 1-10 on how well the criteria matches. Determination of the concept and criteria are weighted differently. Thus, resulting in the product with the highest score that reflects the best design of thin wall structure. The conceptual phase-procedure is known as «Weighted Objectives Method» by Nigel Cross, described in steps in the figure below.
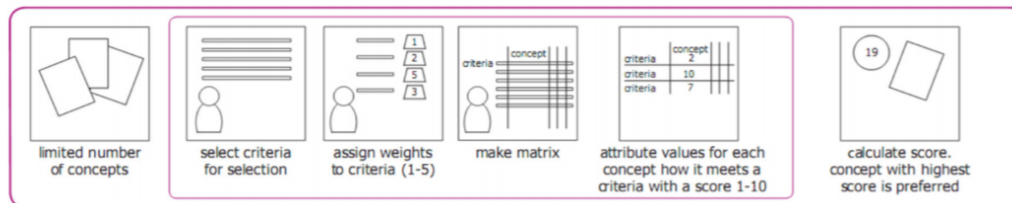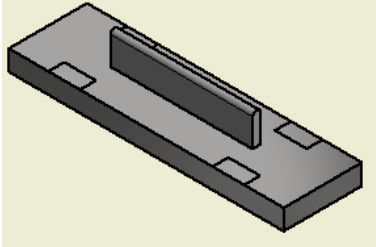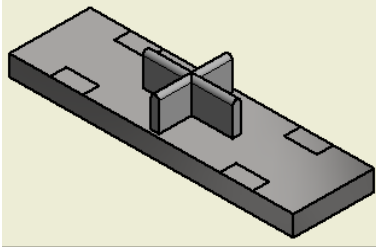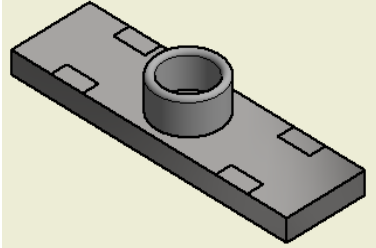
Figure 31: Nigel Cross method "Weighted Objectives Method". Source [64]

Table 11 refers to six different designs of the first created sketches. Each sketch is developed based on these factors: level of difficulties to weld, time and material usage, structure variety to compare RS and deformation result compare to other designs. Practical considerations were taken into account by the evaluation that evaluates the degree of complexity of the height-measurement before and after cut of the TWS. The approach challenge was due to remove the component from the fracture area and then reinstalled at the same spot to be re-measured in a precise way as possible to manage the most accurate measurement.

Sketch of Concept:	Description:
	Sketch of Concept C1 Single stripe: Concept 1 consist of one welding stripe that build layers into a single thin wall structure. C1 structure is easy to weld as with measurement of the height after production and cut of the weldment. Material use during manufacturing is low. The design provides a good visual result of theoretical prediction of distortion and RS. The Single stripe structure has the original dimension of 180x10x40 [mm], during the welding experiment, the length and height will be adjusted to see of it generate the different magnitude of RS. The structure of the single stripe is considered as the original design of a thin wall structure.
	Sketch of Concept C2- 90 degree cross structure: Concept 2 are two single stripe that cross perpendicular where the horizontal stripe are welded along the longitudinal direction and the vertical stripe are welded at the transverse direction of the baseplate. The concept is a degree of complex structure to weld as well as the measurement can be a challenge as it depends on the fracture area after the cut of the structure. Because of stresses behave differently when the structure has an angle, the design can show good and various result from the original single stripe. As the structure covers a large amount of the plate surface, it can cause a higher amount of deformation in the baseplate as well as RS. The cross structure has the original dimension at 110x10x40 [mm] longitudinal direction and 90x10x40 at the transverse direction.
	Sketch of Concept C3- Circular structure: Concept 3 are an circular structure where the weldment path goes 360 degree around. The design is uniquely different from the other concepts, which is challenging to measure as concept C2. The design provides an interesting result as the RS behave differently in this structure. Because the KUKA-robot only can weld straight forward, it makes the design challenging for production. The design has a dimension with an outer diameter at 80 [mm], thickness at 10 [mm] and height 40 [mm].
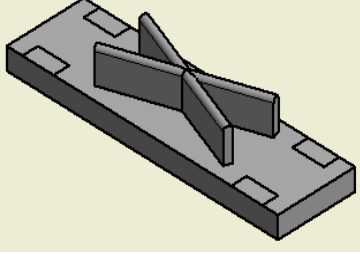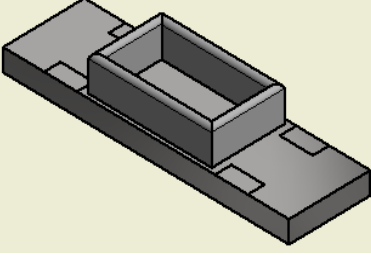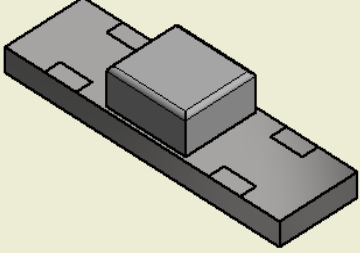
	Sketch of Concept C4- 20 degree cross structure: Concept 4 consist of two single stripe that cross each other at a 20 degree angle along the longitudinal direction of the baseplate. The cross-structure is complex to produce, take the down-cooling and welding sequence into account because the robot needs a change in settings to programmed to weld at a 20 and -20-degree angle. This concept is challenging to measure after cut of the weld but provide good result compared to the single 90-degree cross-structure. Originally dimension of C4 are 180x10x40 [mm].
	Sketch of Concept C5- Hollow Rectangular Structure: Concept 5 are an hallow rectangular structure which has large amount of material and cover large area of the baseplate, which can cause a lot of thermal stresses to the baseplate. The design consist of four single stripes where the dimension along the longitudinal direction are 150x10x40 [mm], and the transverse direction 89x10x40 [mm]. The design is easier to measure compare to the other complex structures as it gives a good comparable result. C5 requires a simple welding process to produce.
	Sketch of Concept C6- Solid Square: Concept 6 are an solid square which require tremendous amount of time and material to produce as well as the area it cover are massive. The design provides a bad result to compare with the other designs as it would generate very high thermal stresses to the baseplate. The dimension of the design is 100x89x40[mm].

Table 11: Sketch of six developed concepts

Table 11 evaluate the concepts according to the weighted objectives method by Nigel Cross's method [64]. The evaluation was determined based on the comment in the table, which reflect the advantages and disadvantages of the design. Together with supervisor Gabor Sziebig, was three concepts estimated as most suitable for GTAW production by the KUKA-30 robot, which provided most comparable results. As shown in table 12 are concept one, two, and four the once with the most significant value based on the given criterion's.

Criteria	Weighting [1-5]	C1	C2	C3	C4	C5	C6
				[1-10]			
Easy to produce	5	5	3	0	3	2	1
Low welding time	4	5	4	3	3	3	1
Amount of material used	4	5	3	3	3	3	1
Comparable result	3	5	4	4	4	2	2
Total		80	55	36	45	40	19

Table 12: Table to test captions and labels

5.1.2   Preparation

Preparations done in the experimental part of the thesis are includes:

- Polishing the surface of the baseplate

- Measuring the welded part and baseplate for the residual stress test

- Cutting off the thin wall structure of the base material

Surface-finish

Before the welding process can start, the baseplate material needs to have a smooth surface to ignite a spark from the arc and achieve a circuit - electricity. Preparation of the material surface is performed by machining, the reason for selecting this method it's due to the glossy surface, and it's effectiveness. The feeding in the milling process was set to 48-65 [mm/sec] for both materials. Depth of the cut depended on the level of oxidation layer in the material, for alloy 304 it was 0,7 [mm] and for X3CrNiMi13-3 0,5 [mm]. Due to the milling cutter's diameter at 160 [mm] and the revolution per minute was set to 380, it generated the spindle speed at 191 [m/min]. The formula for spindle speed used:

$$v = \frac{pi * n * D}{1000} \tag{11}$$

Measurement for the residual test

 When the surface are polished with miller cutter, measuring are then done to establish data for the residual stress test. Measuring method used are with a instrument called "altimeter", which is e precise measuring tool that has an accuracy of 0,01 [mm]. All measurement are preceded from the top of a measuring stone, the stone has a quality of accuracy in height, length and with and are perpendicular to the table. All heights are measured from the surface at the measuring-stone to the top of the surface at the baseplate and thin wall structure. The

measurement are done according to the measuring tape where checkpoints are marked at a given length and measurement at these point are repeated for increasing the accuracy of the measured value.

Figure 32: Measuring device - altimeter. Source: Picture from experiment

Cutting method

Regarding the RS-test by calculation of deformation, the measurement is achieved by measure before and after cut of the TWS. The cut of the structure needs to be precise and possible to provide a fracture area at two points at the sample to reassemble the component for measuring. During the cutting process, the material and welded part can't be compromised as this effect the result of the residual stress test at a high degree. By troubleshooting the problem together with several professors/lectures, four methods were introduced:

- **EmD- electrical discharge machining process** - A method that utilizes charged particles to cut the material. The method provides an exact cut which doesn't have direct contact with the sample during the process. Few companies in Norway had this equipment for disposal, and the distance to these companies was far.

- **Water jet cutting** - The method utilizes high pressure of water jet to cut through a material. This technique was possible to perform in Ballangen. However, the technique had difficulties in cutting a component from a baseplate when the baseplate was bent due to the shrinkage of the weldment.

- **Grinding**- Grinding method use a cutting disk to cut the TWS of the baseplate manually. Problem with this method causes heat problem and can be inaccurate if done by a student.

- **Industrial saw** - A method utilize an industrial saw which generally is used to cut metal plates and large parts. The saw is inaccurate, and the TWS attached to the baseplate doesn't fit in the saw.

- **Milling** - A method that utilizes milling by a cutting edge to cut the thin wall structure. The challenge by this method is the same as the water jet cutting, which included that if the base plate was bent due to the thermal stresses of the weld, it could damage the cutting edge if the stresses would release after the cut and bend the baseplate into the cutting disk during the cutting process. This method could be done at Narvik Campus.

Due to the thin wall structure could hold some internal stresses it could cause deformation of the TWS and baseplate during the cut of the weld. A mobile and flexible method is therefore needed which also could provide a fracture area at the wanted location. Because of those challenges, the grinding process was chosen and performed by an experienced professor, the cutting was executed between the TWS and the top of the baseplate. The structure component was cut along the middle where two small areas at each side of the component were attached to the baseplate, then hammered off the baseplate with a plastic hammer. This provided two areas located at each side that offered the possibility to reconstruct the placement of the thin wall structure on the baseplate for measuring. See attachment for photo's of the fracture area after cut by the grinder.
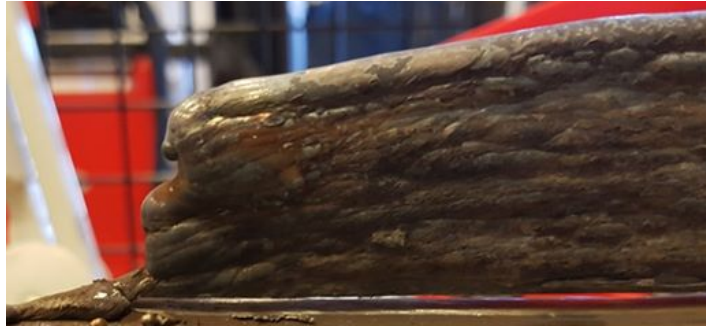
Figure 33: TWS cut from the baseplate and reassembled at the fracture area. Source: Picture from welding experiment

5.1.3 Welding preparation

Before the welding operation could start, several checkpoints needed to be monitored to prevent complication and errors during the welding. The welding preparation checkpoints:

- Measurement of the tungsten electrode, where the point of the electrode should have a distance of 10 [mm] from the shielding cup. Additional should the tungsten possess a pointy end, if not it should be grinded.

- Welding path and angle are set to correct value

- Powersource turned on or should not show any form of error on the display

- Gas flow open and a gas-flow-check should be done before welding

- Air ventilation is turned on

- Polish of the surface on both side if needed

5.2   Welding Experiment - Robot welding by KUKA-30

The first part of the experimental activity is the GTAW by the KUKA-30 robot which was conducted in the machine-lab in Narvik Campus. Based by chapter 4.8 the experimental process was implemented according to the experimental setup illustrated in figure 18 and executed by the practical procedure developed in figure 20. During the welding process, different parameters and designs were utilized to impact the residual stress in the thin wall structures. In this section, parameters and welding operation are addressed, where the WPQR (welding procedure qualification record) are documented in the attachment J.
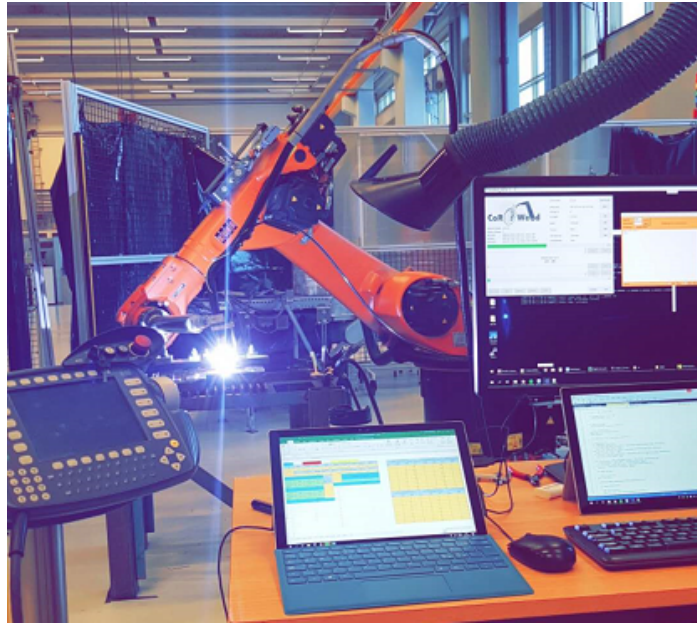
Figure 34: Welding experiment in campus Narvik UiT

5.2.1   Welding operation by KUKA-30

Before welding preparation is done as the robots power source are turned on, the gas flask is opened, and the coordinate system is set for the workpiece. Afterward, welding plan is sett by the KUKA-controller, and the parameters and coordinates are implemented in the welding files. The welding instructions includes four steps:

- Setting coordinate system

- Selection of welding plan

- Monitor the welding preparation

- Define parameters, path, and angle for the welding operation

5.2.1.1   Setting Coordinate System

Before welding at a new baseplate, a new coordinate system for that particular substrate is adjusted accordingly. The new origin of the coordinate system is only set once before the

substrate is fixed to the welding table. X and Y coordinate can be set as wished as long as Z coordinate is set originally at the surface of the baseplate. For this study the coordinate system is set at the point in the lower left corner a5t the workpiece where the axes are positioned in the directions: X-axes along the longitudinal direction, Y-axes transverse and the Z-axes from the surface of the baseplate, illustrated in the figure below:
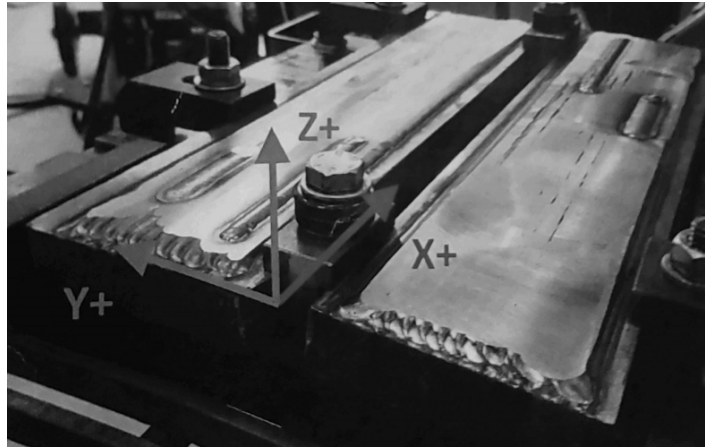
Figure 35: Coordinate system of the workpiece/baseplate. Source [65]

For a new coordinate system to be set in the lower corner of the baseplate, a procedure in the KUKA-controller need to be executed [65]. The procedure for setting the coordinate system at the new workpiece:

1. Set the controller in teach pendant mode

2. Navigate to Setup and select ¿ Measure ¿ Base ¿ 3 point, to select the direction of the axes.

3. Select base number 2 (flat plates)

4. Set measuring tool to 1 (welding torch)

5. Set two point along X and Y-direction to select the axes manually with the controller (see figure 47)

Figure 36: Picture of the welding process

Video of the welding process see appendix 20, video number 19.

5.2.1.2 Selection of welding plan

The welding plan is the file where all information about the welding operation is documented. Before the welding operation is initiated the welding-file needs to be updated (see **??**) and uploaded to the KUKA-central/controller to be able to weld the TWS. In order to make the robot execute the welding plan, a program named "Coroweld" needs to be activated. For activating this program, some setting needs to be selected to program the welding operation of the KUKA-robot:

1. Configures the file by a Submit-Interpret (setting interrupt and change the default file with the subfile coroweld).

2. Run Serial Coroweld file ¿ run Coroweld. manual (coroweld.manual file call on Coroweld RSI file which drives everything in the same file)

NOTES: A submit interrupter is a file that runs independently from other running programs when corowel program are active, it runs parallel with the submit interrupter. RSI (Robot Senter Interface) is an addon to the KUKA-controller which is used to control the robot in real time.

5.2.1.3   Monitor the welding preparation

Control every checkpoint to avoid errors and welding failure. During this part, should all practical instrument be checked and the tungsten-electrode is to be measured before the process can start.

5.2.1.4   Define parameters,path and angle for the welding operation

The welding documentation concerning parameters, coordinates(path), and the robot-angle are saved in a file named "welding_plan .xml". The xml-file is implemented in a program called "Coroweld manual.src" which is the actual program that runs the operation. Initially, the parameters, angle, and welding coordinates are selected in the welding file to establish the values of the welding operation, shown in figure 37 below. The figure shows a clipboard of the welding plan-file of TWS-concept nr.four. First, it states the welding path by establishing a start point in x,y,z-coordinate and then it states the endpoint by a new x,y,z-coordinate, which means the welding path only weld in a linear direction. A ,B and C are the angles around the axes, which in this case are selected to tilt the torch in an angle of 10 degrees. The chosen parameters for this operation are selected to:

- avhc = 2.4 [mm]

- Welding speed = 2.2 [mm/sec]

- Current = 220V

- Wire feeding rate = 1 [mm/sec]

```xml
<weld_plan>
    <header>
        <experimenter>Hans Ivar Arumairasa</experimenter>
        <place>Narvik</place>
        <date>21.01.2019.</date>
        <time>13:00:00.000</time>
        <scan_speed>5</scan_speed>
        <scan_distance>100</scan_distance>
        <workpiece_id>140</workpiece_id>
        <initial_torch_height>2.4</initial_torch_height>
    </header>
    <root_pass>
        <start_point>
            <x>230</x>
            <y>78</y>
            <z>0</z>
            <a>0</a>
            <b>-10</b>
            <c>0</c></pass>
        </end_point>
            <x>389.354</x>
            <y>20</y>
            <z>0</z>
            <a>0</a>
            <b>-10</b>
            <c>0</c>
        <end_point>
        </start_point>
        <pass>
            <y>0.000000</y>
            <z>0</z>
            <a>0</a>
            <b>0</b>
            <c>0</c>
            <weld_job>0</weld_job>
            <avhc_reference>2.400000</avhc_reference>
            <speed>2.200000</speed>
            <current>220</current>
            <wire_feed_rate>1.0000</wire_feed_rate>
            <correction_limit>2</correction_limit>
            <is_used_for_scanning>0</is_used_for_scanning>
```

Figure 37: Welding plan for concept four. Source: welding experiment

When the welding plan is updated in the coroweld file, the teach-pendant mode in the KUKA-controller is changed to automatic mode. Further instructions are then the procedure which takes place after the coroweld file are set:

1. Restart the light curtains and turn on the robot motors

2. Set the robot to home-position (communication are then established)

3. Set robot to measuring (robot travel down to the start position at the workpiece)

4. Start welding

5.3   Welding Parameters

5.3.1   Main Parameters

In the welding operation there are used different set of parameters during the welding process to generate different outcome. The basic parameters which are chosen based on experience of test and fails are [66]:

- avhc - height of the tungsten electrode tip to the baseplate in [mm]

- Welding speed - the speed of the torch along the welding path in [mm/sec]

- Current - flow of the electrical charge, unit in ampere [A]

- Voltage - potential different in charge between two point in the electrical field, unit in volt [V]

- Wire feeding rate - amount of material fed into the welding pool, unit in [mm/sec]

The effect each parameter causes is based upon the research notes from Tania Kerezovic November 2016 which additional support the result in A.

- Voltage: Increase of the voltage [V] wider the with of the weld as the welding pool. It has no direct influence of the penetration of the torch.

- Current: Increase of the current [A] further increase the penetration and with of the weld. Additional higher amount of current influence the weld to be wider and flatter.

- Welding and wire feed - speed: These parameters alone does not influence the appearance of the weld. It is rather the ratio of these which causes effect, example: speed of the torch need to be low enough to allow current to melt the wire which is fed in the melting pool.

- Preheating: If the starting temperature is to low in the material, the deposition of the wire will be decreased. The heat generated uses it's energy to warm up the material first rather than melting the melting pool. It is additional crucial for reducing residual stresses by heating the material to a high temperature before welding as it is the gradually cool it down.

5.3.2   Other Parameters

Along with these five main parameters, is it additionally elaborated other minor-parameters which is based on the outcome of the main parameters. The calculation of those minor parameters are based at Tania's research which is calculated in the WPQR. The equation the each minor-parameters:

$$Deposition rate[D_r] = \frac{13,1 * d^2 * (f * 0,0394) * \eta * 0,4536 * 10}{36} \tag{12}$$

Deposition rate = [g/s],
d = filler wire diameter [mm],
eta = efficiency factor,
f = wire feed [mm/min]

$$\frac{f}{v} = \frac{v_1}{v} \qquad (13) \qquad\qquad \frac{D_r}{v} = [g/mm] \qquad (14)$$

f / v = ratio between wire feeding and welding speed [mm size/mm mat]
v = welding speed [mm/sec]

$$\frac{Q}{D_r} = \frac{kJs}{gmm} \qquad (15) \qquad\qquad \frac{(D_r/v)}{Q} = \frac{g}{kJ} \qquad (16)$$

Q = heat input

$$L = \frac{(l/v)}{f/60} \qquad (17) \qquad\qquad Lm = ((\frac{d}{2}) * (\frac{d}{2}) * 3.14) * L \qquad (18)$$

L = [mm] of wire used
l = lenght of weld
f = wire feed [mm/min]
v = welding speed [mm/sec]
Lm = Volume of wire used [mm$\hat{3}$]

$$\frac{f}{A_v} = (\frac{(f/60)}{v * I}) \qquad (19) \qquad\qquad Lm = ((\frac{d}{2}) * (\frac{d}{2}) * 3.14) * L \qquad (20)$$

f/Av = [mmz/A*mm]
I = current
v = welding speed [mm/sec]

$$FeedHeat = \frac{(0,036 * V * I)}{f} \qquad (21) \qquad\qquad \frac{FeedHeat}{Q} \qquad (22)$$

Feed Heat = [kJ/mmz] V = Voltage [V]
I = Current [A]

5.4   Sources of errors

Welding process by the KUKA-30 robot involved certain errors which occurred due to unknown reasons. The sources of errors delayed continuous progression and compromised the result of the work. The common failures were detected to appear from these sources:

- Tungsten electrode crashes into the surface of the weld, where it normally should stop 2,8 [mm] above the surface. It caused the power source to stop the current flow through the electrode and create an error called "no ignite."

- Wire feeder rate suddenly spat out a tremendous load of material during welding which created half finished welds with parts of wires along the weld.

- Second computer-screen where the program "Double Commander" is initiated and measured sometimes froze and didn't function as it should.

- Spark ignites during welding, creates spots of metal around the welding area.

- System fails

Corrections of those fails were not always the right solution but had in most cases worked. Potentially fix are therefore suggested by troubleshooting the problems based on test and fails - experience.

Tungsten electrode crash

The offset of the tungsten electrode was set to a distance of 50 [mm] from the surface, which caused failure for the robot to measure because the range distance was too long. An adjustment was therefore made to reduce the offset distance to 20 [mm], as the TWS-height increased the distance from tungsten to surface was also increased. Additionally, the tungsten-electrode needed to be sharpened and polished and re-installed, so the tip was 10 [mm] beneath of the ceramic cup at the tool. During welding, the electrode melted several times, and therefore decreased the tip of the tungsten. Which resulted in a non-contact with the electrical-circuit and errors occurred. A solution of the tungsten offset range was to monitor the distance before and after every welding operation. Furthermore, the filler was adjusted several times, which was the leading cause of the problem because the filler was to close to the tungsten and had the wrong setup-height. The filler adjustment was not completely fixed before after several components already were made.

Figure 38: Tungsten electrode crash in sample P2D2. Source: Picture from the welding experiment

During sample P5D1, the right height and angle of the filler-output were discovered and adjusted. As shown in sample P2D2, P1D2, and P4D1, the welded structure had a lot of errors where this adjustment was wrongly placed. Last and final solution was to machine both sides of the plate to secure the circuit-electricity were led through the system. Example of this: P4D2 lost connection after 17 layers, which resulted that the robot could not find a connection to the surface and therefore crashed into the weld-surface. The reason it occurred on the 17-layer, was due to the bending of the material which caused the smooth surface underneath the substrate to avoid the welding table which broke the electric contact. Additional the substrate was not machined at both side, the oxidized spots underneath the plate caused a non-contact surface which would not lead electricity through. Taken those factors into consideration system could then measure it's avhc more precise and enter 2,8-2,4 [mm] near the surface without direct contact.

Feed wire error

At some situations, the wire feeder suddenly fed a considerable amount of material that resulted in a compromised weld, which caused damage from the heat source. The wire feeder also missed the melting pool or went through it with a rapid speed. Reasons for this could be due to the cobber- end-piece of the wire-feeder, which aimed at the surface instead of under the melting pool. Causing the direction of the wire would change to the side of the TWS. The result of this involved the wire didn't melt along the suggested welding path, instead, it created a half melted welding-string which compromised the quality of the weld. The situation often occurs when the surface was uneven and in highly angled terrain where the wire had a problem to interact directly to the welting pool. When the wire went rapidly through the melting pool without melting, it damaged the surface with the heat input. Worse case it decreased the height of the thin wall structure. The suggested fix was to adjust the end-piece height and angle towards the melting pool, which gave perfect result when the right adjustment was set.
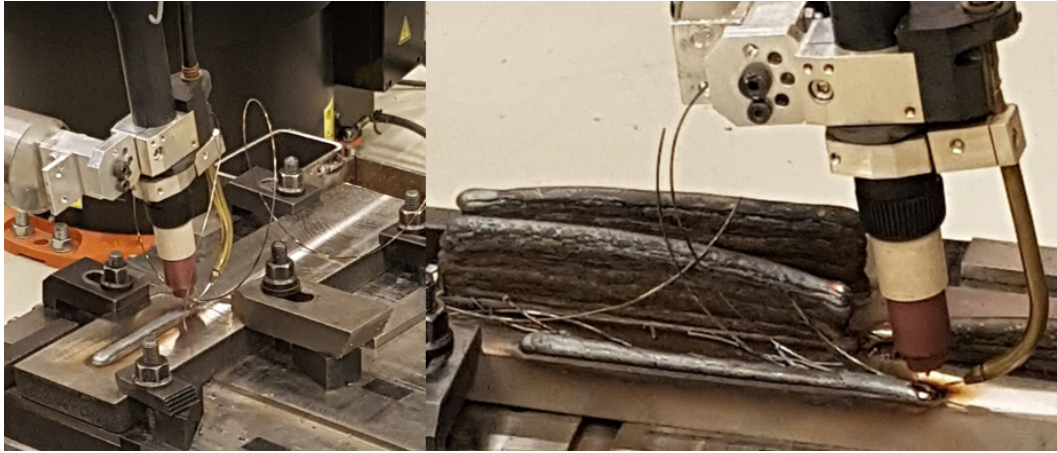
Figure 39: Two cases of wire feed error. Source: Picture from the welding experiment

Sparks and melting spots

The spark ignites during welding could occur from dirty surface or to high heat input, for that reason polishing of the surface was done to provide better contact with the electrode and to prevent it. The high current generated from the first set of parameter resulted in sparks. Parameters with lower current indicated lesser sparks and melting spots. The factor avhc (distance from tungsten to surface) appeared to be too close to the surface, which could be a potential reason for sparks and melting of the electrode. Direct contact can cause a short circuit and stop the welding process instantly. Additionally, when the filler metal caused direct contact to the electrode it generated sparks and melted material at the tungsten. This compromised the quality of the weld and the process.

System error and frozen screens

The frozen screen could easily be handled by unplugging the contact to the screen. The system seemed to stop failing with these corrections, wherein worse cases rebooting of the system was needed. Observations of the welding result illustrated welding with: less current, wire feeding and lower "avhc", fewer errors occurred that resulted in fewer system errors and frozen screen.

Tungsten electrode and wire feeder settings

Additional to uneven surface, the leading causes of tungsten crash and wire feeder errors appeared from compensation between the components. Tungsten electrode and wire feeder were initially installed so the wire feeder would enter the welding pool at the right angle and height. The reason why the tungsten adjustment needed to stick out 10 [mm] outside the shielded cup is to relate to the settings in the welding program.

It bases its parameters (avhc and voltage) on the physical equipment on the robot. If the tungsten melts and decreases in length, would the system try to compensate and generate

higher heat input, which compromises the welded product. If the equipment at robot were not right adjusted would the wire feeder miss the melting pool and lay a layer partially on the sides of the existing layer, causing compromises at the structure. Additionally, the copper-end of the wire feeder would bend if the wire is fed directly into the TWS. Because the wire would keep running even if it didn't enter the melting pool or if it got stuck.

Therefore was figure 42 used visually to re-construct the copper-holder of the wire feeder to the right position, angle, and height when it was bent and change position.
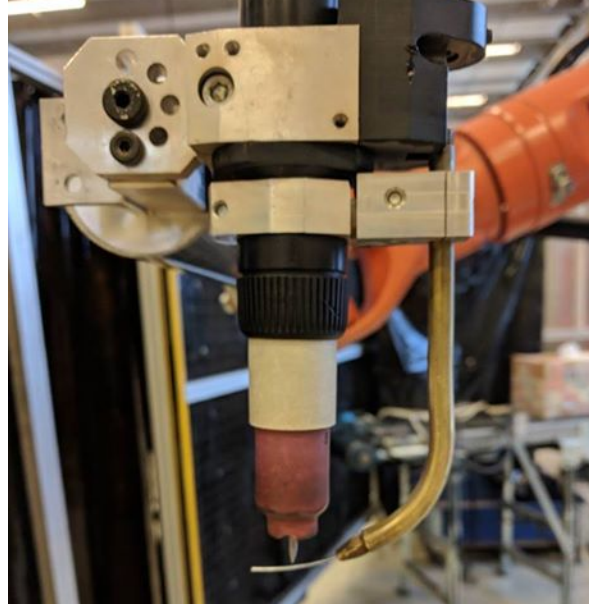
Figure 40: Two cases of wire feed error. Source: Picture from the welding experiment

5.5   Horizontal and vertical direction of the TWS and BP

During this study is the expression as horizontal and vertical direction mentioned, the meaning of those concepts are illustrated by the figure below. The red line illustrates the horizontal direction while the yellow arrow shows the vertical.
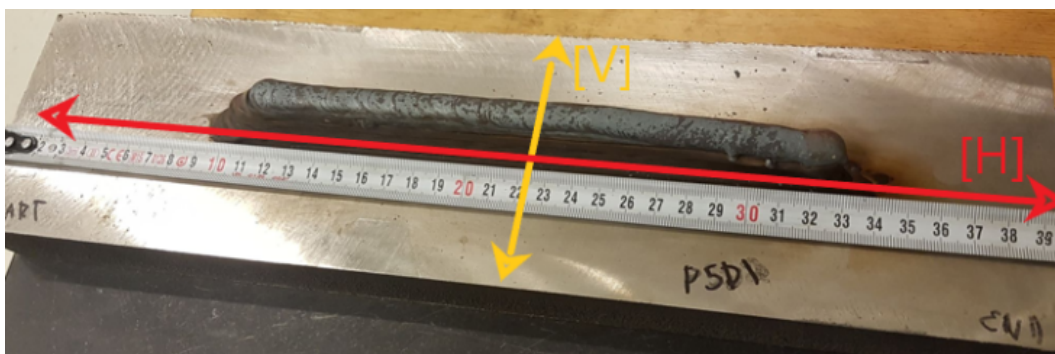
Figure 41: Horizontal and vertical direction

5.6   Positioning the experiment setup with Visual Component (VP)

The experimental setup was initially set up at original position as illustrated in figure 41. Due to the intricate design of 90°and 20°angle cross structures, was the joint at the robot needed to rotate in an un-adjustable angle. In other words could the robot not adjust its joints to position the to-center-point with a 10-degree decline angle at selected coordinates. The main reason why it couldn't is that the robot already by default settings was adjusted in a twisted angle by the joints. Therefore was Visual Component utilized with a digital twin tool to plan the robot's position during welding visually. It was also tested to program the robot to travel through the welding plan-coordinates without activating the torch of the weld, to visually see if the joints and equipment at the robot were compromised.
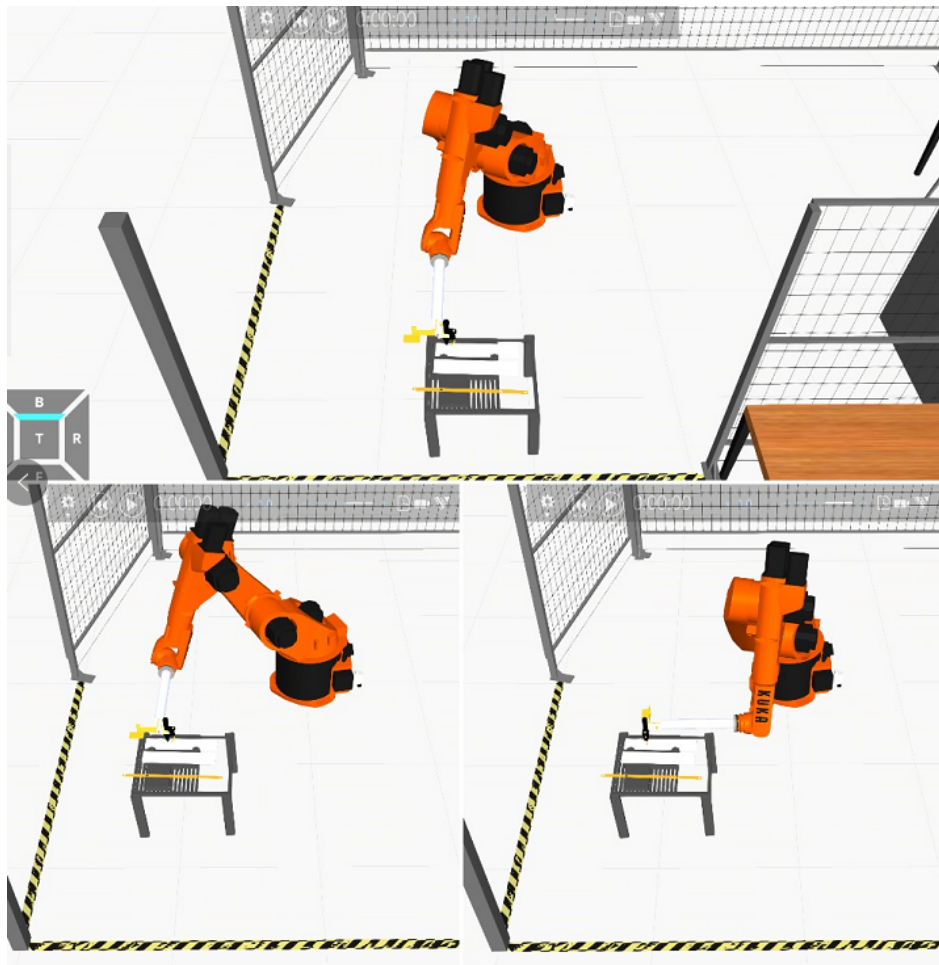
Figure 42: Positioning the welding table with VP. Source: Master thesis "Digital twin simulation with Visual Components" by Halldor Arnarson

6   Practical Experiment - Residual Stress Test

Residual stress test in this study contains two practical experiment methods; ultrasound measurement and calculation based on the measured deformation along the TWS. The practical RS tests are in purpose to give an informative comparison together with the FEM simulation analyzes for investigating the level of disposable the TWS and substrate are after manufactured.

6.1   Ultrasonic residual stress test

Ultrasound measurement was conducted at the laboratory in BiT (Beijing Institute of Technology). The experimental test consisted of an oscillation device developed by the university to give a direct value of the residual stresses. The basic principle of the method is measurement between a reference plate and the welded structure, which is inflicted by RS. The reference material is a raw piece of the wanted material which has a zero-level of RS stresses. The measured RS in the welded TWS is dependant on the changes of signals compare to the reference plate.

6.1.1   Assumption

Initially, the step of the method was to perform a uniaxial tensile test of the reference material to determine the acoustoelastic constant before the actual ultrasound measuring could take place. Because the experiment took place in Beijing-China, the welded component needed to be sent from UiT-Norway, in this case, was the reference block/plate to short to be placed in the tensile-bench. The reference block needed a length of minimum 180-200 [mm] to attach the transducer in the middle to detect the tensile data as the clamps needed a specific area at the end of the brick. The assumption made is a simplified measurement without the uniaxial tensile test, and are alternately performed by the procedure in 6.1.3.

6.1.2   Ultrasound measurement basic principles

The basic principle is based on an original measurement technique which was initially planned to perform, due to the assumption of neglecting the acoustoelastic constant. It was therefore conducted a test of the technique to investigate if it would generate acceptable data. The first step was the preparing of the equipment, which was set up of the oscillation device and selection of the right transducer. A Low frequency provides a deep measurement of the dept, and a high frequency provided a low signal measurement. A normal contact transducer was chosen with a high frequency at 5 MHz to send the signals through the test block, see figure 43 below:
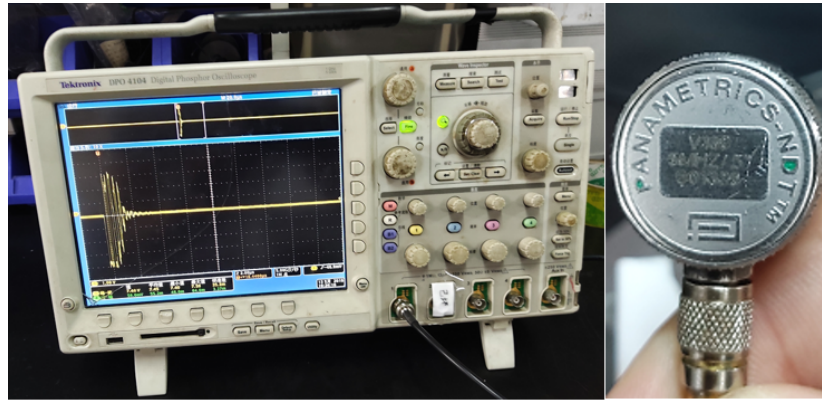
Figure 43: Oscilloscope device at the left side of the picture and transducer at the right side.

A gel was greased between the transducer and material to enhance to signal. The wave was sent out by the transducer and then reflected at the end of the scanned material before received at another or same sensor (depends on the type of transducer). The time it takes for the signal to travel through the block and be received at the end are known as [μs], which are represented at the display of the oscilloscope. When a certain amount of point were measured, an average value was calculated which describe a general value of [μs] for the whole sample. Then the speed is calculated based on the measured thickness of the block, shown below:

$$v = \frac{2 * thickness}{\mu s} \tag{23}$$

Furthermore can the calculation the residual stresses be determine by many ways, an general aspect due to of RS is provided in these formulas:

$$\sigma = E * \epsilon \tag{24}$$

$$\sqrt{\frac{E}{\rho}} --> E = \frac{v}{\rho} \tag{25}$$

$$\sigma = \frac{v * \epsilon}{\rho} \tag{26}$$

6.1.3   Ultrasound measurement procedure

The actual test of ultrasound measurement was performed accordingly to the basic principle. The difference with this technique was the usage of a developed device and software programmed by BiT. The device equal to the oscilloscope presented the signals oscillation and travel speed. However, additional it calculated the residual stresses of that particular signal. Values of RS were then found at different points along the length of the TWS. In additional was the initially transducers changes out with a new signal-sender/cable to be attached to a 45°angle holder. Type of series used in this ultrasound are the accuscan "S".The developed device would then take the angle of calculation into account, see picture beneath:
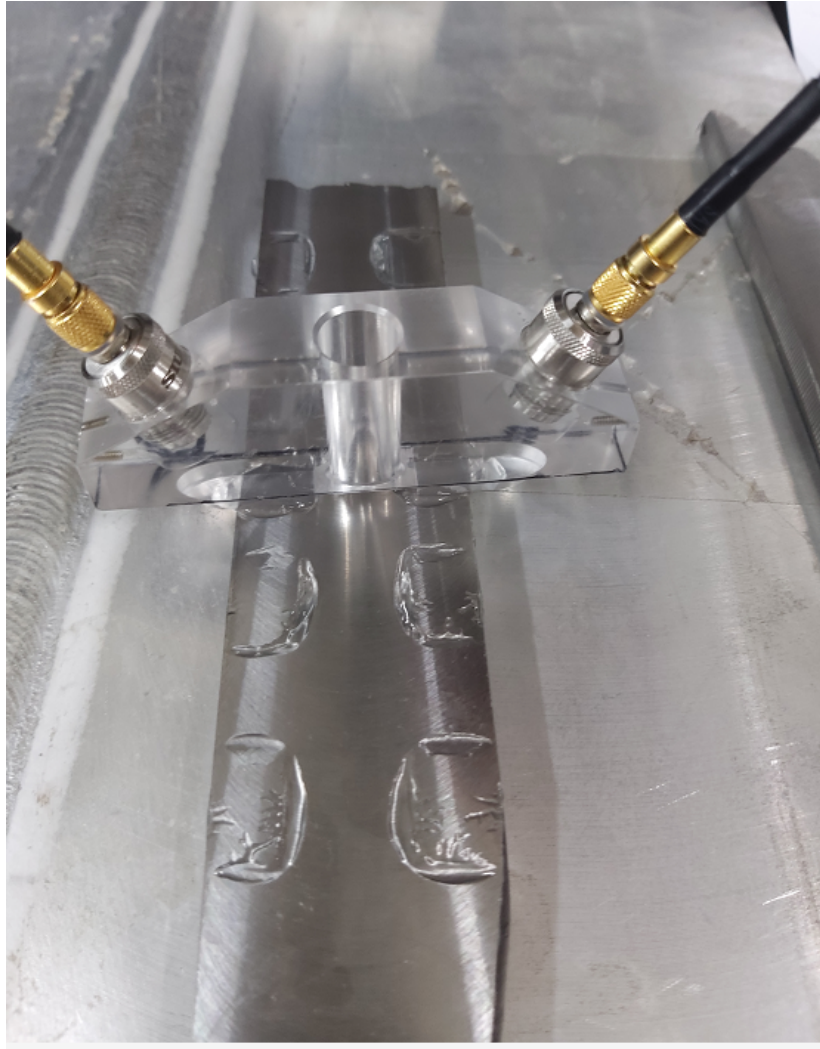
Figure 44: Scanning the welded part by an 45°angle sensor

The device developed by BiT calculated the RS based on a stress factor that depends on the material. During the experiment, the factor for standard stainless steel was used, with a given value at 9,6. This means the values could be rather higher then the actual RS value, if the factor would be changed to one would the result been 9,6 less. Sensor type used is 5M6NT.
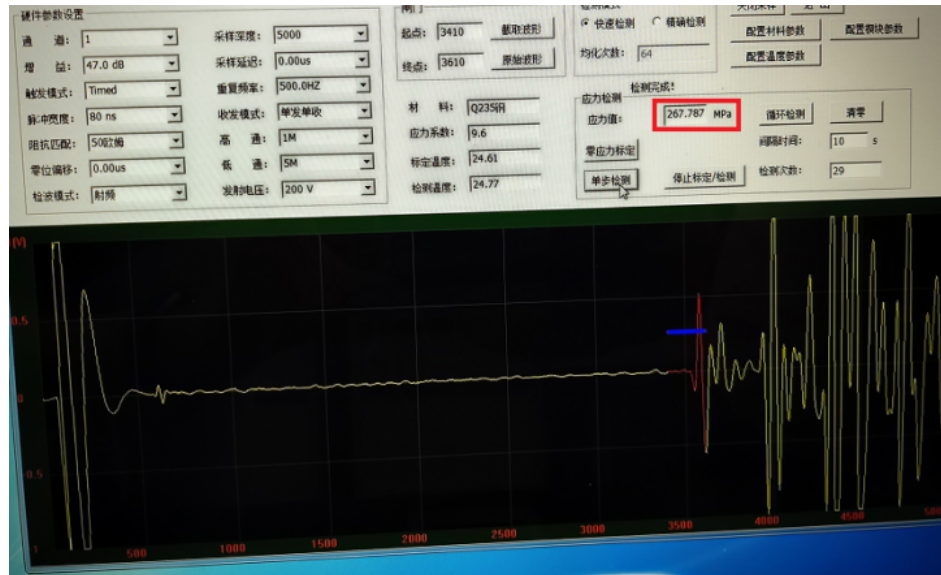
Figure 45: Display from the developed ultrasound device at BiT

Figure 45 shows the screen of the ultrasound measuring device, red marking at the picture illustrates the RS value of the measured sample. The picture below shows the reference block used.

Figure 46: Reference block of the ultrasound test

6.2   Experimental Part 2 - Practical residual stress test

During the experimental part-one, was the TWS accomplished at two different base plate materials. In this process, the heat which extended the material followed cooling which caused shrinkage in the baseplate was due to the heat from the torch, The theoretical assumption is that the component still maintained residual stresses after the weld because of the bent baseplate due to thermal stresses. The stresses could be overloaded to plastic deformation, which makes the distortion permanent. The practical approach involves to cut the welded thin wall structure (TWS) off the baseplate (BP), this would, in theory, made the baseplate and TWS to try to bend back to original deformation because internal stresses would be released. Thus are measurement performed before and after the cut of the welded structure the measure the height of displacement. These data would further be used to calculate residual stresses based on Euler Bernoulli beam theory.

6.2.1   Measuring of TWS and BP

After the preparation, the welded plan documented and updated the measuring (KUKA-robot locate the start position for welding) could take place before the welding operation initiated. The baseplate was fixed at the measuring table, which included a perpendicular table to the floor. An altimeter is then used to measure the baseplate -height with nine measuring points before, after divided the TWS from the substrate. It was performed three measurements. The average data are then used to further calculation. This is achieved to measure the deflection of the TWS and BP from origin state to the new height. The TWS is measured along the longitudinal direction (x-axes) because the stresses are calculated only along the length of the weld. BP is also measured along the longitudinal direction for P1D1, P2D1, P3D1, and P3D1, since the single-string design creates mostly thermal stresses along the longitudinal direction of the BP. However, for the other models which are welded on 90-degree and at 20-degree additional to the single-string weld cover a larger area of the baseplate. Thus are the transverse direction measured at the BP to investigate distortion around x-axes of the plate. The measuring method is done according to 5.1.2.

The height measurement of TWS and BP are shown in appendix B. Sample P5D1, P4D2, and P6D3 are the only samples that were measured before weldment. Each sample that is made by the welding process include a set of parameters [P] and a chosen design [D], for example, P1D1, which means the welded structure with the design number one (concept one) are produced with parameters set one. The welded structures have been measured before the cut of the weld between one-two times. This does not include samples P5D1, P4D1, and P6D3, which have been measured three times. Measurement before the cut of weld has been measured between one-two times among all the samples without P5D1, P4D1, and P6D3, which have been measured three times. Samples which have been measured only one-two times could potential provide failure during the measurement and therefore compromise the result of the residual test method. Because of this, assumptions have been taken into account, see **??**. Thus this method does not generate 100 % accurate answers but instead provide an estimation of the residual stresses.
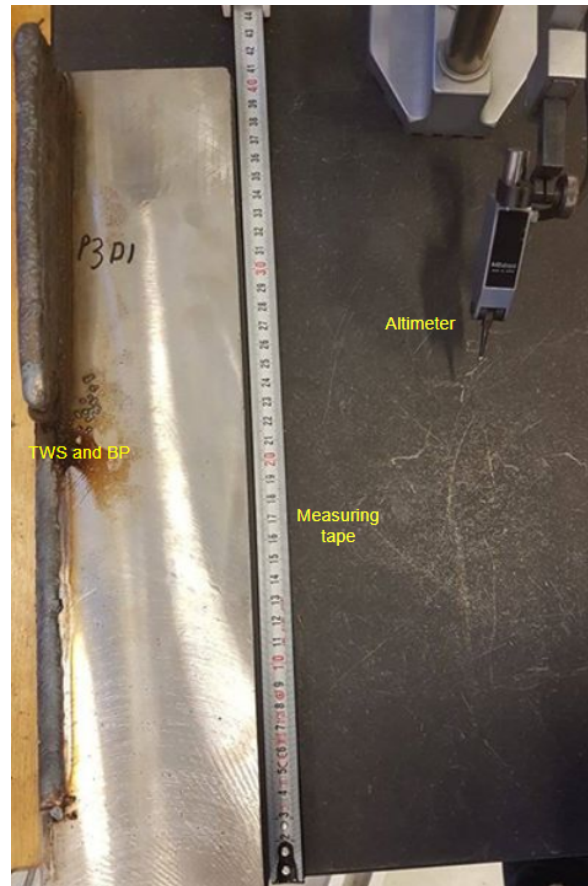
Figure 47: Coordinate system of the workpiece/baseplate. Source [65]

6.2.2 Calculations of the residual stresses

Calculation of the residual stresses in the TWS-component and baseplate are accomplished according to the given assumptions. The thin wall structure is considered as a beam, where Euler-Bernoulli beam theory are used to the purpose of calculating the residual stresses. Due to this theory are a mathematical expression used which are further based on the height measurement from the welded structures (before and after cut of the TWS).

6.2.2.1 Assumptions

During this experiment, the method is assumed to consider the TWS as a beam, because the structure's geometry length has a rectangular area section. Cited from [67] it defines a beam as: "a structure having one of its dimensions much larger than the other two. The axis of the beam is defined along that longer dimension and a cross section normal to this axis is assumed to vary along the span or length of the beam smoothly". The beam is further assumed to be bend underneath the weight of the shrinkage of the thermal stresses by the torch of the GTAW, therefore are the calculation based on pure bending moment due to this. The calculation is performed in excel where the measurement data also are documented. The calculation is simplified based on an assumption of constant tension/compression along the

TWS, because of the high difference in the height of the neutral axis, which compromises the result, see 6.2.2.3.

6.2.2.2 Euler Bernoulli Beam Theory

Euler-Bernoulli beam theory is represented by the formula beneath. The equation describes the relationship between the deflection of the beam and the load applied to cause the deformation. [68] gives the equation for calculating:

$$w = \frac{d^2}{dx^2} * (E * I * \frac{d^2w}{dx^2})$$ (27)

W(x) in this equation represent the deflection of the beam in z-direction, along the x-axis (illustrated in figure 48). Thus q is the distributed load, in other words, force per unit length or pressure being applied to a force per area, it may be a function of x,w, or other variables. I is the section moment area, and E is the elastic modulus which takes stiffness and the design into consideration because this equation is familiar with the classic beam theory, which again is a simplification of the linear theory of elasticity. The equation limits to the small deflection of a beam that is subjected to lateral loads only [68].
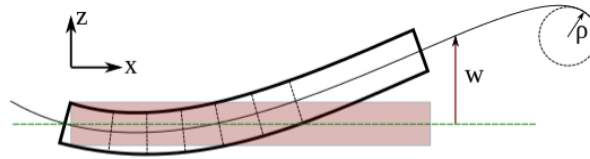
Figure 48: Slope of the neutron axis and deformation (w). Source [69]

Even TWS is considered as a beam, does it not matches the ordinary beam theories as to the situation of fixed end or support along the beam. The displacement which occurs in the beam does not only happens in one or two points but along the whole beam. The ends of the TWS are not supported or have zero displacements as a normal beam calculation. Thus it includes a rigid body movement, which means the beam deforms also rotates. Therefore are the Euler-Bernoulli beam theory used; it is based on the slope (p) of the neutral axis, as illustrated in figure 48. The neutral axis is the axis, which is, in this case, are the half of the height in the TWS when external forces bend the slope of the neutral-axis, it develops a deformation(x) in the z-direction. For a symmetrical beam cross-section about a plane perpendicular to the neutron plane, calculation of the tensile stresses which occurs in the beam including bending moment which causes it may be expressed by:

$$\sigma = -z * E * (\frac{d^2 * w}{dx^2})$$ (28) $$\qquad M = -E * I * (\frac{d^2 * w}{dx^2})$$ (29)

The beam equation is not only capable of calculating deflection, but it can also describe the moment and forces that are interacting with the beam, which allow the possibility to find internal stresses. By utilizing the equations within this theory, it is then possible to know the

residual stresses and deflection of the beams that are under a bending moment. This applies to all beams which are under a small degree of deformation. Even shearing forces stresses are significant, bending moment stresses provides a greater overall impact on the beam in terms of stress concentration. Although the beam is under an effect of forces, the majority of stresses in the beam is located under the surface .
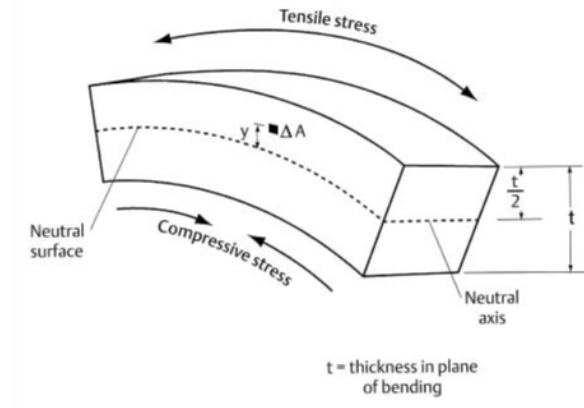
Figure 49: Illustration of cross section at a beam during bending and the location of the neutral axis. Source [69]

6.2.2.3   Calculations

Calculation of the residual stresses is based on the measurement data in appendix B. Before calculation of RS, a new measurement are calculated which is the product of the component/baseplate height divided on two, named z. Then delta-h is then calculated to know the difference in height in a specific point along the x-axis. Delta-height is the product of:

$$h_d = (aftercut - beforecut) \tag{30}$$

Calculation of the residual stresses after measuring includes gathering data to create a graph that describes the deflection (w) and the curvature (w") of the neutral axis of the component. Curvature is the double deviate of the w-graph, or described by p = (1/radius), it tells how strong the bending is in the given point. If w-graph is constant does it means the beam moves up or down like a stiff body, which generates no form of moment/stresses. But if w-graph is linear, it means the beam rotating as a stiff body and again cause no moment/stresses. Before considering the stresses which occur by the deformation into account, a describable slope of the neutral section is required, in other words, a polynomial is needed to describe the slop to generate moment/stresses in the beam. In the case of this study, are the necessary calculation regarded the RS is dependant on three factors: how much the beam is bent (in other words w"), the height of the neutral axis (z) and the elasticity modulus (E) of the material.

Calculation of TWS-component P1D1 is an example to illustrate the calculation method, which utilized at all the samples. Because of the significant difference in the values of the

heights longitudinal to the neutral axis, it generates stresses upon thousands of MPa. There-fore are the calculation simplified to utilize polynomial - second-degree function where only the best-fitted data of the sufficient welding length taken into account. Because the method only can provide a desirable result if there is a small deflection along the x-axis. Best fitting data used are the heights which show coherent height difference along the sufficient welding length — documented in appendix B

Difference before and after cut of TWS			
Delta H in height of the centerline of the **TWS** (height/2)			
Lentgh [mm]	After cut [mm]:	Before cut [mm]:	Delta H [mm]
10	13,86	13,495	0,36
30	16,01	16,14	-0,13
50	18,45	18,405	0,04
70	19,59	19,6	-0,01
90	20,04	19,935	0,10
110	20,21	20,13	0,08
130	20,12	20,015	0,1
150	19,96	19,91	0,05
177	19,62	19,98125	-0,36

Figure 50: Deformation at e given length along the TWS. Source [65]

Delta-h values are then gathered to provide a graph which describes the slope of the neutral axis by a second-degree polynomial:
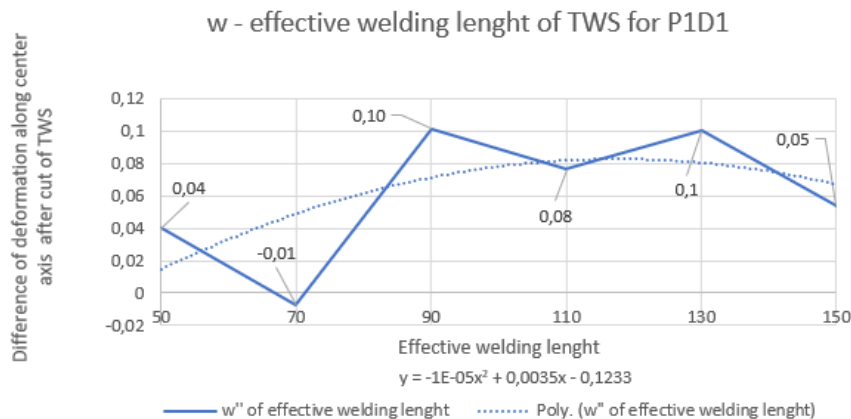
Figure 51: Deformation w(x) along the x-axis of TWS, described by the polynomial function. Source [65]

The first derivative of function-w result at w', which provide knowledge in the decline rate

of the height:
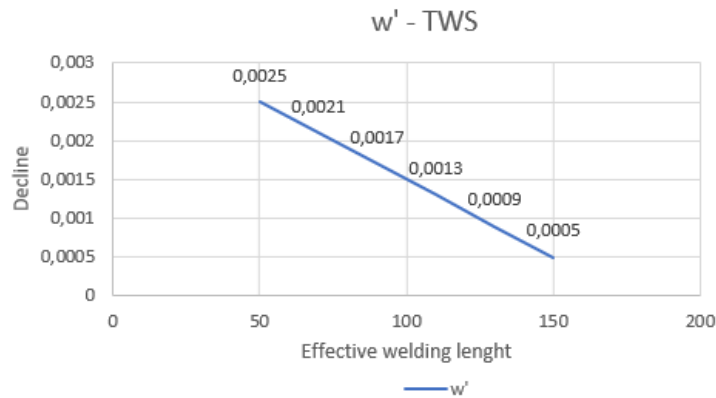
Figure 52: Decline w'(x) along the x-axis of TWS, described by an linear function. Source [65]

The second derivative of function - w (w"), provides knowledge of the amount of bending in a given point.
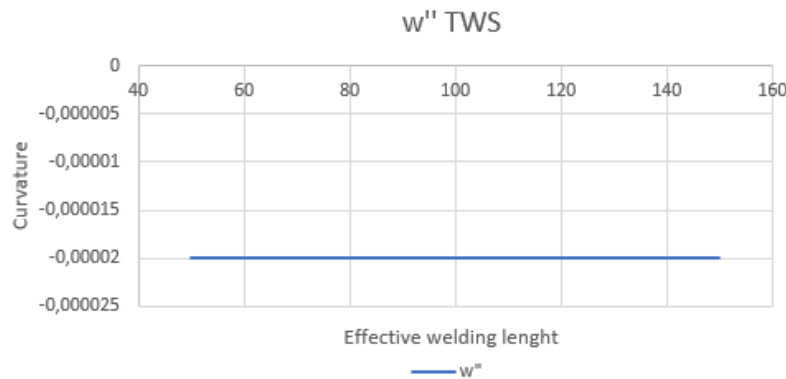
Figure 53: Curvature w"(x) along the x-axis of TWS, described by an constant function. Source [65]

Because of the polynomial we assumed we got an constant curvature along TWS which also result at an constant RS along the longitudinal direction. This result in RS:

$$\sigma = -z * E * \left(\frac{d^2 * w}{dx^2}\right) = 74,5 MPa \tag{31}$$

Double derivative: -0,00002
E-modulus: 200000 MPa
z: 18,62 [mm]

7   Finite Element Method - Simulation

Finite Element Method (FEM) is used to solve physical issues by mathematical models in engineering analysis and structures. The physical problem is related to actual structural components exposed to loads (thermal, structural, fluid, or electromagnetic). ANSYS is a flexible, robust design and optimization package. The simulation program consists of several analysis-environment called analysis-system or transits, these analyses can be connected to provide more realistic results. ANSYS WorkBench is designed to make it easier to simulate multiphysics couplings.
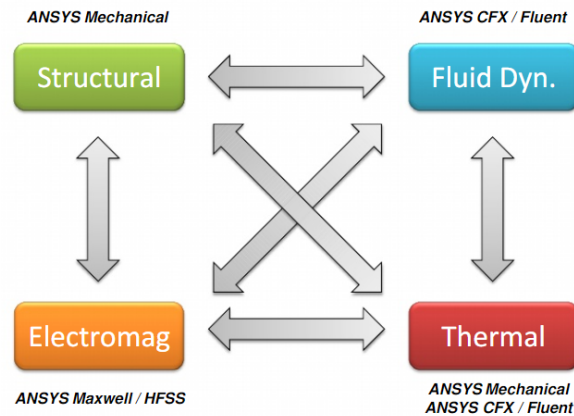
Figure 54: Choices of combination between the different environments. Source [70]

In this study are the component exposed to thermal stresses caused by the welding torch, which result in a multiphysical coupling environment between thermal and structural analysis. Reason for this approach of the GTAW-simulation of the TWS is because of there where lack of license to Additive Manufacturing simulation which would simulate the additive layer-process by the welding. Thus are the assumption made by inflicting thermal stresses with the torch of the GTAW at the surface of the thin wall structure. It is then possible to analyze the residual stresses at the surface which occur during the welding process. Since there is not possible to examine every layer are the simulation simplified to the top layer at every designs/concept, except P1D1 which have been analyzed with two different layers to compare the result by the top-layer analyses of the TWS's.

7.1   ANSYS - Coupling Analysis

The coupling analysis between Thermal transient and Structure transient are connected by one way thermal to structural coupling where the Engineering data (material) and Geometry (design) are the same in both analyses. The coupling analysis is used in the case of all samples, illustrated by the figure below:
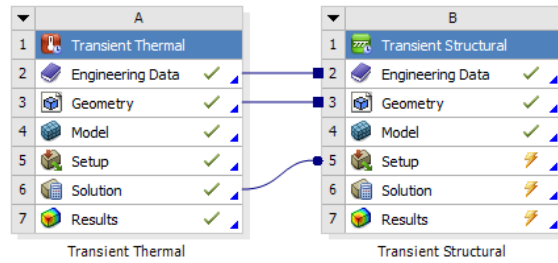
Figure 55: Multiphysical coupling of thermal transient and structural transient

7.1.1 Transient - Thermal and Structural

Reason for selecting transient thermal analysis is to determine temperature which varies over time, is due to simulating the torch of the GTAW, which moves across the TWS longitudinal direction during the welding process. It is common to use the temperature that a transient thermal analysis calculates as input to structural analyses for thermal stress evaluation, which have been done in this study. Many heat transfer applications and problems involve transient thermal analysis, as welding simulation does. A transient thermal analysis follows the same procedures as a steady-state thermal analysis, as both determine temperature, thermal gradients, heat flow rates, and heat flux in a material that are caused by thermal loads, only transient analysis varies over time while steady-state does not vary these load over time. However, does such loads include the following:

- Convection

- Radiation

- Heat flow

- Heat flux

- Constant temperature boundaries

Transient structural is selected to establish displacement, stresses, strains, fix support, and forces that occur in the TWS as a result of the thermal loads. Structural analysis is appropriate for solving problems and present given result as residual stresses.

7.2 Procedure for ANSYS Analysis

A transient thermal analysis is either linear or nonlinear. Dependant on the temperature material properties, convection coefficients or radiation effect can result in non-linear analyses while linear are dependant on a constant material property [71]. In the case of this study, it has been considered a non-linear transient analysis. The procedure for ANSYS analysis consists of three main steps:

- Build the model

- Obtain the solution

- Review the result

7.2.1 Build the Model

The initial step is the create project name and analysis title and then define the element types, material property, and implement the model geometry. The ANSYS element library contains over 80 element types. ANSYS includes the following couple elements: PLANE223, SOLID226, SOLID227.

7.2.2 Obtain the Solution

The second step we define analysis type, options, type of load, and then initiate— finite element solution. Generation of the solution involves three phases [72]:

1. Pre-Processor phase

2. Solution phase

3. Post-Processor phase

Pre-Processing phase is where the conditions and setting are applied, which are based on the material condition and assumptions for the inflicted loads. Solution phase is the generation of those settings. The last step is the outcome of the simulation process, which we can read out the data.

Pre-Processing phase	Solution phase	Post-Processing phase
Material definition	Element and overall matrix formation	Post solution operation
Geometry definition	Analyze settings	Post data printout
Mesh generation	Import load from other transient	Post data scanning
Constraint and load definition	Calculation of displacement, stress, etc.	Post data display

Table 13: Steps description of generating solution

7.2.3 Review the result

When the solution has been generated, the plot of probes and a review of the graphs are done to document the analyzed process. This step is important because the result is used to compare with other results in the thesis. 1

7.3 Modeling for GTAW using FEA

7.3.1 Modeling

As the first step of the simulation was the modeling of TWS and BP. TWS is modeled with three different designs which the first and second design are produced with different dimensions, while the two material for BP has the dimension of 348x99x25 [mm] for material X3CrNiMo13-4 and 397x100x25 [mm] for the material 304L alloy. Welding simulation is

modeled as a single pass in the analysis. The FEA analysis was carried out in two steps. A non-linear transient thermal analysis was first done to implement the heat flow generated by the welding and to obtain a global temperature history of the process. A structural stress analysis was then developed by implementing the thermal loads obtained in the transient thermal environment, that further are used at loading in the stress model. The general purpose of FE package ANSYS was to utilize both thermal and stress analysis as a coupling analysis performed sequentially. The mesh used in the stress analysis was identical to that in the thermal analysis.
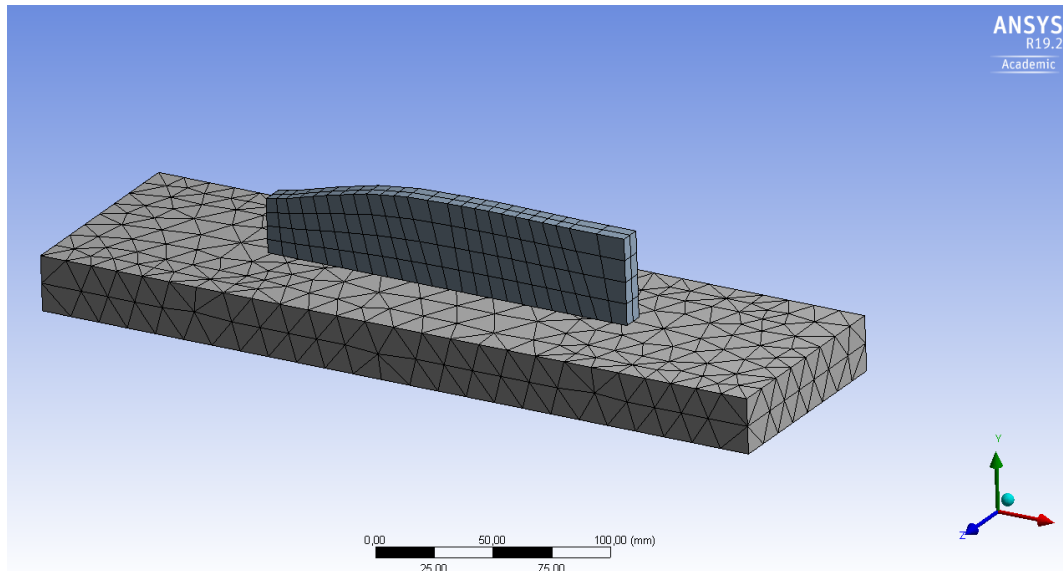
Figure 56: Mesh by sample P1D1 for illustrating

7.3.2 Problem definition

A Finite Element (FE) simulation of the welding process that generates RS in a thin wall structure is presented. The process includes a fusion welding which locally heating the area surface by the torch of the GTAW. Due to the non-uniform temperature distribution during the thermal process, shrinkage occurs when the material expands and cools, which leads to thermal stresses. Incompatible strains that occur due to the dimensional changes correlated with the solidification of the weld metal (WM), metallurgical transformation, and plastic deformation, are sources that inflict RS and distortion to the structures. Welded-induced RS and distortion are crucial for a reliable design of welded structures for further used after production. In this study FE simulation of the welding process, heat flow distribution of heat source, welding-induced RS, and distortion in welded structures are presented.
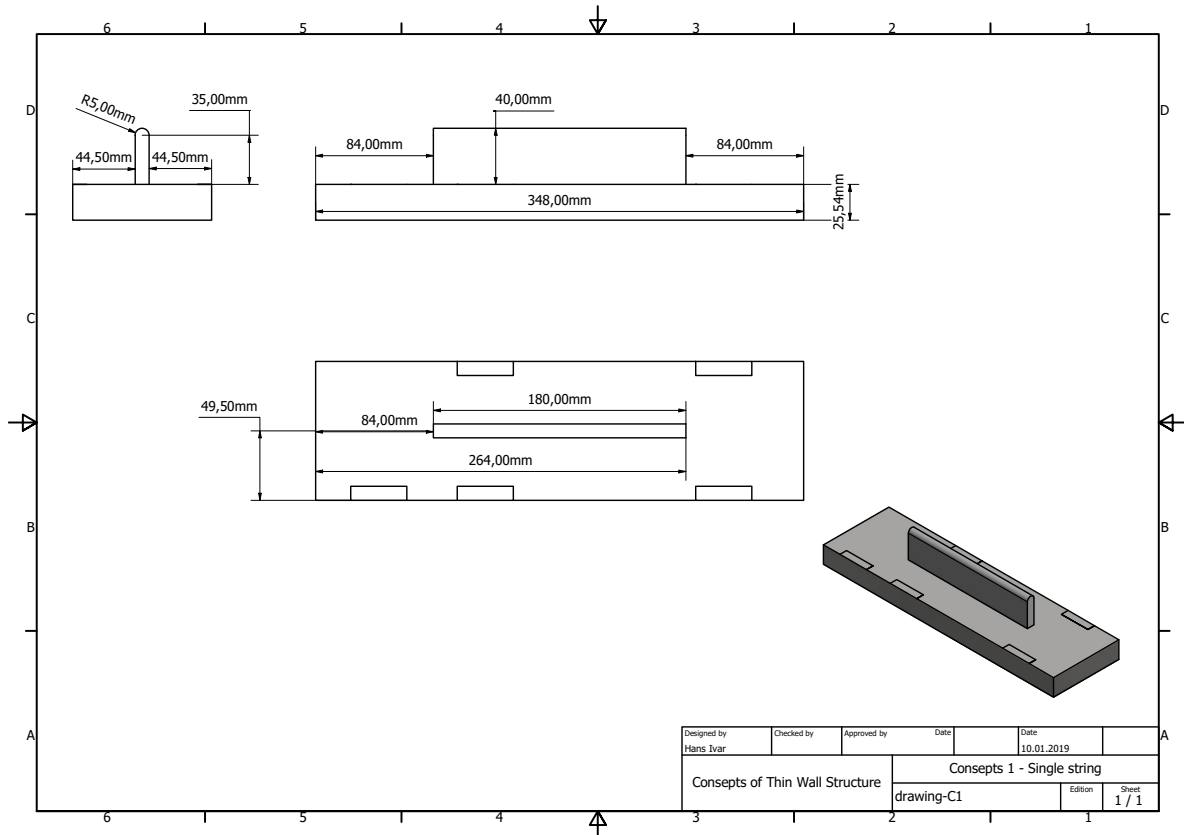
Figure 57: Schematic view of welding path plan of sample P1D1, the rectangle lines on the sides illustrate the location of the clamps to fix the BP. All schematic view of welding plan can be found in attachment 178

7.3.3   Assumption and Restriction

Because the simulation could not be conducted with the additive manufacturing application, which takes every layer of the thin wall structure and its process into account, a simplification was needed. Alternatively, are GTAW with a given heat source simulated with the respect of time. Although it cannot take every layer into account, therefore has a simulation of the top surface at the TWS and the first layer at the baseplate been simulated to provide the result the task description applies. Assumptions during the simulation:

- Heat flow generated from the electrode tungsten is placed at the surface of the TWS which cover the whole width of the structure and a given length for each component, example: 1/9 of the TWS-surface for concept 1.

- Convection applies for TWS when the simulation is analyzed at the TWS.

- Measurement of the RS and deformation are done with the respect of the length of the TWS and BP. Measurement was performed along the edge, because of the height difference it was not possible to create a path in the simulation to measure in the middle of the structure.

7.3.4 Boundary Conditions

One of the essential boundary conditions is edited in the engineering data, where the properties of the material are set. These properties has a huge impact on the behavior of the material and the result of the analyze, shown in table 16. The properties are based upon International Stainless Steel - Martensitic Stainless Steel [73] and AKSteel 304/304L Stainless Steel [74].

Property	Value	Unit
Density	7,7	g cm⁻3
Coefficient of Thermal Expansion	20-400 (C) - 1,16E-05 (K⁻1)	Celsius
Thermal Conductivity	25	W m⁻1 K⁻1
Specific Heat	430	J kg⁻1 K⁻1
Possion ratio	0,31	-

Table 14: Boundary Conditions for material X3CrNiMo13-4

Property	Value	Unit
Density	8,03	g cm⁻3
Coefficient of Thermal Expansion	0-100 (C) - 1,69E-05 (K⁻1), 0-583 (C) - 1,87E-05 (K⁻1)	Celsius
Thermal Conductivity	21,4	W m⁻1 K⁻1
Specific Heat	500	J kg⁻1 K⁻1
Possion ratio	0,31	-

Table 15: Boundary Conditions for material 304L

7.3.4.1 For Thermal Analysis

In the model-structures are the convection located at the surface at the baseplate and inside the structure-component as a result of the heat flow distribution, see figure 58. The room temperature is set as 25 °and the convection value coefficient as 20 W/m$\hat{2}$ °. The thermal analysis is based on the thermal stresses caused by the heat flow due to the GTAW-torch. The heat flow distribution is placed at the top surface of the TWS and BT which
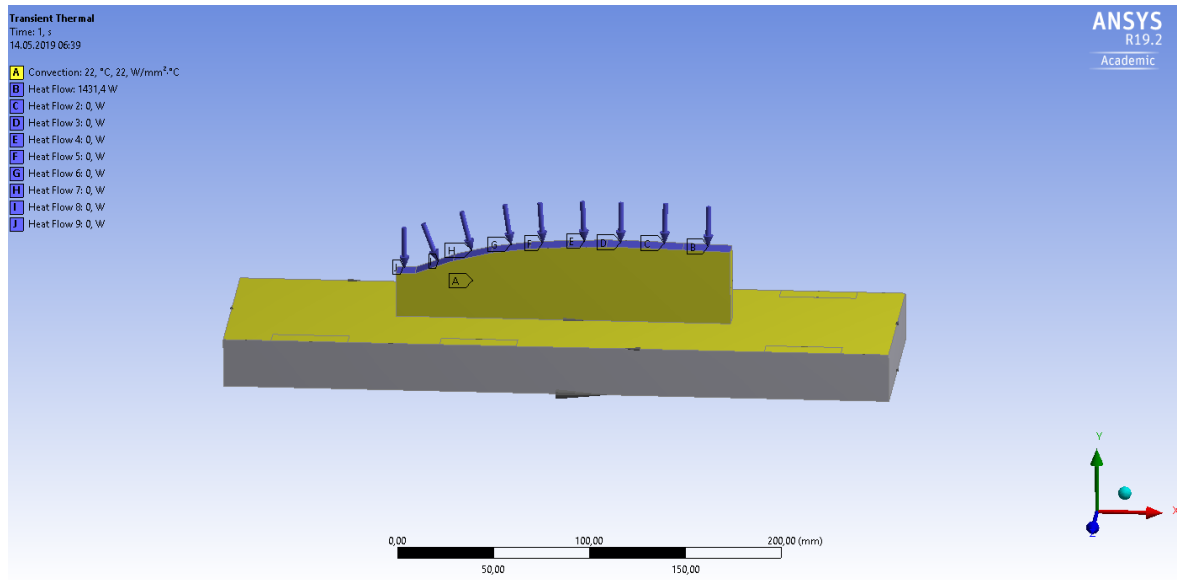
Figure 58: Illustration of heat flow placement at the thermal analysis conditions. Figure shows the placement of heat flow for sample P2D1, which has 9 surfaces and therefore it is 9 heat flow added to each surface.

Reason for adding heat flow to each surface is because they are located at a given height. When the height decrease during the welding process tries the robot to compensate for the height loss by generating a higher voltage, which results in higher heat flow at the TWS surface. It was discovered during the welding experiment of the GTAW-process by WAAM. To generate reality as close as possible are the assumption of estimating the height loss and then apply an estimated heat flow. For instance; the heat flow value along the effective welding area for P1D2 is calculated to be 1431,4 W, an estimated value for the area [J] (illustrated in figure58 are then calculated to a heat flow with value 1533,2 W, which is an estimation of the compensated height loss.

7.3.4.2 For Structural Analysis

Structural boundaries are given by the fixed support which is performed by clamps in the experimental welding process. The fixed support is fixed in any direction at the shown areas at the baseplate-surface, see figure 59. The fixed areas apply for all samples, which is also shown in the schematic welding plans.
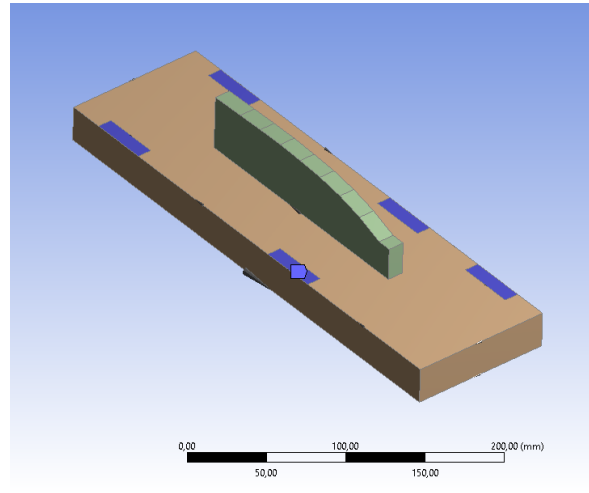
Figure 59: The pupal area illustrate the are the clamps hold the part fixed during welding.

7.3.5   Heat Transfer Analysis

The arc welding process entails melting of the surface and filler metal pursued by solidification of the molten weld metal. The fusion of the metals and solidification during welding correlates with the flow of the heat and are affected by the rate of the heat inside and around the weld metal. The therm thermal efficiency is used in this study to describe the welding process with two efficiency factors; arc efficiency and melting efficiency. Arc efficiency is the factor that are taken into account during the ANSYS simulation. It provide an quantitative measure of the amount of the total arc energy delivered to the welded structure and substrate. Importance of an accurate heat flow parameter in ANSYS is crucial to reflect the reality as much as possible. The qualitative energy balance of a general welding stripe on a substrate where the arc and melting efficiency are taken into account, are illustrated by figure 60. Figure are modified by Niles and Jackson [75]:
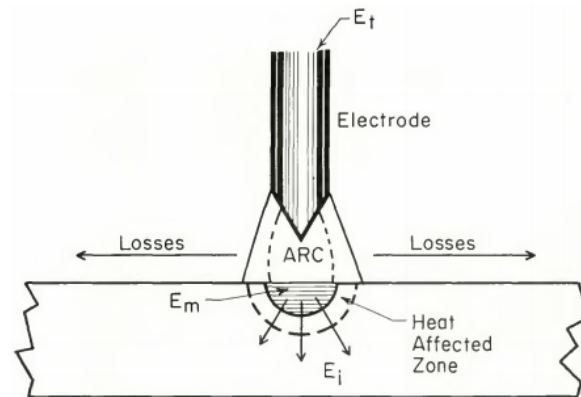
Figure 60: Schematic illustration of the energy distribution of the welding process . Source [75]

The majority of total energy are generated from the welding arc, while the minority is provided by the electrode. The distribution of the generated energy are transferred in two ways;

as a loss to the environment, and the remanding is transferred to the workpiece. Energy transferred to the workpiece are further distributed into two zones; fusion zone which melt a radius into the material (radius are based on the current) and the remaining energy which travel through adjacent base material outside the fusion zone primary by thermal conduction. Energy lost into the base material outside the fusion zone contribute to a local formation called heat-affected zone (HAZ) [76]. In the article of R.W Niles and C.E Jackson [75] they state that welding parameters variation effect the process efficiency by utilizing GTAW process, shown in figure 61. This article are an study of the arc distribution, material response, and changes in welding parameters using GTAW process that shows improved melting and process thermal efficiency as travel speed is increased. Therefore this study is used to base the thermal process efficiency in equation 13, which is further used to calculate the heat flow in the simulation ANSYS. Because my study have similar parameters as avhc = 2.8-2.4 [mm] and welding speed = 2.2-2,3 [mm] it can relate to this study as it also consider current, voltage and cooling into account.
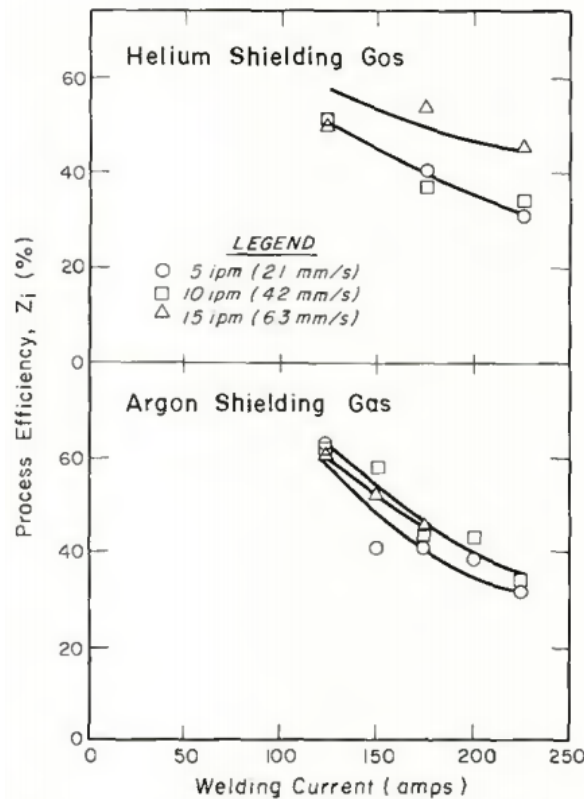
Figure 61: Process efficiency vs welding current for gas tungsten arc surface weld at an HY-80 plate with an avhc at 2.54 [mm] and welding speed at 2.1 [mm] . Source [75]

Figure 61 indicates that when the percentage of total heat decrease the level of current increase with either argon and helium shielding gas. This implies that heat losses from arc increase more rapidly with current level that does the percentage of the total heat entering the base metal. The result from Rykalin by using calorimetric methods he could conclude that the changes in the process efficiency varying from 35% to 65% on a general basis. Thus

the thermal process efficiency eta are therefore determined by the level of current which was used during the welding process to weld the different TWS. When determine the eta, it is an assumption based on figure 61 and the conclusion of the articles [75] [76]. They conclude that the general power efficiency are not the same when the current increase at a given travel speed of the torch. Thus an overestimation are taken into account when assuming the thermal efficiency process to ensure that the heat flow are not to low, see table X.

Calculation of heat flow are based numbers of contributions listed in the table X. Therefore are the heat flow added in ANSYS generated by the formula:

$$Q = I * V * \eta \tag{32}$$

where eta is the total power transfer based on the article of [77]. Thus result in: 250A*16,4V*0,4 = 1640W. The voltage are compensated with the increase in height difference between tungsten and the anode (base material) along the structure, the height difference factor of the electrode is given in [mm] and referred to as avhc.

Sample	Current	Voltage	Efficiency coefficient	Watt
P1D1	250A	16,4V	0,4	1640 W
P2D1	240A	14,2V	0,42	1431,36 W
P3D1	220A	13,5V	0,45	1336,5 W
P1D2	250A	16,4V	0,4	1640 W
P2D2	240A	14,2V	0,42	1431,36 W
P5D1	200A	12.3V	0,5	1230 W
P4D2	220A	12,2V	0,45	1207,8 W
P4D3	220A	12,2V	0,45	1207,8 W

Table 16: Heat flow value based on the parameters used to weld the TWS.

7.3.6 Test of layer assumption

The simulation of WAAM by GTAW in ANSYS has been simplified to an thermal analyzes of the TWS surfaces layer (upper layer of the structure). Initially the application "additive manufacturing" was planed to simulate every layer by taken GTAW into account. This was not done due to restricted access of the licence. Therefor an layer-simulation test is performed to verify the assumption; "every layer inflicted by the same heat source due to the samples set of parameter are equal, hence layer by layer analyzes is taken into account if every layer behave in the same manner when affected by the thermal stresses. The test include thermal analyses of three layer by the TWS-P1D1. Deformation and RS are measure along the longitudinal and transverse direction (along the x-axis) at the samples surface, illustrated by the figure 62 below:
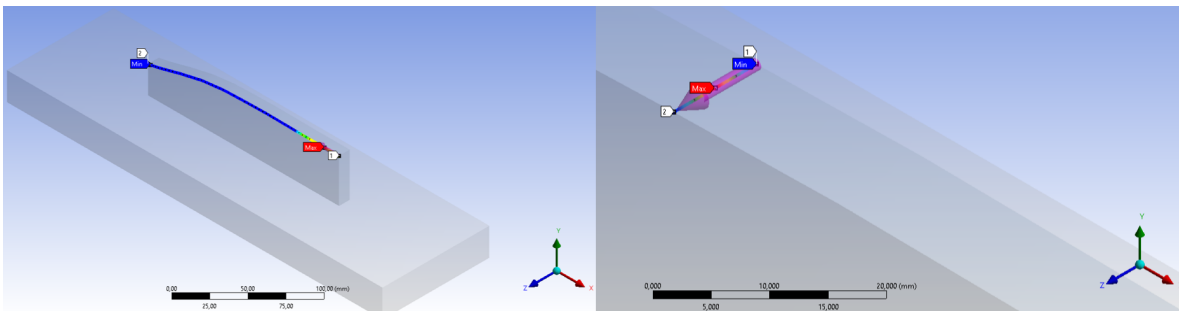
Figure 62: Measurement of the simulations values, longitudinal and transverse direction (along x-axis)

Because of the large amount of documentation are result of the simulated samples presented by graphs of the RS and deformation along the length of the structures. Result are documented in the appendixes:

- Result of the inflicted forces in the samples - Appendix

- Documented videos of the simulations, with and without slipped geometry to illustrate the distribution of the temperature, stresses and deformation along the length of the TWS and BP - Appendix

7.3.6.1 First layer analyses - P1D1x1

Simulation of the first layer indicates an low RS and deformation along longitudinal and transverse direction. Maximum RS occurred in TWS during welding: at 1441 MPa, details of the result, see appendix - figure .
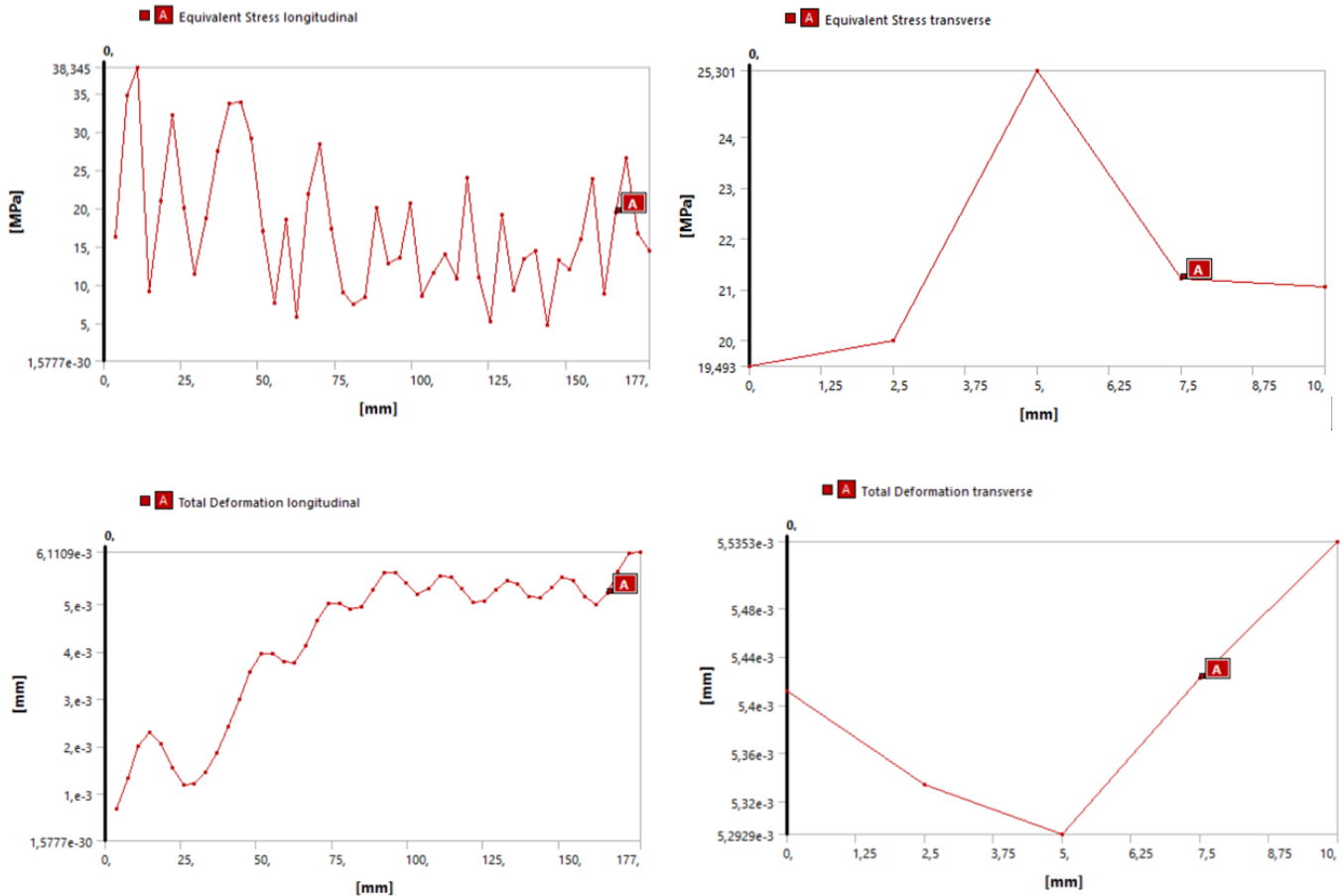
Figure 63: Simulation result of P1D1 first layer

- **RS-longitudinal direction** indicates an frequently amplitude of oscillation with an decreasingly level of RS along the length of the sample, largest stresses occur in peaks along the sample but are mainly highest at the start.

- **RS-transverse direction** indicates the largest amount of RS in the middle of the structure and decline level of stresses at the sides, including the left side with the lowest peak.

- **Deformation-longitudinal direction** indicates an increasingly level of deformation along the length of the sample. Largest deformation occur in the end.

- **Deformation-transverse direction** indicates the largest amount of deflection in the middle of the structure due to tensile stresses and incline level of deformation at the sides.

7.3.6.2   4th layer analyses - P1D1x2

Simulation of the first layer indicates an low RS and deformation along longitudinal and transverse direction. Maximum RS occurred in TWS during welding: at 1566 MPa, details of the result, see appendix - figure .
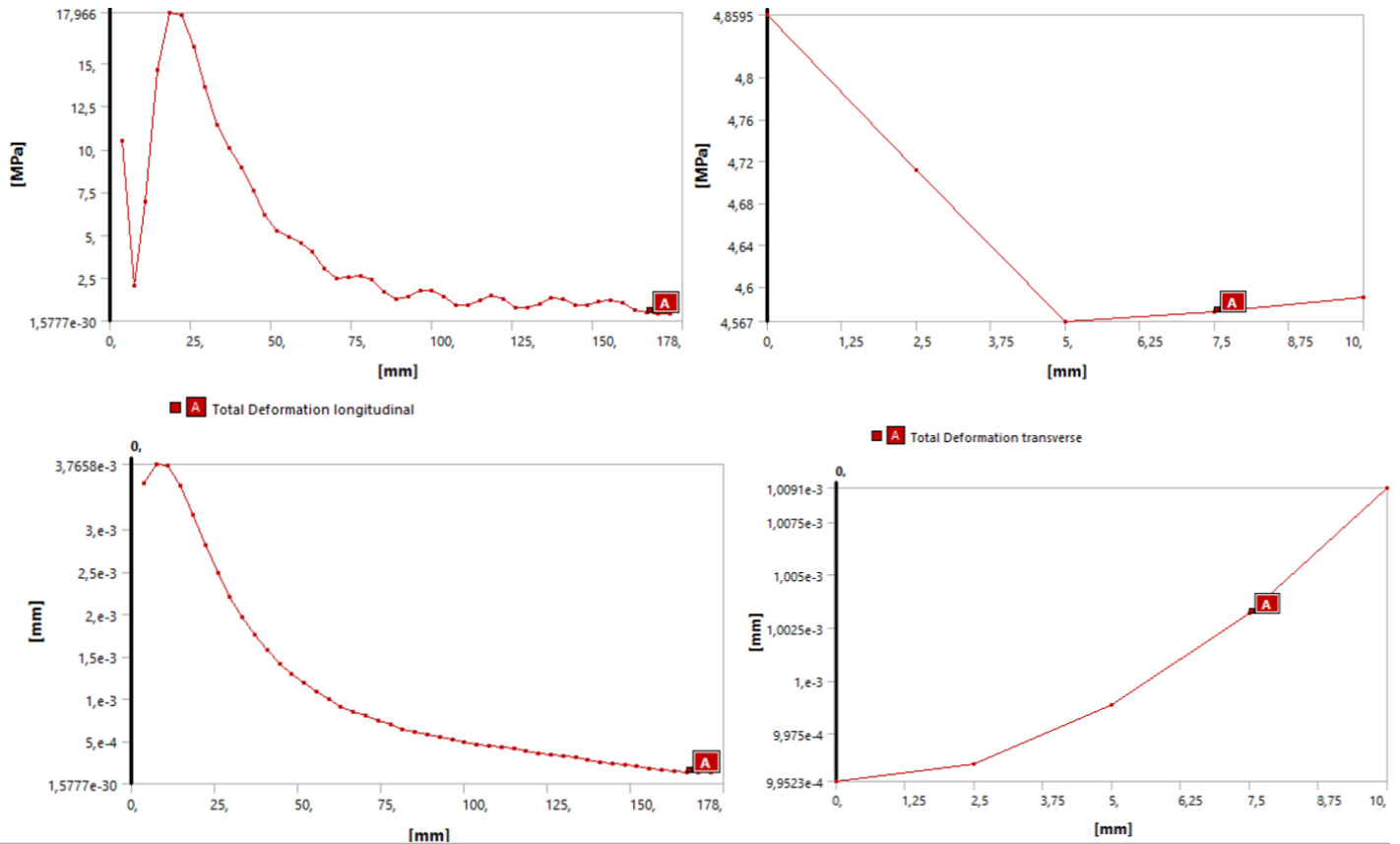
Figure 64: Simulation result of P1D1 4th layer

- **RS-longitudinal direction** indicates an decreasingly level of RS along the length of the sample due to the largest stress which occur at the start.

- **RS-transverse direction** indicates the largest amount of RS occur at the start (left side) where it drops lowest in the middle and then slightly increase at the end. This is due to bending in form of twisting.

- **Deformation-longitudinal direction** indicates an decreasingly level of deformation along the length of the sample. Largest deformation occur in the start.

- **Deformation-transverse direction** indicates an increasingly level along the thickness and has the largest amount of deflection at the end, due to twisting.

7.3.6.3   4th layer analyses - P1D1x3

Simulation of the first layer indicates an low RS and deformation along longitudinal and transverse direction. Maximum RS occurred in TWS during welding: 3.3E-6 MPa, details of the result, see appendix - figure .
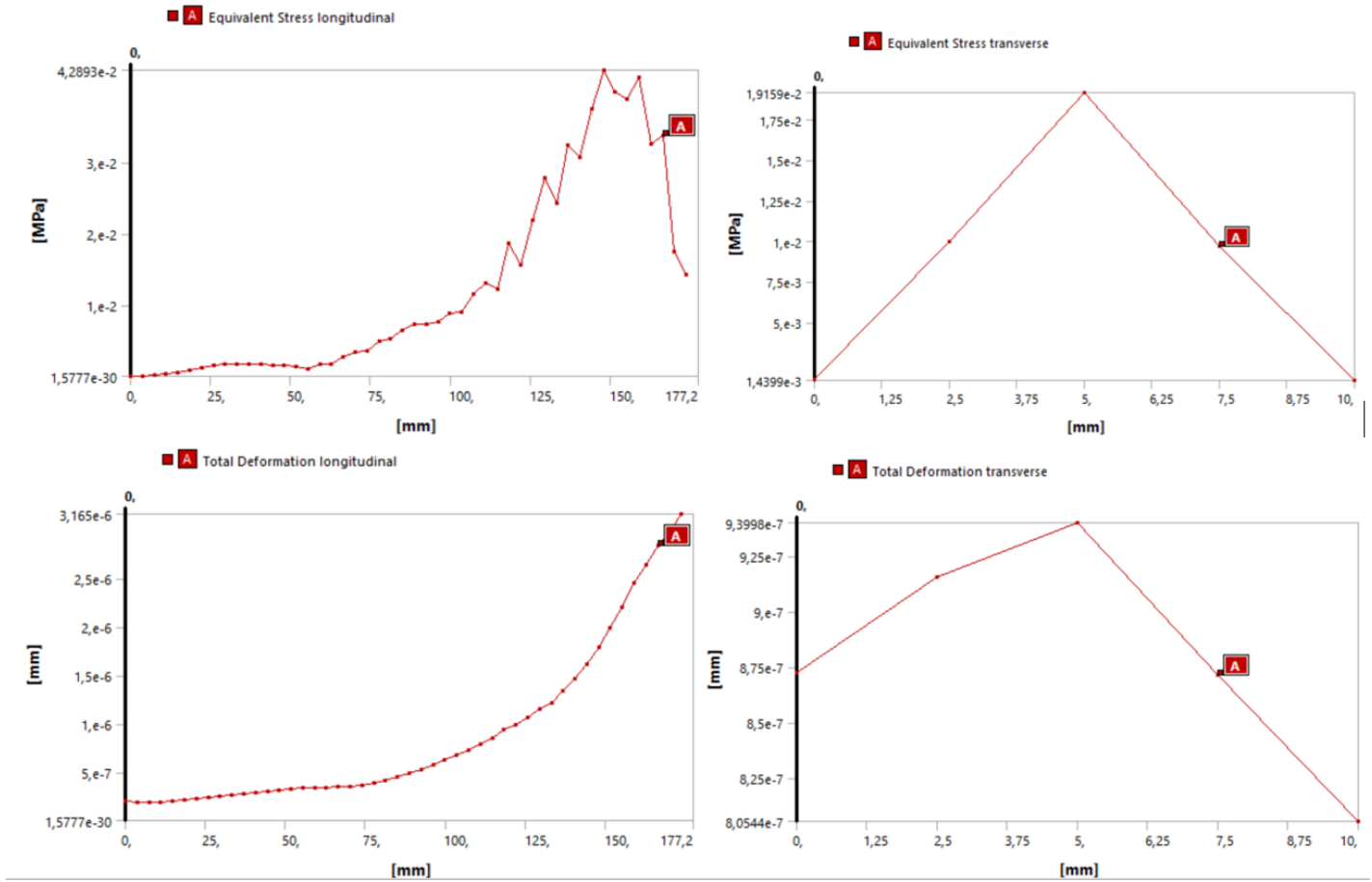
Figure 65: Simulation result of P1D1 4th layer

- **RS-longitudinal direction** indicates an increasingly level of RS along the length of the sample, where the largest stress which occur at the end.

- **RS-transverse direction** indicates the largest amount of RS occur at the middle (tensile stresses) and decline level of stresses at the sides (compressive stresses).

- **Deformation-longitudinal direction** indicates an increasingly level of deformation along the length of the sample. Largest deformation occur at the end, due to bending caused by thermal stresses.

- **Deformation-transverse direction** indicate the largest deformation in the middle, the lowest point is at right side and left side has an higher amount in compare.

7.3.6.4 Assumption of ANSYS-simulation

The result of the three layers of P1D1 present completely different graphs, additional to have different result, shown in appendix . P1D1x1 and P1D1x2 indicates an tremendous high RS due to the fusion zone during welding, while P1D1x3 have a extremely low value of RS. Although the simulation indicate completely different distribution of RS and deformation, the level of value for RS and deformation for all three samples are low. The assumptions are therefore that every layer have an equal amount of stress and deformation where the distribution of these result varies for each layer. Illustrated in appendix video number 1-4 which visually shows an different distribution of the temperature, RS and deformation. See the comparison of the result for the layer-analyze below:
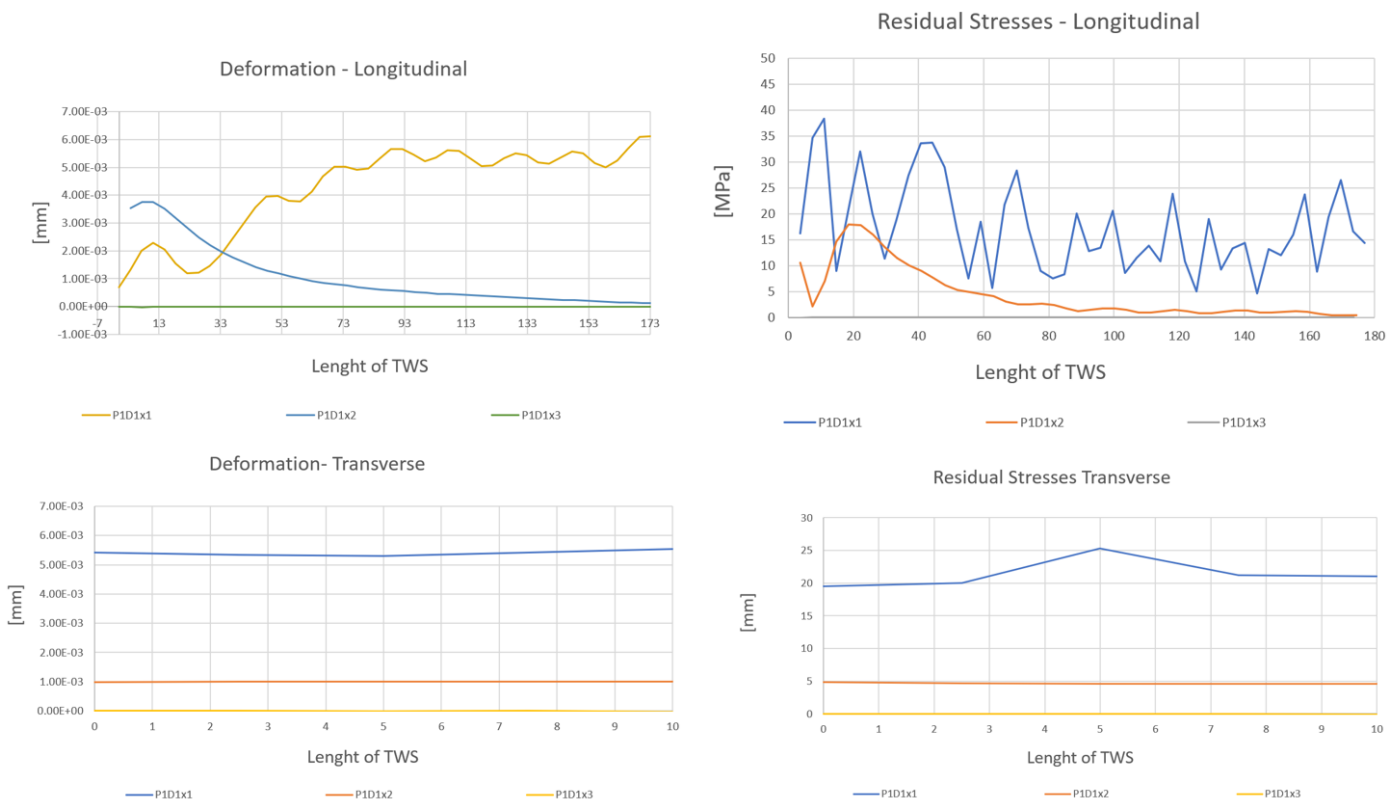
Figure 66: Comparison of result between first, 4th and 8th- welded layer

8 Results

By the stated criterion established in the problem statement (3.3), is the finding result answers the criterion due to the performed experiments and simulation. Thus, this study includes the result within three RS-test methods, simulation, welding experiment, and a welding procedure:

- Pictures of the welded thin wall structure after welding process (welding experiments)

- Residual stress test by calculation of the deformation of the TWS and BT after welding (RS-test method one)

- Residual stress test by ultrasound measurement (RS-test method two)

- ANSYS simulation of the TWS and BP during the welding process to generate residual stress and distortion analyze (RS-test method three)

- Develop a WPQR for the welding process which elaborates the documentation about the TWS welding process (welding procedure)

Tables and graph's present the findings and outcome of this study due to the experiments and simulation-analyze (calculation, ultrasound - experiment, and ANSYS simulation). A comparison of the main results is then made to create an overview of the three methods and their differences. Hand-calculation of the residual stress test are based upon measured deformation of the structure-component before and after the component are cut from the baseplate. Although the calculation is based upon Euler Bernoulli beam theory with a simplification of a polynomial description of the neutral axis height difference, due to noises in the measured data. Thus, these calculated results are presented as a constant value of RS along the length of the TWS. Data generated from the simulation shows temperature, RS and deformation plotted along the length and width of the TWS and BT. Ultrasound measurement method presents only RS-value along the side of the TWS's x-axis. Because of the massive amount of result, the most important data are presented in this chapter in the form of tables and illustrated graphs due to the later comparison.

Result of the initial experiment is presented by pictures of the welded TWS in appendix L. The result illustrates successful welded structures except for samples: P1D2 and P2D2.

8.1 Result - Practical residual stress test

In the initial RS-test (practical experiment) was the difference of height measurement of the neutral axes presented as deformation caused by thermal stresses utilized to calculate the RS by Euler's Bernoulli beam theory. Nine samples were calculated as the result of the experiment, shown in table **??**:

TWS-sample	E-module	z [mm]	w" - H	RS - H [MPa]	z - V	w" - V	RS-V [MPa]
P1D1	2E+5	18,62	-(2E-5)	74,5	-	-	-
P2D1	2E+5	20	-(8E-5)	320	-	-	-
P3D1	193E+3	18,31	-(1E-4)	353,31	-	-	-
P5D1	193E+3	7,36	-(2E-4)	284,09	-	-	-
P1D2	193E+3	8,33	-(8E-4)	1286,7	7,19	-0.0366	50820,4
P2D2	193E+3	8,58	-(6E-3)	9941,04	8,13	-(1,4E-3)	2196,6
P4D2	193E+3	7,58	-(4E-4)	585,5	8,08	-(6,8E-3)	10607,84
P4D3	193E+3	7,98	-(6E-6)	9,24	9,45	-(4E-5)	9.45

Table 17: TWS result from the calculation of the practical experiment for residual stress, see appendix D. Letter "H" stands for horizontal weld and "V"-vertical.

BP-sample	E-module	z [mm]	w" - H	RS - H [MPa]	z - V	w" - V	RS-V [MPa]
P1D1-BP	2E+5	12.69	-(2E-6)	5,07	-	-	-
P2D1-BP	2E+5	20	-(1,4E-5)	56	-	-	-
P3D1-BP	193E+3	20	-(1E-5)	38,6	-	-	-
P5D1-BP	193E+3	20	-(4E-5)	154,4	-	-	-
P1D2-BP	193E+3	12,81	-(6E-6)	14,8	13,95	-(1,8E-6)	48,4
P2D2-BP	193E+3	12,81	-(8E-6)	19,78	13,95	-(1E-5)	27
P4D2-BP	193E+3	11,76	-(4E-6)	9,08	11,56	-(4E-6)	8,89
P4D3-BP	193E+3	12,38	-(1E-5)	23,9	14,13	-(8E-6)	21,82

Table 18: BP result from the calculation of the practical experiment for residual stress, see appendix D. Letter "H" stands for horizontal weld and "V"-vertical.

In appendix F illustrate raw measuring data of the neutral axis height before and after cut of the TWS to illustrate the deformation. The height difference (delta-h) are documented in B, where it shows the actual measured height difference, additional it illustrates the simplified graph of the second degree polynomial which is an estimated graph actual used in the calculation D. The calculated structures by the practical RS-test are chronologically based upon the documentation by attachments:

1. Layer description, welding setting (main and minor parameters) and path coordinates - Appendix A

2. Deformation, height measurement before and after the cut of the TWS (based upon the height measurement result in appendix E) - Appendix F

3. Delta-h (height difference), (based upon the height measurement result in appendix E) - Appendix B

4. Graph of w, w' and w" (neutral axis description by a second degree polynomial) - Appendix C

5. Calculation - Appendix D

8.1.1   P1D1 - Test 1

Welding parameter set one - design one, is the first welded structure. Welding process for P1D1 generated the experiments highest heat input at 1,1 KJ/mm, which is close to the maximum limit for the material at 1,5 KJ/mm. The purpose was to investigate if it generated higher or lower - compression/tension in the material. The welding process had no source of errors during welding. The component was accomplished with 29 layers, which resulted in height at 40,1 [mm] and avr.width at 11,5 [mm]. In additional test-1 generated the highest amount of added material during the GTAW-process. Details of the welding operation for this sample are documented in appendix A - figure 83.
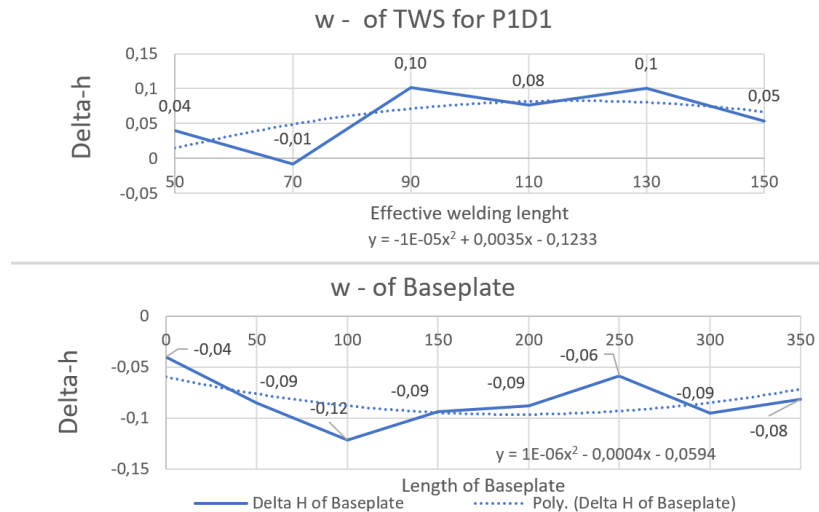
Figure 67: Delta-h of P1D1 described by an estimated second degree polynomial of TWS and BP.

Figure 67 illustrate the height difference along the length of BP as a negative graph and TWS as a positive graph, the functions provided in the figure are the polynomial used in the calculation of the RS. The graph relates to the raw data of height measurement at the neutral axis in F - figure 128.

- **The TWS of P1D1** indicate a general positive deformation along with the sample, which is a strong estimation of the actual delta-h, provided in the appendix B - figure

92. Additional it shows a low negative value of the curvature which is the constant along the horizontal length of the TWS, this causes a low RS value at 74,5 MPa, calculation details are shown in D - figure 112.

- **The BP** indicates a low value in delta-h at the negative estimated polynomial along the length of the substrate. Due to this, the curvature of the BP has a lower value of the TWS at 5,07 MPa along the horizontal length of the substrate.

8.1.2   P2D1 - Test 2

The second set of parameters tested to weld the sample P2D1 was produced with a heat input at 0,89 KJ/mm. The lower amount of power source used in P1D resulted in height at 40 [mm] and an avr.with at 11.3 [mm] caused by 31 deposition layers. The welding process of this test also had a non-significant error of sources. Wire feeding was reduced as the speed increased, generated thinner layers, and a lower amount of heat after weldment, which caused faster production. Layer description can be found in appendix A - figure 84.

Figure 68: Delta-h of P2D1 described by an estimated second degree polynomial of TWS and BP.

Height difference illustrated in figure 68 along the TWS shows a slightly negative graph and the BP as a slightly positive graph. The graph relates to the raw data of height measurement at the neutral axis in F - figure 129.

- **The TWS of P2D1** indicates a decreasingly deformation along with the sample, where the polynomial-curve fit the actual delta-h curve with a good estimation by the provided data in B - figure 93. The curvature appears as a low negative value which is constant

along the length of the TWS, this causes an RS value at 320 MPa, calculation details are shown in D - figure 113.

- **The BP** indicates a smooth steady value for delta-h, shown in figure 68 as less inaccurate match compare to the actual curve at the end of the length of BP. Due to steady low deformation, the curvature appears as a negative low value with an RS at 56 MPa along the horizontal length of the substrate. Details for curvature in BP and TWS are given in appendix C - graph 101.

8.1.3   P3D1 - Test 3

The third set of parameter tested was welded with a heat input at 0,81 KJ/mm. In A - figure 85 we can see one layer was excluded due to an error with the feeding, which caused the wire to miss the welding pool. Layer result included an height at 41,6, avr.width at 10,6 [mm] caused by 34 deposition layers. At this test was the avhc, speed, and feeder - parameters adjusted down.
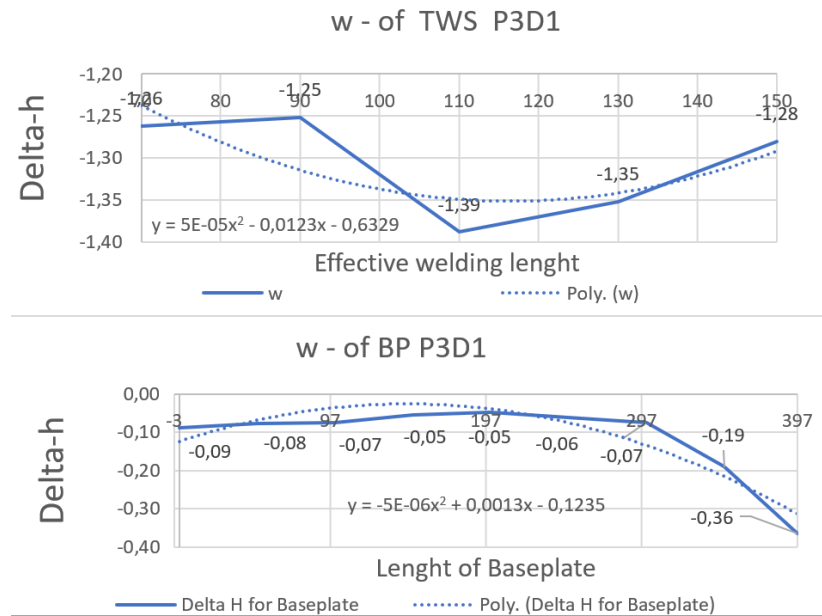
Figure 69: Delta-h of P2D1 described by an estimated second degree polynomial of TWS and BP.

Figure 69 illustrate the height difference along the TWS as a negative graph and BP as a positive graph. The graph relates to the raw data of height measurement at the neutral axis in F - figure 130.

- **TWS of P3D1** indicates an estimated negative deformation along with the sample. The polynomial-curve fit the actual delta-h curve with an exceedingly bad estimation by the provided data in B - figure 94. The curvature of the estimated curve appears as a negative minor-low RS value at 353 MPa, calculation details are shown in D - figure 114.

- **The BP** indicates a positive deformation along the estimated curve which doesn't fit the actual delta-h curve accurate. Nevertheless, are the data of delta-h steady low along the substrate which provide a low negative value of the curvature. Thus, providing a low RS value with 38,6 MPa. Details for curvature in BP and TWS are given in appendix C - graph 102.

8.1.4   P5D1 - Test 5

The fifth set of parameter generated with a lower heat input at 0,67 KJ/mm compares to the first tests. During the welding process, the arc tungsten crashed in the TWS's surface, which led to an error known as short circuit, detail of layer description can be found appendix A - figure 87. The problem was solved with re-adjusted to a new start and end position closer to the center of the TWS. The new set of a parameter included a lower feeding, heat input, and avhc which resulted in height at 30,5 [mm] and avr.width at 10,07 [mm] accomplished at 42 layer depositions.
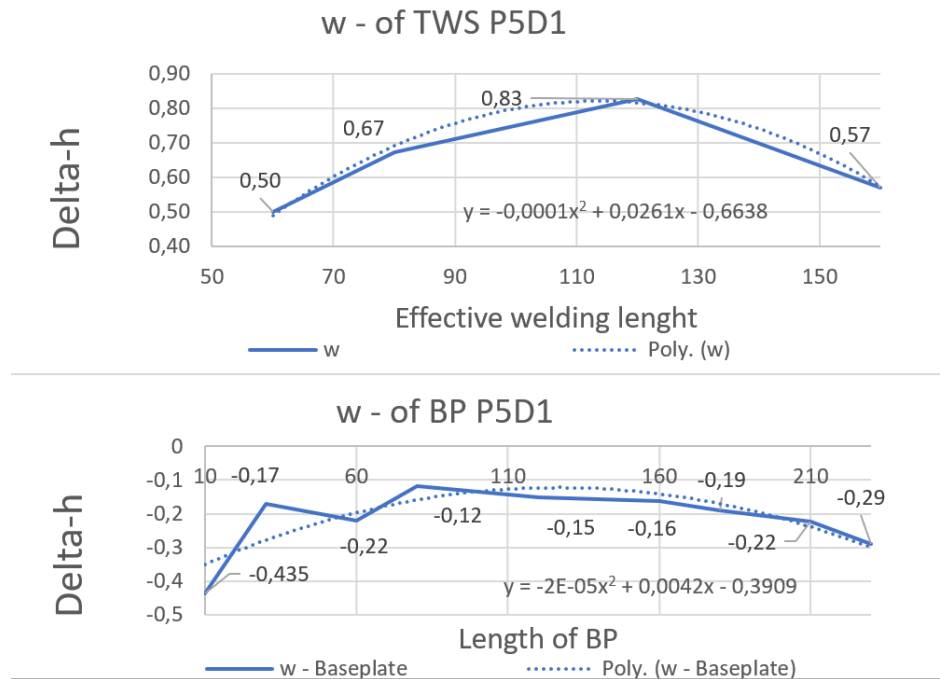
Figure 70: Deformation of the neutral axis along the x-axis.Note: Effective welding length 60-160 [mm]

Figure 70 illustrate the height difference along the TWS and BP as negative graphs. The graphs relate to the raw data of height measurement at the neutral axis in F - figure 131.

- **TWS of P5D1** indicates an estimated positive deformation along TWS. The polynomial curve fits inaccurate compared to the actual delta-h curve due to the provided data in B - figure 95. The curvature of the estimated curve appears as a negative value causing an RS at 284 MPa, calculation details are shown in D - figure 115.

95

- **BP of P5D1** indicates a positive deformation of the estimated polynomial curve along the TWS, the comparison with the actual delta-h curve the estimation is poorly. Although are the data occur general steady, which generate a minor-low negative value of the curvature. Thus, resulting in an RS at 154 MPa. Details for curvature in BP and TWS are given in appendix C - graph 103

8.1.5 P1D2 - Test 6

First set of parameter to weld an 90 °angle structure was welded as an cross with horizontal and vertical walls. Welding process of the design proven difficult due to the vertical walls, this included errors as crash of the tungsten electrode because of the height difference and short welding length. Additional the high heat input from the parameter-set-one caused the component to melt down along the inefficient welding length. Thus it compromised the height of the structure. Layer description addressed in A - figure 88 document the height to be 20,9[mm] and avr.width at 13,23 [mm] with total 11 layer deposited.
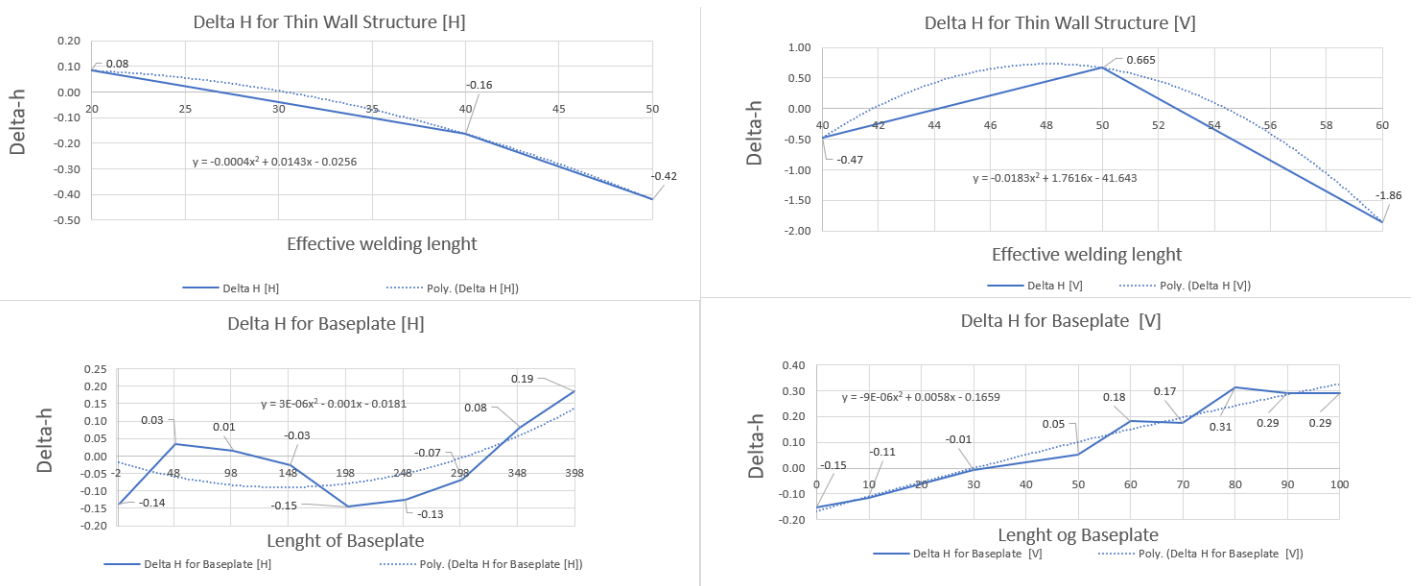
Figure 71: Deformation of the neutral axis along the x-axis.Note: Effective welding length 20-50 [mm] horizontal and 40-60 [mm] vertical direction.

Figure 133 illustrate height difference along the length of the sample at the horizontal [H] and vertical [V] directions based at the raw measurement of the height in F - figure 132. The graphs in figure 133 are commented below for both TWS and BP:

- **TWS[H]** indicates an slightly negative deformation with an poorly estimated polynomial compare to the actual w-curve, details are provided in appendix B - figure 96. The curvature of the simplified graph shows a large value which causes an RS at 1286 MPa. This result is unreal due to the large variation in the delta-h data.

- **TWS[V]** Indicates a large deviation from the deformation-w and the estimated polynomial. The curvature of the sample occurs as tremendous high, causing an RS at 50820 MPA, which is an unreal value due to a large variation of the delta-h data.

- **BP[H]** indicates a positive deformation with a substantial large deviation between the actual curve and the estimated polynomial. The inaccuracy provides a constant negative curvature, due to the profound changes in delta-hit causes RS at 14,8 MPa.

- **BP[V]** indicates a negative deformation where the estimated curve fits poorly to the actual delta-h curve. Although the data are smooth and steady with a low height difference causing the curvature to generate a low RS at 48 MPa, shown in detail in D - figure 116.

8.1.6   P2D2 - Test 7

During the welding production of P2D2 the heat input of 0,89 KJ/mm was used. Because of the short welding length across the vertical direction of the 90 °structure and high power source it created an difficult welding process. Due to this re-positions of the welding path was needed as the tungsten crashed often to the surface because of the height difference. Thus, affected the height and the effective welding length of the TWS. P2D2 resulted with an total height at 15,5 [mm] and avg.witdh at 12,54 after 12 deposited layers, see A - figure 89 for layer and production details.
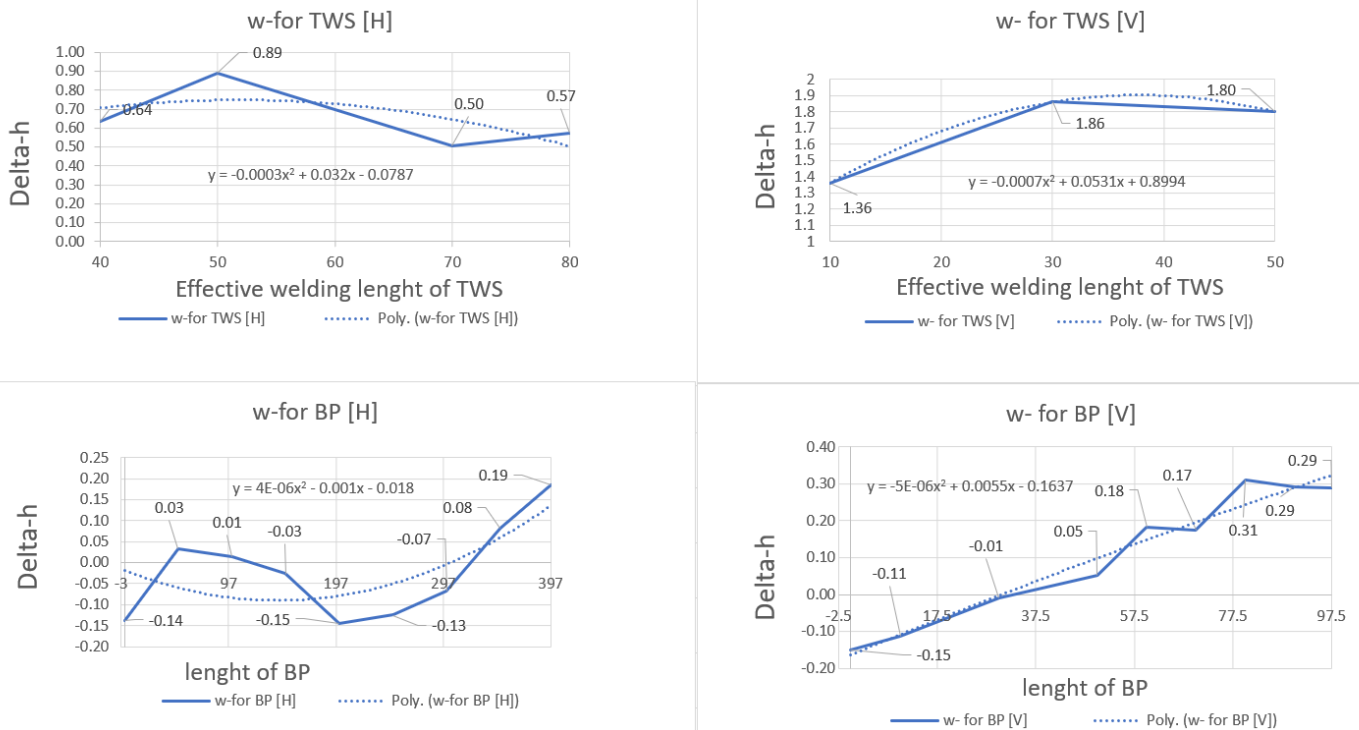
Figure 72: Deformation of the neutral axis along the x-axis.Note: Effective welding length 40-80 [mm] horizontal and 10-50 [mm] vertical direction.

Figure 133 illustrate height difference along the length of the sample at the horizontal [H] and vertical [V] directions based at the raw measurement of the height in F - figure 133. The graphs in figure 133 are commented below for both TWS and BP:

- **TWS[H]** indicates an positive deformation by the estimated polynomial graph which fits the actual curve inaccurate with two large deviation, see B - figure 97. In the curvature of the simplified second-degree polynomial occurs a tremendous large negative value causing the RS at 9941 MPa, which is an unreal data. This is due do to large delta-h values.

- **TWS[V]** Indicates a positive graph of the estimated polynomial curve which provides a poorly estimation. The curvature of delta-h provides a large negative value causing a high RS at 2196 MPa, which also are unreal value. The data of delta-h are too uneven.

- **BP[H]** indicates a strong deviation between the real curve and the estimated polynomial curve. Curvature furthermore provides a low value which generates an RS at 19,78 MPa because of continuous smoothly value of delta-h along the substrate.

- **BP[V]** indicates a positive deformation with a poorly estimated polynomial curve compare to the actual w-curve. Curvature along the sample appears with a low value and causing a low RS at 26,91 MPa because of low and smooth delta-h change along the substrate. See appendix D - figure 117 for detail of the calculation.

8.1.7   P4D2 - Test 8

In the welding process of P4D2 was the horizontal length of the TWS extended and parameter changed, due to the result from P1D2 and P2D2. This resulted in better products for the 90°cross-structure with a longer sufficient welding length, and lesser frequently crashes of the electrode and surface. Although was re-positioning needed because of not enough feeding at the start of the process (build an incline hill at the beginning of the TWS which made the tungsten crash), see A - figure 90 for layer and production details. The structure resulted in height at 19,5[mm] and avr.witdh at 10 [mm] with 13 deposited layers.
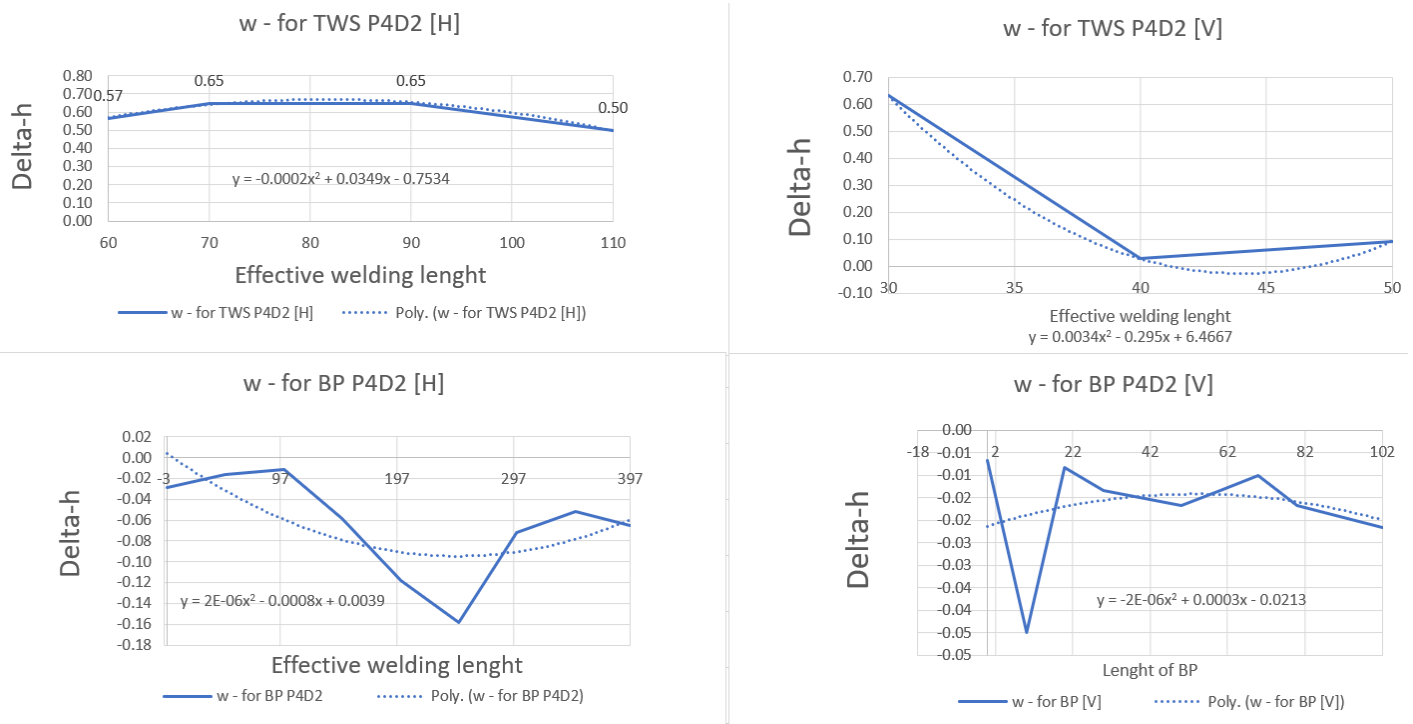
Figure 73: Deformation of the neutral axis along the x-axis. Note: Effective welding length 60-110 [mm] horizontal and 30-50 [mm] vertical direction.

Figure 134 illustrate height difference along the length of the sample at the horizontal [H] and vertical [V] directions based at the raw measurement of the height in F - figure 134. The graphs in figure 134 are commented below for both TWS and BP:

- **TWS[H]** indicates an negative deformation which the estimated polynomial fits acceptable compared to the actual w-curve, details of height difference are documented in B - figure 98. The curvature of the estimated polynomial shows a high value because of the large variety in delta-h data, this resulted in an RS at 566 MPa.

- **TWS[V]** Indicates a positive graph where the estimated polynomial graph fit poorly. The delta-h value has a tremendous amount of variety, which causes a high negative value for the curvature, which furthermore results to a high RS at 10607 MPa. The amount of RS is an unreal value which is caused by the unsteady data in delta-h.

- **BP[H]** indicates a strong deviation between the real curve of deformation and the estimated polynomial curve. Because of the general small millimeter changes along the substrate does the curvature provide an exceedingly low value along with the plate. Thus, resulting in an RS at 9,08 MPa.

- **BP[V]** indicates a negative deformation with a poorly estimated polynomial curve compare to the actual w-curve with a huge difference in deviation at the start of the sample. Curvature along the sample appears with a low value and causing a low RS at 8,89 MPa because of low delta-h change along the substrate. The calculation are shown in appendix D - figure 118 for details.

8.1.8   P4D3 - Test 9

The fourth set of parameters was used to weld the third and last design that included a 20°angle cross-structure. Since the angle of TWS allowed more space at the 100 [mm] width BP, the structure was extended to 180 [mm] in the purpose of extended effective welding length. Due to the parameters, the weldment operation went smoothly with low errors, although some adjustment of narrow the start/end position of the welding stripe was needed. The welding process of test nine resulted an TWS with an total height at 24 [mm] and avr.witdh at 10,56 [mm] with 22 deposited layers, see A - figure 90.
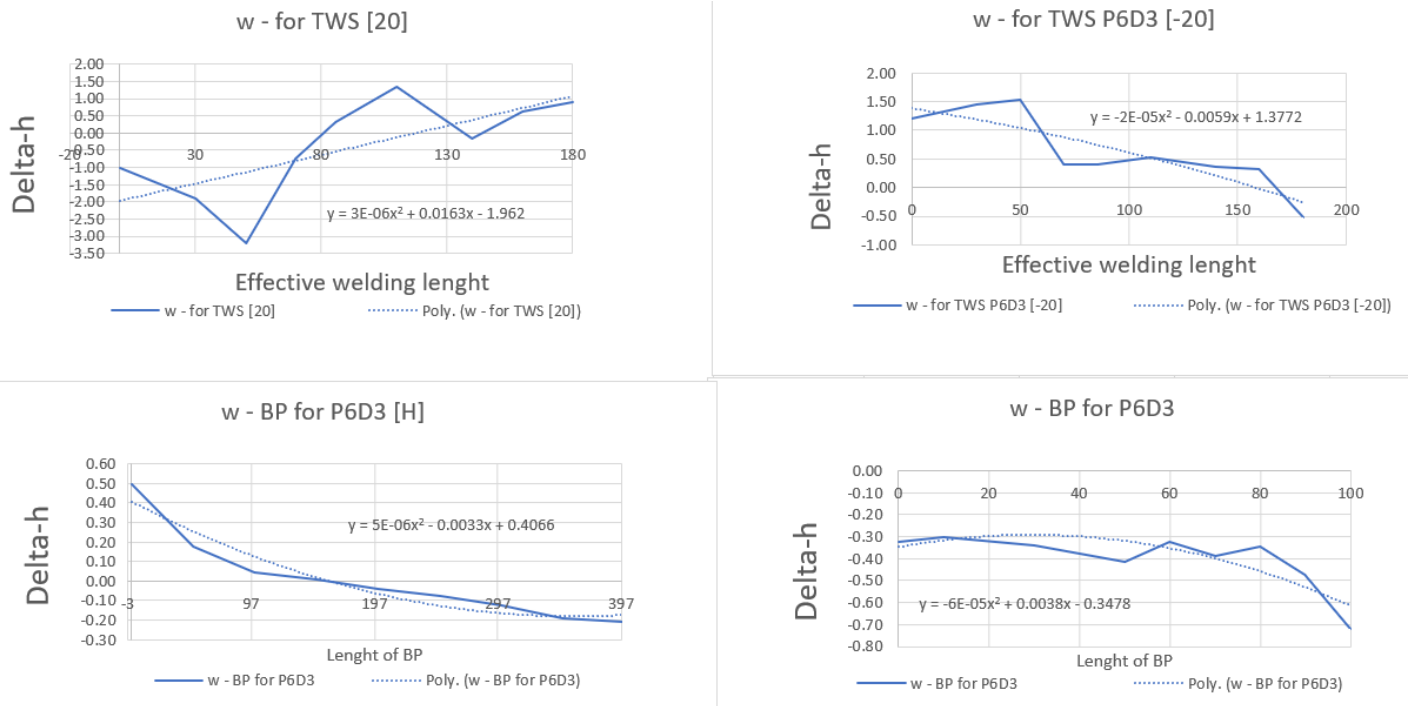
Figure 74: Deformation of the neutral axis along the x-axis.Note: Effective welding length 60-110 [mm] horizontal and 30-50 [mm] vertical direction.

Figure 135 illustrate height difference along the length of the sample at the horizontal [H] and vertical [V] directions based at the raw measurement of the height in F - figure 135. The graphs in figure 135 are commented below for both TWS and BP:

- **TWS[20]** indicates a negative deformation with large deviations between the estimated second-degree polynomial and the actual delta-h curve, based on the data provided in B - figure 99. The curvature of the TWS has a low negative value due to the low value of changes in the delta-h data. This causes a low RS at 9,24 MPa.

- **TWS[V]** Indicates a slightly negative graph where the estimated curve of second degree polynomial fits in an inaccurate manner compare to the actual curve of deformation (w). This is due to the significant deviation as shown. The curvature of the estimated curve provides a low negative value due to small decreasingly data along the vertical weld, causes low RS at 73MPa.

- **BP[H]** indicates a slightly positive deformation curve which the estimated polynomial curve fits poorly. Low height difference data along the horizontal direction provides a low negative value for the curvature, which generates a low RS stress at 23,9 MPa.

- **BP[V]** indicates a negative deformation by the delta-h curve, the estimated second-degree polynomial curve fits deficient in comparison. Although the small variation in height value along the vertical direction of the weld provides a low negative curvature, it generates a low RS at 21,62 MPa, see appendix D - figure 115 for details.

8.2   Result - ANSYS simulation

ANSYS simulation analyzes are based on the assumption made in 7.3.6.4. It states that the simulation considers the result provided at the upper layer at the structure is equal for the rest of the layers. Thus, the RS and deformation provided in the result are equal for the whole TWS. Because of the high amount of data, only TWS are presented in this chapter. The TWS illustrate the result by deformation and RS along the length of the longitudinal and - transverse direction of the TWS. The data of P1D1, P2D1, P3D1, and P5D1 are presented in the same graph for comparison, as P1D2, P2D2, P4D2, and P4D3 also are compared in another graph. Provide a more exceptional aspect of the differences the parameters constitute.

8.2.1   Simulation Result Of TWS: P1D1-P2D1-P3D1-P5D1

Simulation of the single stripe was performed with four kinds of various parameters, developed by the WPQR in Appendix J. The result presents deformation and RS along the longitudinal and transverse direction of the x-axis. Due to the set of parameters, the TWS's has been exposed to different levels of heat input, which has caused high internal stresses in the fusion zone. These stresses decreased rapidly after the welding process (cooling process), illustrated in appendix I. Individual result for each TWS is given in appendix H. Maximum RS and temperature - value in the fusion zone during welding resulted in:

- P1D1 - 1930 MPa at 1597°- details in appendix: H figure 139 for result and I figure 154 for temperature during and after welding.

- P2D1 - 1968 MPa at 1316°- details in appendix H figure 140 for result and I figure 155 for temperature during and after welding.

- P3D1 - 1793 MPa at 797°- details in appendix H figure 141 for result and I figure 156 for temperature during and after welding.

- P5D1 - 2027 MPa at 1341°- details in appendix H figure 142 for result and I figure 157 for temperature during and after welding.

The result from the simulation is presented by:

- Deformation along the length of the TWS (longitudinal and transverse - direction)

- Residual stresses along the length of the TWS (longitudinal and transverse - direction)

8.2.1.1   Deformation along the length of the TWS

The result presents a graph of deformation on a large scale, additionally are a zoomed-in graph with the same result illustrated to provide a detail graph where the values are to low to investigate.
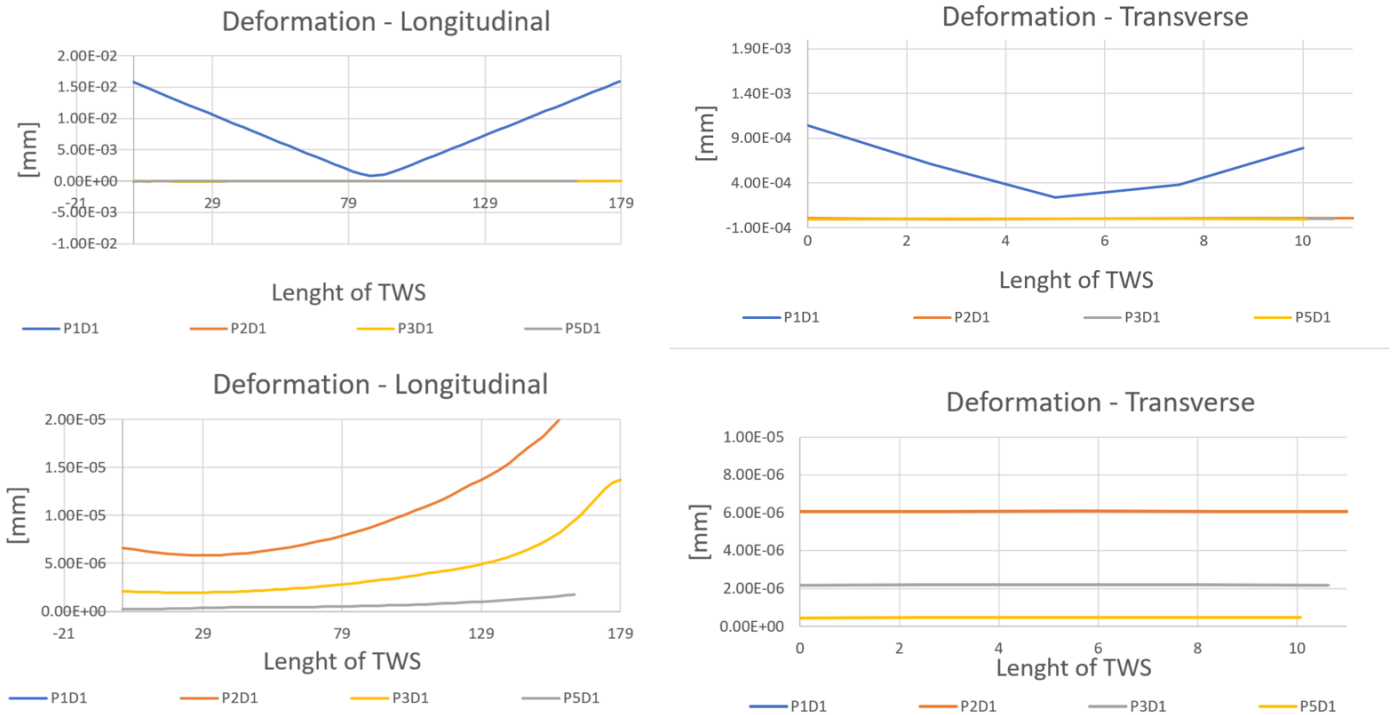
Figure 75: Simulation-result: deformation longitudinal and transverse direction of the x-axis

- **Deformation-longitudinal direction** indicates a large deviation in between P1D1 and the other set of parameters. The geometry of P1D1 illustrate a large deformation at the start and the end of the TWS, while the others have an increased level of deformation with maximum deviation at the end of the sample. See the zoomed graph of the deformation in a longitudinal direction.

- **Deformation-transverse direction** indicates additional a v-formed curve due to bending forces at each side. The deviation of deflection only occurs at sample P1D1, while the other TWS's has a constant value of deformation throughout the length.

8.2.1.2   Residual stresses along the length of the TWS

The result presents a graph of RS on a large scale, additionally are a zoomed-in graph with the same result illustrated to provide a detailed graph where the values are to low to investigate.
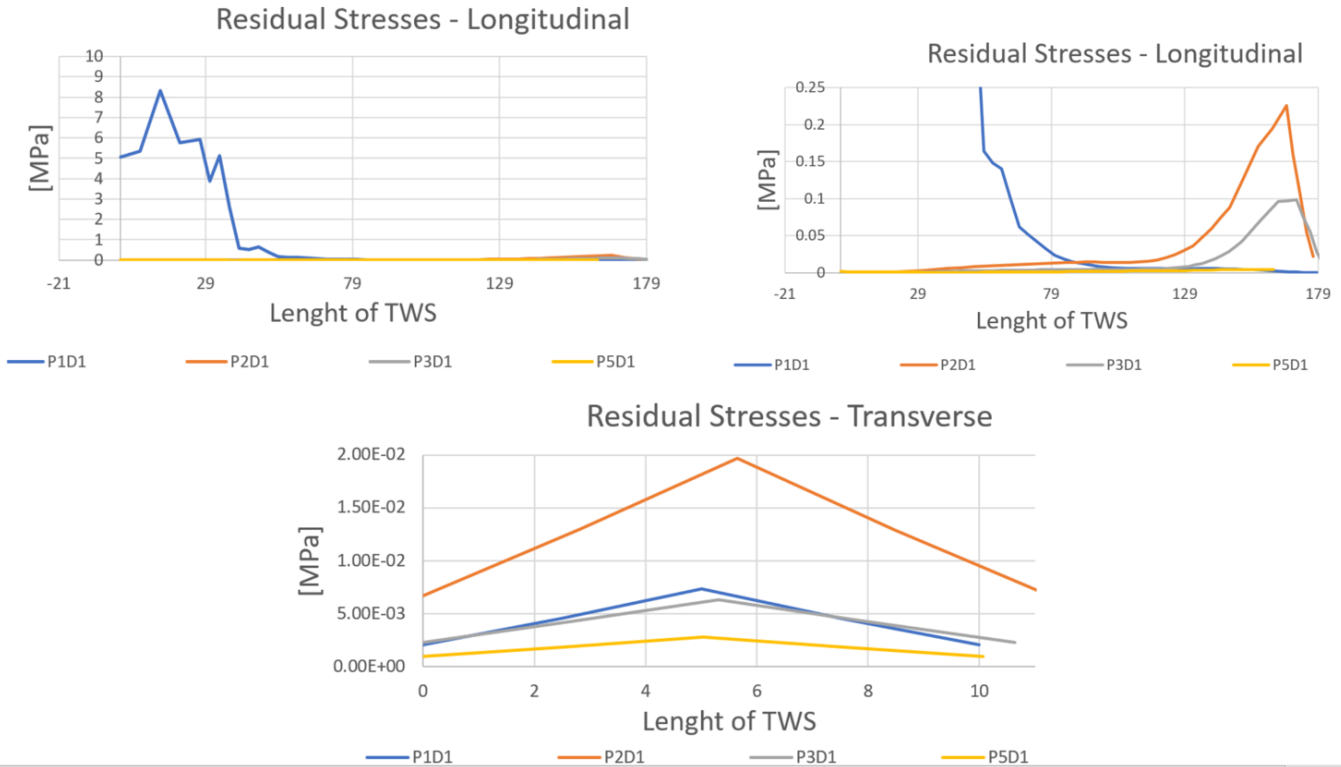
Figure 76: Simulation-result: Residual stresses longitudinal and transverse direction of the x-axis

- **Residual stresses-longitudinal direction** indicates a large deviation in the start of the sample of P1D1 and the other set of parameters. The detailed graph of the longitudinal stresses indicates P5D1 has tremendous low value, equal to zero. The form of the graphs of P2D1 and P3D1 indicates the largest peak of RS at the end of the TWS.

- **Residual stresses-transverse direction** indicates a v-formed behavior of all the samples. Illustrating the stresses, in general, occur in the middle of the thickness in the TWS's. Transverse direction indicates that sample P2D1 has the most considerable amount the RS at 0.002 MPa.

8.2.2   Simulation Result Of TWS: P1D1-P2D2-P4D2

Simulation of 90°angle cross design was performed with three samples with two different set of parameters. Sample P3D3 was not simulated was due to license restriction. The result is presented by eight graphs, which includes deformation and RS along the longitudinal and transverse direction for both horizontal and vertical welding stripe. For the cross-design with 90-degree angle used a long time to cool down than the TWS in general, see appendix I for documentation. The simulated TWS-result are illustrated and documented in appendix H. Maximum RS and temperature value in the fusion zone during the welding resulted in:

- P1D2 - 1968 MPa at 1248°C - details in appendix: H figure 143 for result and I figure 158 for temperature during and after welding.

- P2D2 - 1575 MPa at 1131°C - details in appendix H figure 144 for result and I figure 159 for temperature during and after welding.

- P4D2 - 1555 MPa at 797°C - details in appendix H figure 145 for result and I figure 160 for temperature during and after welding.

The result from the simulation is presented by:

- Deformation-horizontal along the length of the TWS (longitudinal and transverse - direction)

- Deformation-vertical along the length of the TWS (longitudinal and transverse - direction)

- Residual stresses-horizontal along the length of the TWS (longitudinal and transverse - direction)

- Residual stresses-vertical along the length of the TWS (longitudinal and transverse - direction)

8.2.2.1   Deformation along the length of the TWS

The result presents a graph of deformation on a large scale, additionally are a zoomed-in graph with the same result illustrated to provide a detailed graph where the values are to low to investigate.
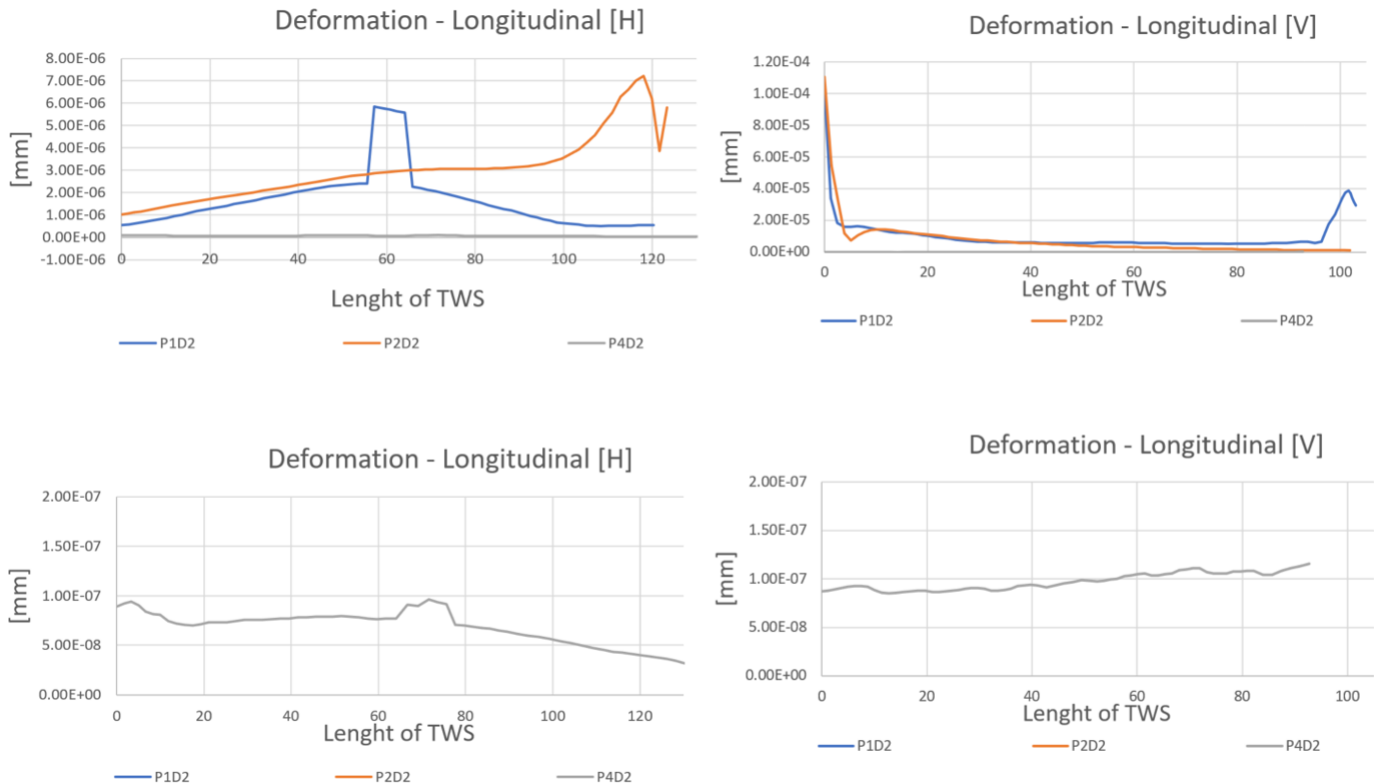
Figure 77: Simulation-result: deformation longitudinal and transverse direction along the horizontal weld

- **Deformation-longitudinal direction - horizontal weld** indicates a large deviation for P1D2 which illustrate the largest peak at the middle of the structure (cross-center) and P2D2 which show the largest amount of RS at the end of the sample. P1D2 and P2D2 occur at a generally low deformation which includes within a range of (1E-05)-(7.5E-06). When zoomed in at the lowest curve of deformation, P4D2, it indicates the largest deviation at the center (Cross of the welds).

- **Deformation-longitudinal direction - vertical weld** indicates a high peak at the start for both P1D2 and P2D2 as they decrease tremendously at a high decline before they hold an almost constant deformation along with the sample. Range of the deformation along the effective welding length is between (9E-06) and (2E-05). P1D2 has a second peak at the end of the weld. P4D2 contain the lowest of deformation around 1E-07 [mm] at an almost constant level has no significant peak.

Deformation along the longitudinal direction in both horizontal and vertical direction has an immense low value, which is at a general level neglectable.

8.2.2.2 Deformation and RS transverse direction of TWS, in horizontal and vertical weld

The result presents a graph of transverse deformation and RS at the horizontal and vertical weld, in a large scale, additionally a zoomed-in graph with the same result illustrated to provide a detailed graph where the values are to low to investigate.
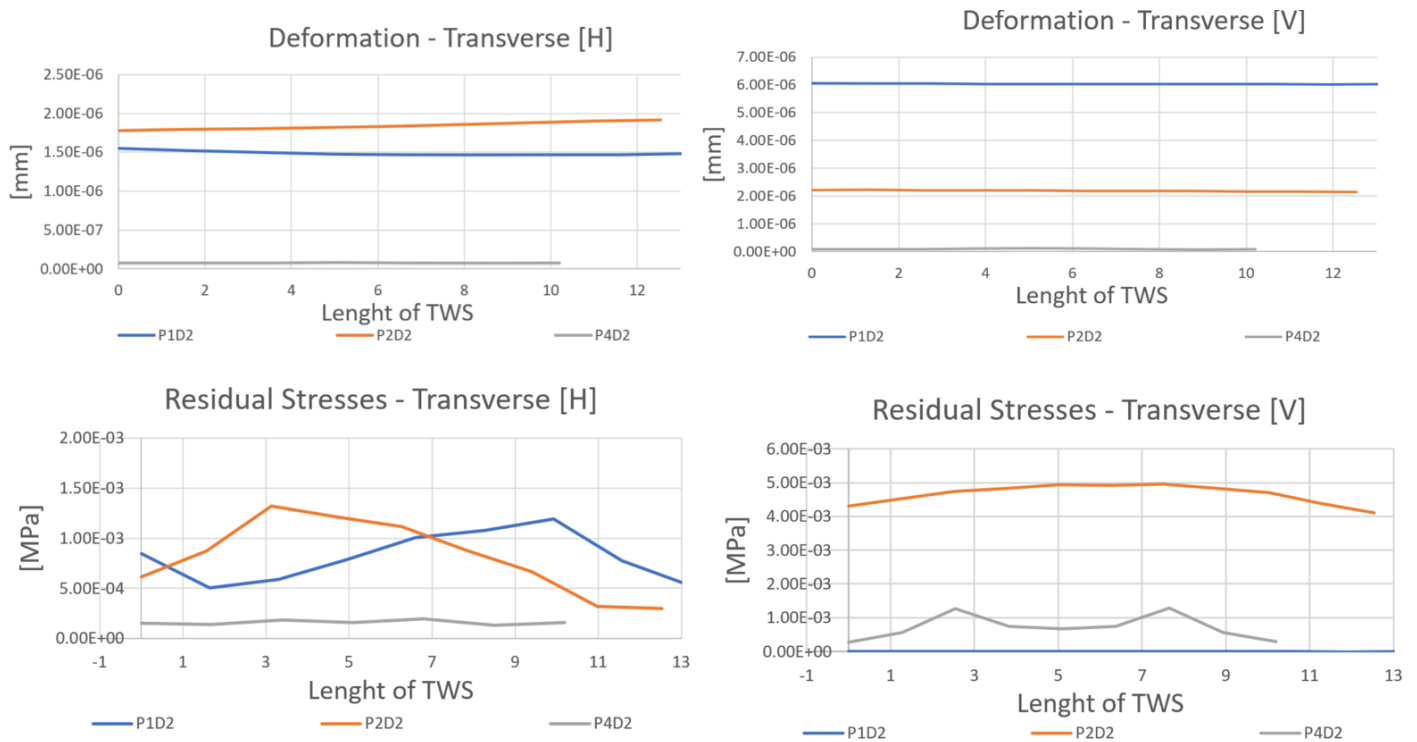
Figure 78: Simulation-result: Transverse direction by deformation (horizontal and vertical) and RS (horizontal and vertical

- **Deformation-transverse direction - horizontal weld** indicates three nearly constant graphs, where P2D2 occur as highest around 1,6E-06 [mm], second highest P1D2 at approximately 1,5E-06 and P4D2 which is close to zero, neglectable in this graph.

- **Deformation-transverse direction - vertical weld** indicates approximately three constant graphs. In this case, P1D2 occur as the highest value with around 6E-06 [mm], P2D2 as second highest at approximately 2E-06 [mm]. As in the horizontal weld are sample P4D2 additionally the lowest in the vertical weld, as neglectable low in this graph.

- **Residual stresses-transverse direction - horizontal weld** indicates P1D2 and P2D2 as an equally large amount of opposite oscillating waves, both peaking at approximately 1,4E-03 [MPa]. P4D2 contains the lowest amount of RS, which is neglectable because of the low level of RS compare to the other samples.

- **Residual stresses-transverse direction - vertical weld** indicates the curve P2D2 as the highest level of RS as it's deformation was lower than P1D2. RS of P1D2 along the

106

vertical weld has the lowest amount, which is close to zero and therefore neglectable in this case. P4D2 appear as the second highest curve of RS, which peaks two times around 1E-03 [MPa].

Deformation and RS along the transverse direction in both horizontal and vertical direction has an immense low value, which is at a general level neglectable.

8.2.2.3   RS longitudinal direction of TWS, in horizontal and vertical weld

The result presents a graph of RS longitudinal direction at the horizontal and vertical weld, in a large scale, additionally a zoomed-in graph with the same result illustrated to provide a detail graph where the values are to low to investigate.
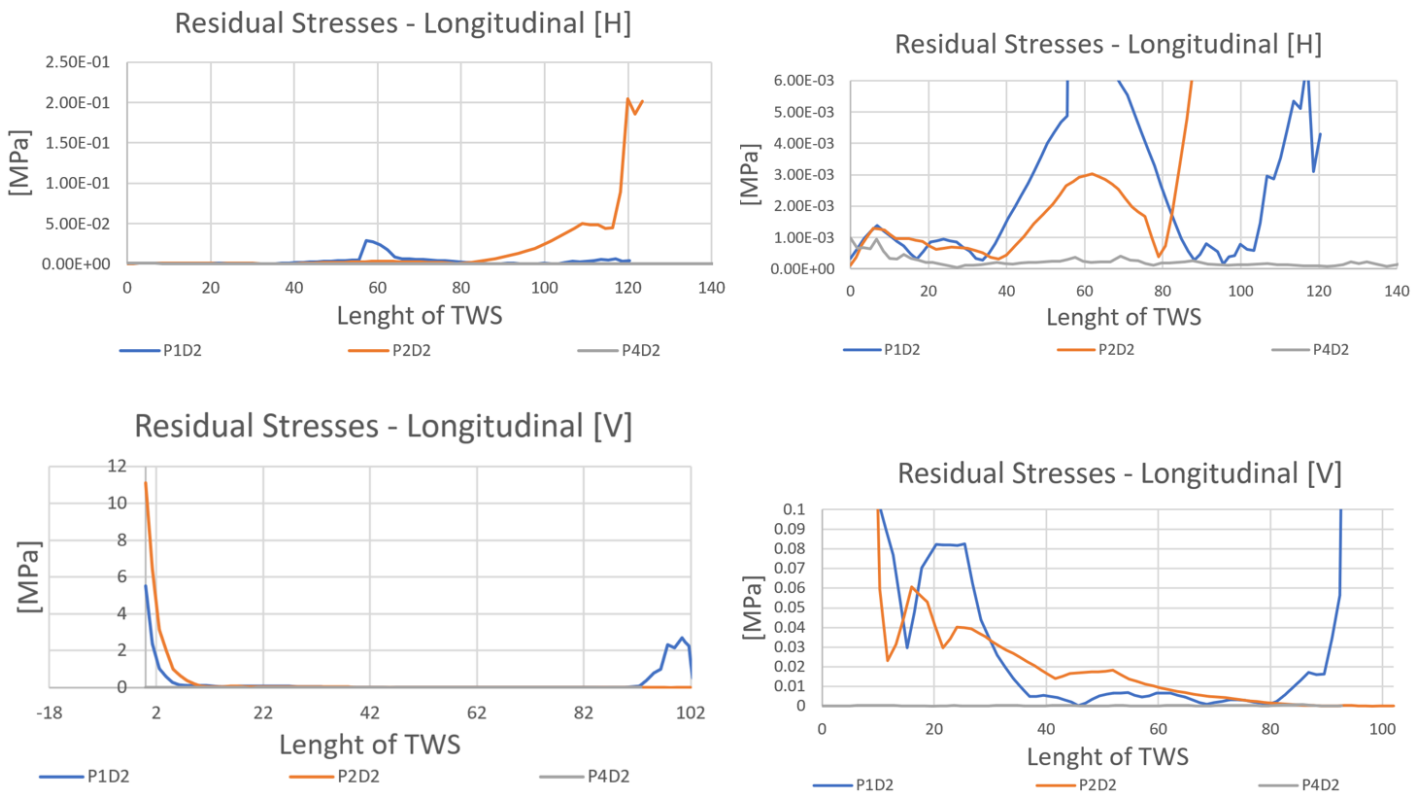
Figure 79: Simulation-result: Residual stresses in longitudinal direction, at horizontal and vertical direction

- **RS-longitudinal direction - horizontal weld** indicates a peak in the center of the cross at P1D2 sample, and a high value at the end of P2D2 compare to P4D2 and P2D2. The investigation from the zoomed-graph shows P2D2 also has a peak at the center cross of the 90°angle structure. P4D2 contain the lowest level of RS, which is below 1E-03 with an approximately constant value along the effective welding length.

- **RS-longitudinal direction - horizontal weld** indicates a tremendously high peak at the start of P2D2 and P1D2 compare to P4D2, P1D2 additional contain a higher peak

at the end of the TWS length. The detailed graph illustrates a low value of RS for both P2D2 and P1D2 along the effective welding length, before P1D2 increase at the end. These values contain below the range of 0.03. P4D2 are below the range of 0.005, which in this comparison is neglectable low.

RS along the longitudinal direction in both horizontal and vertical direction has an immense low value, which is at a general level neglectable.

8.2.3   Simulation Result Of BP: P1D1-P2D1-P3D1-P5D1-P1D2-P2D2-P4D2-P4D3

Simulation of a single stripe structure at the baseplate would inflict thermal stresses and cause shrinkage. Result of simulating design-one at the substrate is done according to present deformation and RS along the longitudinal and transverse direction at the horizontal welding stripe. The cool-down process is described and documented in appendix I as the simulation result of every baseplate are in appendix H. Maximum RS and temperature value in the fusion zone during the welding resulted in:

- P1D2-BP - 2991 MPa at 1152°C - details in appendix: H figure 150 for result and I figure 165 for temperature during and after welding.

- P2D1-BP - 1575 MPa at 1131°C - details in appendix H figure 151 for result and I figure 166 for temperature during and after welding.

- P3D1-BP - 1555 MPa at 797°C - details in appendix H figure 152 for result and I figure 167 for temperature during and after welding.

- P5D1-BP - 1729 MPa at 782°C - details in appendix H figure 149 for result and I figure 164 for temperature during and after welding.

- P1D2-BP - 2890 MPa at 1385°C - details in appendix H figure 149 for result and I figure 164 for temperature during and after welding.

- P2D2-BP - 2521 MPa at 1211°C - details in appendix H figure 149 for result and I figure 164 for temperature during and after welding.

- P4D2-BP - 2719 MPa at 1303°C - details in appendix H figure 149 for result and I figure 164 for temperature during and after welding.

- P4D3-BP - 2187 MPa at 1002°C - details in appendix H figure 149 for result and I figure 164 for temperature during and after welding.

The result from the simulation is presented by:

- Deformation-horizontal along the length of the BP (longitudinal and transverse - direction)

- Deformation-vertical along the length of the BP (longitudinal and transverse - direction)

8.2.3.1   RS and deformation in the longitudinal direction of BP

The result presents a graph of RS and deformation along the longitudinal direction of the substrate, at a large scale, additionally a zoomed-in graph with the same result illustrated to provide a detail graph where the values are to low to inspect.
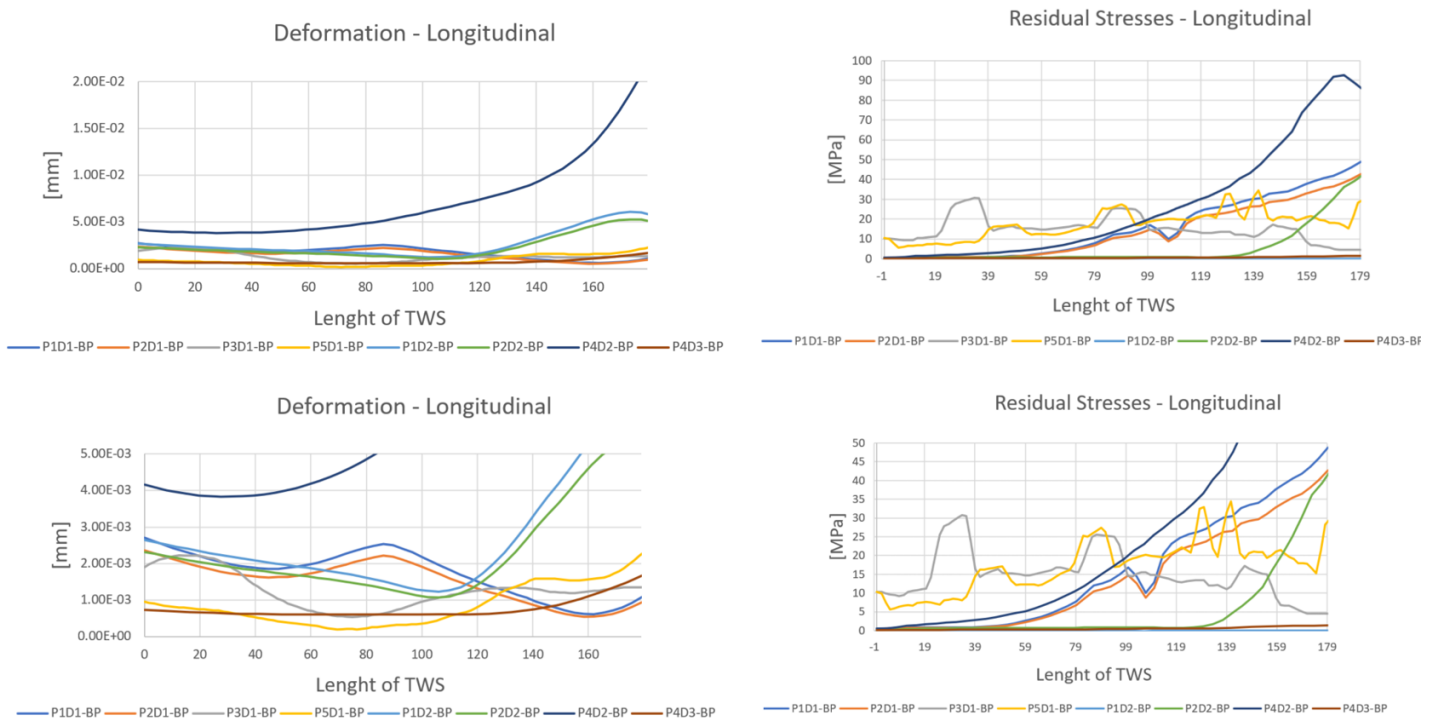
Figure 80: Simulation-result: Residual stresses in longitudinal direction, at horizontal and vertical direction

- **Deformation-longitudinal direction** indicates that the majority has an approximately constant curve with a small deviation at the end. Accept substrate of sample P4D2, which has an increasingly value above the majority of the samples. At the detailed graph below the interference of the graphs are illustrated. The substrate of sample P2D2 and P1D2 stands out as an increase at the end while the others decrease, this occurs approximately in the center of the cross of the 90°angle welded structures.

- **RS-longitudinal direction - horizontal weld** indicates a general behavior of all substrates, as they increase at the end of the sample. P4D2 occur as highest also in the value of RS with the highest peak at 93MPa. Substrate P3D1 and P5D1 act in similar behavior as do P1D1 and P2D1.

RS along longitudinal direction indicates general low for all the substrates, as baseplate P4D2 stands out from the rest of the result. Deformation along longitudinal direction indicates general very low, due to those some substrate can be neglected of the deformation as it also generate an immensely low value of RS.

8.2.3.2   RS and deformation in the transverse direction of BP

The result presents a graph of RS and deformation along the transverse direction of the substrate, at a large scale, additionally a zoomed-in graph with the same result illustrated to provide a detail graph where the values are to low to inspect.
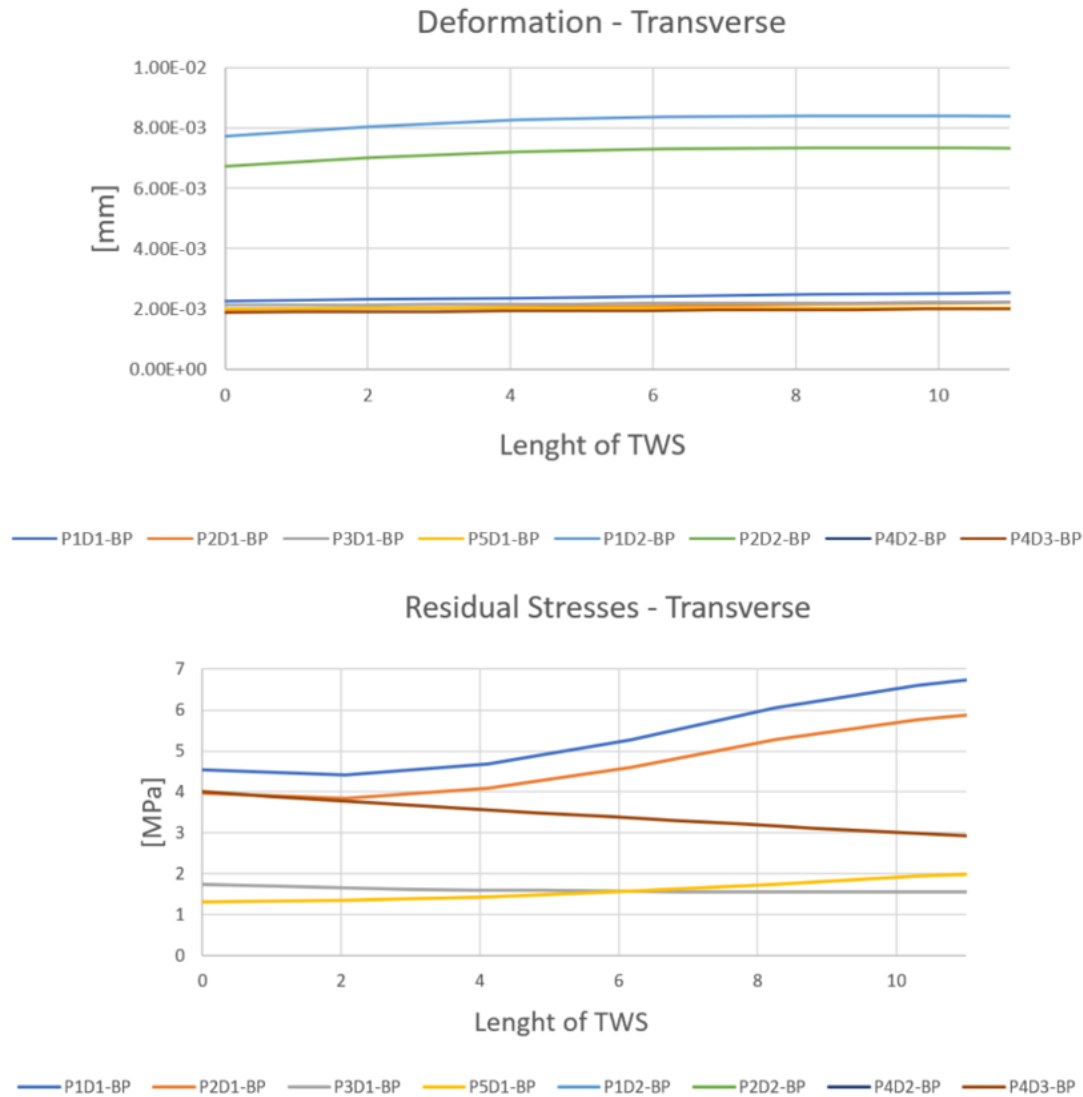
Figure 81: Simulation-result: Residual stresses in longitudinal direction, at horizontal and vertical direction

- **Deformation-transverse direction** indicates the majority of the substrate has an approximately constant curve along the width of the baseplate. The result of P2D2 and P1D2 illustrate a larger value of deformation than the majority of the substrates, where the majority has an immensely low value, which can be considered as neglectable.

- **RS-transverse direction** indicates an overall low value for substrates, which has an approximately equal behavior in this result. P2D1, P1D1, and P4D3 occur as a higher

value within the range 6,5 MPa to 3 MPa, where P1D1 and P2D1 increase at the end of the width.

RS along transverse direction indicates general low for all the substrates, with the highest occurrence above 7 MPa. Deformation along transverse direction illustrates a tremendous low value, which is considered as neglectable.

8.3   Result - Ultrasound Measurement

Ultrasound measurement was performed only at sample P3D1, P2D1, and P1D1 because the other samples had to low height or had to complex structure. The measurement was conducted by five-point along with the sample where measurement along the height was done to take every layer into account. The result contains a constant value of RS along with the height of the TWS, which is divided into five points along with the sample. The substrate was not scanned with ultrasound because the experiment was performed in China, and sending the heavy baseplate would be too expensive. The result is presented in table 19:

Points	RS-P3D1	RS-P2D1	RS-P1D1
1	31.78	197.606	267.787
2	-2.9	136.166	208.267
3	-2.904	118.159	216.907
4	88.296	112.399	184.276
5	33.446	141.199	181.387

Table 19: Ultrasound measurement result

8.4   Comparison of the result

Comparison of the result between the three given methods is arranged in purpose to give an overall view of the result. A direct comparison is presented to state the difference of the outcome of the method and provide an estimated indication of the residual stresses and deformation in the TWS and BP.

8.4.1   Assumptions

Due to the assumptions made regarding the ultrasound measurement in 6.1.1 and calculation of deformation in **??** the value of RS throughout the TWS and BP was stated as constant. Therefore are the result of simulated analyzes simplified to an average value in the purpose of providing an estimated comparison with the result from the experiment of calculation and ultrasound. The result is based upon RS along the longitudinal direction, since there were just three samples which fit the same criteria as the same direction and measurement of RS.

8.4.2   Graphs of the compared result

There are only presented three samples of comparison, due to it was only performed three ultrasound measurement. The three results indicate that the calculation by deformation illustrates the largest amount of RS, ultrasound measurement provided less than half of the value

of the calculation method. At last, the simulation presented the lowest value, which can be neglected compared to the other results.
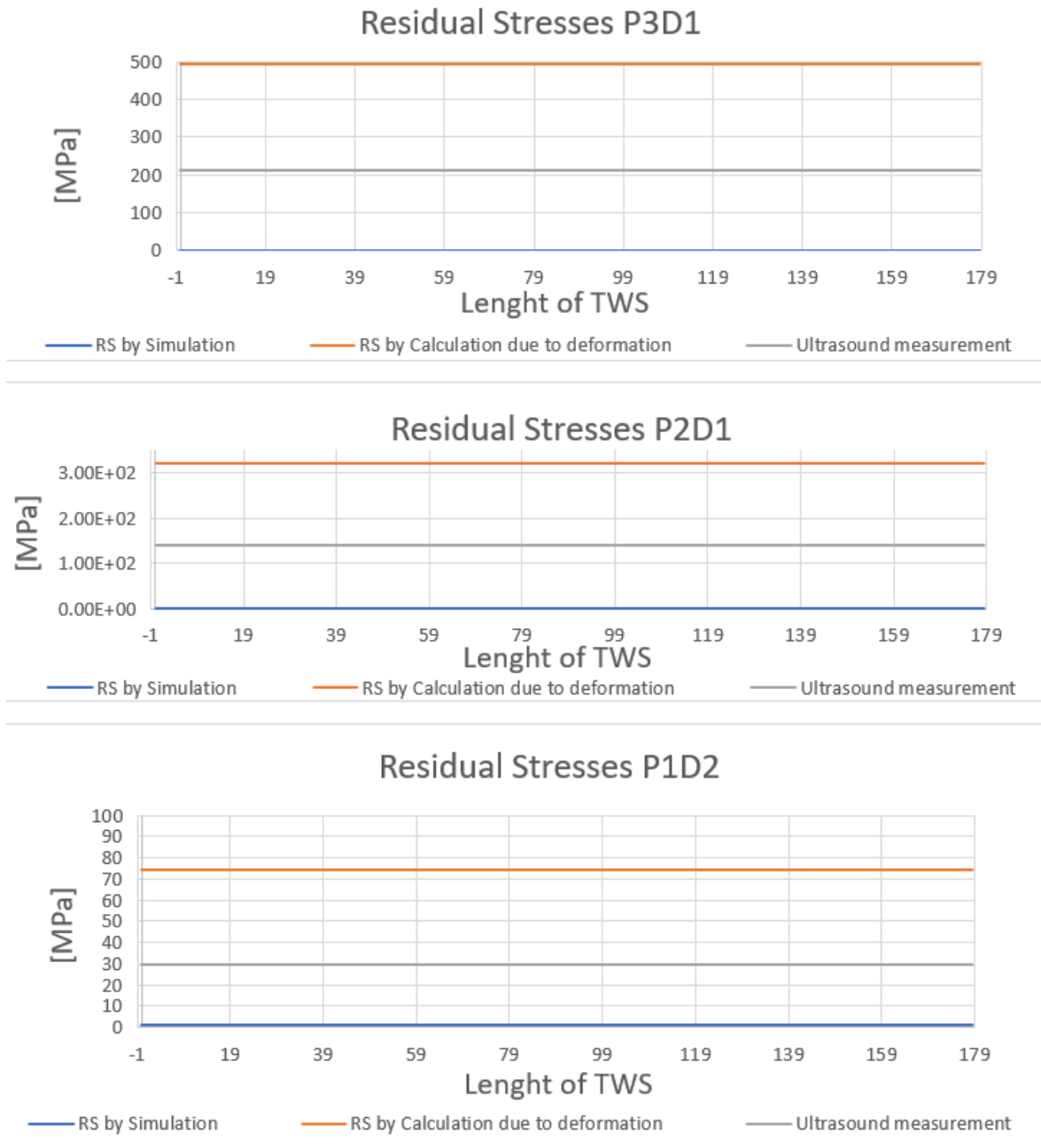
Figure 82: Comparison of the result of simulation, calculation by deformation and ultrasound measurement

8.5 Result - WPQR

Welding procedure qualification record is a developed welding procedure by test and fails by the initial experiment to weld the TWS. The first experiment was to weld the thin wall structure by KUKA-30 robot. The procedure was the first result of the task descriptions. The procedure was developed early due to initiate the welding operations, mentioned in 4.8.3. The purpose of the procedure was to document the structures welding operation and to document the layer description in appendix A. The WPQR contains information about:

- Technique

- Process

- Cleaning

- Filler metal

- Welding plan (position and angle)

- Heat treatment

- Preheat

- Post working heat treatment

- Identification of materials

- Welding Parameter

In appendix, J are WPQR for every sample documented, which represented as the procedure illustrate at the next page for TWS P1D1. Note WPQR number 1,2 and 3 were welded at the other position than the welding planning illustrated at the end of the sheet. Because the welded parts were welded at the same baseplate to save material, this was additional the case with WPQR number six and seven.

9   Discussion

The dissertation involves three practical experiments addition to a FEM-simulation which provided estimated values of the RS and distortion of the TWS and BP. The purpose of comparing the result to create a strong argument for the task description. The initial research entailed a process of WAAM by GTAW to build a layer-wise thin wall structure with the KUKA-30 robot. During the research, it has proven difficulties and potential for improvement, which are elaborated further in this section.

The leading causes of the errors during the welding process were due to the uneven surface of the TWS after the first layers. The sources of errors generally occurred initially between 6th-12th layer, as additional layers made after 6-7[mm], more frequent production failures occurred. High heat input turned out to generate errors concerning decreasing the height and generate melted spots. The reason was due to the selected parameters with high current.

From the result in appendix A and C, it notably indicated the vertical TWS in the 90°structure to possess a steep start and end additional to a low total height of the component. Potential this could emerge from the high heat input which melted down when wire feed error occurred, as the heat only affected the surface instead of melting the wire material. It could potentially compromise the height and form of the thin wall structure. Because of the high level of incline and decline from beginning to the end of the sample, the tungsten crashed, wire feeder missed the melting pool or system has generated a general error. If the length of the TWS had expanded, the sufficient welding length would equally be increased. Thus, causing the inefficient welding length at the start and end of the weld to be further apart. The welding process would then be more capable by laying the welding stripe on top of each other in a more smooth manner and hence preventing the high level of incline. The reason the P4D3 was designed to contain a 20°angle of the cross-structure was to achieve a longer sufficient welding length. By allowing the "horizontal" weld to fit within the substrate by a with at 99 [mm]. If the welding system could compensate for the height difference along the surface, this could solve the majority of the defect in the layers.

The second experiment, calculation by deformation, involved measuring the TWS height before and after it was cut off the substrate by a grinder. By the measured height difference, deformation along the neutral axis in the component could be investigated. The assumption by using Euler Bernoulli beam theory TWS takes a beam into account regarding the calculation. In this theory, the deformation only allowed exceedingly small changes in height along the length of the structure. This appeared as the main issue by the experiments calculation because the factors of generating RS entailed deformation additional to the elasticity modulus and height of the neutral axis. Due to the high values provided from the result in 8.1, it indicates either the height measurement are compromised, or the chosen theory is a wrong assumption to take into account because the deformation is too high for this method.

The measuring device (altimeter) could cause wrongly result when it was not correctly reset at every measure. Additional the samples were re-installed to the fracture area for every measurement which had an impact of the accuracy in the result. The investigation by the result of the base plates indicated a smooth increasingly/decreasingly delta-h along the substrate,

caused a low value of RS for the majority of the results. That was because the deviation occurred mainly caused by the measuring device, and had none fracture area into consideration The most substantial measured value of deformation was detected above 3 [mm] and (-2) [mm], which in practice should not fit the fracture area at both sides of the sample due to the bending of thermal stresses. Which it did, if not the height measurement would not be possible. Thus, it indicates the manual use of altimeter additional with fracture area caused an unsteady measure to originate from human error and equipment failures.

Regarding height measurement of TWS and BP before and after cut of the weld, would enhancement of measuring device be a better choice rather than a difference of calculation technique or a new RS-test method. The main reason is to investigate RS and deformation after internal stresses are relieved for further use of the product. Additional it was not possible to perform another type of RS-test at UiT Campus Narvik. Improvement for the calculation by deformation-test could include utilizing a digital measurement scanner for scanning the TWS and substrate before and after the cut. Although, the cut of the structure-components could potentially cause an issue of providing a fracture area to re-install the component back at the substrate for scanning. Potential methods of cutting the TWS from the substrate were introduced in section 5.1.2, where EmD- electrical discharge machining process could be a suitable candidate. The method by cutting with the grinder at the middle part and then knock the remaining portion off by a plastic hammer to achieve the fracture area distorted the contact area to place the TWS after the cut. Comparable, would the EmD generate a smooth fracture area

FEM-simulation analyzes performed in ANSYS, provided a low value of RS and deformation for both substrate and TWS, due to the assumptions made in 7.3.6.4. Comparison between the simulation and actual welding process was not accurate as of the simulation only considered the top layer of the structure instead of the whole structure. Although the assumption state the simulated result at the top layers regards for every segment of the TWS, does the result only cover a strong estimation of the RS and deformation within the component and substrate. Not all main parameters were taken directly into account. The welding speed was taken into consideration by the selection of the efficient thermal coefficient(figure 61, avhc automatically adjusted the magnitude of the voltage and wire feeder excluded from the simulation. Instead, the welding speed and avhc had an impact on the used parameters for the simulation, involved; voltage, current, and efficient thermal coefficient.
Improvement in the thesis would be to extend the license of the program, to achieve the additive manufacturing application. The app which can be downloaded through the program allows an actual simulation of a wire arc additive manufacturing by TIG welding. If the application could be implemented, the simulation could simulate the actual production process more accurate. Additional it allows simulating larger and more complicated structures, which is why the TWS P4D3 wasn't simulated.

The ultrasound measurement is the last RS-test experiment, by assumptions made in 6.1.1. The test was simplified with excluding the uniaxial tensile test to find the acoustoelastic constant of the material. The majority of the welded structure had a low height below 25 [mm]. Therefore was ultrasound scan was conducted at the three first welded samples with a height at 40 [mm] and above. Reason for this was due to the vertical scan by the transducer

to include all layers within each scan along with the sample. A vertical scan was predicted to provide the most substantial amount of RS. Measurement along the surface at the top layer with a low-frequency transducer could be implemented, by scanning the layers in the longitudinal direction. However, due to not adequate time, it was not performed.

Comparison of the result illustrated in 8.4, based on the assumption given; each RS-test is presented as a constant value through the TWS's. The result in 8.4.2 illustrates a vast difference in the RS-methods of simulation, ultrasound, and calculation by deformation-test. Because the errors of measurement compromise the result in the experiment: calculation by deformation. The RS-values occurs at an unrealistic high value were only a few results of the TWS can be related too. If the stress factor in the ultrasound method decreased from 9.6 to 1 or 2, the RS-result would correspond with the result from the FEA-simulation. However, this was not tested due to not adequate time.

By excluding the compromised measurement in the initial RS-test (calculation by deformation), would the general values for the two experimental methods and the simulation indicate a low value of RS and deformation in TWS and BP. To emphasize are the result generated from the investigation of RS-methods. Are the data a strong estimation compare to the reality, because of the assumption made for each method. The base plate, on the other hand, illustrates a smooth and steady data for both calculations by deformation-test and simulation, see 8.1 and 8.2.3. The reason for this is due to lesser compromised measurement data and assumptions which the TWS needed to gain the result.

The value of RS and deformation was at a general basis estimated low, comparable to the yielding strength at the material, which is 400 MPa. The estimated low data regards only the data which was not he compromised data in the calculation by deformation-test. Additional even though the RS and deformation were at an acceptable value, the TWS's geometry after the welding process was not acceptable for the TWS's with 90°and 20°angle. As shown at the result by the finish produced TWS in L, are sample P1D2, and P2D2 welded samples which were a failure in terms of acceptable welded. The two 90°cross structures were welded with high heat input and a short sufficient welding length along the horizontal TWS. Thus, caused the high and low incline at the start and end of the horizontal TWS of P1D1 and P2D2.

10   Conclusion

Elaborated in the problem statement 3.3 was the wanted outcome of the dissertation revealed. Furthermore is the thesis task descriptions answered according to three experiments (Welding-process, RS-calculation by deformation, ultrasound measurement), FEA-simulation in ANSYS and by WPQR documentation of the weldment. The thesis task outcome is concluded below:

- Outcome of the welded experiment resulted in 9 successfully welding processes, where the two tests P1D2 and D2D2 were deemed to be unacceptable due to short sufficient welding length at the horizontal TWS. The 4th test was excluded from the result due to the inefficient welding process.

- Investigation of the residual stresses and distortion at the thin wall structure and base plate appear as a generally low estimated value (except compromised result due to method error).

- Documented welding process was accomplished by a successful WPQR (welding procedure qualification record).

Critical comment concerning the result of the TWS production process and RS-test's are elaborated based upon the experience from the dissertations-research

For establishing lesser errors and better structure, longer sufficient welding length is obliged. Thus, include longer welds along horizontal and vertically. However, horizontal TWS is feasible with more extensive substrates along the width.

Because delta-h was such a remarkably sensitive factor, and the measure had a high amount of deviation, it states the reason for "high" deformation was due to inaccurate measurement. Thus, this study recommends another measuring device as a digital scanner, if not another RS-test method is implemented.

Due to a large amount of assumption made during the experiments can the research conclude the result are a strong estimation including a low value of RS and deformation in TWS and BP. Thus, the component is highly usable after production. However, this doesn't involve the compromised result due to human and equipment error (measured height of the calculation by deformation-experiment).

Purpose of creating 90°and 20°cross structures was to investigate if it generated a higher value of RS, which turns out it didn't happen by the founding.

Even though the RS and deformation were generally estimated low for all results, was not all TWS possible to weld a height above 40 [mm], due to errors occurred frequently after a height of 6-7 [mm] in the welding process.

Production time was long, mostly due to the cooling of the material after welding. Although, slow cooling is essential to achieve a good (post-welding heat treatment), which reduce RS in the welded part by relieving the thermal stresses.

Wire Arc Additive Manufacturing with Gas Tungsten Arc Welding is not recommended to replace traditional machining and milling technology as current status stands now. The statement regards layer by layer welding to create structures for a certain height above 6-7[mm]. Only single stripe welds and low altitude-TWS does the current system provide acceptable results.

The reason why the current status of welding TWS for higher heights is not recommended is due to the current robot KUKA-30 system. It could only weld linear lines were the welded structures also need machining afterward. Additional to the time-consuming production process, the welding program needs to be further developed. The current equipment and welding program are too limited, by the meaning of this that the robot cannot weld in incline/Decline environment or along uneven surfaces. Additional it cannot weld anything else than straight lines, and it causes welding errors which compromises the TWS.

However, with a more complex robot-system that welds structures in a faster time and provide fewer defects would the question of a better production technique be a different case.

References

[1]   Donghong Ding et al. "Process Planning Strategy for Wire and Arc Additive Manufacturing". In: vol. 363. Oct. 2014. DOI: 10.1007/978-3-319-18997-0_37.

[2]   Vladimir Luzin and Nicholas Hoye. "Stress in Thin Wall Structures Made by Layer Additive Manufacturing". In: (July 2016). DOI: 10.21741/9781945291173-84.

[3]   R.J. Silva, G.F. Barbosa, and J. Carvalho. "Additive Manufacturing of Metal Parts by Welding". In: *IFAC-PapersOnLine.* Volume 48.3 (2015). 15th IFAC Symposium onInformation Control Problems inManufacturing, pp. 2318–2322. ISSN: 2405-8963. DOI: https://doi.org/10.1016/j.ifacol.2015.06.433. URL: http://www.sciencedirect.com/science/article/pii/S2405896315006722.

[4]   E. Halmøy. *Sveiseteknikk.* International series of monographs on physics. Norges tekniske høgskole, Institutt for materialer og bearbeiding, 1993.

[5]   Weldinghistory.org. *Welding History.* 2015. URL: http://www.weldinghistory.org/whfolder/folder/whpre1800.html. (accessed: 10.11.2018).

[6]   www.GoWelding.Org. *The History of Welding.* 2014. URL: http://gowelding.org/articles/history-of-welding/. (accessed: 12.11.2018).

[7]   Jean Cornu. "Basic Definitions in Welding". In: *Fundamentals of Fusion Welding Technology.* Ed. by John Weston. Berlin, Heidelberg: Springer Berlin Heidelberg, 1988, pp. 11–14. ISBN: 978-3-662-11049-2. DOI: 10.1007/978-3-662-11049-2_2. URL: https://doi.org/10.1007/978-3-662-11049-2_2.

[8]   Werner Solken. *Gas Tungsten Arc Welding (GTAW).* 2014. URL: http://www.wermac.org/others/welding_tig_gas-tungsten-arc-welding-process_gtaw.html. (accessed: 12.11.2018).

[9]   R Blondeau. "Metallurgy and mechanics of welding". In: *Welding stainless steels* (Jan. 2008), p. 20.

[10] Jola Lewenski. *Fundamentals of gas tungsten arc welding.* 2003. URL: https://hypertextbook.com/facts/2003/JolaLewinski.shtml. (accessed: 12.11.2018).

[11] M.Arunprasath N.Jeyaprakash Adisu Haile. "Metallurgy and mechanics of welding". In: *The International Journal Of Engineering And Science.* Volume 4 (2015), pp. 11–20.

[12] Do Won Seo, Yang Bae Jeon, and Jae Kyoo Lim. "Effect of Electric Weld Current on Spatter Reduction in Spot Welding Process". In: *Advances in Fracture and Failure Prevention.* Vol. 261. Key Engineering Materials. Trans Tech Publications, Mar. 2004, pp. 1623–1628. DOI: 10.4028/www.scientific.net/KEM.261-263.1623.

[13] S. P. Tewari, Ankur Gupta, and Jyoti Prakash. "EFFECT OF WELDING PARAMETERS ON THE WELDABILITY OF MATERIAL". In: *International Journal of Engineering Science and Technology* Volume 2 (2010), pp. 512–516.

[14]   T.E Abioye. "The Effect of Heat Input on the Mechanical and Corrosion Properties of AISI 304 Electric Arc Weldments". In: *British Journal of Applied Science and Technology* Volume 20 (5 2017).

[15]   Wichan Chuaiphan and Loeshpahn Srijaroenpramong. "Effect of welding speed on microstructures, mechanical properties and corrosion behavior of GTA-welded AISI 201 stainless steel sheets". In: *Journal of Materials Processing Technology* 214.2 (2014), pp. 402–408. ISSN: 0924-0136. DOI: `https://doi.org/10.1016/j.jmatprotec.2013.09.025`. URL: `http://www.sciencedirect.com/science/article/pii/S0924013613003026`.

[16]   Bolarinwa Johnson Kutelu et al. "Review of GTAW Welding Parameters". In: *Journal of Minerals and Materials Characterization and Engineering.* Volume 6.No.5 (2018).

[17]   A Choubey and Vijaykumar Jatti. "Influence of heat input on mechanical properties and microstructure of austenitic 202 grade stainless steel weldments". In: *WSEAS Transactions on Applied and Theoretical Mechanics* Volume 9 (Jan. 2014), pp. 222–228.

[18]   B.Y. Kang et al. "The effect of alternate supply of shielding gases in austenite stainless steel GTA welding". In: *Journal of Materials Processing Technology.* Volume 209.10 (2009), pp. 4722–4727. ISSN: 0924-0136. DOI: `https://doi.org/10.1016/j.jmatprotec.2008.11.035`. URL: `http://www.sciencedirect.com/science/article/pii/S0924013608008315`.

[19]   Prachya Peasura and Anucha Watanapa. "Influence of Shielding Gas on Aluminum Alloy 5083 in Gas Tungsten Arc Welding". In: *Procedia Engineering.* Volume 29 (2012). 2012 International Workshop on Information and Electronics Engineering, pp. 2465–2469. ISSN: 1877-7058. DOI: `https://doi.org/10.1016/j.proeng.2012.01.333`. URL: `http://www.sciencedirect.com/science/article/pii/S1877705812003438`.

[20]   M.Arunprasath N.Jeyaprakash Adisu Haile. "The Parameters and Equipments Used in TIG Welding: A Review". In: *The International Journal Of Engineering And Science.* Volume 4 (2015), pp. 11–20.

[21]   Igor Shishkovsky. "Synthesis of functional gradient parts via RP methods". In: *Rapid Prototyping Journal.* Volume 7,No 4, (2001), pp. 207–211. DOI: `10.1108/13552540110402908`.

[22]   Nikola Knezović and Angela Topić. "Wire and Arc Additive Manufacturing (WAAM) – A New Advance in Manufacturing". In: *New Technologies, Development and Application.* Ed. by Isak Karabegović. Cham: Springer International Publishing, 2019, pp. 65–71.

[23]   IvánTabernero et al. "Study on Arc Welding Processes for High Deposition Rate Additive Manufacturing". In: *Procedia CIRP* 68 (2018). 19th CIRP Conference on Electro Physical and Chemical Machining, 23-27 April 2017, Bilbao, Spain, pp. 358–362. ISSN: 2212-8271. DOI: `https://doi.org/10.1016/j.procir.2017.12.095`. URL: `http://www.sciencedirect.com/science/article/pii/S2212827117310363`.

[24]   Barbosa GF* and Aroca RV. "An IoT-Based Solution for Control and Monitoring of Additive Manufacturing Processes". In: *Journal of Powder Metallurgy Mining.* Volume 6.1 (2017), pp. 1–7. ISSN: 2168-9806. DOI: `10.4172/2168-9806.1000158`. URL: `https://www.omicsonline.org/open-access/an-iotbased-solution-for-control-and-monitoring-of-additivemanufacturing-processes-2168-9806-1000158.php?aid=86466`.

[25]   www.sveis.no. *Nytt utvalg av solidtråder designet for Wire Arc, Additive Manufacturing.* Norsk Sveiseteknisk Forbund. Oslo, 2018.

[26]   C.Shanben, Z.Yuming, and F.Zhili. *Transactions on Intelligent Welding Manufacturing.* Vol. Volume 1. 2520-8519 No.1. Springer Singapore, 2017.

[27]   A. Fallahi, K. Jafarpur, and M.R. Nami. "Analysis of welding conditions based on induced thermal irreversibilities in welded structures: Cases of welding sequences and preheating treatment". In: *Scientia Iranica* 18.3 (2011), pp. 398–406. ISSN: 1026-3098. DOI: `https://doi.org/10.1016/j.scient.2011.05.030`. URL: `http://www.sciencedirect.com/science/article/pii/S1026309811000952`.

[28]   A.G. Olabi and M.S.J. Hashmi. "The effect of post-weld heat-treatment on mechanical-properties and residual-stresses mapping in welded structural steel". In: *Journal of Materials Processing Technology* 55.2 (1995). Conference of the Irish Manufacturing Committee on advanced manufacturing technology, pp. 117–122. ISSN: 0924-0136. DOI: `https://doi.org/10.1016/0924-0136(95)01794-1`. URL: `http://www.sciencedirect.com/science/article/pii/0924013695017941`.

[29]   www.weldpedia.com. *Welding Preheat Considerations.* 2015. URL: `https://www.weldpedia.com/2015/12/welding-preheat-considerations.html`. (accessed: 03.12.2018).

[30]   enginemechanics.tpub.com. *Welding Sequence.* URL: `http://enginemechanics.tpub.com/14119/Figure-7-16-A-Backstep-Sequence-B-Wandering-Seqeunce-208.html`. (accessed: 03.12.2018).

[31]   Y.C. Lin and K.H. Lee. "Effect of preheating on the residual stress in type 304 stainless steel weldment". In: *Journal of Materials Processing Technology* 63.1 (1997), pp. 797–801. ISSN: 0924-0136. DOI: `https://doi.org/10.1016/S0924-0136(96)02727-6`. URL: `http://www.sciencedirect.com/science/article/pii/S0924013696027276`.

[32]   Guangming Fu et al. "Influence of the welding sequence on residual stress and distortion of fillet welded structures". In: *Marine Structures* Volume 46. (2016), pp. 30–55. ISSN: 0951-8339. DOI: `https://doi.org/10.1016/j.marstruc.2015.12.001`. URL: `http://www.sciencedirect.com/science/article/pii/S0951833915001021`.

[33]   Einar Halmøy. *Sveiseteknikk.* 2520-8519. Trondheim, Norges tekniske høgskole, Institutt for materialer og bearbeiding, 1991. URL: `https://urn.nb.no/URN:NBN:no-nb_digibok_2007082404076`.

[34] R. Scott Funderburk. "Key Concept: Postweld Heat Treatment". In: *American Society for Metals* Volume 15.No 2 (1998).

[35] A.G. Olabi and M.S.J. Hashmi. "The effect of post-weld heat-treatment on mechanical-properties and residual-stresses mapping in welded structural steel". In: *Journal of Materials Processing Technology.* Volume 55.No 2. (1995). Conference of the Irish Manufacturing Committee on advanced manufacturing technology, pp. 117–122. ISSN: 0924-0136. DOI: `https://doi.org/10.1016/0924-0136(95)01794-1`. URL: `http://www.sciencedirect.com/science/article/pii/0924013695017941`.

[36] Ravinder Reddy Pinninti. *Simulation of TIG Welding Process.* Dec. 2014. ISBN: ISBN-13:978-3-659-66574-5, ISBN-10: 3659665746, EAN: 9783659665745.

[37] C.L. TSAI and D.S. KIM. "1 - Understanding residual stress and distortion in welds: an overview". In: *Processes and Mechanisms of Welding Residual Stress and Distortion.* Ed. by Zhili Feng. Woodhead Publishing Series in Welding and Other Joining Technologies. Woodhead Publishing, 2005, pp. 3–31. ISBN: 978-1-85573-771-6. DOI: `https://doi.org/10.1533/9781845690939.1.3`. URL: `http://www.sciencedirect.com/science/article/pii/B978185573771650001X`.

[38] Harinadh Vemanaboina, Suresh Akella, and Ramesh Kumar Buddu. "Welding Process Simulation Model for Temperature and Residual Stress Analysis". In: *Procedia Materials Science* 6 (2014). 3rd International Conference on Materials Processing and Characterisation (ICMPC 2014), pp. 1539–1546. ISSN: 2211-8128. DOI: `https://doi.org/10.1016/j.mspro.2014.07.135`. URL: `http://www.sciencedirect.com/science/article/pii/S2211812814005008`.

[39] Ivar Eriksen. "Setup and Interfacing of a KUKA Robotics Lab". Dec. 2017. URL: `http://hdl.handle.net/11250/2490915`.

[40] E. Halmøy. *KUKA Robots.* KR 30, 60-3; KR 30 L16-2. Augsburg, Germany, 1993.

[41] http://www.directindustry.com. *WIRE FEEDER Unit KD 4000 D-11.* 2018. URL: `http://www.directindustry.com/prod/fronius/product-5983-470753.html)`. (accessed: 09.12.2018).

[42] https://www.fronius.com/en. *WIRE FEEDER Unit KD 4000 D-11.* 2018. URL: `https://www.fronius.com/en/downloads#!/searchconfig/%5C%7B%5C%22countryPath%5C%22%5C%3A%5C%22%5C%2Fsitecore%5C%2Fcontent%5C%2FHome%5C%22%5C%2C%5C%22language%5C%22%5C%3A%5C%22en%5C%22%5C%2C%5C%22token%5C%22%5C%3A%5C%228nn9qexafsicopp4cpsaxs%5C%22%5C%2C%5C%22id%5C%22%5C%3A%5C%22b20cdde1-37f9-49a6-8fc7-383ba592f567%5C%22%5C%2C%5C%22searchword%5C%22%5C%3A%5C%22wire%5C%20feeder%5C%22%5C%2C%5C%22dateStart%5C%22%5C%3Anull%5C%2C%5C%22dateEnd%5C%22%5C%3Anull%5C%7D`. (accessed: 09.12.2018).

[43] www.yaang.com. *X3CrNiMo13-4 Standard.* URL: `https://www.yaang.com/data-center/Standard/x3crnimo13-4-standard.html`. (Accessed 10 Mai 2019).

[44] BÖHLERwelding. *BÖHLER EMK 6*. URL: `https://cn.bing.com/search?q=share+latex+cite+pdf&qs=n&form=QBRE&sp=-1&pq=share+latex+cite+pdf&sc=1-20&sk=&cvid=D99EB5540B8346F6BF9425C498EFD99E`. (Accessed 10 Mai 2019).

[45] https://www.fronius.com/en. *WIRE FEEDER Unit KD 4000 D-11*. 2018. URL: `http://www.vabw-service.com/documents/boehler/datenblaetter/en/L1_34457_en__B_Boehler%5C%20emk%5C%206%5C%20NC_de_en_3.pdf?cache=1544363833`. (accessed: 09.12.2018).

[46] KUKA Robot Group. *KR C2 edition 05*. KR 30, 60-3; KR 30 L16-2. Augsburg, Germany, 2007.

[47] http://www.pennstainless.com. *304L Stainless Steel*. 2018. URL: `http://www.pennstainless.com/stainless-grades/300-series-stainless-steel/304l-stainless-steel-2/`. (accessed: 11.12.2018).

[48] www.yaang.com. *X3CrNiMo13-4 Standard*. 2018. URL: `https://www.yaang.com/data-center/Standard/x3crnimo13-4-standard.html`. (accessed: 11.12.2018).

[49] Tomas Maske. "Heavy multi-pass TIG welding". Oct. 2017. URL: `http://hdl.handle.net/10037/11066`.

[50] "Methods of measuring residual stresses in components". In: *Materials Design* 35 (2012). New Rubber Materials, Test Methods and Processes, pp. 572–588. ISSN: 0261-3069. DOI: `https://doi.org/10.1016/j.matdes.2011.08.022`. URL: `http://www.sciencedirect.com/science/article/pii/S0261306911005887`.

[51] K H Kloos E Macherauch. "Measurements and Evaluation of Residual Stresses". In: *Residual Stresses in Science and Technology* (1987), 3s–26s.

[52] "Using finite element and ultrasonic method to evaluate welding longitudinal residual stress through the thickness in austenitic stainless steel plates". In: *Materials Design* 45 (2013), pp. 628–642. ISSN: 0261-3069. DOI: `https://doi.org/10.1016/j.matdes.2012.09.038`. URL: `http://www.sciencedirect.com/science/article/pii/S0261306912006693`.

[53] www.olympus-ims.com. *Ultrasonic Tranducers*. Copyright 2010 by Olympus NDT. (accessed: 25.03.2019).

[54] Fatih Uzun. "Total Residual Stress Measurement by Using Ultrasonic Technique". In: *Gazi University Journal of Science* 24 (Sept. 2010), pp. 135–141.

[55] Jian Lu and Society for Experimental Mechanics (U.S.) *Handbook of measurement of residual stresses*. English. Lilburn, GA : Fairmont Press ; Upper Saddle River, NJ : Distributed by Prentice Hall PTR, 1996. ISBN: 088173229X (Fairmont Press).

[56] Y. Kudryavtsev and J. Kleiman. "Ultrasonic Technique and Equipment for Residual Stresses Measurement". In: *Engineering Applications of Residual Stress, Volume 8*. Ed. by Tom Proulx. New York, NY: Springer New York, 2011, pp. 55–66.

[57]   Yuri Kudryavtsev, Jacob Kleiman, and Helena Polezhayeva. "Ultrasonic Measurement of Residual Stresses in Welded Elements of Ship Structure". In: *Advances in Experimental Mechanics VIII*. Vol. 70. Applied Mechanics and Materials. Trans Tech Publications, Sept. 2011, pp. 273–278. DOI: `10.4028/www.scientific.net/AMM.70.273`.

[58]   T.D.Murnaghan and John Wiley. *Finite Deformation of an elastic solid*. English. New York, 1951.

[59]   D. S. Hughes and J. L. Kelly. "Second-Order Elastic Deformation of Solids". In: *Phys. Rev.* 92 (5 Dec. 1953), pp. 1145–1149. DOI: `10.1103/PhysRev.92.1145`. URL: `https://link.aps.org/doi/10.1103/PhysRev.92.1145`.

[60]   Yashar Javadi and Sergej Hloch. "Employing the L-CR Waves to Measure Longitudinal Residual Stresses in Different Depths of a Stainless Steel Welded Plate". In: *Advances in Materials Science and Engineering* 2013 (Aug. 2013). DOI: `10.1155/2013/746187`.

[61]   VEQTER.co.uk. *X-Ray Diffraction*. URL: `https://www.veqter.co.uk/residual-stress-measurement/x-ray-diffraction`. (accessed: 30.04.2019).

[62]   Osman Anderoglu. "Residual stress measurement using X-ray diffraction". In: (Apr. 2019).

[63]   M. Safarabadi and M.M. Shokrieh. "8 - Understanding residual stresses in polymer matrix composites". In: *Residual Stresses in Composite Materials*. Ed. by Mahmood M. Shokrieh. Woodhead Publishing, 2014, pp. 197–232. ISBN: 978-0-85709-270-0. DOI: `https://doi.org/10.1533/9780857098597.2.197`. URL: `http://www.sciencedirect.com/science/article/pii/B9780857092700500080`.

[64]   Nigel Cross. *Engineering Design Method*. English. John Wiley & Sons; 4th edition, 2008.

[65]   Gabor Sziebig. *Welding Instructions*. English. Narvik Campus - Artic University of Norway.

[66]   Diffen LLC n d. *Current vs Voltage*. URL: `https://www.diffen.com/difference/Current_vs_Voltage`. (accessed: 05.05.2019).

[67]   O. A. Bauchau and J. I. Craig. "Euler-Bernoulli beam theory". In: *Structural Analysis*. Ed. by O. A. Bauchau and J. I. Craig. Dordrecht: Springer Netherlands, 2009, pp. 173–221. DOI: `10.1007/978-90-481-2516-6_5`. URL: `https://doi.org/10.1007/978-90-481-2516-6_5`.

[68]   healthresearchfunding.com. *Euler–Bernoulli beam theory*. URL: `https://healthresearchfundi org/euler-bernoulli-beam-theory-explained/`. (accessed: 08.05.2019).

[69]   www.pocketdentistry.com. *Euler–Bernoulli beam theory*. URL: `https://pocketdentistry.com/2-mechanics-and-mechanical-testing-of-orthodontic-materials/`. (accessed: 08.05.2019, last eddited 20 march 2019).

[70]   Roberto Silva. *2013 ESS CONFERENCE & ANSYS USRES MEETING*. URL: `https://www.academia.edu/24258213/Direct_Coupled_Thermal-Structural_Analysis_in_ANSYS_WorkBench`.

[71] V.S.Ravi1 A.Ramanjaneya Reddy2 P.Hussian Dr. S.Sudhakar Babu. "Non Linear Transient Thermal Analysis of Turbine Blade Cooling". In: *International Journal for Research in Appplied Science and Engineering Technology* 3 (June 2015).

[72] Ravinder Reddy Pinninti. *Simulation of TIG Welding Process*. Dec. 2014. ISBN: ISBN-13:978-3-659-66574-5, ISBN-10: 3659665746, EAN: 9783659665745.

[73] http://www.worldstainless.org. *Martensitic Stainless Steels*. URL: `http://www.worldstainless.org/Files/issf/non-image-files/PDF/ISSF_Martensitic_Stainless_Steels.pdf`. (Accessed 10 Mai 2019).

[74] www.aksteel.com. *304/304L-Stainless Steel*. URL: `https://www.aksteel.com/sites/default/files/2018-01/304304L201706_1.pdf`. (Accessed 10 Mai 2019).

[75] R W Niles and Jackson C E. "Welding thermal efficiency of the GTAW process". In: *Welding Journal 54(1)* (1975), 25s–32s. DOI: `10.1088/0022-3727/6/18/310`.

[76] J N Dupont and A R Marder. "Thermal Efficiency of Arc Weldingprocesses". In: (1995).

[77] M B C Quigley et al. "Heat flow to the workpiece from a TIG welding arc". In: *Journal of Physics D: Applied Physics* 6 (May 2002), p. 2250. DOI: `10.1088/0022-3727/6/18/310`.

Appendices

A Layer and welding path - descriptions for TWS

A.1 Layer and welding path - descriptions P1D1

Test part 1	Parameters of part P1D1:							Max heat input X3CrNiMo13-4: 1,5 [KJ/mm]	
Current: [A]	avhc: [mm]	Welding speed: [mm/sek]	Wire Feed: m/[min]	Voltage: [V]	Heat input [KJ/mm]	f/v [mm zice/mm min]	Deposition rate [g/s]	Q/Dep.Rate [kJs/gmm]	Dep.rate/v [g/mm]
250	2,8	2,2	2	16,4	1,1	0,91	187,3	0,006	85,1
	Gas [L/min]	Welding speed: [mm/min]	Wire Feed: mm/[min]	Dep.rate/v/Q [g/kJ]	[mm] of wire used	Volume of the used wire	f/Av [mmz/Amm]	V*I/f [kJ/mmz]	Feed Heat/Q
	12	132	2000	76,1	2575,8	2911,6	0,061	0,074	0,07

Position coordinates:				Efficiency:	1	Data for Preheat and PWHT to WPQR			
						Avr.height increase[mm	Avr. With [mm]	Arv.Temp after	Avr. Preheat temp:
x0 [mm] =	170	x1 [mm] =	340	Filler Wire dia:	1,2				
y0 [mm] =	15	y1 [mm] =	15	Length of weld [mm]:	170	1,4	11,5	164,1	36,7

Nr.layers:	Hight [mm]:	With [mm] :	Temp after weld	Preheat temp	Nr.layers:	Hight [mm]:	With [mm] :	Temp after weld	Preheat temp
1	2	14	56	35	16	20,5	12	178	44,6
2	4	10	99,2	40	17	22,5	11	210	33
3	5,5	10	90	42	18	23	11,1	211	40
4	7,10	11	106	38	19	25	11	182	39
5	8,1	11	119	45	20	27,1	10,1	217	32
6	8,1	14,5	145	39	21	28,1	12	152	29
7	9	15,1	160	38	22	30	11,5	157	35
8	10,5	10,2	145	30	23	31,5	11,5	203	36
9	11,5	11	140	30	24	32,5	11	215	36
10	13	11	153	36	25	33,9	11,2	200	41
11	14,2	11,5	154	38	26	35	11,4	160	34
12	16,1	12	186	42	27	37,2	11,2	214	41
13	17,7	11,5	143	27	28	39	11	214	34
14	18,1	11,2	168	35	29	40,1	11,5	206	32
15	19,5	11,5	176	43					

Figure 83: Layer and welding path - description for sample P1D1

A.2   Layer and welding path - descriptions P2D1

Test 2		Parameters of part P2D1							Max heat input X3CrNiMo13-4: 1,5 [KJ/mm]
Current: [A]	avho: [mm]	Welding speed: [mm/sek]	Wire Feed: m/[min]	Voltage: [V]	Heat input [KJ/mm]	f/v [mm zice/mm mat]	Deposition rate [g/s]	Q/Dep. Rate [kJs/gmm]	Dep.rate/v [g/mm]
240	2,8	2,3	1,8	14,2	0,89	0,78	168,6	0,005	73,3
	Gas [L/min]	Welding speed: [mm]/[min]	Wire Feed: [mm]/[min]	Dep.rate/v/Q [g/kJ]	[mm] of wire used	Volume of the used wire	f/Av [mmz/Amm]	V*I/f [kJ/mmz]	Feed Heat/Q
	12	138	1800	82,4	2217,4	2506,5	0,054	0,068	0,08
Position coordinates:				Efficiency:	1	Data for Preheat and PWHT to WPQR			
						Avr Hight increase[mm	Avr. With [mm]	Arv. Temp after	Avr. Preheat temp:
x0 [mm] =	5	x1 [mm] =	175	Filler Wire dia:	1,2				
y0 [mm] =	45	y1 [mm] =	45	Length of weld [mm]:	170	1,3	11,3	146,1	46,6
Nr.layers:	Hight [mm]:	With [mm] :	Temp after weld	Preheat temp	Nr.layers:	Hight [mm]:	With [mm] :	Temp after weld	Preheat temp
1	2	10,9	79	35	17	22	11,5	130	45,3
2	4	8,9	101	45,6	18	23,1	12	182	53,3
3	5,5	9,9	93	40	19	24,5	12	124	59
4	6,8	10	80	34	20	25,6	11,5	116,2	46,6
5	7,5	12,4	94	42	21	27	12	195,1	54,1
6	8,5	13	125	40	22	28	11,5	189,9	59,8
7	9,1	12,4	121,6	48	23	29	11,6	145,4	36,4
8	11	11	150	27	24	30	11	153,5	38,2
9	12	11	138,9	50,3	25	32	11	180,8	42,2
10	13	11,5	116	48	26	33,5	10,5	216,7	44,3
11	14,6	11	127,6	61,9	27	34,5	11	115	42,4
12	15,5	11,5	129,5	45	28	36	11	214,7	55,6
13	16,5	12	153,7	45,5	29	37,5	11	165,8	48,8
14	18	12	190,5	57,4	30	39	11	200,3	52,6
15	20	11	155,9	49,6	31	40	10,5	197,9	50,5
16	21	11	156	48	32				

Figure 84: Layer and welding - path description for sample P2D1

A.3   Layer and welding path - descriptions P3D1

Test 3		Parameters of part P3D1						Max heat input 304L alloy: 1,5 [KJ/mm]	
Current: [A]	avhc: [mm]	Welding speed: [mm/sek]	Wire Feed: m/[min]	Voltage: [V]	Heat input [KJ/mm]	f/v [mm zice/mm mat]	Deposition rate [g/s]	Q/Dep.Rate [kJs/gmm]	Dep.rate/v [g/mm]
220,0	2,7	2,2	1,6	13,5	0,81	0,73	168,6	0,005	76,6
	Gas [L/min]	Welding speed: [mm]/[min]	Wire Feed: [mm]/[min]	Dep.rate/v/Q [g/kJ]	[mm] of wire used	Volume of the used wire	f/Av [mmz/Amm]	V''I/f [kJ/mmz]	Feed Heat/Q
	12	132	1800	94,6	2318,2	2620,5	0,062	0,059	0,07

Position coordinates:				Efficiency:	1	Data for Preheat and PWHT to WPQR			
x0 [mm] =	5	x1 [mm] =	175	Filler Wire dia:	1,2	Avr Hight increase[mm	Avr. With [mm]	Arv. Temp after	Avr. Preheat temp:
y0 [mm] =	10	y1 [mm] =	10	Length of weld [mm]:	170	1,2	10,6	169,5	41,7

Nr.layers:	Hight [mm]:	With [mm] :	Temp after weld	Preheat temp	Nr.layers:	Hight [mm]:	With [mm] :	Temp after weld	Preheat temp
2	2	10,5	89	31	18	21,5	10,5	152	54,9
2	4	9	142,6	45	19	23	11	173,5	33,7
3	5	9,5	139,6	44,6	20	24	11	100	37
4	6,5	10	154,6	41,9	21	25	10,7	197,7	38,5
5	7,8	10,2	163,8	43,9	22	26	10,5	168,6	35
6	8,5	11	143,1	44,8	23	28	11	221,6	35,7
7	9,5	11,2	173,4	42,4	24	ERROR WITH FEEDER			
8	10,5	11,5	142	34,5	25	29	10,5	211,1	49
9	12	10,5	130,6	42,8	26	30	10,2	210,7	57
10	13	11,5	159,3	46,3	27	31	10,5	213,9	40,5
11	14	10,5	130	43,2	28	32	11	233,9	41,1
12	15,5	11	202	36,9	29	34	11	230,5	47,2
13	16	11	109,6	31,2	30	35	11	216	33
14	17	11	97,9	35,6	31	36	11	195,4	50,7
15	17,5	10	120	35	32	37,5	11	203	49,8
16	19	11	153,2	34	33	39	10	210	46
17	21	10	183,6	44,2	34	41,6	10,4	220	50

g

Figure 85: Layer and welding path - description for sample P3D1

A.4   Layer and welding path - descriptions P4D1

Test 4		Parameters of part P4D1						Max heat input 304L alloy: 1,5 [KJ/mm]	
								NB Was already welded one welding stripe before emasuring the height.	
Current: [A]	avhc: [mm]	Welding speed: [mm/sek]	Wire Feed: m/[min]	Voltage: [V]	Heat input [KJ/mm]	f/v [mm zice/mm mat]	Deposition rate [g/s]	Q/Dep.Rate [kJs/gmm]	Dep.rate/v [g/mm]
220,0	2,4	2,2	1,47	12,2	0,73	0,67	137,7	0,005	62,6
	Gas [L/min]	Welding speed: [mm]/[min]	Wire Feed: [mm]/[min]	Dep.rate/v/Q [g/kJ]	[mm] of wire used	Volume of the used wire	f/Av [mmz/Amm]	V"l/f [kJ/mmz]	Feed Heat/Q
	12	132	1470	85,5	1893,2	1486,1	0,051	0,066	0,09

Position coordinates for horisontal stripe (from orgin)				Efficiency:	1	Data for Preheat and PWHT to WPQR			
x0 [mm] =	40	x1 [mm] =	140	Filler Wire dia:	1,2	[mm]	[mm]	Arv. Temp after	Avr. Preheat temp:
y0 [mm] =	50	y1 [mm] =	50	Length of weld [mm]:	170				
Origin axes rotation:	A (degree) = 0	B (degree) = -10	C (degree) = 0		Nr.layers:	Hight [mm]:	With [mm] :	Temp after weld	Preheat temp

Nr.layers:	Hight [mm]:	With [mm] :	Temp after weld	Preheat temp
1	1,6	9		
2	2,8	9,5		
3	FAILURE:filler missed the melting pool			
4	4,9	9	Filler went through melting pool	
5	FAILURE:filler missed the melting pool			
6	FAILURE:filler missed the melting pool			
7	7,9	10,6		
8	8,9	10,8		
9	FAILURE:filler missed the melting pool			
10	FAILURE:filler missed the melting pool			
11	10	11		
12	FAILURE:filler missed the melting pool			
13	FAILURE:filler missed the melting pool			
14	11	11		
15	FAILURE:filler missed the melting pool			

Nr.layers:	Hight [mm]:	With [mm] :	Temp after weld	Preheat temp
16	12	11	Filler went through melting pool	
17	13,5	11	Filler went on the side of the melting	
18	NO ARC, REASON CAN BE THAT DEFLECTION PLUSS RUSTY SURFACE UNDER PLATE DONT GIVE CURCUIT			
19				
20				
21				
22				
23				
24				
25				
26				
27				
28				
29				

Figure 86: Layer and welding path - description for sample P4D1

A.5   Layer and welding path - descriptions P5D1

Test 5		Parameters of part P5D1:						Max heat input 304L alloy: 1,5 [KJ/mm]	
Current: [A]	avhc: [mm]	Welding speed: [mm/sek]	Wire Feed: m/[min]	Voltage: [V]	Heat input [KJ/mm]	f/v [mm zice/mm mat]	Deposition rate [g/s]	Q/Dep.Rate [kJs/gmm]	Dep.rate/v [g/mm]
200,0	2,4	2,2	0,85	12,3	0,67	0,39	79,6	0,008	36,2
	Gas [L/min]	Welding speed: [mm]/[min]	Wire Feed: [mm]/[min]	Dep.rate/v/Q [g/kJ]	[mm] of wire used	Volume of the used wire	f/Av [mmz/Amm]	V*I/f [kJ/mmz]	Feed Heat/Q
	12	132	850	53,9	1094,7	859,3	0,032	0,104	0,16

osition coordinates for horisontal stripe (from orgi				Efficiency:	1	Data for Preheat and PVHT to VPQR			
						Avr Hight increase	Avr.Vith [mm]	Arv.Temp after	Avr. Preheat
x0 [mm] =	100	x1 [mm] =	320	Filler Wire dia:	1,2				
y0 [mm] =	50	y1 [mm] =	50	Length of weld [mm]:	170	1,4	10,07		
Origin axes rotation:	A (degree) = 0	B (degree) = -10	C (degree) = 0						

Nr.layers:	Hight [mm]:	Vith [mm]:	Notes:	Nr.layers:	Hight [mm]:	Vith [mm]:	Notes:
1	1	11,8		22	16,5	10	
2	2	9,2		23	17,2	11	
3	3,1	9,5		24	18	10	
4	4	9		25	18,1	10	
5	5	9,4		26	19,4	11	re-adjusted start position: 110-113
6	5,8	10		27	19,9	10	
7	6,4	9,8		28	20,5	10	
8	7	10		29	21	9,5	
9	7,5	10,4		30	22	9,4	
10	8	10,5	re-adjusted start position: 110-105	31	22,5	9,8	re-adjusted start position: 113-117
11	9	11,5		32	22,8	9,6	
12	10	10,9		33	23,5	9,8	re-adjusted start position: 120-125
13	10,5	11		34	24,5	10,3	
14	11,1	10,2		35	25,2	9,6	
15	12	10,5		36	25,5	10	re-adjusted start position: 120-125
16	12	11		37	26,5	9,8	
17	13	9,8	re-adjusted start position: 105-108	38	27	10	
18	13,8	10,3	re-adjusted start position: 108-110	39	28,5	10	
19	14,5	9,4		40	29	10	
20	15	8,8		41	29,6	10	
21	16	10		42	30,5	10	

Figure 87: Layer and welding path - description for sample P5D1

A.6 Layer and welding path - descriptions P1D2

Test 6		Parameters of part P1D2:							Max heat input 304L allov: 1,5 [KJ/mm]	
Current: [A]	avhc: [mm]	Welding speed: [mm/sek]	Wire Feed: m/[min]	Voltage: [V]	Heat input [KJ/mm]	f/v [mm zice/mm mat]	Deposition rate [g/s]	Q/Dep.Rate [kJs/gmm]	Dep.rate/v [g/mm]	
250,0	2,8	2,2	2	16,4	1,12	0,91	168,6	0,007	76,6	
	Gas [L/min]	Welding speed: [mm]/[min]	Wire Feed: [mm]/[min]	Dep.rate/v/Q [g/kJ]	[mm] of wire used	Volume of the used wire	f/Av [mmz/Amm]	V*I/f [kJ/mmz]	Feed Heat/Q	
	12	132	1800	68,5	2318,2	1819,8	0,055	0,082	0,07	

Position coordinates for horisontal stripe (from originally position)				Efficiency:		1	Data for Preheat and PWHT to WPQR			
							Avr Hight increase[mm	Avr. With [mm]	Arv.Temp after	Avr. Preheat temp:
x0 [mm] =	40	x1 [mm] =	140	Filler Wire dia:		1,2				
y0 [mm] =	50	y1 [mm] =	50	Length of weld [mm]:		170	1,8	13,23		
Origin axes rotation:	A (degree) = 0	B (degree) = -10	C (degree) = 0							

Position coordinates for vertikal stripe (turned 90 degree)										
x0 [mm] =	75	x1 [mm] =	75							
y0 [mm] =	85	y1 [mm] =	5							
New axes rotation:	A (degree) = -90	B (degree) = 0	C (degree) = -10							

NB changed:
Horisontal stripe: 40-120 [mm]
Wire Feed to 1,7
Vertikal stripe:80-10 [mm]

Nr.layers:	Hight [mm]:	With [mm] :	Temp after weld	Preheat temp.
1	3	11,5	130	35
2	5	10		
3	7	11		
4	8,9	12		
5	10	15		
6	11,5	13,5		
7	12	14		
8	14,5	13,5		
9	18	15,5		
10	19,5	14		
11	20,9	15,5		

Figure 88: Layer and welding path - description for sample P1D2

A.7   Layer and welding path - descriptions P2D2

Test 7		Parameters of part P2D2:							
								Max heat input 304L alloy: 1,5 [KJ/mm]	
Current: [A]	avhc: [mm]	Welding speed: [mm/sek]	Wire Feed: m/[min]	Voltage: [V]	Heat input [KJ/mm]	f/v [mm zice/mm mat]	Deposition rate [g/s]	Q/Dep.Rate [kJs/gmm]	Dep.rate/v [g/mm]
240	2,8	2,3	1,6	14,2	0,89	0,70	168,6	0,005	73,3
	Gas [L/min]	Welding speed: [mm]/[min]	Wire Feed: [mm]/[min]	Dep.rate/v/Q [g/kJ]	[mm] of wire used	Volume of the used wire	f/Av [mmz/Amm]	V*l/f [kJ/mmz]	Feed Heat/Q
	12	138	1800	82,4	2217,4	1740,7	0,054	0,068	0,08
Position coordinates for horisontal stripe (from originally position)				Efficiency:	1	Data for Preheat and PWHT to WPQR			
						Avr Hight increase[mm]	Avr. With [mm]	Arv. Temp after	Avr. Preheat temp:
x0 [mm] =	230	x1 [mm] =	320	Filler Wire dia:	1,2				
y0 [mm] =	50	y1 [mm] =	50	Length of weld [mm]:	170	1,6	12,54		
Origin axes rotation:	A (degree) = 0	B (degree) = -10	C (degree) = 0						
Position coordinates for vertikal stripe (turned 90 degree)									
x0 [mm] =	270	x1 [mm] =	270						
y0 [mm] =	85	y1 [mm] =	10						
New axes rotation:	A (degree) = -90	B (degree) = 0	C (degree) = -10						
Nr.layers:	Hight [mm]:	With [mm] :	Temp after weld	Preheat temp.					
1	3	8	130	35					
2	5	10							
3	6,8	10,5							
4	8,5	11							
5	9,1	14							
6	10	13							
7	12	14							
8	13	14,5							
9	16,8	13							
10	16	13							
11	18	14							
12	19	15,5							

NB changed parameters from line 11, old once:
Horisontal stripe: 220-320 [mm]
Wire Feed to 1,8
Vertikal stripe:80-5[mm]

Figure 89: Layer and welding path - description for sample P2D2

A.8　Layer and welding path - descriptions P4D2

Test 9		Parameters of part P4D2:						Max heat input 304L alloy: 1,5 [KJ/mm]	
Current: [A]	avhc: [mm]	Welding speed: [mm/sek]	Wire Feed: m/[min]	Voltage: [V]	Heat input [KJ/mm]	f/v [mm zice/mm mat]	Deposition rate [g/s]	Q/Dep.Rate [kJs/gmm]	Dep.rate/v [g/mm]
220,0	2,4	2,2	1	12,2	0,73	0,45	93,6	0,008	42,6
	Gas [L/min]	Welding speed: [mm]/[min]	Wire Feed: [mm]/[min]	Dep.rate/v/Q [g/kJ]	[mm] of wire used	Volume of the used wire	f/Av [mmz/Amm]	V*l/f [kJ/mmz]	Feed Heat/Q
	12	132	1000	58,2	1287,9	1011,0	0,034	0,097	0,13

Position coordinates for horisontal stripe (from originally position)				Efficiency:	1	Data for Preheat and PWHT to WPQR			
						Avr Hight increase[mm]	Avr. With [mm]	Arv. Temp after	Avr. Preheat temp:
x0 [mm] =	160	x1 [mm] =	300	Filler Wire dia:	1,2				
y0 [mm] =	51	y1 [mm] =	51	Length of weld [mm]:	170	1,0	10,17894737		

Origin axes rotation:	A (degree) = 0	B (degree) = -10	C (degree) = 0			Nr.layers:	Hight [mm]:	With [mm] :	Temp after weld	Preheat temp

Position coordinates for vertikal stripe (turned 90 degree)						12	13,1	9,8	re-adjusted start position: Stripe(V):x=222, y0=85-y1=7 Stripe (H): x=175-x1=290, y=51
x0 [mm] =	222	x1 [mm] =	222		13	14,9	10	
y0 [mm] =	95	y1 [mm] =	5		14	15,1	10	
New axes rotation:	A (degree) = -90	B (degree) = 0	C (degree) = -10		15	16,1	10	re-adjusted start position: Stripe(V):x=222, y0=82-y1=12 Stripe (H): x=175-x1=280, y=51
Nr.layers:	Hight [mm]:	With [mm] :	Temp after weld	Preheat temp	16	17,1	10	
1	1,8	10,5			17	18,1	10,5	
2	3,9	9,2			18	19	10	re-adjusted start position: Stripe(V):x=222, y0=80-y1=15 Stripe (H): x=185-x1=275, y=51
3	4,8	10,9			19	19,5	10	
4	6,1	10,1						
5	7,1	10,1						
6	8,1	10,1						
7	9,1	10,1	re-adjusted start position: Stripe(V):x=222, y=90 Stripe (H): x=165, y=51					
8	9,8	11,1						
9	10	11	Electrode was crocked, resulted in an angular weld with low					
10	11,5	10						
11	12,1	10	re-adjusted start position: Stripe(V):x=222, y=87 Stripe (H): x=170, y=51					

Figure 90: Layer and welding path - description for sample P4D2

A.9   Layer and welding path - descriptions P4D3

Test 8		Parameters of part P4D3:						Max heat input 304L alloy	
Current: [A]	avhc: [mm]	Welding speed:	Wire Feed: m/[min]	Voltage: [V]	Heat input [KJ/mm]	f/v [mm zice/mm mat]	Deposition rate [g/s]	Q/Dep.Rate [kJs/gmm]	Dep.rate/v [g/mm]
220,0	2,4	2,2	1	12,2	0,73	0,45	93,6	0,008	42,6
	Gas [L/min]	Welding speed:	Wire Feed: [mm]/[min]	Dep.rate/v/Q [g/kJ]	[mm] of wire used	Volume of the used wire	f/Av [mmz/Amm]	V•I/f [kJ/mmz]	Feed Heat/Q
	12	132	1000	58,2	1287,9	1011,0	0,034	0,097	0,13

Position coordinates for angled stripe (turned 20 degree)				Efficiency:	1	Data for Preheat and PWHT to WPQR			
						Avr Hight increase[mm]	Avr.With [mm]	Arv.Temp after welding(degree)	Avr. Preheat temp:
x0 [mm] =	230	x1 [mm] =	389,354	Filler Wire dia:	1,2				
y0 [mm] =	20	y1 [mm] =	78	Length of weld [mm]:	170	1,1	10,56		
Origin axes rotation:	A (degree) = 20	B (degree) = -10	C (degree) = 0			Nr.layers:	Hight [mm]:	With [mm] :	Temp after weld [degree]:	Preheat temp.

Position coordinates for angled stripe (turned -20 degree)					Nr.layers:	Hight [mm]:	With [mm] :		
					10	12,1	11		
x0 [mm] =	230	x1 [mm] =	389,354		11	13	11	re-adjusted start position: Stripe(-20):x=240, y=74,36 Stripe(20): x=240, y=23,64	
y0 [mm] =	78	y1 [mm] =	20		12	14	12		
New axes rotation:	A (degree) = -20	B (degree) = -10	C (degree) = 0		13	15	12		

Nr.layers:	Hight [mm]:	With [mm] :	Temp after weld [degree]	Preheat temp.	Nr.layers	Hight	With		
					14	16,2	10		
1	1,4	12			15	17	10	re-adjusted start position: Stripe(-20):x=245, y=72,54 Stripe(20): x=245 y=25,46	
2	2,1	11							
3	4	10			16	18	9,8		
4	5,5	10			17	19	9,5		
5	7	10,4			18	20	11,9	re-adjusted start position: Stripe(-20):x=250, y=70,721 Stripe(20): x=250 y=27,279	
6	8	9,8			19	21,1	11		
7	9	10			20	22,1	9,5		
8	10	11			21	23	10		
9	11	10,5			22	24	10		

Figure 91: Layer and welding path - description for sample P4D3

B   Delta-H (height difference) and Average height measurement for TWS

Measurement for the neutral axis used in the calculation for finding w". These measurement are based upon the measured values of the sample in appendix E

B.1   Delta-H and Average height measurement - P1D1

	Average measurment of two			Average measurment of two				Difference before and after cut of TWS		
	Height of the **base-plate** from the left corner BEFORE cut of weld[H]:			Height of the **thin wall structure** from the lowest corner to the highest BEFORE cut of weld[H]:				**Delta-H** in height of the centerline of the **TWS** (height/2)		
Point:	Length [mm]:	Height [mm]:	Point:	Length [mm]:	Height of TWS + BP [mm]:	Height of only TWS	Lentgh [mm]	After cut [mm]:	Before cut [mm]:	Delta H [mm]
1	0	27,68	1	10	54,67	26,99	10	13,86	13,495	0,36
2	50	26,22	2	30	58,5	32,28	30	16,01	16,14	-0,13
3	100	25,17	3	50	61,98	36,81	50	18,45	18,405	0,04
4	150	24,72	4	70	63,92	39,2	70	19,59	19,6	-0,01
5	200	24,73	5	90	64,6	39,87	90	20,04	19,935	0,10
6	250	24,92	6	110	65,18	40,26	110	20,21	20,13	0,08
7	300	25,27	7	130	65,3	40,03	130	20,12	20,015	0,1
8	350	25,59	8	150	65,41	39,82	150	19,96	19,91	0,05
Average height:		25,5375	9	177	65,5	39,9625	177	19,62	19,98125	-0,36
	Average measurment of four			Average measurment of four				Difference before and after cut of TWS		
	Height of the **base-plate** from the lowest corner to highest AFTER the cut of the			Height of the **thin wall structure** from the lowest corner to the highest AFTER cut of weld[H]:				**Delta-H** in height of the centerline in **Baseplate.** (height/2)		
Point:	Length [mm]:	Height [mm]:	Point:	Length [mm]:	Height of TWS + BP [mm]:	Height of only TWS	Lentgh [mm]	After cut [mm]:	Before cut [mm]:	Delta H [mm]
1	0	27,6	1	10	55,32	27,72	0	13,8	13,84	-0,04
2	50	26,05	2	30	58,08	32,03	50	13,025	13,11	-0,09
3	100	24,93	3	50	61,82	36,89	100	12,46375	12,585	-0,12
5	150	24,53	4	70	63,72	39,19	150	12,26625	12,36	-0,09
5	200	24,56	5	90	64,63	40,07	200	12,2775	12,365	-0,09
6	250	24,80	6	110	65,22	40,41	250	12,40125	12,46	-0,06
7	300	25,08	2)	130	65,31	40,23	300	12,54	12,635	-0,09
8	350	25,43	8	150	65,36	39,93	350	12,71375	12,795	-0,08
Average height:		25,371875	9	177	64,61	39,23				0

Figure 92: Deformation of neutral axis for P1D1. Documented by the measurement in appendix 120

B.2   Delta-H and Average height measurement - P2D1

Average measurment of two			Average measurment of two					Difference before and after cut of TWS			
Height of the **base-plate** from the lowest corner to highest BEFORE cut of weld[H]:			Height of the **thin wall structure** from the lowest corner to the highest BEFORE cut of weld[H]:					**Delta-H** in height of the centerline of the **TWS** (height/2)			
Point:	Length [mm]:	Height [mm]:	Point:	Length [mm]:	Height of TWS + BP [mm]:	Height of only TWS:		Length [mm]:	After cut	Before cut	Delta H
1	0	27,68	1	10	51,27	23,59		10	12,81	11,795	1,02
2	50	26,22	2	30	57,2	30,98		30	16,31	15,49	0,82
3	100	25,17	3	50	61,03	35,86		50	18,46	17,93	0,53
4	150	24,72	4	70	63,38	38,66		70	19,73	19,33	0,40
5	200	24,73	5	90	64,63	39,9		90	20,29	19,95	0,34
6	250	24,92	6	110	65,55	40,63		110	20,54	20,315	0,23
7	300	25,27	7	130	65,71	40,44		130	20,28	20,22	0,06
8	350	25,53	8	150	65,48	39,89		150	19,86	19,945	-0,08
Avrage hight:		25,54	9	175	64,78	39,24		175	19,55	19,62	-0,07
Average measurment of three			Average measurment of three					Difference before and after cut of TWS			
Height of the **base-plate** from the lowest corner to highest AFTER the cut of the			Height of the **thin wall structure** from the lowest corner to the highest AFTER cut of the weld[H]:					**Delta-H** in height of the centerline in **Baseplate.** (height/2)			
Point:	Length [mm]:	Height [mm]:	Point:	Length [mm]:	Height of TWS + BP [mm]:	Height of only TWS:		Length [mm]:	After cut	Before cut	Delta H
1	0	26,5	1	10	52,13	25,63		0	13,25	13,84	-0,59
2	50	25,42	2	30	58,03	32,61		50	12,71	13,11	-0,40
3	100	24,72	3	50	61,64	36,93		100	12,36	12,585	-0,23
4	150	24,50	4	70	63,96	39,46		150	12,25	12,36	-0,11
5	200	24,58	5	90	65,15	40,57		200	12,29	12,365	-0,08
6	250	24,80	6	110	65,88	41,09		250	12,40	12,46	-0,06
7	300	25,17	7	130	65,74	40,57		300	12,59	12,635	-0,05
8	350	25,54	8	150	65,27	39,72		350	12,77	12,795	-0,02
Avrage hight:		25,15	9	175	64,26	39,10					

Figure 93: Deformation of neutral axis for P2D1. Documented by the measurement in appendix 121

B.3   Delta-H and Average height measurement - P3D1

Average measurment of one			Average measurment of one				Difference before and after cut of TWS			
Height of the **base-plate** from the lowest corner to highest BEFORE cut of weld[H]:			Height of the **thin wall structure** from the lowest corner to the highest BEFORE cut of weld[H]:				**Delta-H** in height of the centerline of the **TWS** (height/2)			
Point:	Length [mm]:	Height [mm]:	Point:	Length [mm]:	Height of TWS + BP [mm]:	Height of only TWS	Length [mm]:	After cut	Before cut	Delta H
1	0	25,26	1	10	55,39	30,13	10	13,21	15,065	-1,85
2	50	25,19	2	30	59,13	33,94	30	15,16	16,97	-1,81
3	100	25,08	3	50	63,31	38,23	50	18,08	19,115	-1,04
4	150	25	4	70	66,15	41,15	70	19,31	20,575	-1,26
5	200	24,98	5	90	67,45	42,47	90	19,98	21,235	-1,25
6	250	25,04	6	110	67,97	42,93	110	20,08	21,465	-1,39
7	300	25,39	7	130	68,16	42,77	130	20,03	21,385	-1,35
8	350	26,26	8	150	68,42	42,16	150	19,80	21,08	-1,28
9	398	27,36	9	180	68,66	41,3	180	19,10	20,65	-1,56

Average measurment of three			Average measurment of three				Difference before and after cut of TWS			
Height of the **base-plate** from the lowest corner to highest AFTER the cut of the			Height of the **thin wall structure** from the lowest corner to the highest AFTER cut of the weld[H]:				**Delta-H** in height of the centerline in **Baseplate.** (height/2)			
Point:	Length [mm]:	Height [mm]:	Point:	Length [mm]:	Height of TWS + BP [mm]:	Height of only TWS	Length [mm]:	After cut	Before cut	Delta H
1	0	25,08	1	10	51,51	26,42	0	12,54	12,63	-0,09
2	50	25,04	2	30	55,36	30,33	50	12,52	12,595	-0,08
3	100	24,93	3	50	61,09	36,16	100	12,47	12,54	-0,07
4	150	24,89	4	70	63,52	38,63	150	12,45	12,5	-0,05
5	200	24,88	5	90	64,85	39,97	200	12,44	12,49	-0,05
6	250	24,92	6	110	65,07	40,15	250	12,46	12,52	-0,06
7	300	25,24	7	130	65,31	40,07	300	12,62	12,695	-0,07
8	350	25,88	8	150	65,48	39,60	350	12,94	13,13	-0,19
9	397	26,63	9	180	64,82	38,19	397	13,32	13,68	-0,36

g

Figure 94: Deformation of neutral axis for P3D1. Documented by the measurement in appendix 122

B.4   Delta-H and Average height measurement - P5D1

Average measurment of two			Average measurment of two				Difference			
Height of the **base-plate** from the left corner BEFORE welding[H]:			Height of the **thin wall structure** from the lowest corner to the highest BEFORE cut of the weld[H]:				**Delta-H** in height of the centerline of the **TWS** (height/2)			
Point:	Length [mm]:	Height [mm]:	Point:	Length [mm]:	Height of TWS + BP [mm]:	Height of only TWS [mm]	Length [mm]:	After cut	Before cut	Delta H
1	0	24,97	1	10	35,51	10,54	10	5,30	5,27	0,03
2	50	24,95	2	30	56,07	31,12	30	15,60	15,56	0,04
3	100	24,94	3	60	55,02	30,08	60	15,54	15,04	0,50
4	150	24,88	4	80	54,39	29,51	80	15,43	14,755	0,67
5	200	24,79	5	120	54,06	29,27	120	15,46	14,635	0,83
6	250	24,79	6	160	52,68	27,89	160	14,52	13,945	0,57
7	300	24,82	7	180	49,68	24,86	180	12,65	12,43	0,22
8	350	24,9	8	210	45,3	20,4	210	10,15	10,2	-0,05
9	398	24,96	9	230	42,59	17,63	230	8,00	8,815	-0,82
Average of height:		24,89								

Average measurment of two			Average measurment of three				Difference			
Height of the **base-plate** from the lowest corner to the highest, AFTER weld[H]:			Height of the **thin wall structure** from the lowest corner to the highest AFTER cut of weld[H]:				**Delta-H** in height of the centerline in **Baseplate.** (height/2)			
Point:	Length [mm]:	Height [mm]:	Point:	Length [mm]:	Height of TWS + BP [mm]:	Height of only TWS [mm]	Length [mm]:	After cut	Before cut	Delta H
1	0	26,1	1	10	36,7	10,6	10	12,62	13,05	-0,435
2	50	25,54	2	30	56,74	31,2	30	12,60	12,77	-0,17
3	100	25	3	60	56,08	31,08	60	12,28	12,5	-0,22
4	150	24,66	4	80	55,52	30,86	80	12,21	12,33	-0,12
5	200	24,6	5	120	55,53	30,93	120	12,15	12,3	-0,15
6	250	24,79	6	160	53,82	29,03	160	12,23	12,395	-0,16
7	300	25,23	7	180	50,53	25,30	180	12,43	12,615	-0,19
8	350	25,76	8	210	46,06	20,30	210	12,66	12,88	-0,22
9	398	26,53	9	230	42,53	16,00	230	12,98	13,265	-0,29
Average of height:		25,36								

Figure 95: Deformation of neutral axis for P5D1. Documented by the measurement in appendix 123

B.5　Delta-H and Average height measurement - P1D2

Average measurement of one

Height of the base-plate from the lowest corner to the highest BEFORE cut of weld:

Point:	Length [mm]:	Height [mm]:
1	0	27,48
2	50	25,35
3	100	25,19
4	150	25,2
5	200	25,23
6	250	25,2
7	300	25,26
8	350	25,55
9	338	25,31
Average Height:		25,66

Height of the base-plate from the lowest corner to the highest BEFORE cut of weld:

Point:	Length [mm]:	Height [mm]:
1	0	27,48
2	10	27,56
3	30	27,56
4	50	27,77
5	60	27,67
6	70	27,8
7	80	27,61
8	90	27,72
9	100	27,8
Average Height:		27,66

Height of the thin wall structure from the lowest corner to the highest BEFORE cut of weld [H]:

Point:	Length [mm]:	Height of TWS + BP [mm]:	Height of only TWS [mm]
1	0	34,63	7,21
2	10	46,36	21,01
3	20	47,34	22,15
4	40	47,08	21,88
5	50	45,8	20,57
6	70	40,63	15,43
7	80	38,35	13,03
8	90	32,47	6,92
9	110	28,37	2,46

Height of the thin wall structure from the lowest corner to the highest BEFORE cut of weld [V]:

Point:	Length [mm]:	Height of TWS + BP [mm]:	Height of only TWS [mm]
1	0	37,6	10,12
2	10	38,85	11,23
3	30	39,18	11,62
4	40	47,22	19,45
5	50	45,34	18,27
6	60	45,57	17,77
7	70	39,84	12,23
8	80	37,62	9,3
9	90	27,3	0,1

Difference before and after cut of TWS — Delta H in height of the centerline of the TWS [H] (height/2):

Length [mm]:	After cut	Before cut	Delta H
0	8,79	3,605	5,18
10	10,73	10,505	0,22
20	11,16	11,075	0,08
40	10,78	10,94	-0,16
50	9,87	10,285	-0,42
70	8,33	7,715	0,61
80	6,88	6,545	0,33
90	5,43	3,46	2,03
110	2,95	1,23	1,72

Difference before and after cut of TWS — Delta H in height of the centerline in BP [H] (height/2):

Length [mm]:	After cut [mm]:	Before cut [mm]	Delta H [mm]
0	13,60	13,74	-0,14
50	13,01	12,375	0,03
100	12,61	12,535	0,01
150	12,57	12,6	-0,03
200	12,47	12,615	-0,15
250	12,48	12,6	-0,13
300	12,56	12,63	-0,07
350	12,86	12,775	0,08
338	13,14	12,955	0,13

Average measurement of three

Height of the base-plate from the lowest corner to highest AFTER the cut of the weld [H]:

Point:	Length [mm]:	Height [mm]:
1	0	27,20
2	50	26,02
3	100	25,22
4	150	25,15
5	200	24,34
6	250	24,35
7	300	25,12
8	350	25,71
9	338	26,28
Average Height:		25,62

Height of the base-plate from the lowest corner to highest AFTER the cut of the weld [V]:

Point:	Length [mm]:	Height [mm]:
1	0	27,18
2	10	27,33
3	30	27,54
4	50	27,87
5	60	28,03
6	70	28,15
7	80	28,23
8	90	28,30
9	100	28,38
Average Height:		27,83

Height of the thin wall structure from the lowest corner to the highest AFTER cut of weld [H]:

Point:	Length [mm]:	Height of TWS + BP [mm]:	Height of only TWS [mm]
1	0	44,77	17,57
2	10	47,47	21,46
3	20	47,54	22,32
4	40	46,70	21,55
5	50	44,67	19,73
6	70	41,61	16,66
7	80	38,88	13,76
8	90	36,63	10,98
9	110	32,19	5,31

Height of the thin wall structure from the lowest corner to the highest AFTER cut of weld [V]:

Point:	Length [mm]:	Height of TWS + BP [mm]:	Height of only TWS [mm]
1	0	38,46	11,23
2	10	45,10	17,77
3	30	45,78	18,23
4	40	46,38	18,50
5	50	47,63	19,60
6	60	42,2	14,05
7	70	38,88	10,65
8	80	35,80	7,50
9	90	30,31	2,54

Difference before and after cut of TWS — Delta H in height of the centerline of the TWS [V] (height/2):

Length [mm]:	After cut	Before cut	Delta H
0	5,64	5,06	0,58
10	8,89	5,645	3,24
30	9,12	5,81	3,31
40	9,25	9,725	-0,47
50	9,80	9,135	0,665
60	7,03	8,885	-1,86
70	5,32	6,115	-0,79
80	3,75	4,95	-1,2
90	1,27	0,05	1,22

Difference before and after cut of TWS — Delta H in height of the centerline in BP [V] (height/2):

Length [mm]:	After cut [mm]:	Before cut [mm]	Delta H [mm]
0	13,53	13,74	-0,15
10	13,67	13,78	-0,11
30	13,77	13,78	-0,01
50	13,34	13,885	0,05
60	14,02	13,835	0,18
70	14,07	13,9	0,17
80	14,12	13,605	0,31
90	14,15	13,86	0,23
100	14,13	13,9	0,23

Figure 96: Deformation of neutral axis for P5D1. Documented by the measurement in appendix **??**

B.6 Delta-H and Average height measurement - P2D2

Top table:

	Average measurement of two		Average measurement of two		Average measurement of two			Average measurement of two			Difference before and after cut of TWS				Difference before and after cut of TWS			
	Height of the **base-plate** from the lowest corner to the highest BEFORE cut of weld		Height of the **base-plate** from the lowest corner to the highest BEFORE cut of weld		Height of the **thin wall structure** from the lowest corner to the highest BEFORE cut of weld [H]			Height of the **thin wall structure** from the lowest corner to the highest BEFORE cut of weld [V]			**Delta-H** in height of the centerline of the TWS [H] (height/2)				**Delta-H** in height of the centerline in BP [H]. (height/2)			
Point:	Length [mm]	Height [mm]	Point:	Length [mm]	Height [mm]	Point:	Length [mm]	Height of TWS + BP [mm]	Height of only TWS [mm]	Point:	Length [mm]	Height of TWS + BP [mm]	Height of only TWS [mm]	Length [mm]	After cut	Before cut	Delta H	Length [mm]	After cut [mm]	Before cut [mm]	Delta H [mm]
1	0	27,48	1	0	27,48	1	0	36,65	9,17	1	0	41,43	13,95	0	6,35	4,585	1,77	0	13,60	13,74	-0,14
2	50	25,95	2	10	27,56	2	10	40,54	14,59	2	10	40,8	13,24	10	8,74	7,295	1,45	50	13,01	12,975	0,03
3	100	25,19	3	30	27,56	3	20	42,74	17,55	3	30	39,86	12,3	20	9,12	8,775	0,35	100	12,61	12,535	0,01
4	150	25,2	4	50	27,77	4	40	42,27	17,07	4	50	40,37	13,2	40	9,17	8,535	0,64	150	12,57	12,6	-0,03
5	200	25,23	5	60	27,67	5	50	42,64	17,41	5	60	43,21	15,54	50	9,60	8,705	0,89	200	12,47	12,615	-0,15
6	250	25,2	6	70	27,8	6	70	40,56	15,36	6	70	42,37	15,17	70	8,19	7,68	0,50	250	12,48	12,6	-0,13
7	300	25,26	7	80	27,61	7	80	37,81	12,55	7	80	42,11	14,5	80	6,85	6,275	0,57	300	12,56	12,63	-0,07
8	350	25,55	8	90	27,72	8	110	33,14	7,59	8	90	37	3,28	110	5,33	3,735	1,60	350	12,86	12,775	0,08
9	397	25,91	9	97,5	27,8	9	120	30,05	4,14	9	97,5	30	2,2	120	3,12	2,07	1,05	397	13,14	12,955	0,19
Average Height:		25,71	Average Height:		27,66																

Bottom table:

	Average measurement of three			Average measurement of three			Average measurement of three		Average measurement of three			Difference before and after cut of TWS				Difference before and after cut of TWS			
	Height of the **thin wall structure** from the lowest corner to the highest AFTER cut of weld [H]			Height of the **thin wall structure** from the lowest corner to the highest AFTER cut of weld [V]			Height of the **base-plate** from the lowest corner to highest AFTER the cut of the		Height of the **base-plate** from the lowest corner to highest AFTER the cut of the			**Delta-H** in height of the centerline of the TWS [V] (height/2)				**Delta-H** in height of the centerline in BP [V]. (height/2)			
Point:	Length [mm]	Height of TWS + BP [mm]	Height of only TWS [mm]	Point:	Length [mm]	Height of TWS + BP [mm]	Height of only TWS [mm]	Point:	Length [mm]	Height [mm]	Point:	Length [mm]	Height [mm]	Length [mm]	After cut	Before cut	Delta H	Length [mm]	After cut [mm]	Before cut [mm]	Delta H [mm]
1	0	33,90	12,70	1	0	42,62	15,44	1	0	27,20	1	0	27,18	0	7,72	6,975	0,745	0	13,53	13,74	-0,15
2	10	43,50	17,48	2	10	43,29	15,36	2	50	26,02	2	10	27,33	10	7,98	6,62	1,36	10	13,67	13,78	-0,11
3	20	43,47	18,25	3	30	43,56	16,02	3	100	25,22	3	30	27,54	30	8,01	6,15	1,86	30	13,77	13,78	-0,01
4	40	43,43	18,34	4	50	44,67	16,80	4	150	25,15	4	50	27,87	50	8,40	6,6	1,80	50	13,94	13,885	0,05
5	50	44,13	19,13	5	60	42,43	14,39	5	200	24,34	5	60	28,03	60	7,20	7,77	-0,57	60	14,02	13,835	0,18
6	70	41,32	16,37	6	70	40,53	12,38	6	250	24,95	6	70	28,15	70	6,19	7,585	-1,395	70	14,07	13,9	0,17
7	80	38,82	13,70	7	80	38,63	10,40	7	300	25,12	7	80	28,23	80	5,20	7,25	-2,05	80	14,12	13,805	0,31
8	110	36,50	10,79	8	90	36,43	8,12	8	350	25,71	8	90	28,30	90	4,06	4,64	-0,58	90	14,15	13,86	0,29
9	120	32,52	6,24	9	97,5	34,13	5,75	9	397	26,28	9	97,5	28,38	97,5	2,88	1,1	1,775	97,5	14,19	13,9	0,29
								Average Height:		25,62	Average Height:		27,83								

Figure 97: Deformation of neutral axis for P2D2. Documented by the measurement in appendix 124

B.7 Delta-H and Average height measurement - P4D2

Average measurment of three — Height of the base-plate from the lowest corner to highest

Point	Length [mm]	Height [mm]
1	0	23,04
2	50	23,09
3	100	23,15
4	150	23,17
5	200	23,19
6	250	23,48
7	300	24,24
8	357	24,85
		23,53
Average Height:		23,53

Average measurment of three — Height of the base-plate from the lowest corner to highest

Point	Length [mm]	Height [mm]
1	0	23,05
2	10	22,95
3	20	23,02
4	30	23,02
5	50	23,02
6	60	23,04
7	70	23,07
8	80	23,07
9	102	23,14
Average Height:		23,04

Average measurment of three — Height of the thin wall structure from the lowest corner to the highest BEFORE cut of

Point	Length [mm]	Height of TWS + BP	Height of only TWS
1	10	31,43	8,34
2	20	36,28	13,16
3	40	40,59	17,41
4	60	40,73	17,44
5	70	42,29	18,86
6	90	40,02	16,22
7	110	37,63	13,25
8	130	34,34	9,39
9	150	28,21	4,55

Average measurment of three — Height of the thin wall structure from the lowest corner to the highest BEFORE cut of

Point	Length [mm]	Height of TWS + BP	Height of only TWS
1	10	36,77	13,71
2	20	41,29	18,26
3	30	40,86	17,82
4	40	41,73	18,68
5	50	42,65	19,59
6	60	40,15	17,09
7	70	36,915	13,83
8	80	34,68	11,57
9	90	31,54	8,35

Difference before and after cut of TWS — Delta-H in height of the centerline of the TWS [H]

Length [mm]	After cut	Before cut	Delta H
10	4,41	4,17	0,25
20	6,88	6,58	0,30
40	9,17	8,71	0,46
60	9,29	8,72	0,57
70	10,08	9,43	0,65
90	8,76	8,11	0,65
110	7,13	6,63	0,50
130	4,97	4,69	0,27
150	2,48	2,28	0,20

Difference before and after cut of TWS — Delta-H in height of the centerline in BP [H]. (height/2)

Length [mm]	Before weld [mm]	After cut [mm]	Before cut [mm]	Delta H [mm]
0	11,49	11,52	11,55	-0,03
50	11,53	11,54	11,56	-0,02
100	11,58	11,58	11,59	-0,01
150	11,64	11,59	11,645	-0,06
200	11,71	11,60	11,715	-0,12
250	11,79	11,74	11,9	-0,16
300	11,88	12,12	12,19	-0,07
350	11,97	12,43	12,48	-0,05
397	11,7	11,77	11,83	-0,06

Average measurment of three — Height of the base-plate from the lowest corner to the highest

Point	Length [mm]	Height [mm]
1	0	23,09
2	50	23,12
3	100	23,18
4	150	23,29
5	200	23,43
6	250	23,8
7	300	24,38
8	357	24,96
		23,66
Average Height:		23,66

Average measurment of three — Height of the base-plate from the lowest corner to the highest

Point	Length [mm]	Height [mm]
1	0	23,06
2	10	23,04
3	20	23,04
4	30	23,05
5	50	23,06
6	60	23,06
7	70	23,09
8	80	23,11
9	102	23,18
Average Height:		23,08

Average measurment of three — Height of the thin wall structure from the lowest corner to the highest AFTER cut of

Point	Length [mm]	Height of TWS + BP	Height of only TWS
1	10	31,86	8,83
2	20	36,85	13,77
3	40	41,49	18,33
4	60	41,74	18,57
5	70	43,35	20,15
6	90	41	17,52
7	110	38,49	14,25
8	130	34,78	9,93
9	150	28,48	4,95

Average measurment of three — Height of the thin wall structure from the lowest corner to the highest AFTER cut of

Point	Length [mm]	Height of TWS + BP	Height of only TWS
1	10	32,39	9,34
2	20	38,04	15,09
3	30	42,11	19,09
4	40	41,75	18,73
5	50	42,80	19,77
6	60	43,56	20,52
7	70	40,72	17,65
8	80	37,03	13,96
9	90	34,48	11,34

Difference before and after cut of TWS — Delta-H in height of the centerline of the TWS [V]

Length [mm]	After cut	Before cut	Delta H
10	4,67	6,86	-2,19
20	7,55	9,13	-1,58
30	9,54	8,91	0,63
40	9,37	9,34	0,03
50	9,89	9,80	0,09
60	10,26	8,54	1,72
70	8,83	6,91	1,91
80	6,98	5,79	1,19
90	5,67	4,18	1,49

Difference before and after cut of TWS — Delta-H in height of the centerline in BP [V]. (height/2)

Length [mm]	Before weld [mm]	After cut [mm]	Before cut [mm]	Delta H [mm]
0	11,62	11,53	11,53	-0,01
10	11,61	11,47	11,52	-0,04
20	11,61	11,51	11,52	-0,01
30	11,62	11,51	11,52	-0,01
50	11,63	11,51	11,53	-0,02
60	11,64	11,52	11,53	-0,01
70	11,66	11,53	11,54	-0,01
80	11,67	11,54	11,55	-0,02
102	11,7	11,57	11,59	-0,02

Figure 98: Deformation of neutral axis for P4D2. Documented by the measurement in appendix **??**

B.8   Delta-H and Average height measurement - P4D3

Top table (BEFORE cut)

Average measurement of one — Height of the base-plate from the			Average measurement of one — Height of the base-plate from the			Average measurement of one — Height of the thin wall structure from the lowest corner to the highest BEFORE cut of				Average measurement of one — Height of the thin wall structure from the lowest corner to the highest BEFORE cut of				Average measurement of three — Height of the base-plate from the			Difference before and after cut of TWS — Delta H in height of the centerline of the TWS [20]				Difference before and after cut of TWS — Delta H in height of the centerline in BP [H] (height/2)				
Point	Length [mm]	Height [mm]	Point	Length [mm]	Height [mm]	Point	Length [mm]	Height of TWS+BP	Height of only TWS	Point	Length [mm]	Height of TWS+BP	Height of only TWS	Point	Length [mm]	Height [mm]	Length [mm]	After cut [mm]	Before cut [mm]	Delta H [mm]	Length [mm]	Before weld [mm]	After cut [mm]	Before cut [mm]	Delta H [mm]
1	0	24,16	1	0	24,16	1	0	34,45	7,65	1	0	35,7	8,9	1	0	25,81	0	2,80	3,83	-1,03	0	12,08	13,40	12,90	0,50
2	50	24,15	2	10	24,16	2	30	43,76	18,06	2	30	42,47	16,77	2	50	25,34	30	7,11	9,03	-1,92	50	12,075	12,85	12,67	0,18
3	100	24,16	3	30	24,11	3	50	46,21	21,27	3	50	43,87	18,93	3	100	24,85	50	7,43	10,64	-3,21	100	12,08	12,47	12,42	0,05
4	150	24,16	4	50	24,11	4	70	47,95	23,51	4	70	47,91	23,47	4	150	24,42	70	11,00	11,76	-0,76	150	12,08	12,22	12,21	0,01
5	200	24,16	5	60	24,11	5	85,5	50,5	26,3	5	85,5	50,52	26,32	5	200	24,28	85,5	13,48	13,15	0,33	200	12,08	12,10	12,14	-0,04
6	250	24,16	6	70	24,11	6	110	45,16	20,97	6	110	45,15	20,96	6	250	24,34	110	11,83	10,49	1,34	250	12,08	12,10	12,17	-0,07
7	300	24,16	7	80	24,1	7	140	45,04	20,85	7	140	44,83	20,64	7	300	24,43	140	10,27	10,43	-0,15	300	12,08	12,10	12,22	-0,12
8	350	24,18	8	90	24,1	8	160	39,03	14,83	8	160	38,53	14,33	8	350	24,58	160	8,06	7,42	0,64	350	12,09	12,10	12,29	-0,19
9	398	24,18	9	100	24,1	9	180	32,44	8,2	9	180	32,7	8,46	9	398	24,66	180	4,99	4,10	0,89	398	12,09	12,12	12,33	-0,21

Bottom table (AFTER cut)

Average measurement of one — Height of the base-plate from the			Average measurement of one — Height of the base-plate from the			Average measurement of three — Height of the thin wall structure from the lowest corner to the highest AFTER cut of				Average measurement of three — Height of the thin wall structure from the lowest corner to the highest AFTER cut of				Average measurement of three — Height of the base-plate from the			Difference before and after cut of TWS — Delta H in height of the centerline of the TWS [-20]				Difference before and after cut of TWS — Delta H in height of the centerline in BP [V] (height/2)				
Point	Length [mm]	Height [mm]	Point	Length [mm]	Height [mm]	Point	Length [mm]	Height of TWS+BP	Height of only TWS	Point	Length [mm]	Height of TWS+BP	Height of only TWS	Point	Length [mm]	Height [mm]	Length [mm]	After cut [mm]	Before cut [mm]	Delta H [mm]	Length [mm]	Before weld [mm]	After cut [mm]	Before cut [mm]	Delta H [mm]
1	0	26,8	1	0	26,8	1	0	31,41	5,60	1	0	37,1	11,29	1	0	26,15	0	5,65	4,45	1,20	0	12,08	13,08	13,40	-0,32
2	50	25,70	2	10	27,09	2	30	39,57	14,22	2	30	45,01	19,67	2	10	26,49	30	9,83	8,39	1,45	10	12,08	13,25	13,55	-0,30
3	100	24,94	3	30	27,21	3	50	39,71	14,86	3	50	46,84	21,99	3	30	26,53	50	11,00	9,47	1,53	30	12,06	13,27	13,61	-0,34
4	150	24,44	4	50	28,05	4	70	46,42	22,00	4	70	48,68	24,26	4	50	27,22	70	12,13	11,74	0,40	50	12,06	13,61	14,03	-0,42
5	200	24,2	5	60	28,21	5	85,5	51,2	26,96	5	85,5	51,40	27,11	5	60	27,57	85,5	13,56	13,16	0,40	60	12,06	13,78	14,11	-0,32
6	250	24,19	6	70	28,61	6	110	48,0	23,65	6	110	46,36	22,03	6	70	27,83	110	11,01	10,48	0,53	70	12,06	13,92	14,31	-0,39
7	300	24,19	7	80	29,09	7	140	44,98	20,55	7	140	45,78	21,35	7	80	28,40	140	10,68	10,32	0,35	80	12,05	14,20	14,55	-0,35
8	350	24,2	8	90	29,52	8	160	40,69	16,11	8	160	39,56	14,99	8	90	28,57	160	7,49	7,17	0,33	90	12,05	14,29	14,76	-0,48
9	398	24,24	9	100	29,82	9	180	34,64	9,98	9	180	32,07	7,41	9	100	28,38	180	3,71	4,23	-0,52	100	12,05	14,19	14,91	-0,72

Figure 99: Deformation of neutral axis for P4D3. Documented by the measurement in appendix 127

C Graph of the polynomial-curve which describe neutral axis of the TWS and BP

The graphs in this appendix are based on the data from B.

C.1 Graph - P1D1
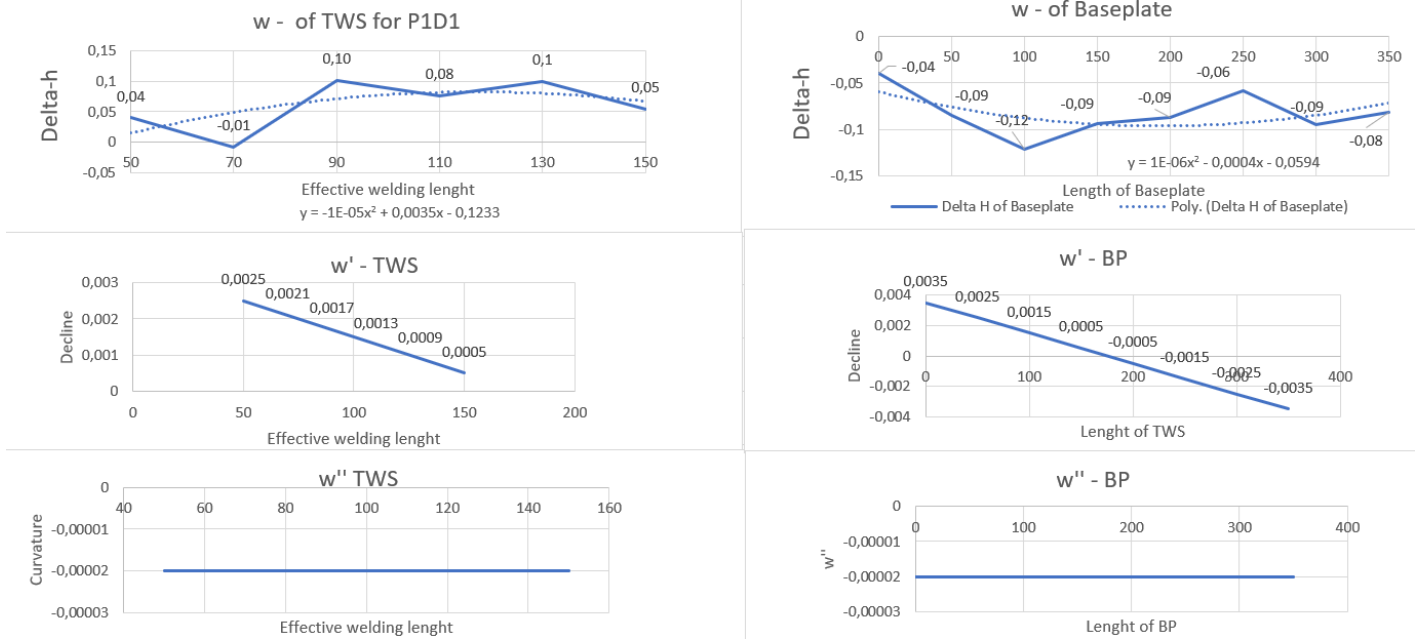
Figure 100: Graph of deformation (W), decline/increase (w') and the curvature (w"). Based on the data documented in appendix 92

C.2   Graph - P2D1
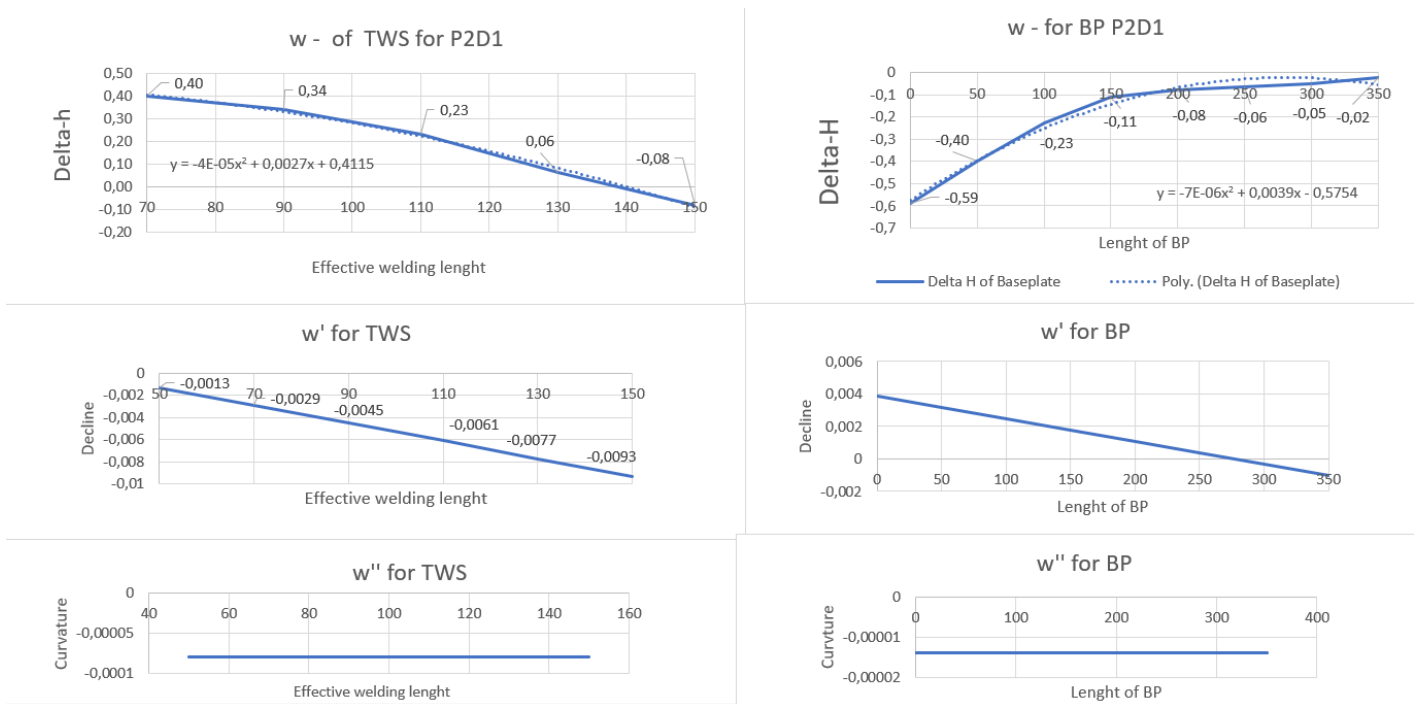
Figure 101: Graph of deformation (W), decline/increase (w') and the curvature (w"). Based on the data documented in appendix 93

C.3   Graph - P3D1
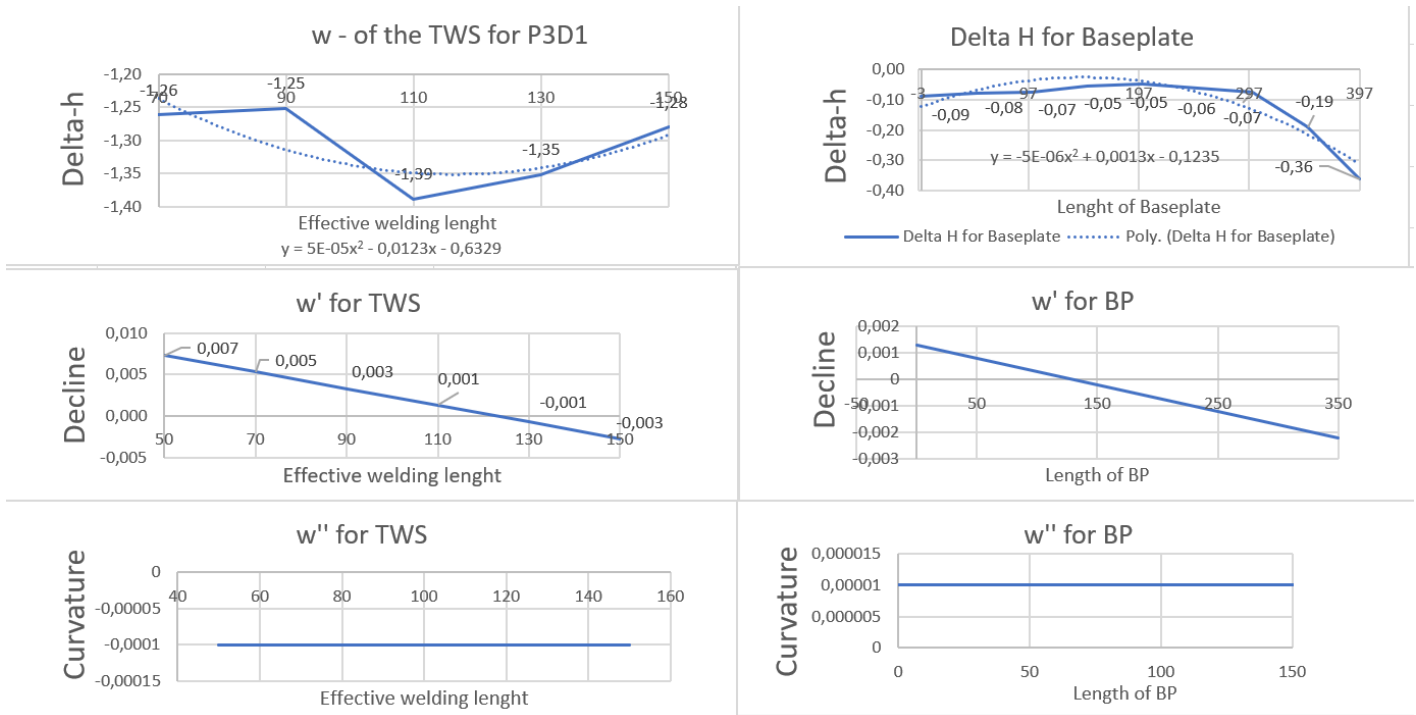
Figure 102: Graph of deformation (W), decline/increase (w') and the curvature (w").Based on the data documented in appendix 94

C.4   Graph - P5D1
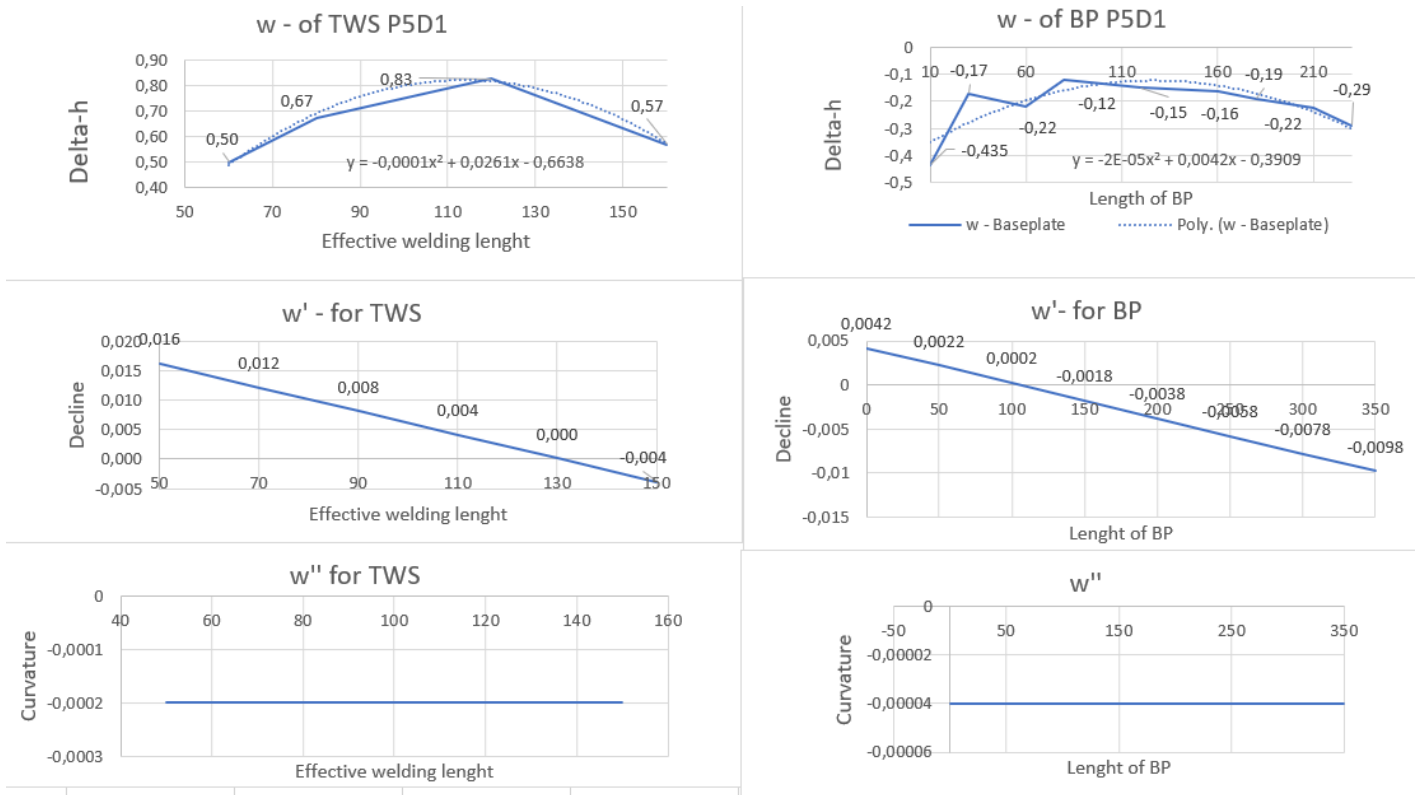
Figure 103: Graph of deformation (W), decline/increase (w') and the curvature (w").Based on the data documented in appendix 95

C.5   Graph - P1D2 - TWS
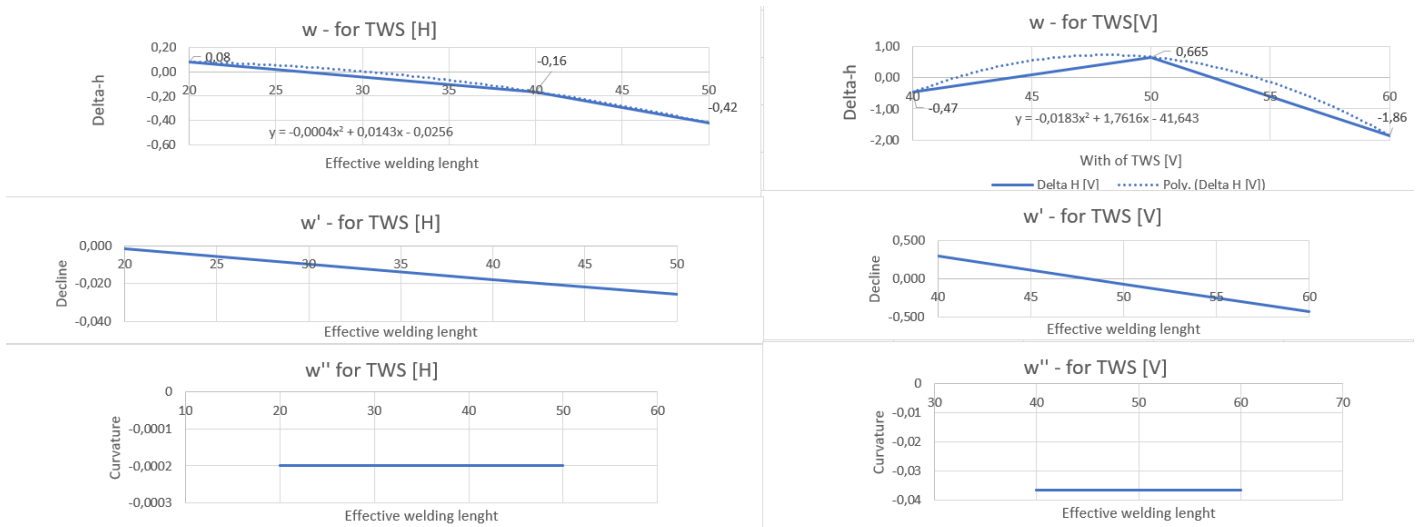
Figure 104: Graph of deformation (W), decline/increase (w') and the curvature (w"). Based on the data documented in appendix 96

C.6   Graph - P1D2 - BP
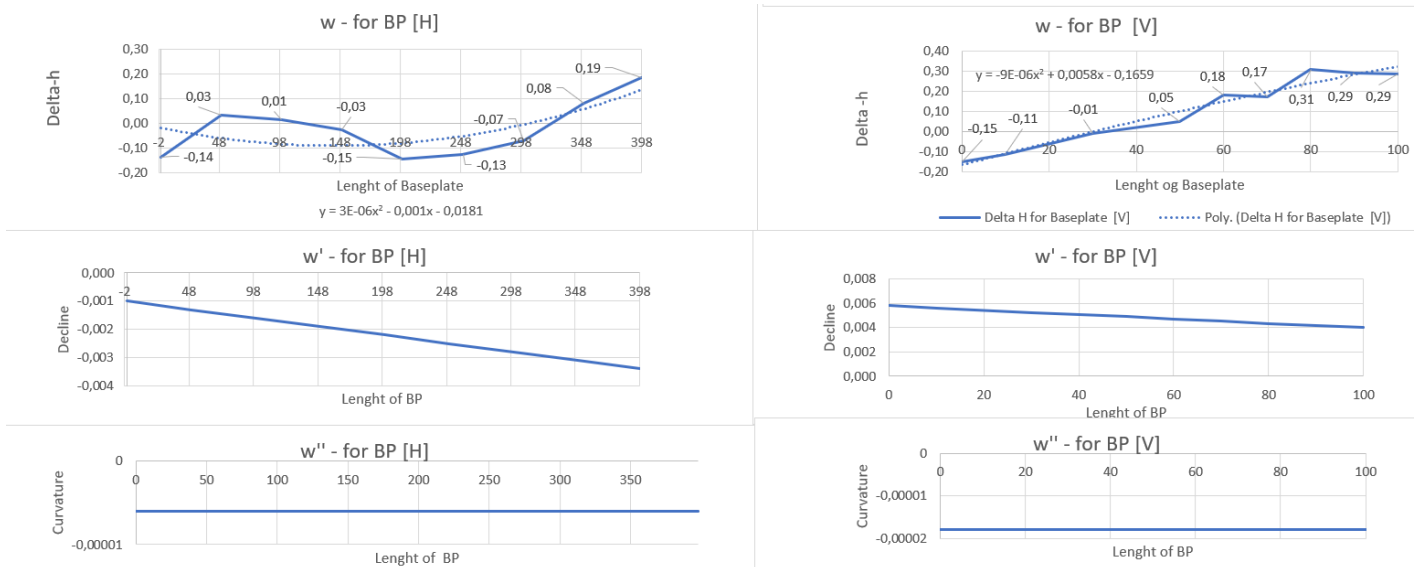
Figure 105: Graph of deformation (W), decline/increase (w') and the curvature (w"). Based on the data documented in appendix 96

C.7   Graph - P2D2 - TWS
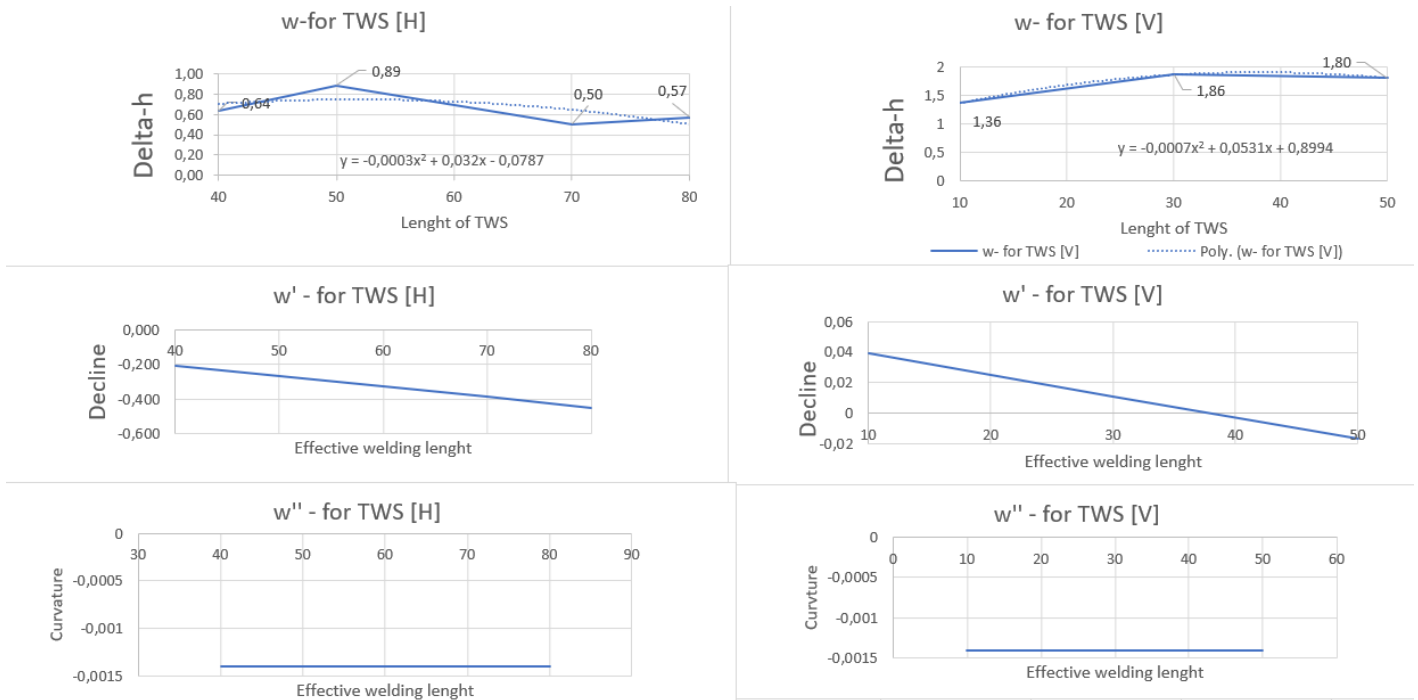
Figure 106: Graph of deformation (W), decline/increase (w') and the curvature (w"). Based on the data documented in appendix 97

C.8   Graph - P2D2 - BP
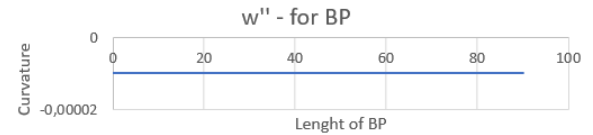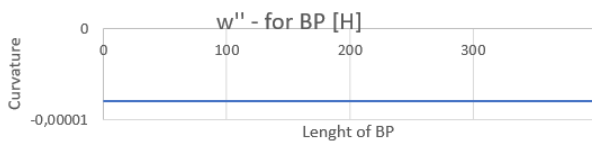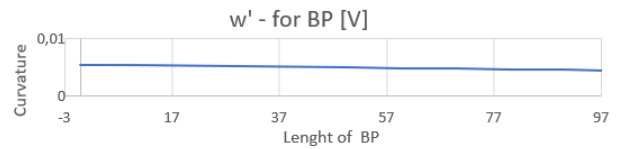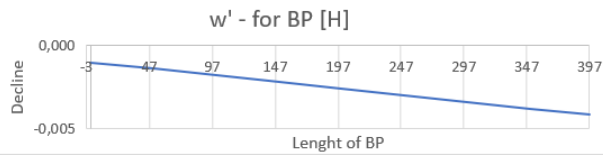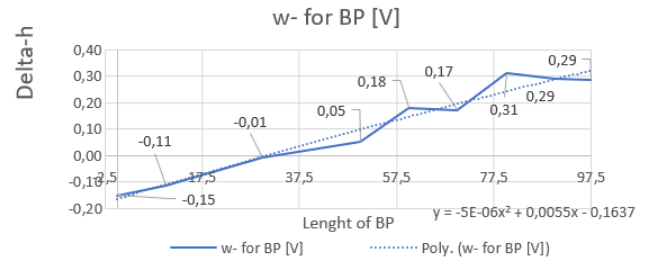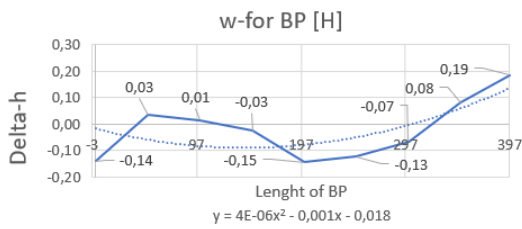
Figure 107: Graph of deformation (W), decline/increase (w') and the curvature (w"). Based on the data documented in appendix 97

C.9   Graph - P4D2 - TWS
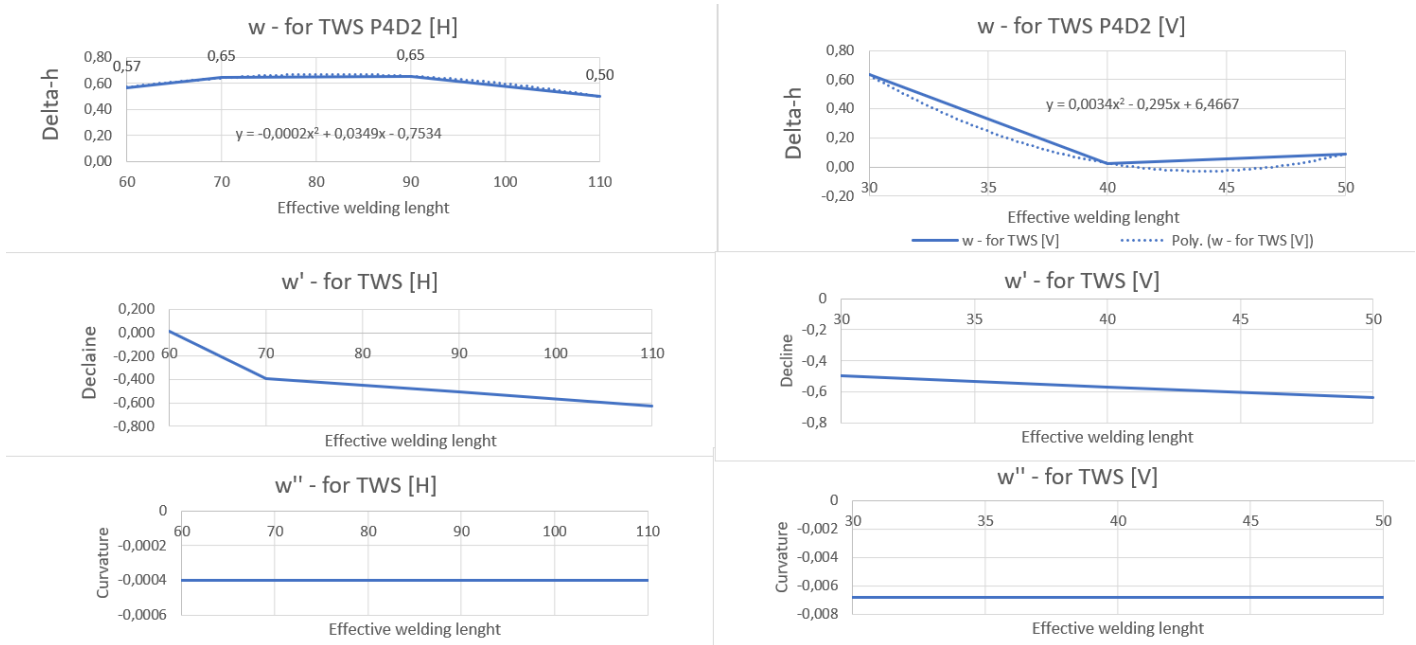
Figure 108: Graph of deformation (W), decline/increase (w') and the curvature (w"). Based on the data documented in appendix 98

C.10   Graph - P4D2 - BP
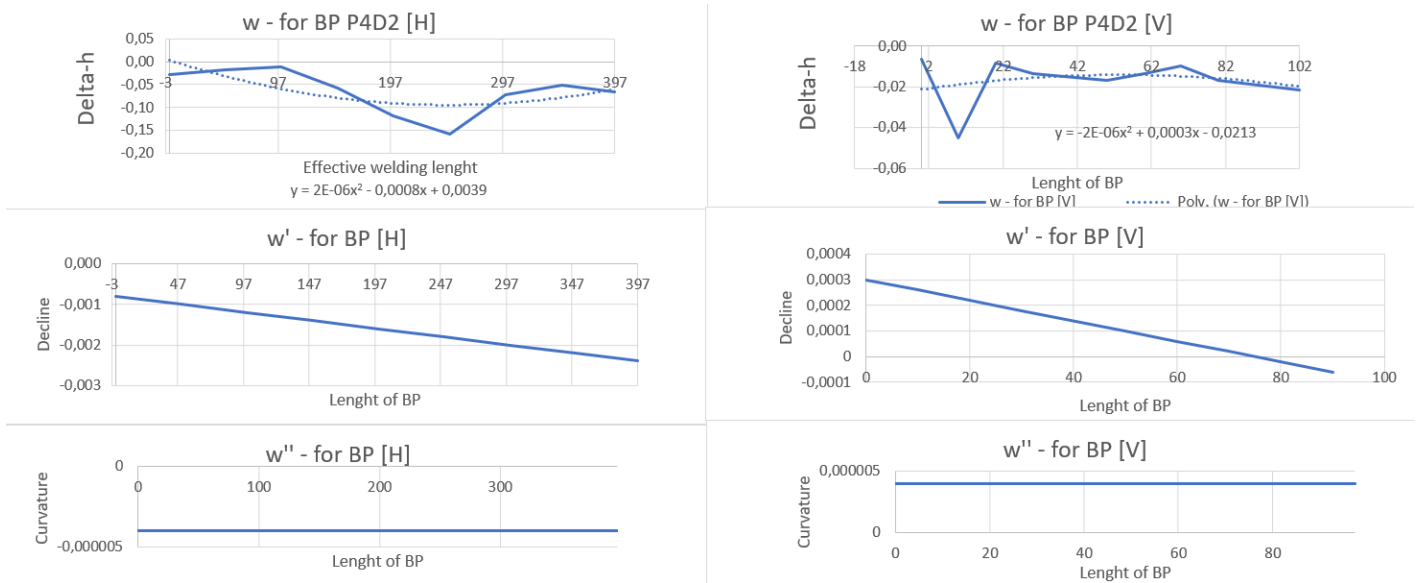
Figure 109: Graph of deformation (W), decline/increase (w') and the curvature (w"). Based on the data documented in appendix 98

C.11   Graph - P4D3 - TWS
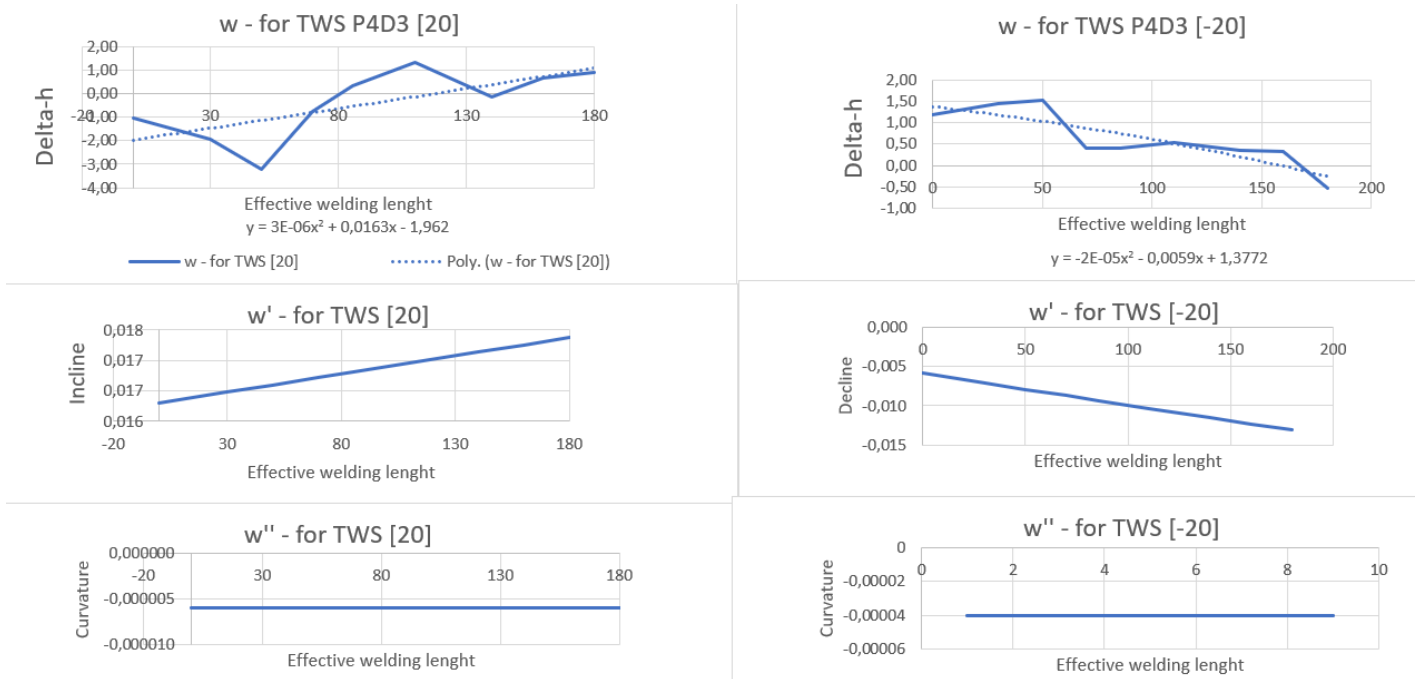
Figure 110: Graph of deformation (W), decline/increase (w') and the curvature (w"). Based on the data documented in appendix 97

C.12   Graph - P4D3 - BP
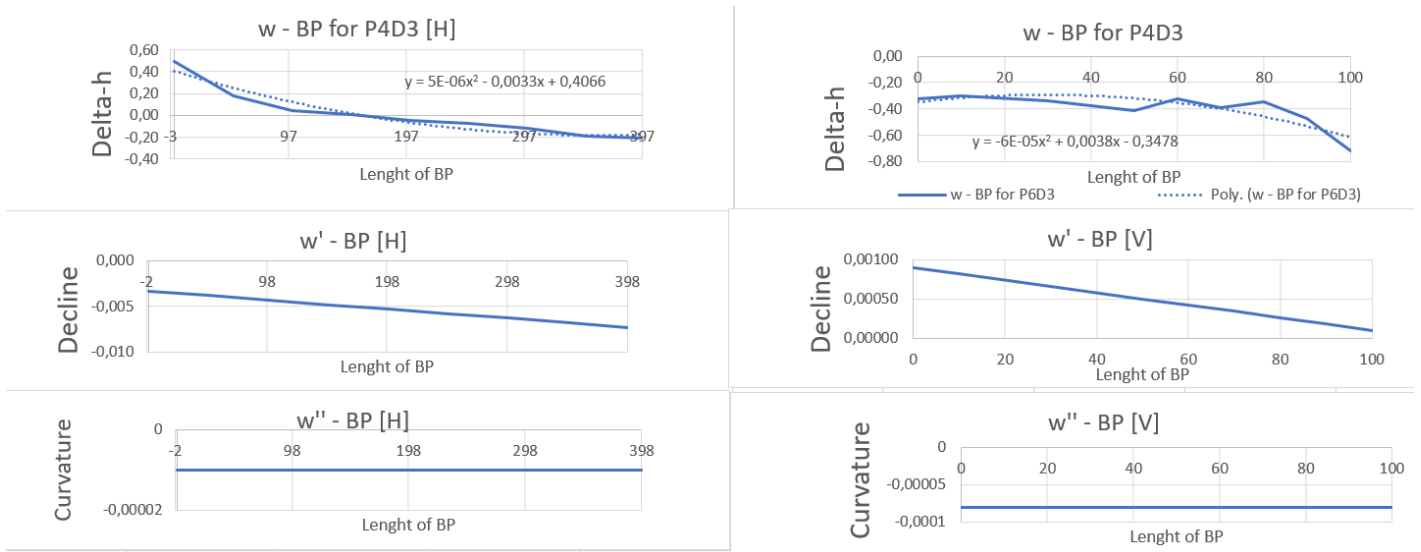
Figure 111: Graph of deformation (W), decline/increase (w') and the curvature (w"). Based on the data documented in appendix 99

D   Calculation of the practical experiment - calculating the residual stresses

D.1   Calculation of sample P1D1

• **Function of the effective welding lenght of TWS**			
Delta H:	(-(1*10^-5)*x^2+(0.0035)*x-0.1233)		
w'	0,0035-0,00002*x		
w''	-0,00002		
• **Residual stresses along the TWS**			
Residual stress [N/mm^2]	74,4939	Formula for residual stress:	$\sigma = \dfrac{Mz}{I} = -zE\,\dfrac{\mathrm{d}^2 w}{\mathrm{d}x^2}.$
z=	18,62		
• **Function of the BP height difference**			
w:	((1*10^-6)*x^2-(0,0004)*x-0,0594		
w' :	(0,0035-0,00002*x)		
w'':	0,000002		
• **Residual stresses along the BP**			
Residual stress [N/mm^2]	5,07	Formula for residual stress:	$\sigma = \dfrac{Mz}{I} = -zE\,\dfrac{\mathrm{d}^2 w}{\mathrm{d}x^2}.$
z=	12,69		

Figure 112: Calculation of RS based on the data documented in appendix 92

D.2 Calculation of sample P2D1

• Function of the delta-h along TWS				
w	(-(4*10^-5)*x^2+(0,0027)*x+0,4115)			
w'	(0,0027-0,00008*)			
w''	(-0,00008)			
• Residual stresses in the TWS:				$\sigma = \dfrac{Mz}{I} = -zE\,\dfrac{\mathrm{d}^2 w}{\mathrm{d}x^2}.$
Residual stress [N/mm^2]	320		Formula for residual stress:	
z=	20			
• Function of the BP height difference				
w	(-(7*10^-6)*x^2+0,0039*x-0,5754)			
w'	(-0.000014*(-278.571+x))			
w''	-0,000014			
• Curvature:	-0,000014			
• Residual stresses along the BP:				$\sigma = \dfrac{Mz}{I} = -zE\,\dfrac{\mathrm{d}^2 w}{\mathrm{d}x^2}.$
Residual stress [N/mm^2]	56		Formula for residual stress:	
z=	20			

Figure 113: Calculation of RS based on the data documented in appendix 92

D.3   Calculation of sample P3D1

• **Function of delta-h along TWS**					
w	(-(5*10^-5)*x^2+0.0123x - 0.6329)				
w'	(0.0001 (-123 + x))				
w"	(-0.0001)		**Curvature:**	-0,0001	$$\sigma = \frac{Mz}{I} = -zE\,\frac{\mathrm{d}^2 w}{\mathrm{d}x^2}.$$
• **Residual stresses along the TWS:**					
Residual stress [N/mm^2]	353,31			Formula for residual stress:	
z=	18,31				
• **Function of the BP height difference**					
w	(-(5*10^-6)*x^2+0,0013*x-0,1235)				
w'	(0,0013-0,00001*x)				
w"	-0,00001				
• Curvature:	-0,00001				
• **Residual stresses along the BP:**					$$\sigma = \frac{Mz}{I} = -zE\,\frac{\mathrm{d}^2 w}{\mathrm{d}x^2}.$$
Residual stress [N/mm^2]	38,6			Formula for residual stress:	
z=	20				

Figure 114: Calculation of RS based on the data documented in appendix 92

D.4   Calculation of sample P5D1

• Function of the effective welding lenght of TWS				
w	(-(0,0001)*x^2+0,0261*x-0,6638)			
w'	(0,0261-0,0002*x)			
w"	-0,0002			
• Residual stresses that occur at given point due to the moment:				$\sigma = \dfrac{Mz}{I} = -zE\,\dfrac{\mathrm{d}^2 w}{\mathrm{d}x^2}.$
Residual stress [N/mm^2]	284,09		Formula for residual stress:	
z=	7,36			
• Function of the BP height difference				
w	(-(2*10^-5)*x^2+(0,0042)*x-0,3909)			
w'	(0,0042-0,00004*x)			
w"	-0,00004			
• Curvature:	-0,00004			
• Residual stresses that occur at given point due to the moment:				$\sigma = \dfrac{Mz}{I} = -zE\,\dfrac{\mathrm{d}^2 w}{\mathrm{d}x^2}.$
Residual stress [N/mm^2]	154,4		Formula for residual stress:	
z=	20			

Figure 115: Calculation of RS based on the data documented in appendix 92

D.5 Calculation of sample P1D2

• Function of delta-h along the TWS [H]				• Function of delta-h along the TWS [V]		
w	(-(0,0004)*x^2+0,0143*x-0,0256)			w	(-(0,0183)*x^2+1,7616*x-41,643)	
w'	(0,0143-0,0008*x)			w'	(1,7616-0,0366*x)	
w''	-0,0008			w''	-0.0366	
• Residual stresses :				• Residual stresses :		
Residual stress [N/mm^2]	1286,07			Residual stress [N/mm^2]	50820,36	
z=	8,33			z=	7,19	
Formula for residual stress:	$\sigma = \dfrac{Mz}{I} = -zE\dfrac{\mathrm{d}^2 w}{\mathrm{d}x^2}.$			Formula for residual stress:	$\sigma = \dfrac{Mz}{I} = -zE\dfrac{\mathrm{d}^2 w}{\mathrm{d}x^2}.$	
• Function of delta-h along the BP [H]				• Function of delta-h along the BP [V]		
w	(-(3*10^-6)*x^2-0,001*x-0,0181			w	(-(9*10^-6)*x^2+0,0058*x-0,1659)	
w'	(-6×10^-6*(166,667+x))			w'	(-0,000018*(-322.222+x))	
w''	(-(6*10^-6))			w''	-0,000018	
• Curvature:	-0,000006			• Curvature:	-0,000018	
• Residual stresses :				• Residual stresses :		
Residual stress [N/mm^2]	14,83483778			Residual stress [N/mm^2]	48,44686	
z=	12,81			z=	13,95	

Figure 116: Calculation of RS based on the data documented in appendix 92

D.6 Calculation of sample P2D2

• Function of delta-h along the TWS [H]				• Function of delta-h along the TWS [V]		
w	(-(0,003)*x^2+0,032*x-0,0787)			w	(-(0,0007)*x^2+0,0531*x+0,8994)	
w'	(0,032-0,006*x)			w'	(0,0531-0,0014*x)	
w''	-0,006			w''	-0,0014	
• Residual stresses:				• Residual stresses:		
Residual stress [N/mm^2]	9941,04			Residual stress [N/mm^2]	2196,58	
z=	8,58			z=	8,13	
Formula for residual stress:	$\sigma = \dfrac{Mz}{I} = -zE\,\dfrac{\mathrm{d}^2 w}{\mathrm{d}x^2}.$			Formula for residual stress:	$\sigma = \dfrac{Mz}{I} = -zE\,\dfrac{\mathrm{d}^2 w}{\mathrm{d}x^2}.$	
• Function of delta-h along the BP [H]				• Function of delta-h along the BP [V]		
w	(-(4*10^-6)*x^2-0,001*x-0,018)			w	(-(5*10^-6)*x^2+0,0055*x-0,1637)	
w'	(-0.001-(8×10^-6)*x)			w'	(0,0055-0,00001*x)	
w''	-0,000008			w''	-0,00001	
• Curvature:	-0,000008			• Curvature:	-0,00001	
• Residual stresses:				• Residual stresses:		
Residual stress [N/mm^2]	19,78	z=	12,81	Residual stress [N/mm^2]	26,91	z=	13,95

Figure 117: Calculation of RS based on the data documented in appendix 92

D.7   Calculation of sample P4D2

• Function of delta-h along the TWS [H]				• Function of delta-h along the TWS [V]			
w	(-(0,0002)*x^2+0,0349*x-0,7534)			w	(-(0,0034)*x^2-0,295*x+6,4667)		
w'	(0,0349-0,0004*x)			w'	(-0,295-0,0068*x)		
w"	-0,0004			w"	-0,0068		
• Residual stresses:				• Residual stresses:			
Residual stress [N/mm^2]	585,50	z=	7,58	Residual stress [N/mm^2]	10607,84	z=	8,08
Formula for residual stress:	$\sigma = \dfrac{Mz}{I} = -zE\,\dfrac{\mathrm{d}^2 w}{\mathrm{d}x^2}.$			Formula for residual stress:	$\sigma = \dfrac{Mz}{I} = -zE\,\dfrac{\mathrm{d}^2 w}{\mathrm{d}x^2}.$		
• Function of delta-h along BP [H]				• Function of delta-h along the BP [V]			
w	(-(2*10^-6)*x^2-0,0008*x+0,0039)			w	(-(2*10^-6)*x^2+(0,0003)*x-0,0213)		
w'	(-0,0008-(4×10^-6)*x)			w'	(0,0003-(4×10^-6)*x)		
w"	-0,000004			w"	-0,000004		
• Curvature:	-0,000004			• Curvature:	0,000004		
• Residual stresses that occur at given point due to the moment:				• Residual stresses that occur at given point due to the moment:			
Residual stress [N/mm^2]	9,08	z=	11,76	Residual stress [N/mm^2]	8,89	z=	11,52

Figure 118: Calculation of RS based on the data documented in appendix 92

D.8   Calculation of sample P4D3

• Function of delta-h along the TWS [H]				• Function of delta-h along the TWS [V]			
w	(-(0,0002)*x^2+0,0349*x-0,7534)			w	(-(0,0034)*x^2-0,295*x+6,4667)		
w'	(0,0349-0,0004*x)			w'	(-0,295-0,0068*x)		
w"	-0,0004			w"	-0,0068		
• Residual stresses:				• Residual stresses:			
Residual stress [N/mm^2]	585,50	z=	7,58	Residual stress [N/mm^2]	10607,84	z=	8,08
Formula for residual stress:	$\sigma = \dfrac{Mz}{I} = -zE\,\dfrac{\mathrm{d}^2w}{\mathrm{d}x^2}.$			Formula for residual stress:	$\sigma = \dfrac{Mz}{I} = -zE\,\dfrac{\mathrm{d}^2w}{\mathrm{d}x^2}.$		
• Function of delta-h along BP [H]				• Function of delta-h along the BP [V]			
w	(-(2*10^-6)*x^2-0,0008*x+0,0039)			w	(-(2*10^-6)*x^2+(0,0003)*x-0,0213)		
w'	(-0,0008-(4×10^-6)*x)			w'	(0,0003-(4×10^-6)*x)		
w"	-0,000004			w"	-0,000004		
• Curvature:	-0,000004			• Curvature:	0,000004		
• Residual stresses that occur at given point due to the moment:				• Residual stresses that occur at given point due to the moment:			
Residual stress [N/mm^2]	9,08	z=	11,76	Residual stress [N/mm^2]	8,89	z=	11,52

Figure 119: Calculation of RS based on the data documented in appendix 92

E Height measurement for TWS - Documentation for the delta-h values

E.1 Height measurement - P1D1

Measurement 1 — Height of the **BP** from the lowest corner to highest AFTER the cut of the weld[H]:			Measurement 1 — Height of the **TWS** from the lowest corner to the highest AFTER cut of weld[H]:			Measurement 2 — Height of the **BP** from the lowest corner to highest AFTER the cut of the weld[H]:			Measurement 2 — Height of the **TWS** from the lowest corner to the highest AFTER cut of weld[H]:		
Point:	Length [mm]:	Height [mm]:	Point:	Length [mm]:	Height [mm]:	Point:	Length [mm]:	Height [mm]:	Point:	Length [mm]:	Height [mm]:
1	0	27,58	1	1	55,47	1	0	27,61	1	1	55,3
2	50	26,07	2	3	58,14	2	50	26,04	2	3	58,3
3	100	24,88	3	5	61,9	3	100	24,96	3	5	61,77
5	150	24,55	4	7	63,87	5	150	24,52	4	7	63,8
5	200	24,57	5	9	64,72	5	200	24,55	5	9	64,85
6	250	24,79	6	11	65,17	6	250	24,81	6	11	65,57
7	300	25,11	7	13	65,37	7	300	25,06	7	13	65,57
8	350	25,43	8	15	65,5	8	350	25,43	8	15	65,7
9	398		9	17,7	64,96	9	398		9	17,7	64,96

Measurement 3 — Height of the **BP** from the lowest corner to highest AFTER the cut of the weld[H]:			Measurement 3 — Height of the **TWS** from the lowest corner to the highest AFTER cut of weld[H]:			Measurement 4 — Height of the **BP** from the lowest corner to highest AFTER the cut of the weld[H]:			Measurement 4 — Height of the **TWS** from the lowest corner to the highest AFTER cut of weld[H]:		
Point:	Length [mm]:	Height [mm]:	Point:	Length [mm]:	Height [mm]:	Point:	Length [mm]:	Height [mm]:	Point:	Length [mm]:	Height [mm]:
1	0	27,6	1	1	55,25	1	0	27,61	1	1	55,25
2	50	26,05	2	3	57,93	2	50	26,04	2	3	57,93
3	100	24,91	3	5	61,8	3	100	24,96	3	5	61,8
5	150	24,54	4	7	63,6	5	150	24,52	4	7	63,6
5	200	24,55	5	9	64,47	5	200	24,55	5	9	64,47
6	250	24,8	6	11	65,06	6	250	24,81	6	11	65,06
7	300	25,09	7	13	65,15	7	300 xliii	25,06	7	13	65,15
8	350	25,42	8	15	65,11	8	350	25,43	8	15	65,11
9	398		9	17,7	64,25	9	398		9	17,7	64,25

E.2 Height measurement - P2D1

Measurement 1 – Height of the TWS from the lowest corner to the highest AFTER cut of the weld[H]:			Measurement 1 – Height of the BP from the lowest corner to highest AFTER the cut of the weld[H]:			Measurement 2 – Height of the TWS from the lowest corner to the highest AFTER cut of the weld[H]:			Measurement 2 – Height of the BP from the lowest corner to highest AFTER the cut of the weld[H]:		
Point:	Length [mm]:	Height [mm]:	Point:	Length [mm]:	Height [mm]:	Point:	Length [mm]:	Height [mm]:	Point:	Length [mm]:	Height [mm]:
1	10	64,58	1	0	26,51	1	10	64,1	1	0	26,5
2	30	65,45	2	50	25,45	2	30	65,19	2	50	25,38
3	50	65,93	3	100	24,71	3	50	65,58	3	100	24,73
4	70	66,01	4	150	24,51	4	70	65,8	4	150	24,48
5	90	65,25	5	200	24,57	5	90	65,14	5	200	24,57
6	110	64,12	6	250	24,78	6	110	63,98	6	250	24,8
7	130	61,67	7	300	25,2	7	130	61,7	7	300	25,16
8	150	58,1	8	348,5	25,57	8	150	58	8	348,5	25,53
9	175	52,08	9	398		9	175	52,22	9		

Measurement 3 – Height of the TWS from the lowest corner to the highest AFTER cut of the weld[H]:			Measurement 3 – Height of the BP from the lowest corner to highest AFTER the cut of the weld[H]:		
Point:	Length [mm]:	Height [mm]:	Point:	Length [mm]:	Height [mm]:
1	10	64,09	1	0	26,49
2	30	65,16	2	50	25,43
3	50	65,7	3	100	24,72
4	70	65,84	4	150	24,52
5	90	65,06	5	200	24,59
6	110	63,78	6	250	24,81
7	130	61,55	7	300 xlv	25,15
8	150	58	8	348,5	25,53
9	175	52,08	9		

E.3 Height measurement - P3D1

Measurement 1 — Height of the BP from the lowest corner to highest AFTER the cut of the weld[H]:			Measurement 1 — Height of the TWS from the lowest corner to the highest AFTER cut of the weld[H]:			Measurement 2 — Height of the BP from the lowest corner to highest AFTER the cut of the weld[H]:			Measurement 2 — Height of the TWS from the lowest corner to the highest AFTER cut of the weld[H]:		
Point:	Length [mm]:	Height [mm]:	Point:	Length [mm]:	Height [mm]:	Point:	Length [mm]:	Height [mm]:	Point:	Length [mm]:	Height [mm]:
1	0	25,53	1	10	55,94	1	0	24,86	1	10	49,23
2	50	25,44	2	30	60,04	2	50	24,86	2	30	52,95
3	100	25,28	3	50	63,48	3	100	24,76	3	50	56,2
4	150	25,21	4	70	65,72	4	150	24,73	4	70	58,55
5	200	25,14	5	90	66,97	5	200	24,76	5	90	59,96
6	250	25,07	6	110	67,26	6	250	24,84	6	110	60,1
7	300	25,43	7	130	67,62	7	300	25,15	7	130	60,27
8	350	26,03	8	150	67,83	8	350	25,81	8	150	60,4
9	397	26,73	9	176	67,22	9	397	26,6	9	176	59,83

Measurement 3 — Height of the BP from the lowest corner to highest AFTER the cut of the weld[H]:			Measurement 3 — Height of the TWS from the lowest corner to the highest AFTER cut of the weld[H]:		
Point:	Length [mm]:	Height [mm]:	Point:	Length [mm]:	Height [mm]:
1	0	24,86	1	10	49,35
2	50	24,81	2	30	53,1
3	100	24,76	3	50	63,6
4	150	24,74	4	70	66,29
5	200	24,75	5	90	67,62
6	250	24,85	6	110	67,86
7	300	25,15	7	130	68,04
8	350	25,8	8	150	68,21
9	397	26,57	9	176	67,42

xlvii

E.4 Height measurement - P5D1

| Measurement 1 | | | Measurement 1 | | | Measurement 2 | | | Measurement 2 | | |
| Height of the **TWS** from the lowest corner to the highest AFTER cut of weld[H]: | | | Height of the **BP** from the lowest corner to highest AFTER the cut of the weld[H]: | | | Height of the **TWS** from the lowest corner to the highest AFTER cut of weld[H]: | | | Height of the **BP** from the lowest corner to highest AFTER the cut of the weld[H]: | | |
Point:	Length [mm]:	Height [mm]:	Point:	Length [mm]:	Height [mm]:	Point:	Length [mm]:	Height [mm]:	Point:	Length [mm]:	Height [mm]:
1	10	36,16	1	0	25,24	1	10	37,41	1	0	25,25
2	30	56,47	2	50	24,86	2	30	56,7	2	50	24,9
3	60	56,03	3	100	24,57	3	60	56	3	100	24,57
4	80	55,38	4	150	24,44	4	80	55,47	4	150	24,43
5	120	55,39	5	200	24,3	5	120	55,42	5	200	24,31
6	160	53,7	6	250	24,45	6	160	53,71	6	250	24,5
7	180	50,36	7	300	24,86	7	180	50,45	7	300	24,87
8	210	45,96	8	350	25,3	8	210	45,86	8	350	25,35
9	230	42,25	9	387	25,91	9	230	42,67	9	387	26,01

| Measurement 3 | | | Measurement 3 | | |
| Height of the **TWS** from the lowest corner to the highest AFTER cut of weld[H]: | | | Height of the **BP** from the lowest corner to highest AFTER the cut of the weld[H]: | | |
Point:	Length [mm]:	Height [mm]:	Point:	Length [mm]:	Height [mm]:
1	10	36,53	1	0	25,2
2	30	57,05	2	50	25,84
3	60	56,21	3	100	24,54
4	80	55,7	4	150	24,4
5	120	55,77	5	200	24,29
6	160	54,05	6	250	24,45
7	180	50,79	7	300 xlix	24,82
8	210	46,35	8	350	25,29
9	230	42,66	9	387	25,94

E.5   Height measurement - P2D2

Measurement 1 — Height of the **thin wall structure** from the lowest corner to the highest AFTER cut of weld [H]:

Point:	Length [mm]:	Height [mm]:
1	1	39,9
2	2	43,55
3	3	43,55
4	4	43,46
5	5	44,07
6	7	41,31
7	8	38,82
8	9	36,444
9	11	32,53

Measurement 1 — Height of the **thin wall structure** from the lowest corner to the highest AFTER cut of weld [V]:

Point:	Length [mm]:	Height [mm]:
1	1	42,66
2	2	43,33
3	3	43,63
4	4	44,63
5	5	42,45
6	6	40,57
7	7	38,71
8	8	36,34
9	9	33,93

Measurement 2 — Height of the **thin wall structure** from the lowest corner to the highest AFTER cut of weld [H]:

Point:	Length [mm]:	Height [mm]:
1	1	39,86
2	2	43,38
3	3	43,47
4	4	43,38
5	5	44,05
6	7	41,14
7	8	38,73
8	9	36,67
9	11	32,31

Measurement 2 — Height of the **thin wall structure** from the lowest corner to the highest AFTER cut of weld [V]:

Point:	Length [mm]:	Height [mm]:
1	1	42,52
2	2	43,32
3	3	43,52
4	4	44,67
5	5	42,4
6	6	40,51
7	7	38,74
8	8	36,56
9	9	34,31

Measurement 3 — Height of the **thin wall structure** from the lowest corner to the highest AFTER cut of weld [H]:

Point:	Length [mm]:	Height [mm]:
1	1	39,95
2	2	43,56
3	3	43,38
4	4	43,62
5	5	44,27
6	7	41,51
7	8	38,92
8	9	36,39
9	11	32,72

Measurement 3 — Height of the **thin wall structure** from the lowest corner to the highest AFTER cut of weld [V]:

Point:	Length [mm]:	Height [mm]:
1	1	42,67
2	2	43,23
3	3	43,54
4	4	44,71
5	5	42,43
6	6	40,5
7	7	38,44
8	8	36,38
9	9	34,14

Measurement 1 — Height of the **base-plate** from the lowest corner to highest AFTER the cut of the weld[H]:

Point:	Length	Height
1	0	27,2
2	50	26,05
3	100	25,23
4	150	25,14
5	200	25,03
6	250	24,96
7	300	25,16
8	350	25,73
9	398	26,28

Measurement 1 — Height of the **base-plate** from the lowest corner to highest AFTER the cut of the weld[V]:

Point:	Length	Height
1	0	27,21
2	1	27,37
3	3	27,53
4	5	27,86
5	6	28,02
6	7	28,14
7	8	28,22
8	9	28,31
9	10	28,3

Measurement 2 — Height of the **base-plate** from the lowest corner to highest AFTER the cut of the weld[H]:

Point:	Length	Height
1	0	27,19
2	50	25,98
3	100	25,23
4	150	25,15
5	200	24,9
6	250	24,92
7	300	25,05
8	350	25,7
9	398	26,28

Measurement 2 — Height of the **base-plate** from the lowest corner to highest AFTER the cut of the weld[V]:

Point:	Length	Height
1	0	27,17
2	1	27,31
3	3	27,64
4	5	27,88
5	6	28,04
6	7	28,18
7	8	28,24
8	9	28,3
9	10	28,42

Measurement 3 — Height of the **base-plate** from the lowest corner to highest AFTER the cut of the weld[H]:

Point:	Length	Height
1	0	27,22
2	50	26,02
3	100	25,2
4	150	25,15
5	200	24,89
6	250	24,97
7	300	25,16
8	350	25,71
9	398	26,28

Measurement 3 — Height of the **base-plate** from the lowest corner to highest AFTER the cut of the weld[V]:

Point:	Length	Height
1	0	27,15
2	1	27,32
3	3	27,46
4	5	27,88
5	6	28,04
6	7	28,12
7	8	28,24
8	9	28,3
9	10	28,41

Figure 124: Measurement of the total height, for TWS and BP

E.6   Height measurement - P4D2- part 1

Measurement 1 — Height of the TWS from the lowest corner to the highest BEFORE cut of weld [H]:

Point:	Length	Height
1	10	31,41
2	20	35,92
3	40	40,61
4	60	40,72
5	70	42,38
6	90	40,05
7	110	37,64
8	130	34,17
9	150	28,18

Measurement 1 — Height of the TWS from the lowest corner to the highest BEFORE cut of weld [V]:

Point:	Length[mm]:	Height [mm]:
1	10	37,05
2	20	41,34
3	30	40,89
4	40	41,66
5	50	42,66
6	60	40,21
7	70	36,84
8	80	34,89
9	90	31,71

Measurement 2 — Height of the TWS from the lowest corner to the highest BEFORE cut of weld [H]:

Point:	Length[mm]:	Height [mm]:
1	10	31,38
2	20	36,13
3	40	40,52
4	60	40,76
5	70	42,24
6	90	40,04
7	110	37,67
8	130	34,4
9	150	28,26

Measurement 2 — Height of the TWS from the lowest corner to the highest BEFORE cut of weld [V]:

Point:	Length[mm]:	Height [mm]:
1	10	36,55
2	20	41,24
3	30	40,87
4	40	41,74
5	50	42,62
6	60	40,23
7	70	36.91
8	80	34,48
9	90	31,46

Measurement 3 — Height of the TWS from the lowest corner to the highest BEFORE cut of weld [H]:

Point:	Length[mm]:	Height [mm]:
1	10	31,5
2	20	36,8
3	40	40,64
4	60	40,7
5	70	42,24
6	90	39,96
7	110	37,59
8	130	34,46
9	150	28,2

Measurement 3 — Height of the TWS from the lowest corner to the highest BEFORE cut of weld [V]:

Point:	Length[mm]:	Height [mm]:
1	10	36,72
2	20	41,3
3	30	40,83
4	40	41,78
5	50	42,66
6	60	40,01
7	70	36,99
8	80	34,67
9	90	31,44

Measurement 1 — Height of the BP from the lowest corner to highest BEFORE the cut of the weld[H]:

Point:	Length	Height
1	0	23,1
2	50	23,12
3	100	23,18
4	150	23,29
5	200	23,43
6	250	23,8
7	300	24,38
8	357	24,96

Measurement 1 — Height of the BP from the lowest corner to highest BEFORE the cut of the weld[V]:

Point:	Length[mm]:	Height [mm]:
1	0	23,08
2	10	23,05
3	20	23,05
4	30	23,07
5	50	23,07
6	60	23,09
7	70	23,1
8	80	23,12
9	102	23,2

Measurement 2 — Height of the BP from the lowest corner to highest BEFORE the cut of the weld[H]:

Point:	Length[mm]:	Height [mm]:
1	0	23,1
2	50	23,12
3	100	23,19
4	150	23,29
5	200	23,43
6	250	23,8
7	300	24,38
8	357	24,96

Measurement 2 — Height of the BP from the lowest corner to highest BEFORE the cut of the weld[V]:

Point:	Length[mm]:	Height [mm]:
1	0	23,06
2	10	23,04
3	20	23,04
4	30	23,03
5	50	23,05
6	60	23,06
7	70	23,08
8	80	23,1
9	102	23,17

Measurement 3 — Height of the BP from the lowest corner to highest BEFORE the cut of the weld[H]:

Point:	Length[mm]:	Height [mm]:
1	0	23,08
2	50	23,12
3	100	23,16
4	150	23,29
5	200	23,43
6	250	23,8
7	300	24,38
8	357	24,95

Measurement 3 — Height of the BP from the lowest corner to highest BEFORE the cut of the weld[V]:

Point:	Length[mm]:	Height [mm]:
1	0	23,05
2	10	23,02
3	20	23,03
4	30	23,04
5	50	23,05
6	60	23,04
7	70	23,08
8	80	23,1
9	102	23,18

Measurement 1 — Height of the TWS from the lowest corner to the highest AFTER cut of weld [H]:

Point:	Length	Height
1	10	31,87
2	20	36,45
3	40	41,38
4	60	41,74
5	70	43,19
6	90	40,87
7	110	38,44
8	130	34,76
9	150	28,52

Measurement 1 — Height of the TWS from the lowest corner to the highest AFTER cut of weld [V]:

Point:	Length[mm]:	Height [mm]:
1	1	32,69
2	2	37,82
3	3	42,05
4	4	41,72
5	5	42,81
6	6	43,55
7	7	40,69
8	8	37,44
9	9	34,63

Measurement 2 — Height of the TWS from the lowest corner to the highest AFTER cut of weld [H]:

Point:	Length[mm]:	Height [mm]:
1	10	31,82
2	20	36,74
3	40	41,32
4	60	41,6
5	70	43,11
6	90	40,87
7	110	38,24
8	130	34,74
9	150	28,02

Figure 125: Measurement of the total height, for TWS and BP

E.7   Height measurement - P4D2 - part 2

Measurement 2 — Height of the **TWS** from the lowest corner to the highest AFTER cut of weld [V]:

Point:	Length[mm]:	Height [mm]:
1	1	32,47
2	2	38,48
3	3	42,35
4	4	41,75
5	5	42,85
6	6	43,55
7	7	40,87
8	8	36,74
9	9	34,5

Measurement 3 — Height of the **TWS** from the lowest corner to the highest AFTER cut of weld [H]:

Point:	Length[mm]:	Height [mm]:
1	10	31,9
2	20	37,37
3	40	41,76
4	60	41,89
5	70	43,74
6	90	41,26
7	110	38,78
8	130	34,85
9	150	28,9

Measurement 3 — Height of the **TWS** from the lowest corner to the highest AFTER cut of weld [V]:

Point:	Length[mm]:	Height [mm]:
1	1	32
2	2	37,81
3	3	41,93
4	4	41,79
5	5	42,73
6	6	43,58
7	7	40,59
8	8	36,91
9	9	34,31

Measurement 1 — Height of the **BP** from the lowest corner to highest AFTER the cut of the weld[H]:

Point:	Length	Height
1	0	23,04
2	50	23,11
3	100	23,15
4	150	23,16
5	200	23,22
6	250	23,48
7	300	24,25
8	357	24,86

Measurement 1 — Height of the **BP** from the lowest corner to highest AFTER the cut of the weld[V]:

Point:	Length	Height
1	0	23,03
2	10	22,95
3	20	23,03
4	30	23
5	50	23,01
6	60	23,03
7	70	23,06
8	80	23,06
9	102	23,14

Measurement 2 — Height of the **BP** from the lowest corner to highest AFTER the cut of the weld[H]:

Point:	Length	Height
1	0	23,04
2	50	23,08
3	100	23,16
4	150	23,16
5	200	23,2
6	250	23,53
7	300	24,25
8	357	24,85

Measurement 2 — Height of the **BP** from the lowest corner to highest AFTER the cut of the weld[V]:

Point:	Length	Height
1	0	23,05
2	10	22,94
3	20	23
4	30	23,02
5	50	23,01
6	60	23,02
7	70	23,05
8	80	23,07
9	102	23,12

Measurement 3 — Height of the **BP** from the lowest corner to highest AFTER the cut of the weld[H]:

Point:	Length	Height
1	0	23,03
2	50	23,07
3	100	23,15
4	150	23,2
5	200	23,16
6	250	23,44
7	300	24,21
8	357	24,85

Measurement 3 — Height of the **BP** from the lowest corner to highest AFTER the cut of the weld[V]:

Point:	Length	Height
1	0	23,07
2	10	22,95
3	20	23,04
4	30	23,04
5	50	23,05
6	60	23,06
7	70	23,09
8	80	23,09
9	102	23,16

Measurement 1 — Height of the **BP** from the lowest corner to highest BEFORE weld[H]:

Point:	Length	Height
1	0	22,99
2	50	23,07
3	100	23,16
4	150	23,27
5	200	23,42
6	250	23,58
7	300	23,76
8	357	23,94

Measurement 1 — Height of the **BP** from the lowest corner to highest BEFORE weld[V]:

Point:	Length	Height
1	0	23,25
2	10	23,2
3	20	23,22
4	30	23,23
5	50	23,26
6	60	23,26
7	70	23,31
8	80	23,32
9	102	23,4

Measurement 2 — Height of the **BP** from the lowest corner to highest BEFORE weld[H]:

Point:	Length	Height
1	0	22,98
2	50	23,06
3	100	23,16
4	150	23,29
5	200	23,41
6	250	23,58
7	300	23,77
8	357	23,93

Measurement 2 — Height of the **BP** from the lowest corner to highest BEFORE weld[V]:

Point:	Length	Height
1	0	23,24
2	10	23,24
3	20	23,23
4	30	23,23
5	50	23,25
6	60	23,29
7	70	23,31
8	80	23,34
9	102	23,4

Figure 126: Measurement of the total height, for TWS and BP

E.8   Height measurement - P4D3

Measurement 1 Height of the TWS from the lowest corner to the highest AFTER cut of weld [20]:			Measurement 1 Height of the TWS from the lowest corner to the highest AFTER cut of weld [-20]:			Measurement 2 Height of the TWS from the lowest corner to the highest AFTER cut of weld [20]:			Measurement 2 Height of the TWS from the lowest corner to the highest AFTER cut of weld [-20]:			Measurement 3 Height of the TWS from the lowest corner to the highest AFTER cut of weld [20]:			Measurement 3 Height of the TWS from the lowest corner to the highest AFTER cut of weld [-20]:		
Point:	Length [mm]:	Height [mm]:	Point:	Length [mm]:	Height [mm]:	Point:	Length [mm]:	Height [mm]:	Point:	Length [mm]:	Height [mm]:	Point:	Length [mm]:	Height [mm]:	Point:	Length [mm]:	Height [mm]:
1	0	32,5	1	0	36,7	1	0	30,89	1	0	37,31	1	0	30,83	1	0	37,29
2	30	40,08	2	30	44,98	2	30	39,28	2	30	45	2	30	39,34	2	30	45,05
3	50	43,4	3	50	46,61	3	50	42,75	3	50	46,92	3	50	32,97	3	50	46,98
4	70	46,34	4	70	48,51	4	70	46,32	4	70	48,71	4	70	46,6	4	70	48,83
5	85,5	50,91	5	85,5	51,36	5	85,5	51,3	5	85,5	51,4	5	85,5	51,53	5	85,5	51,43
6	110	47,45	6	110	46,31	6	110	48,18	6	110	46,35	6	110	48,33	6	110	46,43
7	140	44,31	7	140	45,85	7	140	46,14	7	140	45,78	7	140	44,49	7	140	45,72
8	160	39,72	8	160	40,31	8	160	41,21	8	160	39,26	8	160	41,14	8	160	39,12
9	180	34,62	9	180	32,34	9	180	35,12	9	180	31,68	9	180	34,17	9	180	32,2

Measurement 1 Height of the BP from the lowest corner to highest AFTER the cut of the weld[H]:			Measurement 1 Height of the BP from the lowest corner to highest AFTER the cut of the weld[V]:			Measurement 2 Height of the BP from the lowest corner to highest AFTER the cut of the weld[H]:			Measurement 2 Height of the BP from the lowest corner to highest AFTER the cut of the weld[V]:			Measurement 3 Height of the BP from the lowest corner to highest AFTER the cut of the weld[H]:			Measurement 3 Height of the BP from the lowest corner to highest AFTER the cut of the weld[V]:		
Point:	Length [mm]:	Height [mm]:	Point:	Length [mm]:	Height [mm]:	Point:	Length [mm]:	Height [mm]:	Point:	Length [mm]:	Height [mm]:	Point:	Length [mm]:	Height [mm]:	Point:	Length [mm]:	Height [mm]:
1	0	25,77	1	0	26,22	1	0	25,88	1	0	26,1	1	0	25,77	1	0	26,13
2	50	25,42	2	1	26,5	2	50	25,35	2	1	26,47	2	50	25,26	2	1	26,5
3	100	24,84	3	3	27,23	3	100	24,85	3	3	25,49	3	100	24,85	3	3	26,88
4	150	24,43	4	5	27,96	4	150	24,4	4	5	25,88	4	150	24,44	4	5	27,82
5	200	24,28	5	6	28,24	5	200	24,28	5	6	26,2	5	200	24,29	5	6	28,26
6	250	24,33	6	7	28,48	6	250	24,34	6	7	26,46	6	250	24,34	6	7	28,56
7	300	24,44	7	8	29,03	7	300	24,43	7	8	27,23	7	300	24,43	7	8	28,93
8	350	24,58	8	9	29,33	8	350	24,58	8	9	27,22	8	350	24,57	8	9	29,16
9	398	24,66	9	10	29,03	9	398	24,66	9	10	27,24	9	398	24,66	9	10	28,88

Figure 127: Measurement of the total height, for TWS and BP

F Deformation

Raw measuring data of the height of the neutral axis along the length of the thin wall structures. Before and after cut of the weld are presented as two graphs which illustrate the deformation when the stresses are released.
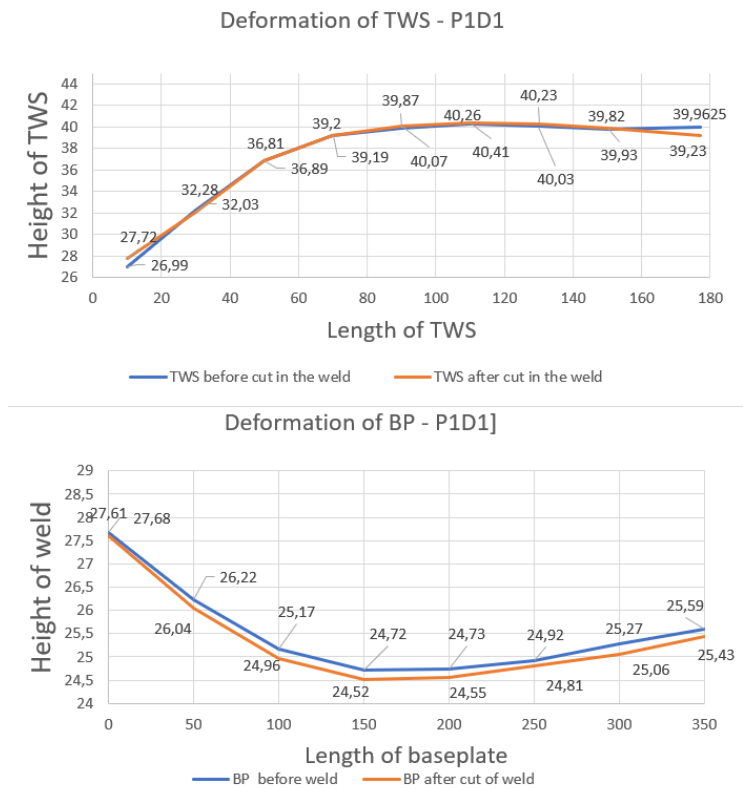
Figure 128: Deformation of the neutral axis along the x-axis.Note: Effective welding length 50-150 [mm]
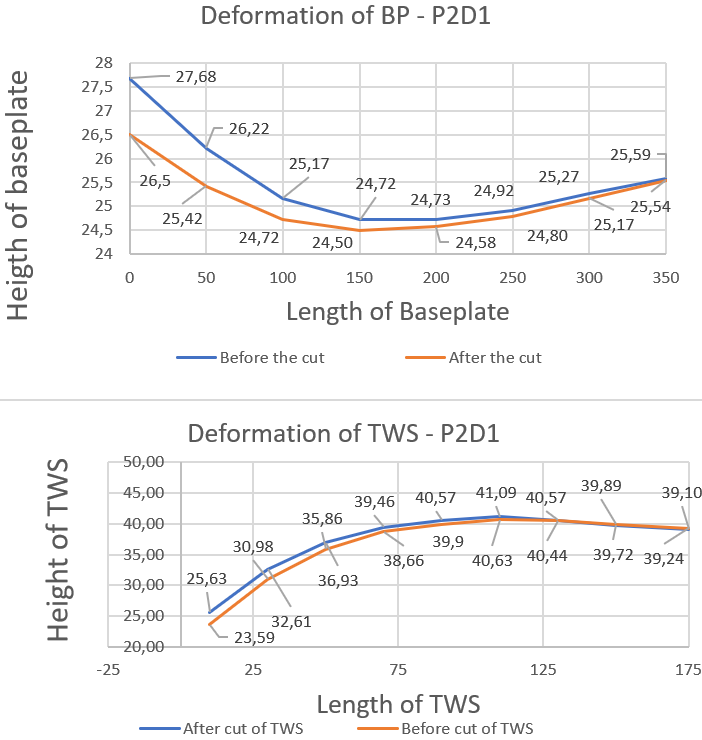
Figure 129: Deformation of the neutral axis along the x-axis. Note: Effective welding length 50-150 [mm]

Deformation of BP - P3D1

Deformation of TWS - P3D1
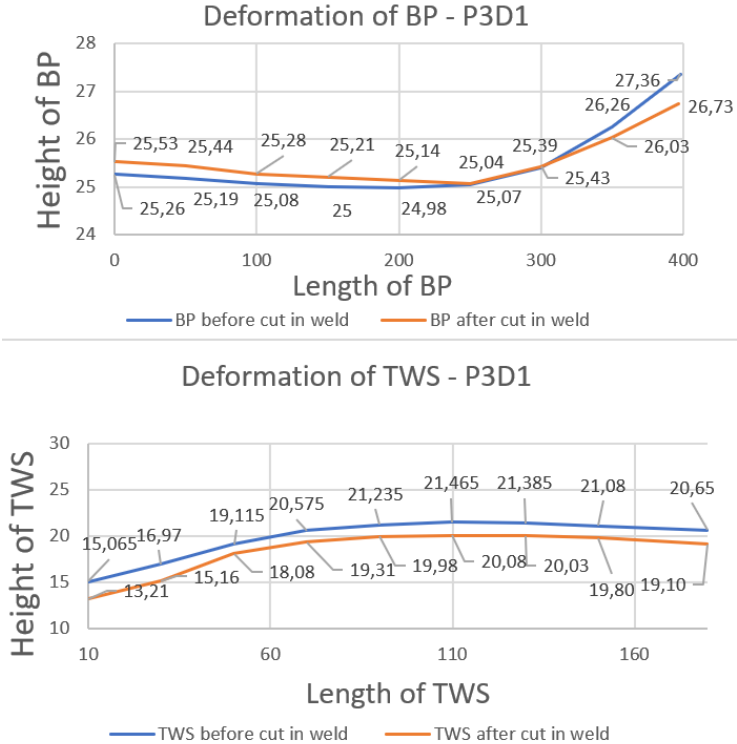
Figure 130: Deformation of the neutral axis along the x-axis.Note: Effective welding length 50-150 [mm]
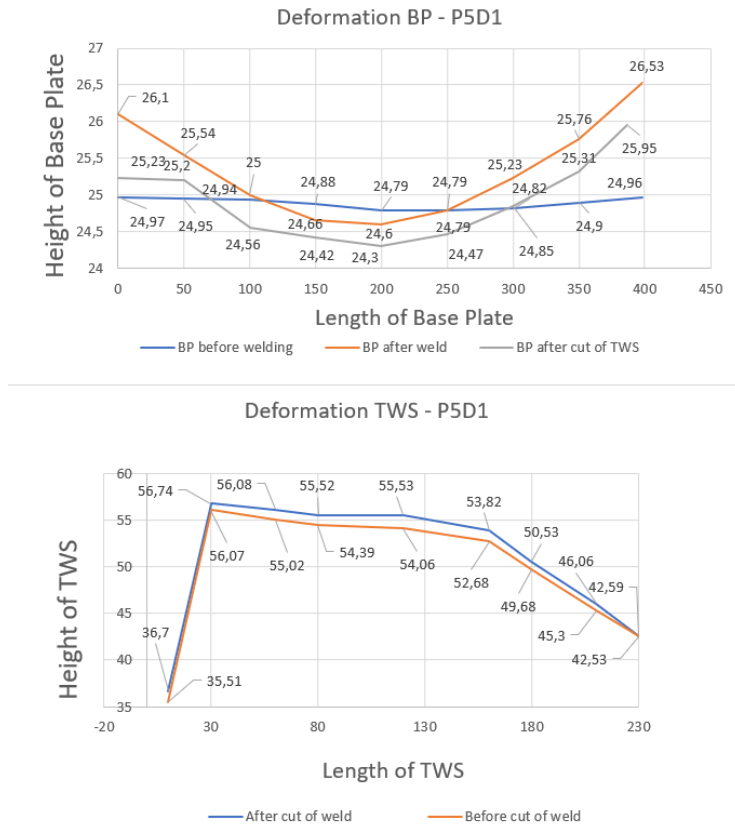
Figure 131: Deformation of the neutral axis along the x-axis.Note: Effective welding length 50-150 [mm]
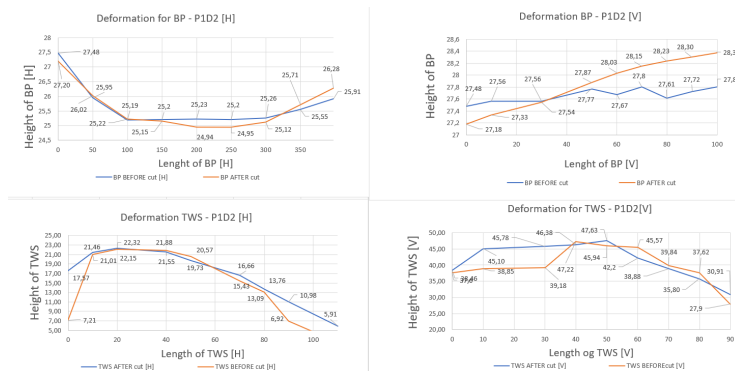
Figure 132: Deformation of the neutral axis along the x-axis.Note: Effective welding length 50-150 [mm]
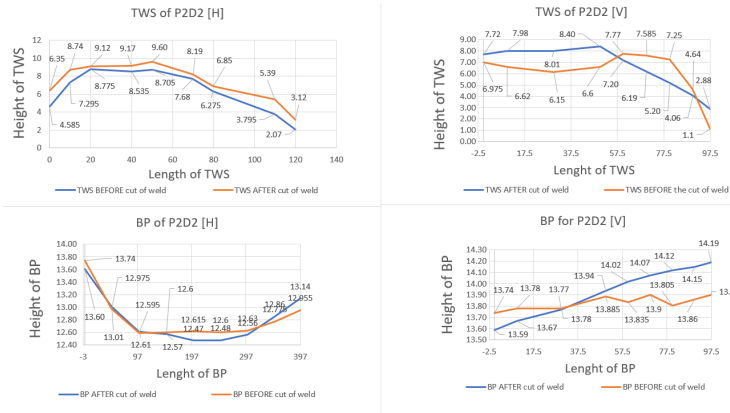
Figure 133: Deformation of the neutral axis along the x-axis.Note: Effective welding length 50-150 [mm]
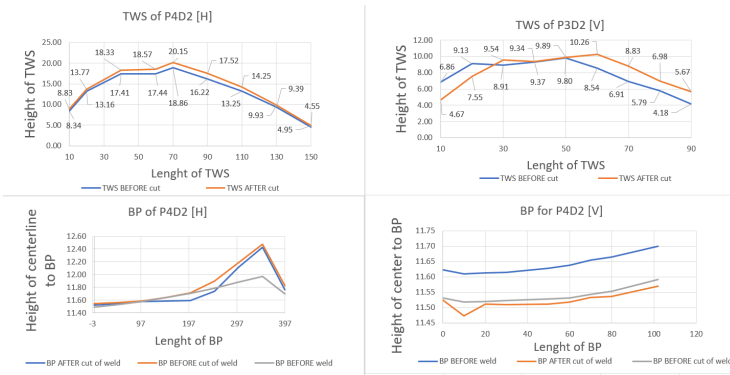
Figure 134: Deformation of the neutral axis along the x-axis.Note: Effective welding length 50-150 [mm]
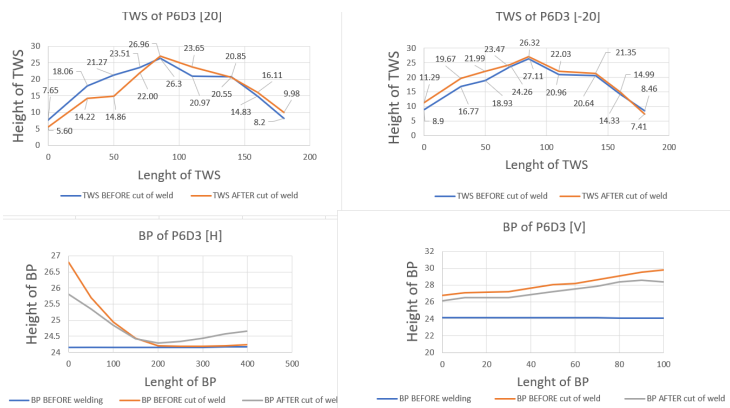
Figure 135: Deformation of the neutral axis along the x-axis.Note: Effective welding length 50-150 [mm]

G   Youtube-Videoes

Number	Description	URL
1a	Temperature distribution of sample P1D1	`https://www.youtube.com/watch?v=938xA8j95Uw`
1b	Temperature of sample P1D1 - sliced geometry	`https://www.youtube.com/watch?v=zRFeSkpVWrw`
1c	Residual stresses distribution of sample P1D1	`https://www.youtube.com/watch?v=C4h6vuvi4rY`
1d	Residual stresses of sample P1D1 - sliced geometry	`https://www.youtube.com/watch?v=VJfWlOO6FFA`
1e	Deformation distribution of sample P1D1	`https://www.youtube.com/watch?v=eQanCGMf_ps`
1f	Deformation distribution of sample P1D1 - sliced geometry	`https://www.youtube.com/watch?v=A7NMbfy6NUY`
2a	Temperature distribution of sample P1D1x1	`https://www.youtube.com/watch?v=Fk7uozomc-I`
2b	Temperature distribution of sample P1D1x1 - sliced geometry	`https://www.youtube.com/watch?v=K5K_2Tmp1-I`
2c	Residual stress distribution of sample P1D1x1	`https://www.youtube.com/watch?v=mlGksFY7GL4`
2d	Residual stress distribution of sample P1D1x1 - sliced geometry	`https://www.youtube.com/watch?v=WB2yPKixiCY`
2e	Deformation distribution of sample P1D1x1	`https://www.youtube.com/watch?v=0rMKht3ZM5g`
2f	Deformation distribution of sample P1D1x1 - sliced geometry	`https://www.youtube.com/watch?v=FMetWm--8a4`
3a	Temperature distribution of sample P1D1x2	`https://www.youtube.com/watch?v=Fk7uozomc-I`
3b	Temperature distribution of sample P1D1x2 - sliced geometry	`https://www.youtube.com/watch?v=Ef1eYpPQ4ps`
3c	Residual stress distribution of sample P1D1x2	`https://www.youtube.com/watch?v=PcrjiJvOrQQ`
3d	Residual stress distribution of sample P1D1x2 - sliced geometry	`https://www.youtube.com/watch?v=2-K5uIQ0kaA`
3e	Deformation distribution of sample P1D1x2	`https://www.youtube.com/watch?v=tErwSgV8mnY`
3f	Deformation distribution of sample P1D1x2 - sliced geometry	`https://www.youtube.com/watch?v=Edrmg5953d0`

4a	Temperature distribution of sample P1D1x3	https://www.youtube.com/watch?v=jy-AoDM_c-U
4b	Temperature distribution of sample P1D1x3 - sliced geometry	https://www.youtube.com/watch?v=NAiOCALMOWE
4c	Residual stress distribution of sample P1D1x3	https://www.youtube.com/watch?v=pE2ScBnJwG8
4d	Residual stress distribution of sample P1D1x3 - sliced geometry	https://www.youtube.com/watch?v=lxFvEEajhdI
4e	Deformation distribution of sample P1D1x3	https://www.youtube.com/watch?v=aIjSePWR85s
4f	Deformation distribution of sample P1D1x3 - sliced geometry	https://www.youtube.com/watch?v=-Or-aOjQuDw
5a	Temperature distribution of sample P2D1	https://www.youtube.com/watch?v=oeSGnpdSnR8
5b	Temperature distribution of sample P2D1 - sliced geometry	https://www.youtube.com/watch?v=5v84YB9gyEY
5c	Residual stress distribution of sample P2D1	https://www.youtube.com/watch?v=yi2cfHqaack
5d	Residual stress distribution of sample P2D1 - sliced geometry	https://www.youtube.com/watch?v=y5ewC37wARM
5e	Deformation distribution of sample P2D1	https://www.youtube.com/watch?v=drON0x6PC6E
5f	Deformation distribution of sample P2D1 - sliced geometry	https://www.youtube.com/watch?v=Hw4szhmuyBE
6a	Temperature distribution of sample P3D1	https://www.youtube.com/watch?v=m633vzIUN7Q
6b	Temperature distribution of sample P3D1 - sliced geometry	https://www.youtube.com/watch?v=xBqbJ8PUEf8
6c	Residual stress distribution of sample P3D1	https://www.youtube.com/watch?v=NmZ2geNV-g8
6d	Residual stress distribution of sample P3D1 - sliced geometry	https://www.youtube.com/watch?v=jFDyHx9EIzs
6e	Deformation distribution of sample P3D1	https://www.youtube.com/watch?v=sqkrHJMOhIo
6e	Deformation distribution of sample P3D1 - sliced geometry	https://www.youtube.com/watch?v=FQaDnB8-BNA
7a	Temperature distribution of sample P5D1	https://www.youtube.com/watch?v=L34fnlAW7Gg
7b	Temperature distribution of sample P5D1 - sliced geometry	https://www.youtube.com/watch?v=nv0s53ThO1w

7c	Residual stress distribution of sample P5D1	https://www.youtube.com/watch?v=7F5o2Wspfyg
7d	Residual stress distribution of sample P5D1 - sliced geometry	https://www.youtube.com/watch?v=bnHxEz-j4WI
7e	Deformation distribution of sample P5D1	https://www.youtube.com/watch?v=ENhVeXPUgVw
7f	Deformation distribution of sample P5D1 - sliced geometry	https://www.youtube.com/watch?v=C5GMN1dUlqo
8a	Temperature distribution of sample P1D2	https://www.youtube.com/watch?v=X3ffjqv1QJY
8b	Temperature distribution of sample P1D2 - sliced geometry	https://www.youtube.com/watch?v=Gao50IHJhE8
8c	Residual stress distribution of sample P1D2	https://www.youtube.com/watch?v=SjKtyE8ntGo
8d	Residual stress distribution of sample P1D2 - sliced geometry	https://www.youtube.com/watch?v=eZqSgJ45_ck
8e	Deformation distribution of sample P1D2	https://www.youtube.com/watch?v=rcqybwt4--I
8e	Deformation distribution of sample P1D2 - sliced geometry	https://www.youtube.com/watch?v=I5J6Ly72LR8
9a	Temperature distribution of sample P2D2	https://www.youtube.com/watch?v=OwQgm3XHhdk
9b	Temperature distribution of sample P2D2 - sliced geometry	https://www.youtube.com/watch?v=RzyEClzWGg0
9c	Residual stress distribution of sample P2D2	https://www.youtube.com/watch?v=pXaM4WqVql0
9d	Residual stress distribution of sample P2D2 - sliced geometry	https://www.youtube.com/watch?v=cNmWWgg1w2g
9e	Deformation distribution of sample P2D2	https://www.youtube.com/watch?v=_4_spXRK8oo
9f	Deformation distribution of sample P2D2 - sliced geometry	https://www.youtube.com/watch?v=zeVScrGdqKY
10a	Temperature distribution of sample P4D2	https://www.youtube.com/watch?v=gA7b73AAcl0
10b	Temperature distribution of sample P4D2 - sliced geometry	https://www.youtube.com/watch?v=N2Neyvw24Cw
10c	Residual stress distribution of sample P4D2	https://www.youtube.com/watch?v=8fJLrD3XM5I
10d	Residual stress distribution of sample P4D2 - sliced geometry	https://www.youtube.com/watch?v=94flm2scgEM

10e	Deformation distribution of sample P4D2	`https://www.youtube.com/watch?v=trh0RuWd0fw`
10f	Deformation distribution of sample P4D2 - sliced geometry	`https://www.youtube.com/watch?v=MHfXKd-YP0o`
11a	Temperature distribution of sample P1D1-BT	`https://www.youtube.com/watch?v=r3L0jMsJaGI`
11b	Temperature distribution of sample P1D1-BT - sliced geometry	`https://www.youtube.com/watch?v=1Gp1OnmkCfQ`
11c	Residual stress distribution of sample P1D1-BT	`https://www.youtube.com/watch?v=BwWEuF7bYdM`
11d	Residual stress distribution of sample P1D1-BT - sliced geometry	`https://www.youtube.com/watch?v=3G3HWf9MaVM`
11e	Deformation distribution of sample P1D1-BT	`https://www.youtube.com/watch?v=-udxqOfYdtk`
11f	Deformation distribution of sample P1D1-BT - sliced geometry	`https://www.youtube.com/watch?v=MnPNcrXfqZI`
12a	Temperature distribution of sample P2D1-BT	`https://www.youtube.com/watch?v=imwDMuVA9C0`
12b	Temperature distribution of sample P2D1-BT - sliced geometry	`https://www.youtube.com/watch?v=EN9kNOIXvVA`
12c	Residual stress distribution of sample P2D1-BT	`https://www.youtube.com/watch?v=En5gqv4iSuA`
12d	Residual stress distribution of sample P2D1-BT - sliced geometry	`https://www.youtube.com/watch?v=BnJRMtinGOY`
12e	Deformation distribution of sample P2D1-BT	`https://www.youtube.com/watch?v=JZOUIYlsElQ`
12f	Deformation distribution of sample P2D1-BT - sliced geometry	`https://www.youtube.com/watch?v=JZOUIYlsElQ`
13a	Temperature distribution of sample P3D1-BT	`https://www.youtube.com/watch?v=B-Rq_KOcPrA`
13b	Temperature distribution of sample P3D1-BT - sliced geometry	`https://www.youtube.com/watch?v=J8_ofp9Ka44`
13c	Residual stress distribution of sample P3D1-BT	`https://www.youtube.com/watch?v=NmZ2geNV-g8`
13d	Residual stress distribution of sample P3D1-BT - sliced geometry	`https://www.youtube.com/watch?v=jFDyHx9EIzs`
13e	Deformation distribution of sample P3D1-BT	`https://www.youtube.com/watch?v=OoGq_H9ViUY`
13f	Deformation distribution of sample P3D1-BT - sliced geometry	`https://www.youtube.com/watch?v=7oNNZ0klZxs`

14a	Temperature distribution of sample P5D1-BT	https://www.youtube.com/watch?v=cxVYMrz0rtM
14b	Temperature distribution of sample P5D1-BT - sliced geometry	https://www.youtube.com/watch?v=g_oPJ-u20lI
14c	Residual stress distribution of sample P5D1-BT	https://www.youtube.com/watch?v=umUyaIEMAmQ&feature=youtu.be
14d	Residual stress distribution of sample P5D1-BT - sliced geometry	https://www.youtube.com/watch?v=bnHxEz-j4WI
14e	Deformation distribution of sample P5D1-BT	https://www.youtube.com/watch?v=Qzz5O3yaxl4
14f	Deformation distribution of sample P5D1-BT - sliced geometry	https://www.youtube.com/watch?v=9RRGvzBT6Y4
15a	Temperature distribution of sample P1D2-BT	https://www.youtube.com/watch?v=cF9R9lb9ZLc
15b	Temperature distribution of sample P1D2-BT - sliced geometry	https://youtu.be/yOh9FKIFkcc
15c	Residual stress distribution of sample P1D2-BT	https://www.youtube.com/watch?v=PIfo4D4l7f0
15d	Residual stress distribution of sample P1D2-BT - sliced geometry	https://www.youtube.com/watch?v=7yvuxx4cyAw
15e	Deformation distribution of sample P1D2-BT	https://www.youtube.com/watch?v=VrToa4f2Njo
15f	Deformation distribution of sample P1D2-BT - sliced geometry	https://www.youtube.com/watch?v=PKpvfMU7z58
16a	Temperature distribution of sample P2D2-BT	https://www.youtube.com/watch?v=MRohFhI1iFs
16b	Temperature distribution of sample P2D2-BT - sliced geometry	https://youtu.be/vTJxt2JCnxk
16c	Residual stress distribution of sample P2D2-BT	https://youtu.be/POJkbEJ4LYA
16d	Residual stress distribution of sample P2D2-BT - sliced geometry	https://youtu.be/Wkq7M61X1qc
16e	Deformation distribution of sample P2D2-BT	https://youtu.be/ISYFHfo8xMI
16f	Deformation distribution of sample P2D2-BT - sliced geometry	https://youtu.be/_yUwA-AB6-w
17a	Temperature distribution of sample P4D2-BT	https://youtu.be/BibLV955cig
17b	Temperature distribution of sample P4D2-BT - sliced geometry	https://www.youtube.com/watch?v=_yUwA-AB6-w

17c	Residual stress distribution of sample P4D2-BT	https://www.youtube.com/watch?v=POJkbEJ4LYA
17d	Residual stress distribution of sample P4D2-BT - sliced geometry	https://www.youtube.com/watch?v=POJkbEJ4LYA
17e	Deformation distribution of sample P4D2-BT - sliced geometry	https://youtu.be/f_G3YsaacLY
17f	Deformation distribution sample P4D2-BT - sliced geometry	https://www.youtube.com/watch?v=_yUwA-AB6-w
18a	Temperature distribution of sample P4D3-BT	https://youtu.be/j1OXvQf2N_I
18b	Temperature distribution of sample P4D3-BT - sliced geometry	
18c	Residual stress distribution of sample P4D3-BT	https://youtu.be/5DkxsyXP5ow
18d	Residual stress distribution of sample P4D3-BT - sliced geometry	https://youtu.be/ZmRMCrQ9EZs
18e	Deformation stress distribution of sample P4D3-BT	https://youtu.be/j1OXvQf2N_I
18f	Deformation distribution of sample P4D3-BT - sliced geometry	https://youtu.be/BSm4tkDguS4
19	Video of the welding process	https://youtu.be/uc5ZIUVPEJA

Table 20: Video's that illustrate the distribution of the results: temperature,residual stresses and deformation

H Result value of RS and deformation along the length longitudinal and transverse direction of the TWS

H.1 P1D1x1 - Result

Object Name	Equivalent Stress	Normal Stress	Directional Deformation	Total Deformation	Total Deformation longitudinal	Equivalent Stress longitudinal	Equivalent Stress transverse
State	Solved						
Scope							
Scoping Method	Geometry Selection				Path		
Geometry	All Bodies						
Path					Path		Path 2
Definition							
Type	Equivalent (von-Mises) Stress	Normal Stress	Directional Deformation	Total Deformation		Equivalent (von-Mises) Stress	
By	Time						
Display Time	0,90125 s	Last					
Calculate Time History	Yes						
Identifier							
Suppressed	No						
Orientation			X Axis				
Coordinate System			Global Coordinate System				
Integration Point Results							
Display Option	Averaged					Averaged	
Average Across Bodies	No					No	
Results							
Minimum	9,0118e-004 MPa	-78,845 MPa	-8,1071e-004 mm	0, mm	6,8579e-004 mm	4,6951 MPa	19,493 MPa
Maximum	1441,1 MPa	67,768 MPa	7,2039e-003 mm	7,3097e-003 mm	6,1109e-003 mm	38,345 MPa	25,301 MPa
Average	23,104 MPa	-2,6664 MPa	1,3598e-003 mm	1,4259e-003 mm	4,2595e-003 mm	17,264 MPa	21,414 MPa
Minimum Occurs On	Baseplate P1D1	TWS P1D1x1		Baseplate P1D1		TWS P1D1x1	
Maximum Occurs On	TWS P1D1x1						
Minimum Value Over Time							
Minimum	4,1141e-004 MPa	-1654, MPa	-3,217e-002 mm	0, mm	9,3748e-005 mm	1,3392e-002 MPa	4,9916 MPa
Maximum	3,4358e-003 MPa	-78,845 MPa	-4,7434e-004 mm	0, mm	2,2147e-003 mm	5,116 MPa	443,27 MPa
Maximum Value Over Time							
Minimum	115,24 MPa	67,761 MPa	7,1664e-003 mm	7,3092e-003 mm	6,1106e-003 mm	38,024 MPa	11,409 MPa
Maximum	1441,1 MPa	521,81 MPa	3,4195e-002 mm	3,4562e-002 mm	3,0073e-002 mm	1290,1 MPa	744,22 MPa
Information							
Time	1, s	20, s					
Load Step	1						
Substep	1	20					
Iteration Number	7	68					

Figure 136: Simulation result of the first layer at sample P1D1

H.2   P1D1x2 - Result

Object Name	Equivalent Stress	Normal Stress	Directional Deformation	Total Deformation	Equivalent Stress longitudinal	Total Deformation longitudinal	Total Deformation transverse	Equivalent Stress transverse
State					Solved			
Scope								
Scoping Method		Geometry Selection				Path		
Geometry				All Bodies				
Path						Path		Path 2
Definition								
Type	Equivalent (von-Mises) Stress	Normal Stress	Directional Deformation	Total Deformation	Equivalent (von-Mises) Stress	Total Deformation		Equivalent (von-Mises) Stress
By					Time			
Display Time	0,90125 s				Last			
Calculate Time History					Yes			
Identifier								
Suppressed					No			
Orientation			X Axis					
Coordinate System			Global Coordinate System					
Integration Point Results								
Display Option	Averaged				Averaged			Averaged
Average Across Bodies	No				No			No
Results								
Minimum	3,3579e-004 MPa	-49,224 MPa	-7,0113e-003 mm	0, mm	0,39874 MPa	1,3327e-004 mm	9,9523e-004 mm	4,567 MPa
Maximum	1566, MPa	13,824 MPa	6,2025e-004 mm	7,0851e-003 mm	17,966 MPa	3,7658e-003 mm	1,0091e-003 mm	4,8595 MPa
Average	25,466 MPa	-2,0824 MPa	-4,4096e-004 mm	4,8569e-004 mm	4,3221 MPa	1,053e-003 mm	1,0005e-003 mm	4,6609 MPa
Minimum Occurs On	Baseplate P1D1	TWS P1D1x2		Baseplate P1D1		TWS P1D1x2		
Maximum Occurs On	TWS P1D1x2	Baseplate P1D1				TWS P1D1x2		
Minimum Value Over Time								
Minimum	1,8299e-004 MPa	-1622,5 MPa	-5,415e-002 mm	0, mm	4,1401e-002 MPa	1,0992e-004 mm	1,5409e-004 mm	4,567 MPa
Maximum	8,0812e-003 MPa	-49,224 MPa	-6,9725e-003 mm	0, mm	2,7725 MPa	2,7801e-003 mm	2,6054e-002 mm	503,2 MPa
Maximum Value Over Time								
Minimum	58,03 MPa	13,798 MPa	6,2025e-004 mm	7,0525e-003 mm	17,966 MPa	3,7166e-003 mm	2,9979e-004 mm	4,8592 MPa
Maximum	1566, MPa	436,35 MPa	5,9051e-002 mm	6,5191e-002 mm	1490,8 MPa	5,034e-002 mm	2,7313e-002 mm	1126,3 MPa

Figure 137: Simulation result of the 4th layer at sample P1D1

H.3   P1D1x3 - Result

Object Name	Total Deformation	Directional Deformation	Normal Stress	Equivalent Stress	Total Deformation longitudinal	Equivalent Stress longitudinal	Total Deformation transverse	Equivalent Stress transverse
State					Solved			
Scope								
Scoping Method		Geometry Selection				Path		
Geometry					All Bodies			
Path						Path		Path 2
Definition								
Type	Total Deformation	Directional Deformation	Normal Stress	Equivalent (von-Mises) Stress	Total Deformation	Equivalent (von-Mises) Stress	Total Deformation	Equivalent (von-Mises) Stress
By					Time			
Display Time					Last			
Calculate Time History					Yes			
Identifier								
Suppressed					No			
Orientation		X Axis						
Coordinate System		Global Coordinate System						
Results								
Minimum	0, mm	-3,2875e-006 mm	-3,9445e-002 MPa	5,4531e-007 MPa	1,919e-007 mm	4,4551e-005 MPa	8,0544e-007 mm	1,4399e-003 MPa
Maximum	3,3786e-006 mm	6,6703e-007 mm	2,9086e-002 MPa	5,099e-002 MPa	3,165e-006 mm	4,2893e-002 MPa	9,3998e-007 mm	1,9159e-002 MPa
Average	3,7414e-007 mm	4,2744e-008 mm	-1,8382e-003 MPa	3,3318e-003 MPa	8,7616e-007 mm	1,2355e-002 MPa	8,8099e-007 mm	8,3744e-003 MPa
Minimum Occurs On	Baseplate P1D1	TWS P1D1x4		Baseplate P1D1		TWS P1D1x4		
Maximum Occurs On					TWS P1D1x4			
Minimum Value Over Time								
Minimum	0, mm	-3,2875e-006 mm	-3,9445e-002 MPa	5,4529e-007 MPa	1,919e-007 mm	4,4551e-005 MPa	8,0544e-007 mm	1,4399e-003 MPa
Maximum	0, mm	-3,2875e-006 mm	-3,9445e-002 MPa	5,4534e-007 MPa	1,9191e-007 mm	4,4551e-005 MPa	8,0544e-007 mm	1,4399e-003 MPa
Maximum Value Over Time								
Minimum	3,3786e-006 mm	6,6703e-007 mm	2,9086e-002 MPa	5,099e-002 MPa	3,165e-006 mm	4,2893e-002 MPa	9,3997e-007 mm	1,9159e-002 MPa
Maximum	3,3786e-006 mm	6,6703e-007 mm	2,9086e-002 MPa	5,099e-002 MPa	3,165e-006 mm	4,2893e-002 MPa	9,3998e-007 mm	1,9159e-002 MPa
Information								

Figure 138: Simulation result of the 4th layer at sample P1D1

H.4   P1D1 - Result

Object Name	Equivalent Stress	Normal Stress	Directional Deformation	Total Deformation	Equivalent Stress longitudinal - low Surface	Equivalent Stress longitudinal - top Surface	Total Deformation longitudinal	Equivalent Stress transverse	Total Deformation transverse
State	Solved								
Scope									
Scoping Method	Geometry Selection				Path				
Geometry	All Bodies								
Path					Path	Path 2		Path 3	
Definition									
Type	Equivalent (von-Mises) Stress	Normal Stress	Directional Deformation	Total Deformation	Equivalent (von-Mises) Stress		Total Deformation	Equivalent (von-Mises) Stress	Total Deformation
By	Time					Result Set		Time	
Display Time	0,90125 s		Last					Last	
Calculate Time History	Yes								
Identifier									
Suppressed	No								
Orientation		X Axis							
Coordinate System		Global Coordinate System							
Set Number						1,			
Integration Point Results									
Display Option	Averaged				Averaged			Averaged	
Average Across Bodies	No				No			No	
Results									
Minimum	9,5705e-005 MPa	-6,3401e-002 MPa	-8,8549e-003 mm	1,3332e-004 mm	6,9822e-004 MPa	1,2516e-004 MPa	7,9446e-004 mm	2,0833e-003 MPa	2,4172e-004 mm
Maximum	638,83 MPa	4,9076e-002 MPa	8,8365e-003 mm	3,2387e-002 mm	2,9402e-003 MPa	8,3323 MPa	1,5894e-002 mm	7,3557e-003 MPa	1,0402e-003 mm
Average	2,9835 MPa	7,6949e-004 MPa	-8,1448e-007 mm	1,5246e-002 mm	1,585e-003 MPa	0,91914 MPa	8,0915e-003 mm	4,1487e-003 MPa	6,1328e-004 mm
Minimum Occurs On	Baseplate P1D1	TWS P1D1	Baseplate P1D1	TWS P1D1	Baseplate P1D1	TWS P1D1			
Maximum Occurs On	TWS P1D1		Baseplate P1D1			TWS P1D1			
Minimum Value Over Time									
Minimum	2,9859e-006 MPa	-1983,9 MPa	-7,9782e-002 mm	7,1567e-008 mm	6,557e-004 MPa	5,635e-005 MPa	3,489e-006 mm	2,0833e-003 MPa	6,1562e-006 mm
Maximum	9,7293e-003 MPa	-6,3401e-002 MPa	-3,5868e-004 mm	1,0802e-003 mm	3,0365 MPa	0,79142 MPa	7,8956e-003 mm	259,14 MPa	2,6057e-002 mm
Maximum Value Over Time									
Minimum	4,9886e-002 MPa	4,9076e-002 MPa	1,1544e-003 mm	1,185e-003 mm	2,9402e-003 MPa	4,8972e-002 MPa	1,1286e-003 mm	7,3557e-003 MPa	6,2198e-006 mm
Maximum	1930,9 MPa	1085,9 MPa	4,0695e-002 mm	8,5215e-002 mm	16,201 MPa	1117,2 MPa	7,7327e-002 mm	861,73 MPa	3,1575e-002 mm

Figure 139: Simulation result of the TWS P1D1

H.5   P2D1 - Result

Object Name	Equivalent Stress	Normal Stress	Directional Deformation	Total Deformation	Equivalent Stress longitudinal	Total Deformation longitudinal	Equivalent Stress transverse	Total Deformation transverse
State	Solved						
Scope							
Scoping Method	Geometry Selection				Path			
Geometry	All Bodies						
Path					Path		Path 2	
Definition							
Type	Equivalent (von-Mises) Stress	Normal Stress	Directional Deformation	Total Deformation	Equivalent (von-Mises) Stress	Total Deformation	Equivalent (von-Mises) Stress	Total Deformation
By	Time						
Display Time	0,90125 s	Last						
Calculate Time History	Yes						
Identifier							
Suppressed	No						
Orientation		X Axis						
Coordinate System		Global Coordinate System						
Integration Point Results							
Display Option	Averaged				Averaged		Averaged	
Average Across Bodies	No				No		No	
Results							
Minimum	5,3062e-005 MPa	-0,28649 MPa	-2,9636e-005 mm	0, mm	2,0641e-004 MPa	5,8375e-006 mm	6,6297e-003 MPa	6,0789e-006 mm
Maximum	480,12 MPa	0,22054 MPa	7,2503e-006 mm	3,0416e-005 mm	0,22527 MPa	3,0416e-005 mm	1,9649e-002 MPa	6,0884e-006 mm
Average	2,8763 MPa	2,2986e-004 MPa	1,5624e-007 mm	2,8938e-006 mm	3,7733e-002 MPa	1,2129e-005 mm	1,178e-002 MPa	6,0837e-006 mm
Minimum Occurs On	Baseplate P2D1	TWS P2D1		Baseplate P2D1	TWS P2D1			
Maximum Occurs On	TWS P2D1						
Minimum Value Over Time							
Minimum	3,0992e-007 MPa	-1795,9 MPa	-8,2608e-002 mm	0, mm	1,7287e-005 MPa	2,6264e-007 mm	6,6297e-003 MPa	2,692e-006 mm
Maximum	3,5416e-003 MPa	-0,28649 MPa	-2,9636e-005 mm	0, mm	1,024 MPa	7,4211e-003 mm	203,72 MPa	2,3884e-002 mm
Maximum Value Over Time							
Minimum	0,24632 MPa	0,22054 MPa	7,2503e-006 mm	3,0416e-005 mm	0,22527 MPa	3,0416e-005 mm	1,9649e-002 MPa	3,9638e-006 mm
Maximum	1752,4 MPa	969,2 MPa	3,6679e-002 mm	8,6839e-002 mm	1053,6 MPa	7,946e-002 mm	673,15 MPa	2,8698e-002 mm

Figure 140: Simulation result of the TWS P2D1

H.6 P3D1 - Result

Object Name	Equivalent Stress	Normal Stress	Directional Deformation	Total Deformation	Equivalent Stress longitudinal	Equivalent Stress transverse	Total Deformation longitudinal	Total Deformation transverse
State					Solved			
Scope								
Scoping Method		Geometry Selection			Path			
Geometry					All Bodies			
Path					Path	Path 2	Path	Path 2
Definition								
Type	Equivalent (von-Mises) Stress	Normal Stress	Directional Deformation	Total Deformation	Equivalent (von-Mises) Stress		Total Deformation	
By					Time			
Display Time	0,90125 s				Last			
Calculate Time History					Yes			
Identifier								
Suppressed					No			
Orientation			X Axis					
Coordinate System			Global Coordinate System					
Integration Point Results								
Display Option	Averaged				Averaged			
Average Across Bodies	No				No			
Results								
Minimum	2,3343e-004 MPa	-0,12245 MPa	-1,3736e-005 mm	0, mm	3,2304e-005 MPa	2,3576e-003 MPa	1,9454e-006 mm	2,162e-006 mm
Maximum	848,37 MPa	9,7097e-002 MPa	2,5668e-006 mm	1,3797e-005 mm	9,8641e-002 MPa	6,3784e-003 MPa	1,3748e-005 mm	2,1771e-006 mm
Average	8,8346 MPa	2,89e-004 MPa	8,1759e-008 mm	1,4012e-006 mm	1,4581e-002 MPa	3,9544e-003 MPa	4,3668e-006 mm	2,1714e-006 mm
Minimum Occurs On	P3D1\Solid1	TWS of P3D1\Solid1		P3D1\Solid1	TWS of P3D1\Solid1			
Maximum Occurs On					TWS of P3D1\Solid1			
Minimum Value Over Time								
Minimum	2,1347e-006 MPa	-1881, MPa	-7,0582e-002 mm	0, mm	3,2304e-005 MPa	2,3576e-003 MPa	1,9454e-006 mm	2,162e-006 mm
Maximum	7,8769e-003 MPa	-0,12245 MPa	-1,3736e-005 mm	0, mm	0,45259 MPa	271,56 MPa	6,9499e-003 mm	2,2801e-002 mm
Maximum Value Over Time								
Minimum	0,10303 MPa	9,7097e-002 MPa	2,5668e-006 mm	1,3797e-005 mm	9,8641e-002 MPa	6,3784e-003 MPa	1,3748e-005 mm	2,1771e-006 mm
Maximum	1793,2 MPa	849,19 MPa	4,2335e-002 mm	7,4807e-002 mm	923,34 MPa	850,29 MPa	6,9458e-002 mm	2,7067e-002 mm

Figure 141: Simulation result of the TWS P3D1

H.7   P5D1 - Result

Object Name	Equivalent Stress	Directional Deformation	Total Deformation	Equivalent Stress longitudinal	Equivalent Stress transverse	Total Deformation longitudinal	Total Deformation transverse	Equivalent Stress longitudinal[V]	Equivalent Stress transverse [V]	Total Deformation longitudinal [V]	Total Deformation transverse [V]
State				Solved				Suppressed			
Scope											
Scoping Method	Geometry Selection			Path							
Geometry				All Bodies							
Path				Path	Path 2	Path	Path 2				
Definition											
Type	Equivalent (von-Mises) Stress	Directional Deformation	Total Deformation	Equivalent (von-Mises) Stress		Total Deformation		Equivalent (von-Mises) Stress		Total Deformation	
By				Time							
Display Time	0,90125 s			Last							
Calculate Time History				Yes							
Identifier											
Suppressed				No				Yes			
Orientation		X Axis									
Coordinate System		Global Coordinate System									
Integration Point Results											
Display Option	Averaged			Averaged				Averaged			
Average Across Bodies	No			No				No			
Results											
Minimum	2,8271e-004 MPa	-1,1651e-006 mm	0, mm	2,3592e-004 MPa	9,423e-004 MPa	2,3089e-007 mm	4,8182e-007 mm				
Maximum	2005,1 MPa	5,1792e-006 mm	5,3341e-006 mm	3,8298e-002 MPa	2,8193e-003 MPa	5,3341e-006 mm	4,8731e-007 mm				
Average	6,284 MPa	-4,3438e-008 mm	5,0884e-007 mm	5,5842e-003 MPa	1,6938e-003 MPa	1,442e-006 mm	4,8423e-007 mm				
Minimum Occurs On	Baseplate P4D1	TWS P4D1	Baseplate P4D1	TWS P4D1							
Maximum Occurs On				TWS P4D1							
Minimum Value Over Time											
Minimum	6,401e-007 MPa	-5,7661e-002 mm	0, mm	2,3592e-004 MPa	9,423e-004 MPa	2,3089e-007 mm	4,8182e-007 mm				
Maximum	7,3959e-003 MPa	-1,1651e-006 mm	0, mm	0,8715 MPa	151,09 MPa	2,5224e-003 mm	1,7212e-002 mm				
Maximum Value Over Time											
Minimum	4,6013e-002 MPa	5,1792e-006 mm	5,3341e-006 mm	3,8298e-002 MPa	2,8193e-003 MPa	5,3341e-006 mm	4,8731e-007 mm				
Maximum	2027,6 MPa	3,8309e-002 mm	6,1043e-002 mm	1067,6 MPa	600,21 MPa	5,4062e-002 mm	1,9783e-002 mm				

Figure 142: Simulation result of the TWS P5D1

H.8   P1D2 - Result

Object Name	Equivalent Stress	Directional Deformation	Total Deformation	Equivalent Stress longitudinal [H]	Equivalent Stress Transverse [H]	Total Deformation longitudinal [H]	Total Deformation transverse [H]	Equivalent Stress longitudinal [V]	Equivalent Stress transverse [V]	Total Deformation longitudinal [V]	Total Deformation transverse [V]
State						Solved					
Scope											
Scoping Method		Geometry Selection					Path				
Geometry						All Bodies					
Path				Path	Path 2	Path	Path 2	Path 3	Path 4	Path 3	Path 4
Definition											
Type	Equivalent (von-Mises) Stress	Directional Deformation	Total Deformation		Equivalent (von-Mises) Stress		Total Deformation		Equivalent (von-Mises) Stress		Total Deformation
By						Time					
Display Time	0,90125 s					Last					
Calculate Time History						Yes					
Identifier											
Suppressed						No					
Orientation		X Axis									
Coordinate System		Global Coordinate System									
Integration Point Results											
Display Option	Averaged				Averaged				Averaged		
Average Across Bodies	No				No				No		
Results											
Minimum	1,794e-004 MPa	-1,5322e-004 mm	0, mm	1,5814e-004 MPa	5,0417e-004 MPa	5,0484e-007 mm	1,4656e-006 mm	3,9451e-004 MPa	4,5142e-003 MPa	5,1108e-006 mm	6,02e-006 mm
Maximum	1002,6 MPa	1,6179e-004 mm	3,342e-004 mm	2,8832e-002 MPa	1,1906e-003 MPa	5,838e-006 mm	1,5508e-006 mm	5,5072 MPa	2,0352e-002 MPa	1,0153e-004 mm	6,0622e-006 mm
Average	11,035 MPa	1,177e-009 mm	3,0518e-006 mm	3,4426e-003 MPa	8,1325e-004 MPa	1,6325e-006 mm	1,4896e-006 mm	0,33971 MPa	1,3112e-002 MPa	1,1664e-005 mm	6,0324e-006 mm
Minimum Occurs On	Baseplate P1D2	TWS P1D2 [V]	Baseplate P1D2			TWS P1D2				TWS P1D2 [V]	
Maximum Occurs On	TWS P1D2		TWS P1D2 [V]		TWS P1D2	TWS P1D2 [V]	TWS P1D2			TWS P1D2 [V]	
Minimum Value Over Time											
Minimum	3,308e-007 MPa	-6,6127e-002 mm	0, mm	1,224e-004 MPa	1,9998e-004 MPa	2,4043e-007 mm	1,4656e-006 mm	1,427e-005 MPa	7,0416e-005 MPa	6,5864e-007 mm	8,9225e-007 mm
Maximum	4,1394e-003 MPa	-5,1724e-005 mm	0, mm	6,1146 MPa	501,37 MPa	9,1445e-003 mm	4,2253e-002 mm	4,3968 MPa	375,96 MPa	9,5485e-003 mm	6,2209e-002 mm
Maximum Value Over Time											
Minimum	8,1112 MPa	5,5039e-005 mm	1,0306e-004 mm	2,8832e-002 MPa	1,1906e-003 MPa	5,838e-006 mm	1,5508e-006 mm	6,2493e-004 MPa	2,3336e-004 MPa	9,2467e-007 mm	1,0888e-006 mm
Maximum	1968,4 MPa	6,5551e-002 mm	7,0951e-002 mm	1397,4 MPa	1004,7 MPa	6,7022e-002 mm	4,4437e-002 mm	786,34 MPa	1010,7 MPa	6,7322e-002 mm	6,409e-002 mm

Figure 143: Simulation result of the TWS P1D2

H.9   P2D2 - Result

Object Name	Equivalent Stress	Directional Deformation	Total Deformation	Equivalent Stress longitudinal [H]	Equivalent Stress Transverse [H]	Total Deformation longitudinal [H]	Total Deformation transverse [H]	Equivalent Stress longitudinal [V]	Equivalent Stress transverse [V]	Total Deformation longitudinal [V]	Total Deformation transverse [V]
State						Solved					
						Scope					
Scoping Method		Geometry Selection					Path				
Geometry						All Bodies					
Path				Path	Path 2	Path	Path 2	Path 3	Path 4	Path 3	Path 4
						Definition					
Type	Equivalent (von-Mises) Stress	Directional Deformation	Total Deformation		Equivalent (von-Mises) Stress		Total Deformation		Equivalent (von-Mises) Stress		Total Deformation
By						Time					
Display Time	0,90125 s					Last					
Calculate Time History						Yes					
Identifier											
Suppressed						No					
Orientation		X Axis									
Coordinate System		Global Coordinate System									
						Integration Point Results					
Display Option	Averaged				Averaged				Averaged		
Average Across Bodies	No				No				No		
						Results					
Minimum	1,794e-004 MPa	-1,5322e-004 mm	0, mm	1,5814e-004 MPa	5,0417e-004 MPa	5,0484e-007 mm	1,4656e-006 mm	3,9451e-004 MPa	4,5142e-003 MPa	5,1108e-006 mm	6,02e-006 mm
Maximum	1002,6 MPa	1,6179e-004 mm	3,342e-004 mm	2,8832e-002 MPa	1,1906e-003 MPa	5,838e-006 mm	1,5508e-006 mm	5,5072 MPa	2,0352e-002 MPa	1,0153e-004 mm	6,0622e-006 mm
Average	11,035 MPa	1,177e-009 mm	3,0518e-006 mm	3,4426e-003 MPa	8,1325e-004 MPa	1,6325e-006 mm	1,4896e-006 mm	0,33971 MPa	1,3112e-002 MPa	1,1664e-005 mm	6,0324e-006 mm
Minimum Occurs On	Baseplate P1D2	TWS P1D2 [V]	Baseplate P1D2		TWS P1D2				TWS P1D2 [V]		
Maximum Occurs On	TWS P1D2		TWS P1D2 [V]		TWS P1D2	TWS P1D2 [V]	TWS P1D2		TWS P1D2 [V]		
						Minimum Value Over Time					
Minimum	3,308e-007 MPa	-6,6127e-002 mm	0, mm	1,224e-004 MPa	1,9998e-004 MPa	2,4043e-007 mm	1,4656e-006 mm	1,427e-005 MPa	7,0416e-005 MPa	6,5864e-007 mm	8,9225e-007 mm
Maximum	4,1394e-003 MPa	-5,1724e-005 mm	0, mm	6,1146 MPa	501,37 MPa	9,1445e-003 mm	4,2253e-002 mm	4,3968 MPa	375,96 MPa	9,5485e-003 mm	6,2209e-002 mm
						Maximum Value Over Time					
Minimum	8,1112 MPa	5,5039e-005 mm	1,0306e-004 mm	2,8832e-002 MPa	1,1906e-003 MPa	5,838e-006 mm	1,5508e-006 mm	6,2493e-004 MPa	2,3336e-004 MPa	9,2467e-007 mm	1,0888e-006 mm
Maximum	1968,4 MPa	6,5551e-002 mm	7,0951e-002 mm	1397,4 MPa	1004,7 MPa	6,7022e-002 mm	4,4437e-002 mm	786,34 MPa	1010,7 MPa	6,7322e-002 mm	6,409e-002 mm

Figure 144: Simulation result of the TWS P2D2

H.10   P4D2 - Result

Object Name	Equivalent Stress	Directional Deformation	Total Deformation	Equivalent Stress longitudinal [H]	Equivalent Stress transverse[H]	Total Deformation longitudinal[H]	Total Deformation transverse [H]	Equivalent Stress longitudinal[V]	Equivalent Stress transverse [V]	Total Deformation longitudinal [V]	Total Deformation transverse [V]
State						Solved					
Scope											
Scoping Method		Geometry Selection					Path				
Geometry						All Bodies					
Path				Path	Path 2	Path	Path 2	Path 3	Path 4	Path 3	Path 4
Definition											
Type	Equivalent (von-Mises) Stress	Directional Deformation	Total Deformation	Equivalent (von-Mises) Stress		Total Deformation		Equivalent (von-Mises) Stress		Total Deformation	
By						Time					
Display Time	0,90125 s					Last					
Calculate Time History						Yes					
Identifier											
Suppressed						No					
Orientation		X Axis									
Coordinate System		Global Coordinate System									
Integration Point Results											
Display Option	Averaged			Averaged				Averaged			
Average Across Bodies	No			No				No			
Results											
Minimum	2,0596e-004 MPa	-9,5182e-008 mm	0, mm	5,038e-005 MPa	1,3131e-004 MPa	1,3439e-008 mm	7,7193e-008 mm	6,9026e-005 MPa	2,6956e-004 MPa	8,5343e-008 mm	8,7158e-008 mm
Maximum	991, MPa	1,4163e-007 mm	1,6655e-007 mm	9,824e-004 MPa	1,9775e-004 MPa	9,6088e-008 mm	7,9132e-008 mm	7,4049e-004 MPa	1,2805e-003 MPa	1,1565e-007 mm	1,1248e-007 mm
Average	5,0648 MPa	1,0818e-008 mm	4,9405e-008 mm	2,4533e-004 MPa	1,609e-004 MPa	6,3127e-008 mm	7,8105e-008 mm	2,5103e-004 MPa	7,0734e-004 MPa	9,7132e-008 mm	9,7277e-008 mm
Minimum Occurs On	BP P4D2	TWS [V] P4D2	BP P4D2	TWS [H] P4D2				TWS [V] P4D2			
Maximum Occurs On		TWS [H] P4D2				TWS [V] P4D2	TWS [H] P4D2	TWS [V] P4D2			
Minimum Value Over Time											
Minimum	2,6369e-008 MPa	-4,945e-002 mm	0, mm	2,5679e-005 MPa	3,4285e-005 MPa	2,4455e-009 mm	5,8491e-008 mm	1,6541e-006 MPa	4,0782e-005 MPa	5,0269e-008 mm	5,0804e-009 mm
Maximum	4,2355e-003 MPa	-9,5182e-008 mm	0, mm	1,4109 MPa	188,9 MPa	2,9383e-003 mm	2,0615e-002 mm	1,0426 MPa	480,19 MPa	8,5198e-003 mm	3,715e-002 mm
Maximum Value Over Time											
Minimum	1,0122e-002 MPa	1,3998e-007 mm	1,6655e-007 mm	9,8239e-004 MPa	1,8855e-004 MPa	8,7895e-008 mm	6,3587e-008 mm	7,266e-005 MPa	6,3981e-004 MPa	1,1565e-007 mm	5,8603e-008 mm
Maximum	1555,3 MPa	4,7402e-002 mm	5,6289e-002 mm	848,06 MPa	545,02 MPa	4,8172e-002 mm	2,2397e-002 mm	947,31 MPa	1267,9 MPa	5,3866e-002 mm	3,8872e-002 mm

Figure 145: Simulation result of the TWS P4D2

H.11   P1D1-BP - Result

Object Name	Equivalent Stress	Normal Stress	Directional Deformation	Total Deformation	Equivalent Stress longitudinal	Equivalent Stress transverse	Total Deformation longitudinal	Total Deformation transverse
State					Solved			
Scope								
Scoping Method			Geometry Selection			Path		
Geometry					All Bodies			
Path					Path	Path 2	Path	Path 2
Definition								
Type	Equivalent (von-Mises) Stress	Normal Stress	Directional Deformation	Total Deformation	Equivalent (von-Mises) Stress		Total Deformation	
By					Time			
Display Time	0,90125 s				Last			
Calculate Time History					Yes			
Identifier								
Suppressed					No			
Orientation			X Axis					
Coordinate System			Global Coordinate System					
Integration Point Results								
Display Option	Averaged				Averaged			
Average Across Bodies	No				No			
Results								
Minimum	3,8334e-003 MPa	-73,809 MPa	-3,5911e-003 mm	0, mm	0,52022 MPa	4,4045 MPa	6,1854e-004 mm	8,4405e-004 mm
Maximum	2885,3 MPa	30,47 MPa	4,357e-003 mm	5,8095e-003 mm	74,326 MPa	44,59 MPa	5,6054e-003 mm	3,1407e-003 mm
Average	15,366 MPa	-6,3581 MPa	2,7568e-005 mm	2,6853e-003 mm	24,99 MPa	11,592 MPa	2,272e-003 mm	2,497e-003 mm
Minimum Occurs On					P1D1-BT-FreeParts			
Maximum Occurs On					P1D1-BT-FreeParts			
Minimum Value Over Time								
Minimum	1,0738e-004 MPa	-3505,9 MPa	-4,7719e-002 mm	0, mm	2,6717e-003 MPa	9,9849e-003 MPa	1,6396e-006 mm	3,7732e-005 mm
Maximum	9,1098e-002 MPa	-73,711 MPa	-3,0304e-003 mm	0, mm	2,1765 MPa	27,797 MPa	3,2266e-003 mm	1,1777e-002 mm
Maximum Value Over Time								
Minimum	80,037 MPa	30,47 MPa	2,5979e-003 mm	5,8095e-003 mm	74,326 MPa	0,18553 MPa	3,5362e-003 mm	4,3985e-005 mm
Maximum	2991,3 MPa	365,71 MPa	5,0576e-002 mm	0,10502 mm	2660,7 MPa	1753, MPa	9,0936e-002 mm	6,4803e-002 mm

Figure 146: Simulation result of the baseplate-P1D1

H.12   P2D1-BP - Result

Object Name	Equivalent Stress	Normal Stress	Directional Deformation	Total Deformation	Equivalent Stress longitudinal	Total Deformation longitudinal	Equivalent Stress transverse	Total Deformation transverse
State					Solved			
Scope								
Scoping Method			Geometry Selection			Path		
Geometry					All Bodies			
Path					Path		Path 2	
Definition								
Type	Equivalent (von-Mises) Stress	Normal Stress	Directional Deformation	Total Deformation	Equivalent (von-Mises) Stress	Total Deformation	Equivalent (von-Mises) Stress	Total Deformation
By					Time			
Display Time	0,90125 s				Last			
Calculate Time History					Yes			
Identifier								
Suppressed					No			
Orientation			X Axis					
Coordinate System			Global Coordinate System					
Integration Point Results								
Display Option	Averaged				Averaged		Averaged	
Average Across Bodies	No				No		No	
Results								
Minimum	5,3062e-005 MPa	-0,28649 MPa	-2,9636e-005 mm	0, mm	2,0641e-004 MPa	5,8375e-006 mm	6,6297e-003 MPa	6,0789e-006 mm
Maximum	480,12 MPa	0,22054 MPa	7,2503e-006 mm	3,0416e-005 mm	0,22527 MPa	3,0416e-005 mm	1,9649e-002 MPa	6,0884e-006 mm
Average	2,8763 MPa	2,2986e-004 MPa	1,5624e-007 mm	2,8938e-006 mm	3,7733e-002 MPa	1,2129e-005 mm	1,178e-002 MPa	6,0837e-006 mm
Minimum Occurs On	Baseplate P2D1		TWS P2D1	Baseplate P2D1		TWS P2D1		
Maximum Occurs On					TWS P2D1			
Minimum Value Over Time								
Minimum	3,0992e-007 MPa	-1795,9 MPa	-8,2608e-002 mm	0, mm	1,7287e-005 MPa	2,6264e-007 mm	6,6297e-003 MPa	2,692e-006 mm
Maximum	3,5416e-003 MPa	-0,28649 MPa	-2,9636e-005 mm	0, mm	1,024 MPa	7,4211e-003 mm	203,72 MPa	2,3884e-002 mm
Maximum Value Over Time								
Minimum	0,24632 MPa	0,22054 MPa	7,2503e-006 mm	3,0416e-005 mm	0,22527 MPa	3,0416e-005 mm	1,9649e-002 MPa	3,9638e-006 mm
Maximum	1752,4 MPa	969,2 MPa	3,6679e-002 mm	8,6839e-002 mm	1053,6 MPa	7,946e-002 mm	673,15 MPa	2,8698e-002 mm

Figure 147: Simulation result of the baseplate-P2D1

H.13   P3D1-BP - Result

Object Name	Equivalent Stress	Normal Stress	Directional Deformation	Total Deformation	Equivalent Stress longitudinal	Equivalent Stress transverse	Total Deformation longitudinal	Total Deformation transverse
State					Solved			
Scope								
Scoping Method		Geometry Selection				Path		
Geometry				All Bodies				
Path					Path	Path 2	Path	Path 2
Definition								
Type	Equivalent (von-Mises) Stress	Normal Stress	Directional Deformation	Total Deformation	Equivalent (von-Mises) Stress		Total Deformation	
By					Time			
Display Time	0,90125 s				Last			
Calculate Time History					Yes			
Identifier								
Suppressed					No			
Orientation			X Axis					
Coordinate System			Global Coordinate System					
Integration Point Results								
Display Option		Averaged				Averaged		
Average Across Bodies		No				No		
Results								
Minimum	1,8496e-003 MPa	-35,126 MPa	-1,8862e-003 mm	0, mm	4,4182 MPa	15,499 MPa	5,3866e-004 mm	5,6713e-004 mm
Maximum	895,96 MPa	12,445 MPa	2,097e-003 mm	3,9676e-003 mm	30,82 MPa	17,247 MPa	2,2252e-003 mm	1,2303e-003 mm
Average	8,2661 MPa	-3,0754 MPa	1,7116e-004 mm	1,6971e-003 mm	14,91 MPa	16,238 MPa	1,2615e-003 mm	9,6591e-004 mm
Minimum Occurs On					P3D1-BT-FreeParts			
Maximum Occurs On					P3D1-BT-FreeParts			
Minimum Value Over Time								
Minimum	1,1771e-004 MPa	-2257,9 MPa	-2,4256e-002 mm	0, mm	5,8355e-003 MPa	0,212 MPa	1,5733e-005 mm	6,1864e-005 mm
Maximum	2,1164e-002 MPa	-35,126 MPa	-1,8862e-003 mm	0, mm	29,973 MPa	431,15 MPa	5,6086e-003 mm	3,6978e-002 mm
Maximum Value Over Time								
Minimum	33,983 MPa	12,445 MPa	1,5376e-003 mm	3,9676e-003 mm	30,82 MPa	0,21518 MPa	2,2252e-003 mm	6,2343e-005 mm
Maximum	1793,6 MPa	254,36 MPa	2,1218e-002 mm	5,9827e-002 mm	1550,5 MPa	572,36 MPa	5,3448e-002 mm	4,614e-002 mm

Figure 148: Simulation result of the baseplate-P3D1

H.14   P5D1-BP - Result

Object Name	Equivalent Stress	Normal Stress	Directional Deformation	Total Deformation	Equivalent Stress longitudinal	Equivalent Stress transverse	Total Deformation longitudinal	Total Deformation transverse
State					Solved			
Scope								
Scoping Method		Geometry Selection				Path		
Geometry				All Bodies				
Path					Path	Path 2	Path	Path 2
Definition								
Type	Equivalent (von-Mises) Stress	Normal Stress	Directional Deformation	Total Deformation	Equivalent (von-Mises) Stress		Total Deformation	
By					Time			
Display Time	0,90125 s				Last			
Calculate Time History					Yes			
Identifier								
Suppressed					No			
Orientation			X Axis					
Coordinate System			Global Coordinate System					
Integration Point Results								
Display Option		Averaged				Averaged		
Average Across Bodies		No				No		
Results								
Minimum	3,0585e-004 MPa	-35,003 MPa	-1,8854e-003 mm	0, mm	5,6132 MPa	16,58 MPa	1,9507e-004 mm	3,5773e-004 mm
Maximum	830,21 MPa	8,5679 MPa	1,9548e-003 mm	2,7023e-003 mm	34,494 MPa	18,151 MPa	2,3007e-003 mm	1,0273e-003 mm
Average	6,3552 MPa	-3,4952 MPa	2,5307e-005 mm	1,44e-003 mm	17,337 MPa	17,3 MPa	8,493e-004 mm	7,5993e-004 mm
Minimum Occurs On					P5D1-BT-FreeParts			
Maximum Occurs On					P5D1-BT-FreeParts			
Minimum Value Over Time								
Minimum	9,6778e-006 MPa	-2038,9 MPa	-2,1783e-002 mm	0, mm	2,1336e-003 MPa	3,5862e-002 MPa	3,1993e-006 mm	1,9143e-005 mm
Maximum	1,4119e-002 MPa	-35,003 MPa	-1,0951e-003 mm	0, mm	34,368 MPa	428,55 MPa	6,6102e-003 mm	3,4678e-002 mm
Maximum Value Over Time								
Minimum	36,955 MPa	8,5679 MPa	1,1007e-003 mm	2,4147e-003 mm	18,127 MPa	3,5988e-002 MPa	3,5445e-004 mm	1,9332e-005 mm
Maximum	1729,8 MPa	261,7 MPa	2,1538e-002 mm	5,4698e-002 mm	1586,6 MPa	584,85 MPa	4,748e-002 mm	4,3074e-002 mm

Figure 149: Simulation result of the baseplate-P5D1

H.15 P1D2-BP - Result

Object Name	Equivalent Stress	Normal Stress	Directional Deformation	Total Deformation	Equivalent Stress longitudinal	Equivalent Stress transverse	Total Deformation longitudinal	Total Deformation transverse
State					Solved			
Scope								
Scoping Method			Geometry Selection			Path		
Geometry			All Bodies					
Path					Path	Path 2	Path	Path 2
Definition								
Type	Equivalent (von-Mises) Stress	Normal Stress	Directional Deformation	Total Deformation	Equivalent (von-Mises) Stress		Total Deformation	
By					Time			
Display Time	0,90125 s				Last			
Calculate Time History					Yes			
Identifier								
Suppressed					No			
Orientation			X Axis					
Coordinate System			Global Coordinate System					
Integration Point Results								
Display Option	Averaged				Averaged			
Average Across Bodies	No				No			
Results								
Minimum	1,1987e-003 MPa	-66,119 MPa	-5,2281e-003 mm	0, mm	6,4519e-002 MPa	11,709 MPa	1,2299e-003 mm	3,167e-003 mm
Maximum	2527,5 MPa	44,483 MPa	6,5671e-003 mm	1,7487e-002 mm	57,075 MPa	41,32 MPa	9,5438e-003 mm	8,4519e-003 mm
Average	16,476 MPa	-5,3787 MPa	9,5492e-004 mm	5,9431e-003 mm	10,25 MPa	26,832 MPa	4,0637e-003 mm	7,0953e-003 mm
Minimum Occurs On					P1D2-BT-FreeParts			
Maximum Occurs On					P1D2-BT-FreeParts			
Minimum Value Over Time								
Minimum	6,5175e-005 MPa	-3551, MPa	-5,7509e-002 mm	0, mm	3,654e-003 MPa	0,12391 MPa	1,0783e-005 mm	8,8343e-005 mm
Maximum	1,7288e-002 MPa	-66,062 MPa	-1,4953e-003 mm	0, mm	0,41024 MPa	82,854 MPa	2,5467e-003 mm	3,6765e-002 mm
Maximum Value Over Time								
Minimum	65,157 MPa	44,483 MPa	1,6357e-003 mm	3,5832e-003 mm	57,075 MPa	0,61228 MPa	2,3491e-003 mm	1,3139e-004 mm
Maximum	2890,2 MPa	671,02 MPa	6,6616e-002 mm	0,15165 mm	2457,3 MPa	2388,4 MPa	0,13684 mm	0,14011 mm

Figure 150: Simulation result of the baseplate-P1D2

H.16 P2D2-BP - Result

Object Name	Equivalent Stress	Normal Stress	Directional Deformation	Total Deformation	Equivalent Stress longitudinal	Equivalent Stress transverse	Total Deformation longitudinal	Total Deformation transverse
State					Solved			
Scope								
Scoping Method			Geometry Selection			Path		
Geometry			All Bodies					
Path					Path	Path 2	Path	Path 2
Definition								
Type	Equivalent (von-Mises) Stress	Normal Stress	Directional Deformation	Total Deformation	Equivalent (von-Mises) Stress		Total Deformation	
By					Time			
Display Time	0.90125 s				Last			
Calculate Time History					Yes			
Identifier								
Suppressed					No			
Orientation			X Axis					
Coordinate System			Global Coordinate System					
Integration Point Results								
Display Option	Averaged				Averaged			
Average Across Bodies	No				No			
Results								
Minimum	1.0388e-003 MPa	-57.709 MPa	-4.5626e-003 mm	0. mm	5.6326e-002 MPa	10.22 MPa	1.0734e-003 mm	2.7634e-003 mm
Maximum	2201.3 MPa	38.825 MPa	5.7314e-003 mm	1.5261e-002 mm	49.814 MPa	36.063 MPa	8.3293e-003 mm	7.3762e-003 mm
Average	14.306 MPa	-4.6946 MPa	8.3343e-004 mm	5.1867e-003 mm	8.9457 MPa	23.418 MPa	3.5464e-003 mm	6.1921e-003 mm
Minimum Occurs On					P1D2-BT-FreeParts			
Maximum Occurs On					P1D2-BT-FreeParts			
Minimum Value Over Time								
Minimum	5.6874e-005 MPa	-3103. MPa	-4.9872e-002 mm	0. mm	3.1886e-003 MPa	0.10813 MPa	9.4101e-006 mm	7.7093e-005 mm
Maximum	1.5089e-002 MPa	-57.659 MPa	-1.3048e-003 mm	0. mm	0.35669 MPa	71.916 MPa	2.213e-003 mm	3.1995e-002 mm
Maximum Value Over Time								
Minimum	56.868 MPa	38.825 MPa	1.4274e-003 mm	3.127e-003 mm	49.814 MPa	0.53431 MPa	2.05e-003 mm	1.1466e-004 mm
Maximum	2521.9 MPa	582.5 MPa	5.7834e-002 mm	0.13179 mm	2143.6 MPa	2080.7 MPa	0.11888 mm	0.12177 mm

Figure 151: Simulation result of the baseplate-P2D2

H.17 P4D2-BP - Result

Object Name	Equivalent Stress	Normal Stress	Directional Deformation	Total Deformation	Equivalent Stress longitudinal	Equivalent Stress transverse	Total Deformation longitudinal	Total Deformation transverse
State					Solved			
Scope								
Scoping Method		Geometry Selection				Path		
Geometry				All Bodies				
Path					Path	Path 2	Path	Path 2
Definition								
Type	Equivalent (von-Mises) Stress	Normal Stress	Directional Deformation	Total Deformation		Equivalent (von-Mises) Stress		Total Deformation
By					Time			
Display Time	0,90125 s				Last			
Calculate Time History					Yes			
Identifier								
Suppressed					No			
Orientation			X Axis					
Coordinate System			Global Coordinate System					
Integration Point Results								
Display Option		Averaged				Averaged		
Average Across Bodies		No				No		
Results								
Minimum	9,4624e-004 MPa	-109,12 MPa	-7,3554e-003 mm	0, mm	0,52299 MPa	15,216 MPa	3,8309e-003 mm	2,4408e-002 mm
Maximum	2303,7 MPa	58,239 MPa	1,322e-002 mm	3,0501e-002 mm	109,76 MPa	63,05 MPa	2,9384e-002 mm	2,9737e-002 mm
Average	16,965 MPa	-23,088 MPa	1,7715e-003 mm	9,9035e-003 mm	35,127 MPa	36,154 MPa	1,1035e-002 mm	2,6865e-002 mm
Minimum Occurs On					P4D2-BT-FreeParts			
Maximum Occurs On					P4D2-BT-FreeParts			
Minimum Value Over Time								
Minimum	4,6248e-005 MPa	-3152,2 MPa	-4,6425e-002 mm	0, mm	1,8702e-003 MPa	0,10512 MPa	5,2272e-006 mm	6,6356e-005 mm
Maximum	3,0143e-002 MPa	-109,02 MPa	-1,316e-003 mm	0, mm	0,85451 MPa	107,79 MPa	6,1232e-003 mm	5,4545e-002 mm
Maximum Value Over Time								
Minimum	180,84 MPa	58,239 MPa	1,9251e-003 mm	3,1517e-003 mm	109,76 MPa	0,25118 MPa	2,0596e-003 mm	9,3208e-005 mm
Maximum	2719,2 MPa	502,24 MPa	5,402e-002 mm	0,1557 mm	2316,2 MPa	1691,4 MPa	0,13972 mm	0,14263 mm

Figure 152: Simulation result of the baseplate-P4D2

H.18 P4D3-BP - Result

Object Name	Equivalent Stress	Normal Stress	Directional Deformation	Total Deformation	Equivalent Stress longitudinal [-20]	Equivalent Stress transverse[-20]	Total Deformation longitudinal [20]	Total Deformation transverse[20]
State					Solved			
Scope								
Scoping Method		Geometry Selection				Path		
Geometry				All Bodies				
Path					Path	Path 3	Path 2	Path 4
Definition								
Type	Equivalent (von-Mises) Stress	Normal Stress	Directional Deformation	Total Deformation		Equivalent (von-Mises) Stress		Total Deformation
By					Time			
Display Time	0,90125 s				Last			
Calculate Time History					Yes			
Identifier								
Suppressed					No			
Orientation			X Axis					
Coordinate System			Global Coordinate System					
Integration Point Results								
Display Option		Averaged				Averaged		
Average Across Bodies		No				No		
Results								
Minimum	1,0984e-003 MPa	-40,347 MPa	-2,6863e-003 mm	0, mm	4,4437 MPa	14,362 MPa	5,4997e-004 mm	3,242e-003 mm
Maximum	1993,8 MPa	25,358 MPa	9,7569e-003 mm	1,4145e-002 mm	33,362 MPa	15,777 MPa	1,0444e-002 mm	3,4483e-003 mm
Average	10,243 MPa	-2,527 MPa	1,2915e-003 mm	4,3988e-003 mm	18,256 MPa	15,102 MPa	4,0793e-003 mm	3,3713e-003 mm
Minimum Occurs On					P4D3-BT-FreeParts			
Maximum Occurs On					P4D3-BT-FreeParts			
Minimum Value Over Time								
Minimum	4,6233e-005 MPa	-2589,1 MPa	-2,9507e-002 mm	0, mm	3,0595e-004 MPa	0,14721 MPa	8,7613e-006 mm	4,7741e-005 mm
Maximum	8,2476e-003 MPa	-40,347 MPa	-1,122e-003 mm	0, mm	34,948 MPa	445,51 MPa	1,0623e-002 mm	3,753e-002 mm
Maximum Value Over Time								
Minimum	46,748 MPa	25,358 MPa	1,523e-003 mm	2,5396e-003 mm	0,22387 MPa	0,19448 MPa	1,6124e-003 mm	5,3177e-005 mm
Maximum	2187,1 MPa	287,25 MPa	5,8155e-002 mm	7,4839e-002 mm	1882,1 MPa	807,42 MPa	6,6389e-002 mm	5,1554e-002 mm

Figure 153: Simulation result of the baseplate-P4D3

I Temperature during welding time - Simulation

Simulation has set 10-20 second after welding process too illustrate how the temperature decrease after welding.
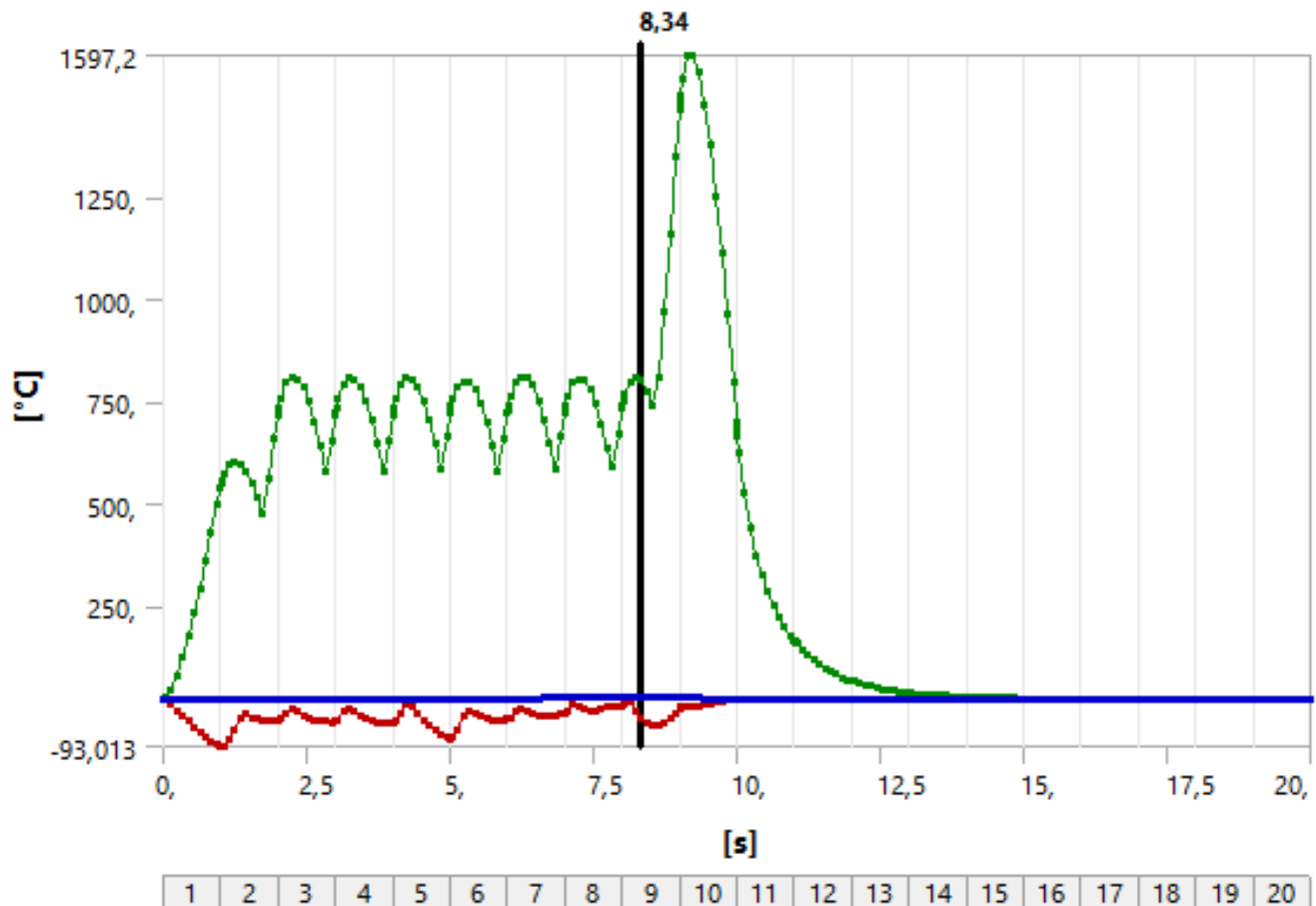
I.1 Temperature - P1D1

Figure 154: Maximum temperature at 1597°following by a rapid cooling, during a duration in 20 second
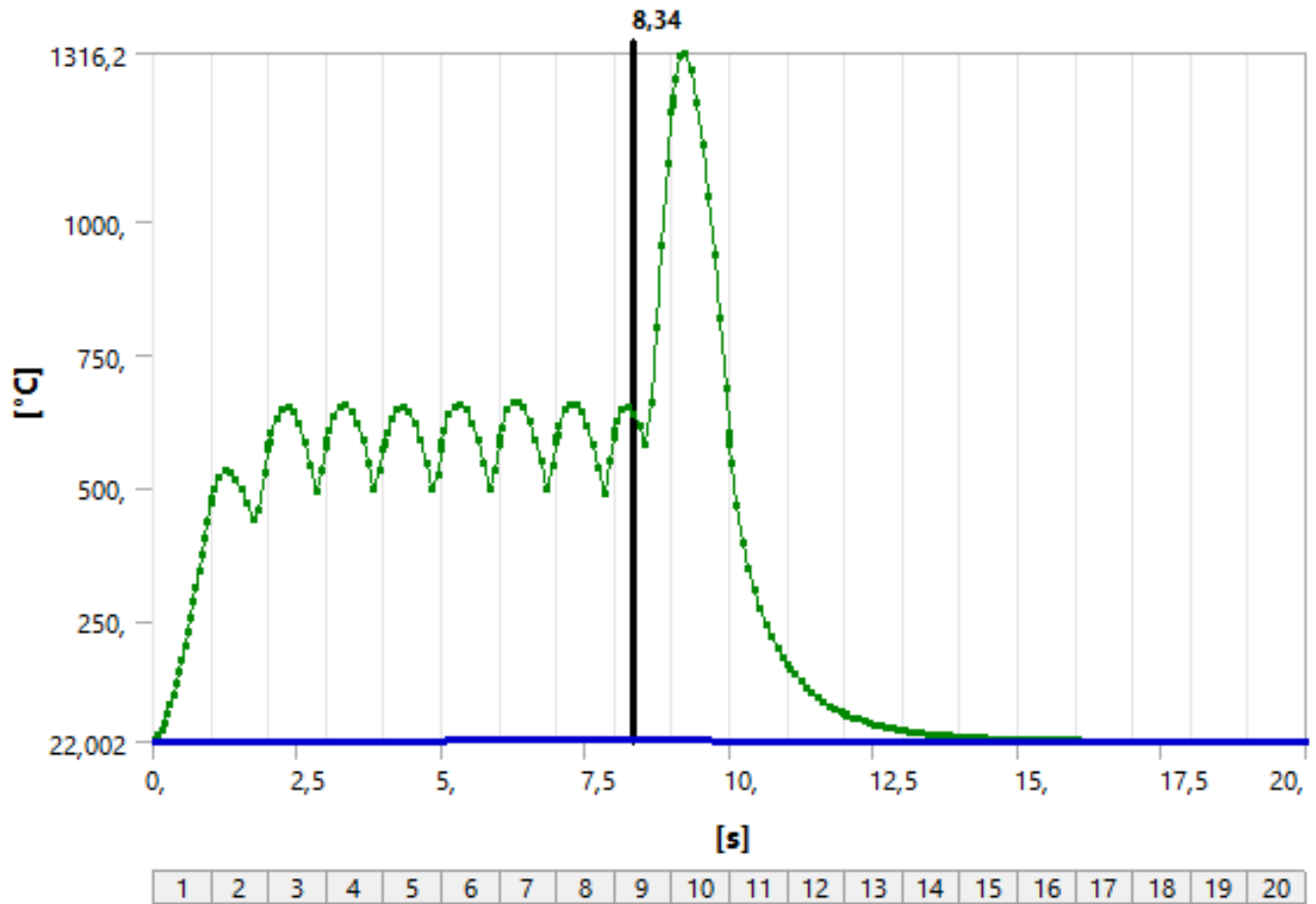
I.2 Temperature - P2D1

Figure 155: Maximum temperature at 1316°following by a rapid cooling, during a duration in 20 second
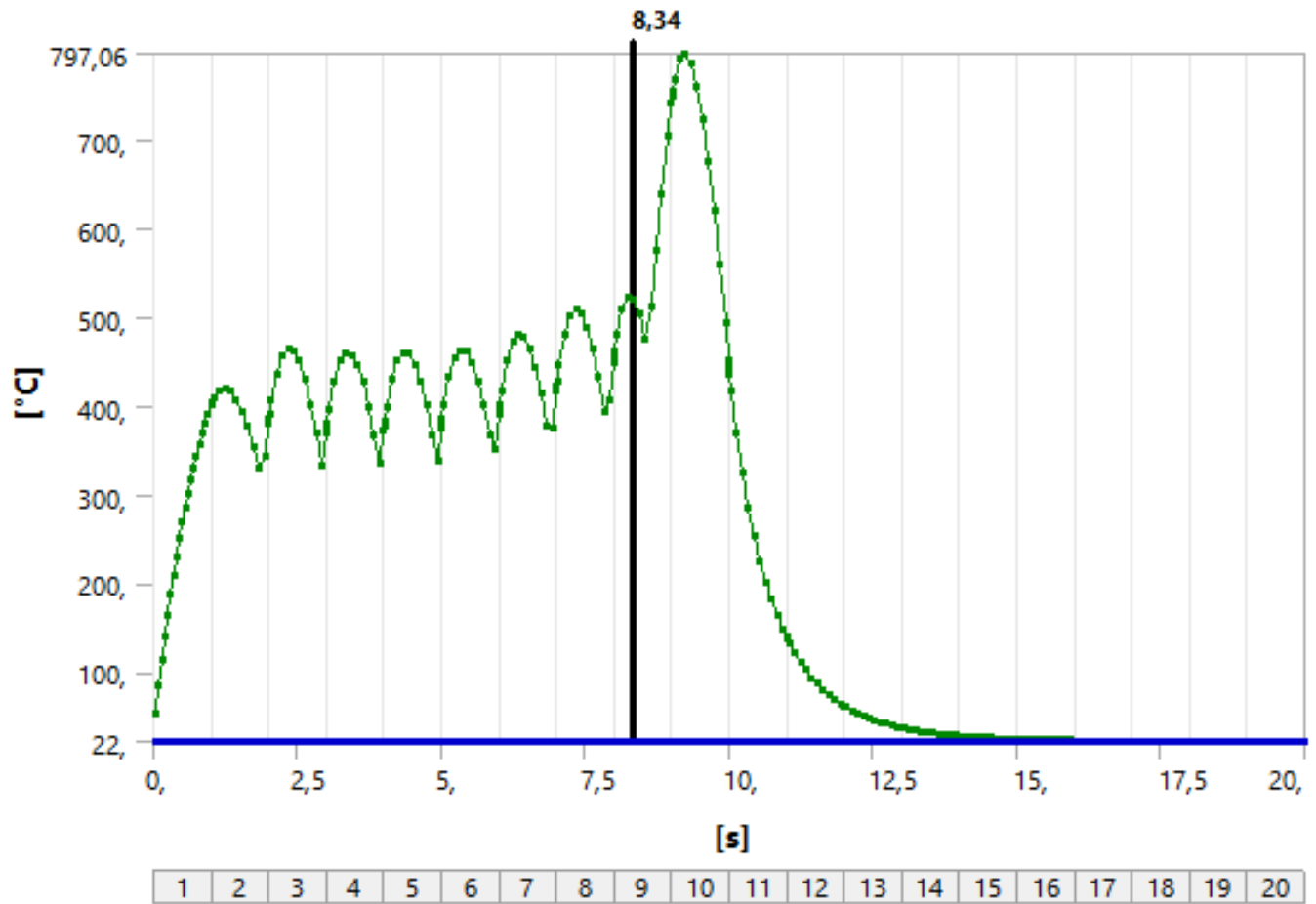
I.3   Temperature - P3D1

Figure 156: Maximum temperature at 797°following by a rapid cooling, during a duration in 20 second
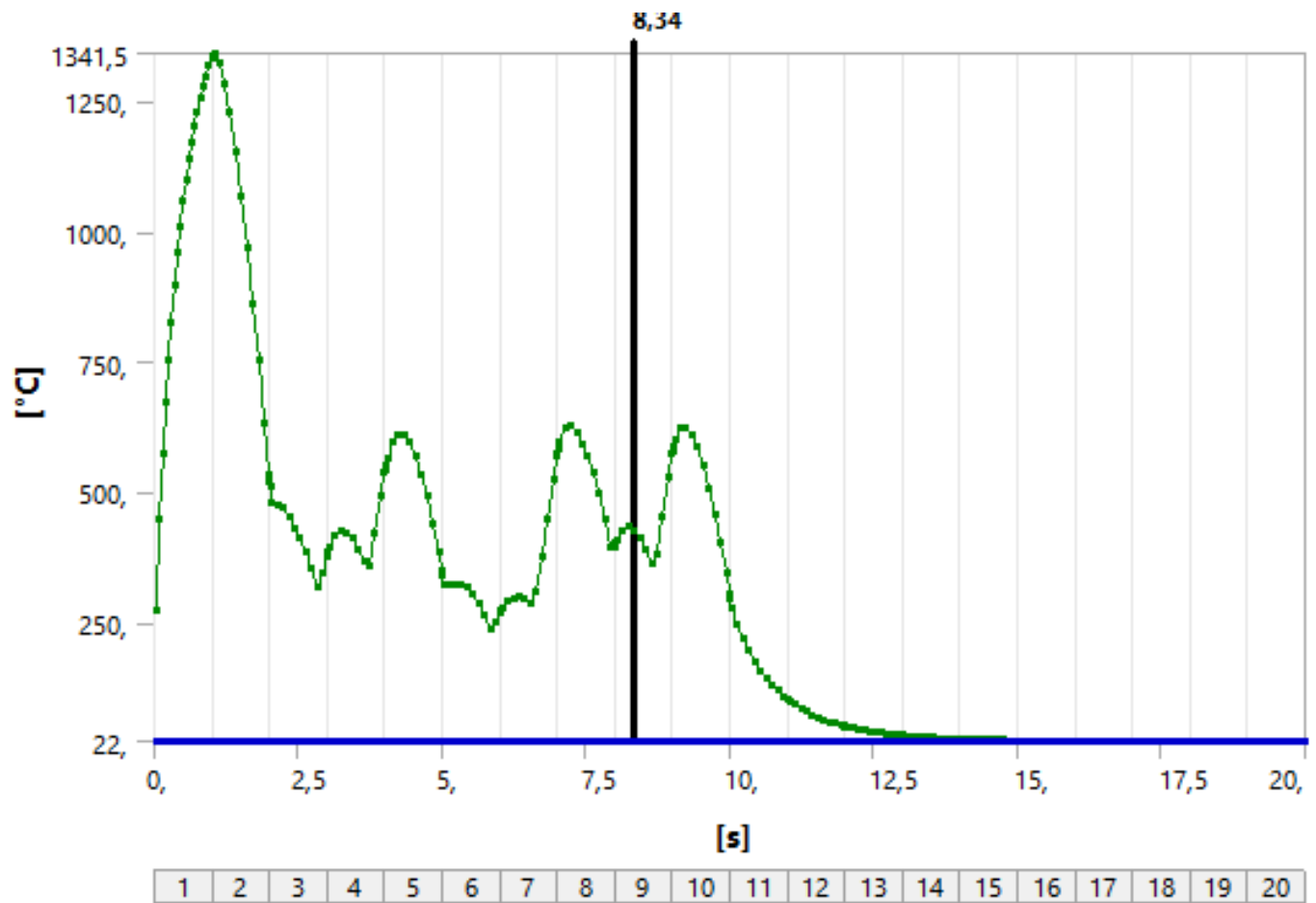
I.4   Temperature - P5D1

Figure 157: Maximum temperature at 1341°following by a rapid cooling, during a duration in 20 second

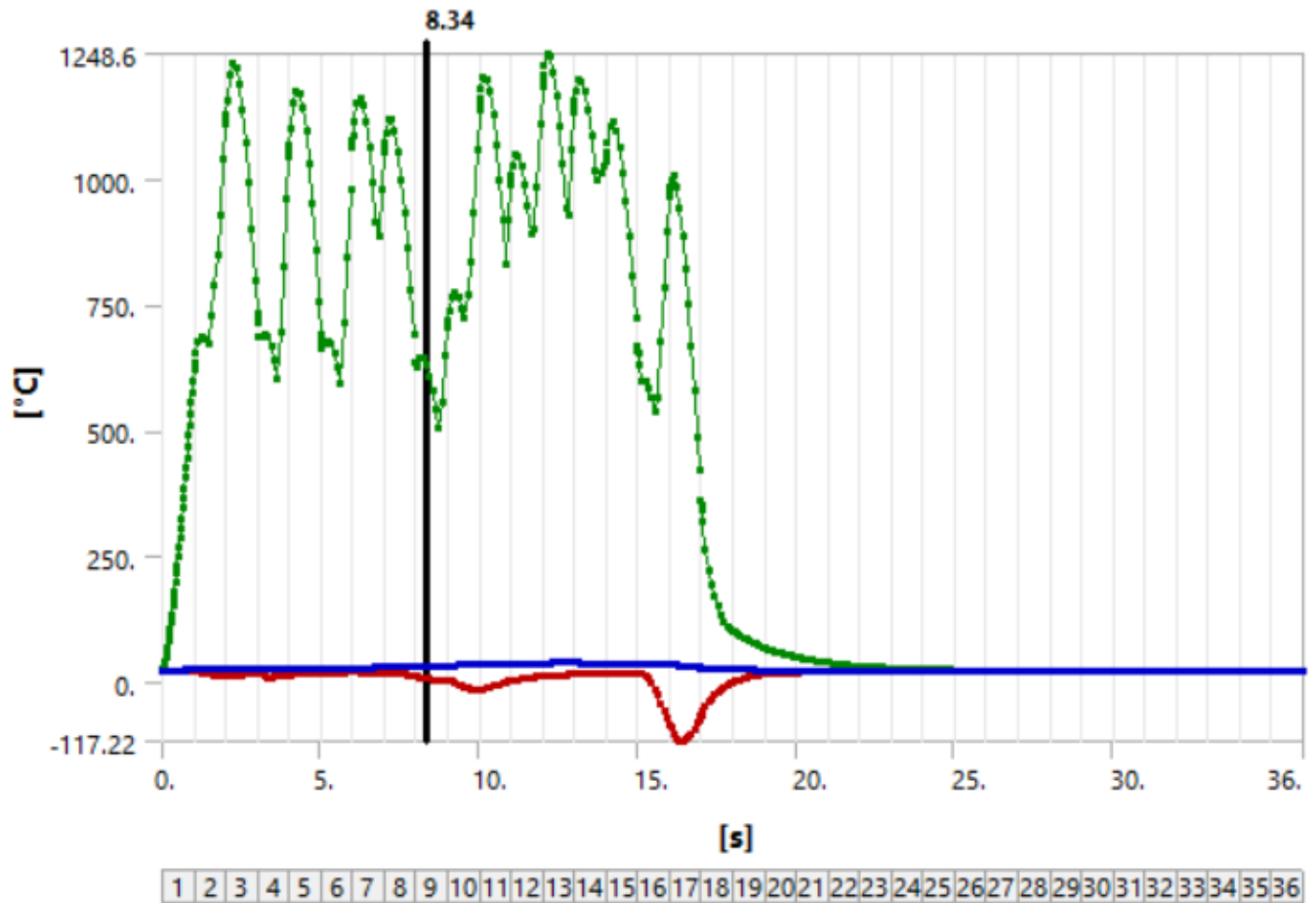## I.5   Temperature - P1D2

Figure 158: Maximum temperature at 1248°following by a rapid cooling, during a duration in 36 second

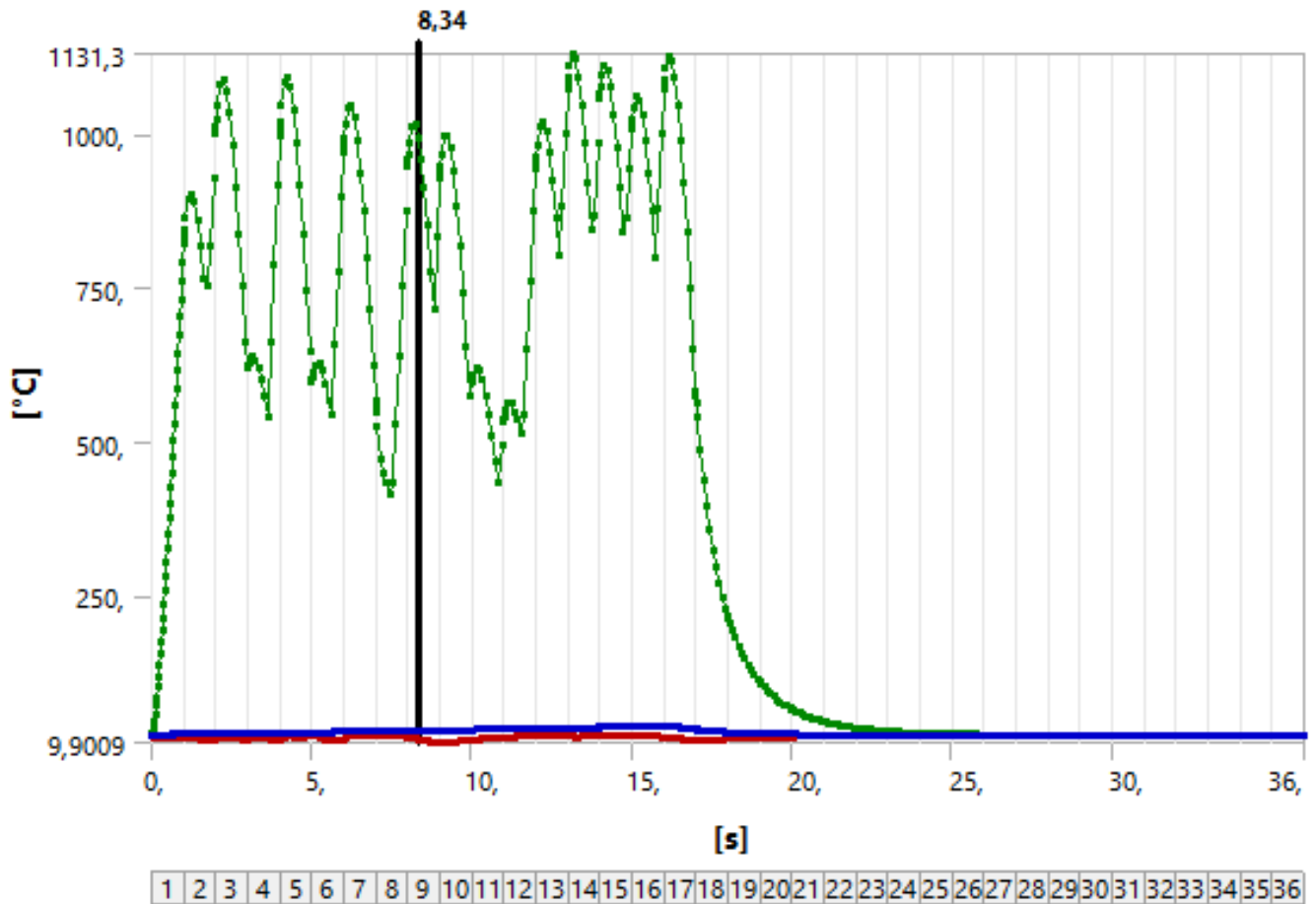## I.6   Temperature - P2D2

Figure 159: Maximum temperature at 1131°following by a rapid cooling, during a duration in 36 second
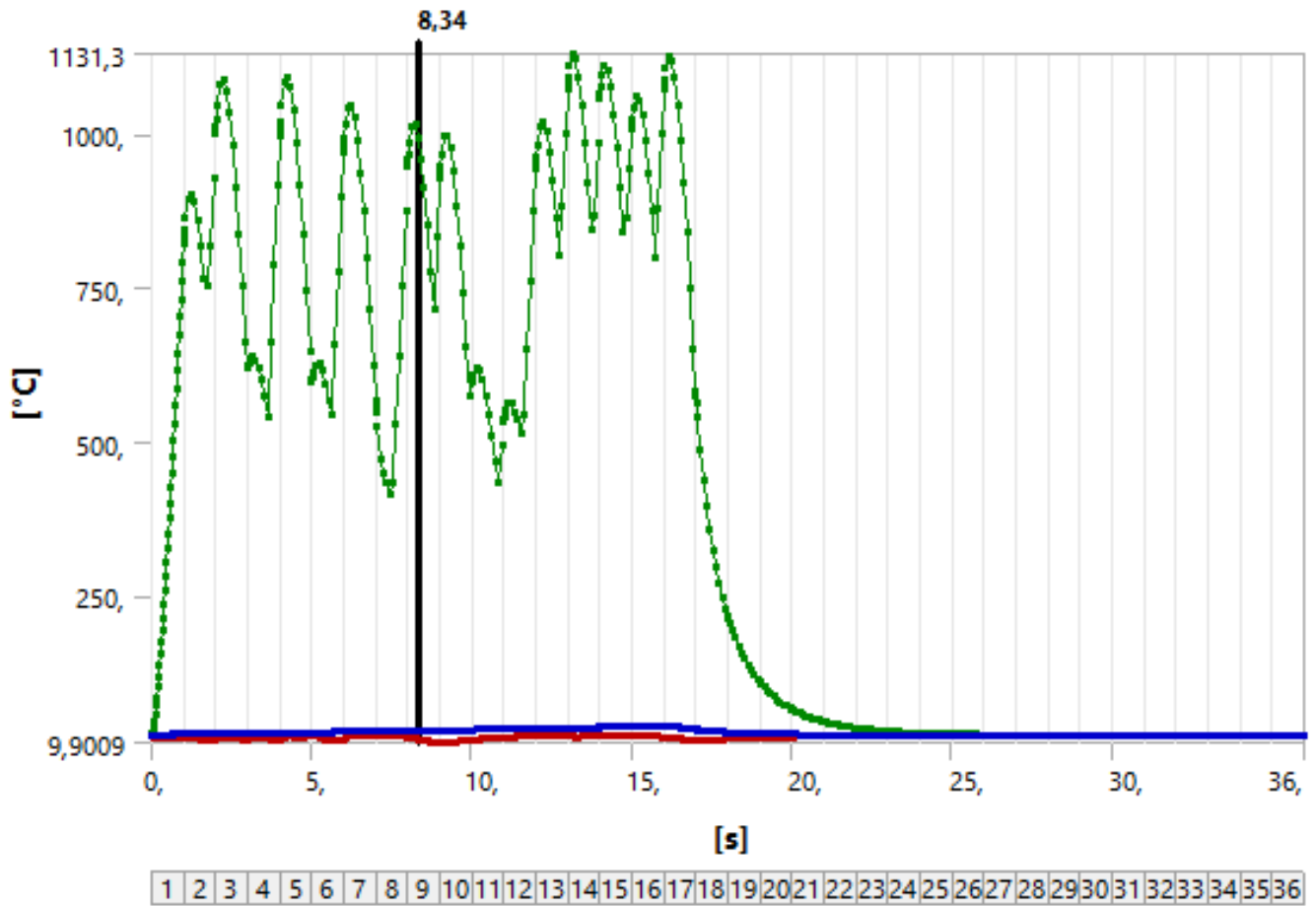
I.7   Temperature - P4D2

Figure 160: Maximum temperature at 1121°following by a rapid cooling, during a duration in 36 second

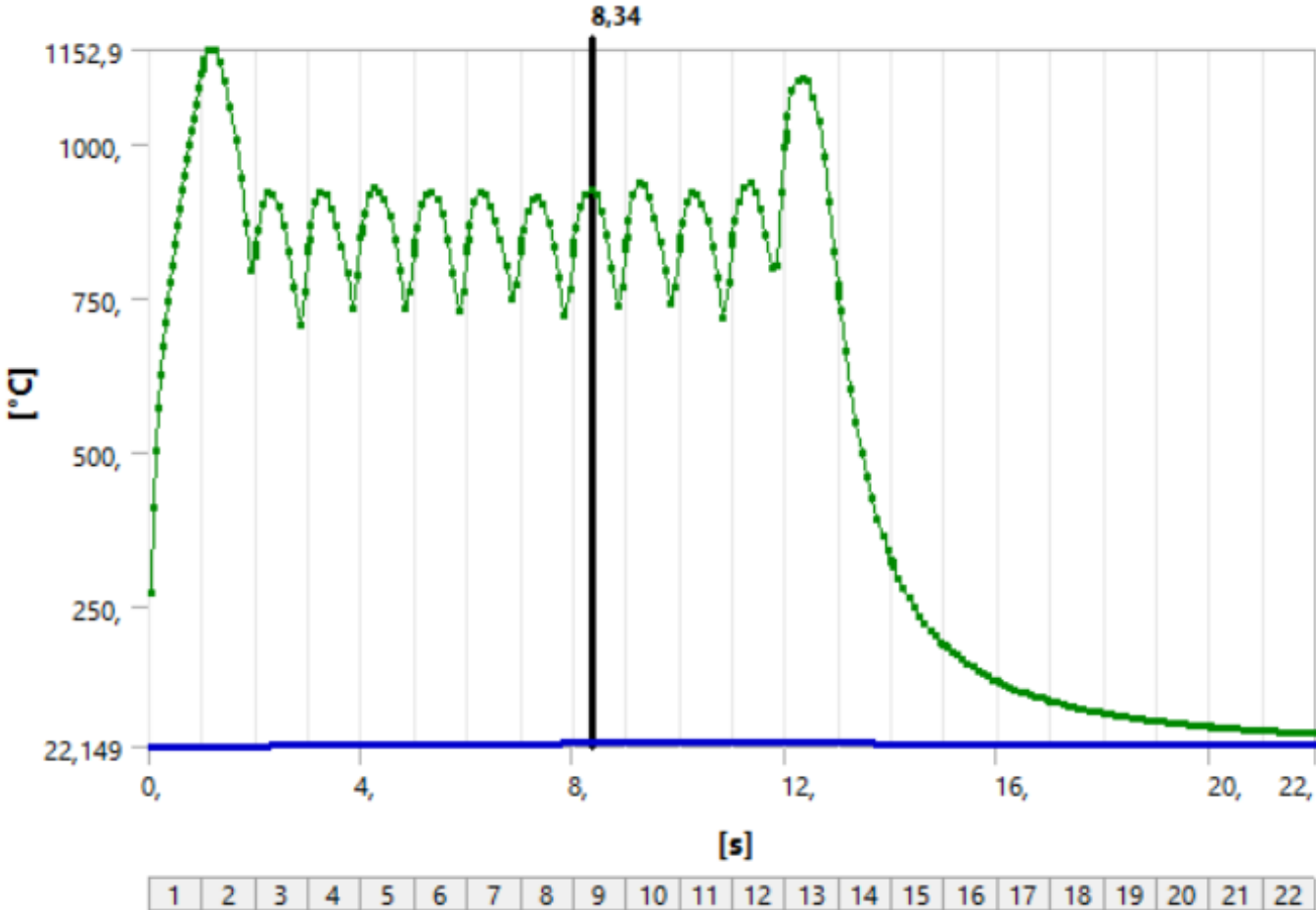## I.8   Temperature - P1D1-BP

Figure 161: Maximum temperature at 1152°following by a rapid cooling, during a duration in 22 second

I.9   Temperature - P2D1-BP

Figure 162: Maximum temperature at 1009°following by a rapid cooling, during a duration in 22 second

I.10 Temperature - P3D1-BP

Figure 163: Maximum temperature at 803°following by a rapid cooling, during a duration in 20 second

I.11   Temperature - P5D1-BP

Figure 164: Maximum temperature at 782°following by a rapid cooling, during a duration in 36 second

I.12   Temperature - P1D2-BP
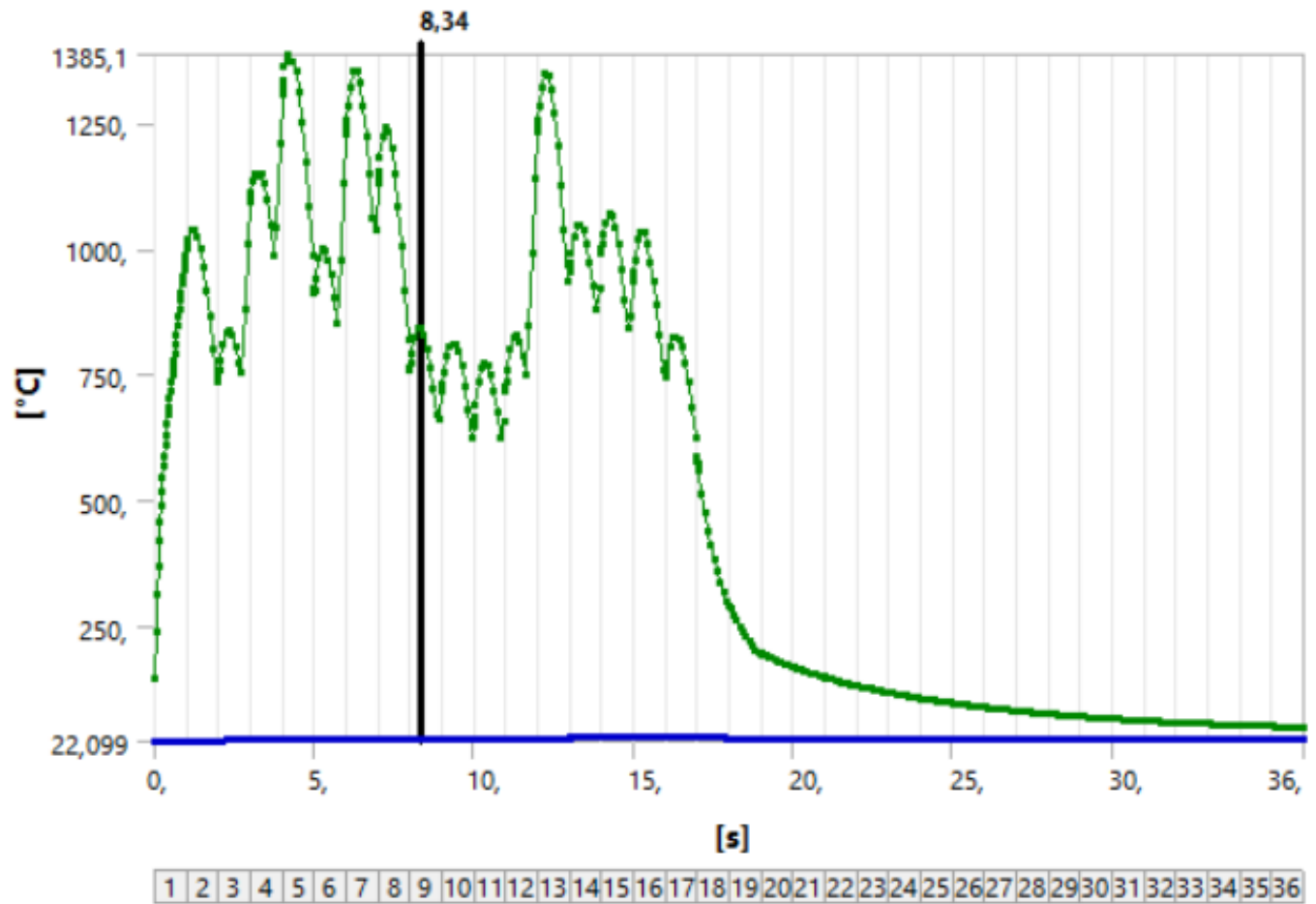
Figure 165: Maximum temperature at 1385°following by a rapid cooling, during a duration in 36 second

I.13   Temperature - P2D2-BP
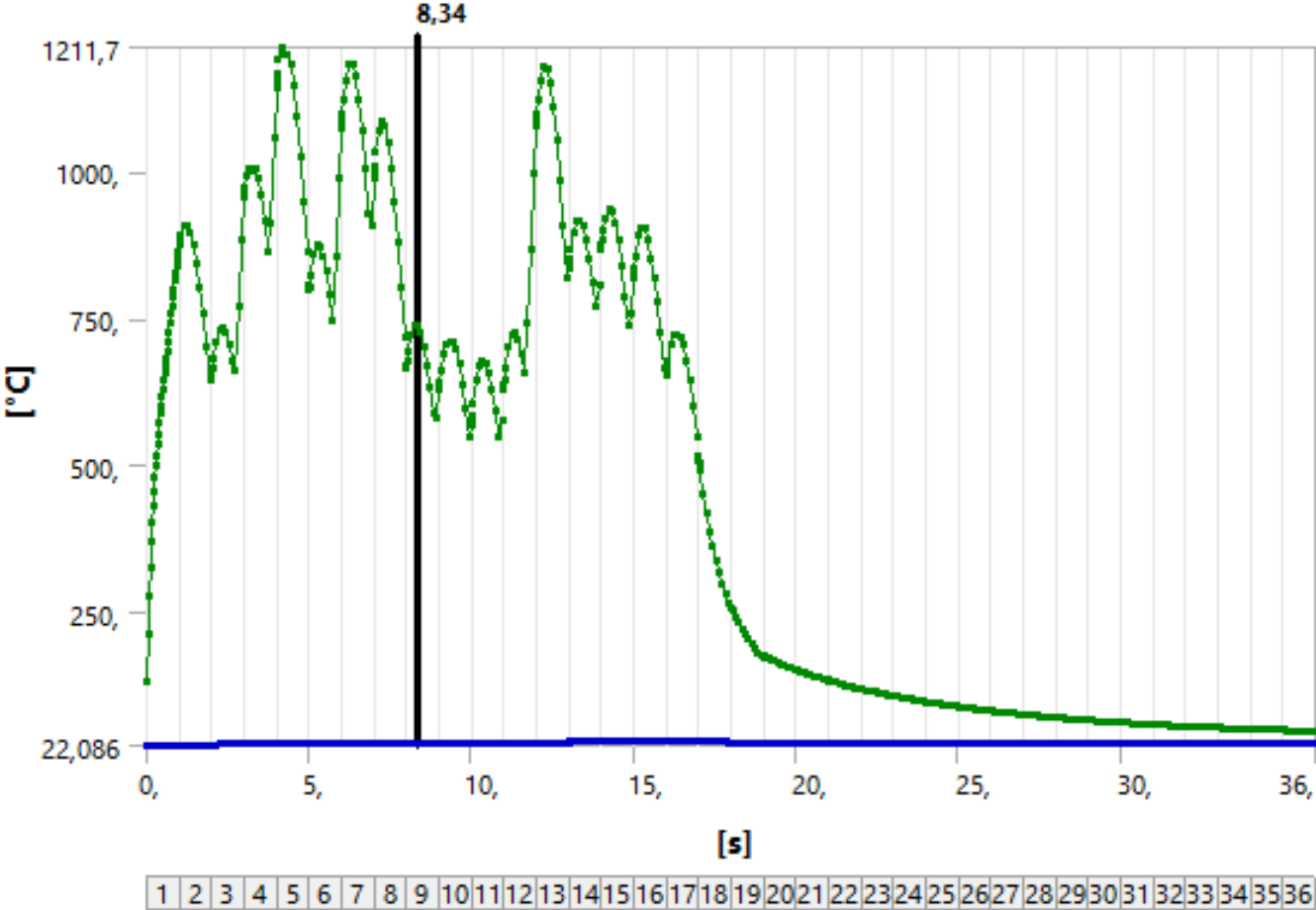
Figure 166: Maximum temperature at 1211°following by a rapid cooling, during a duration in 36 second

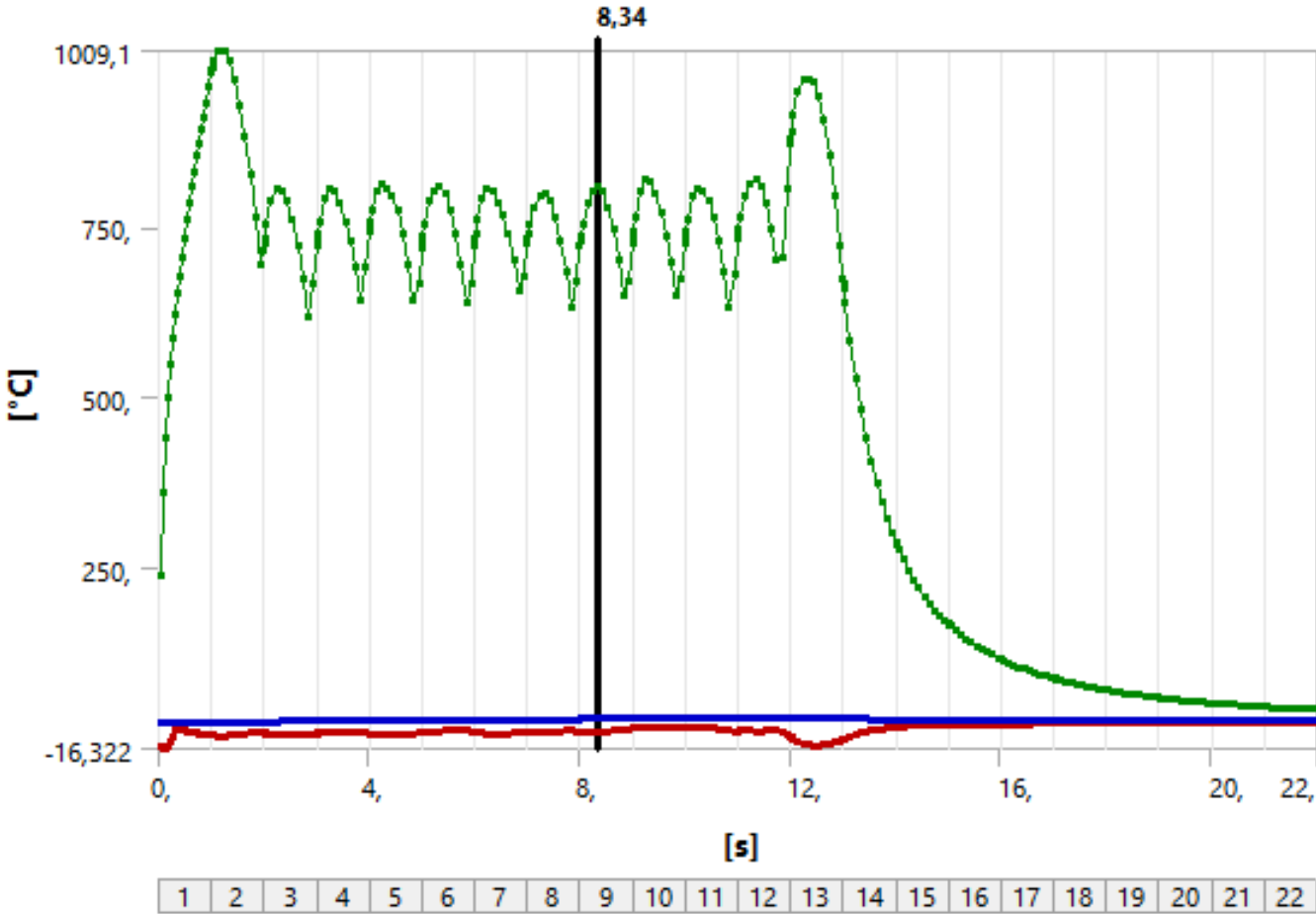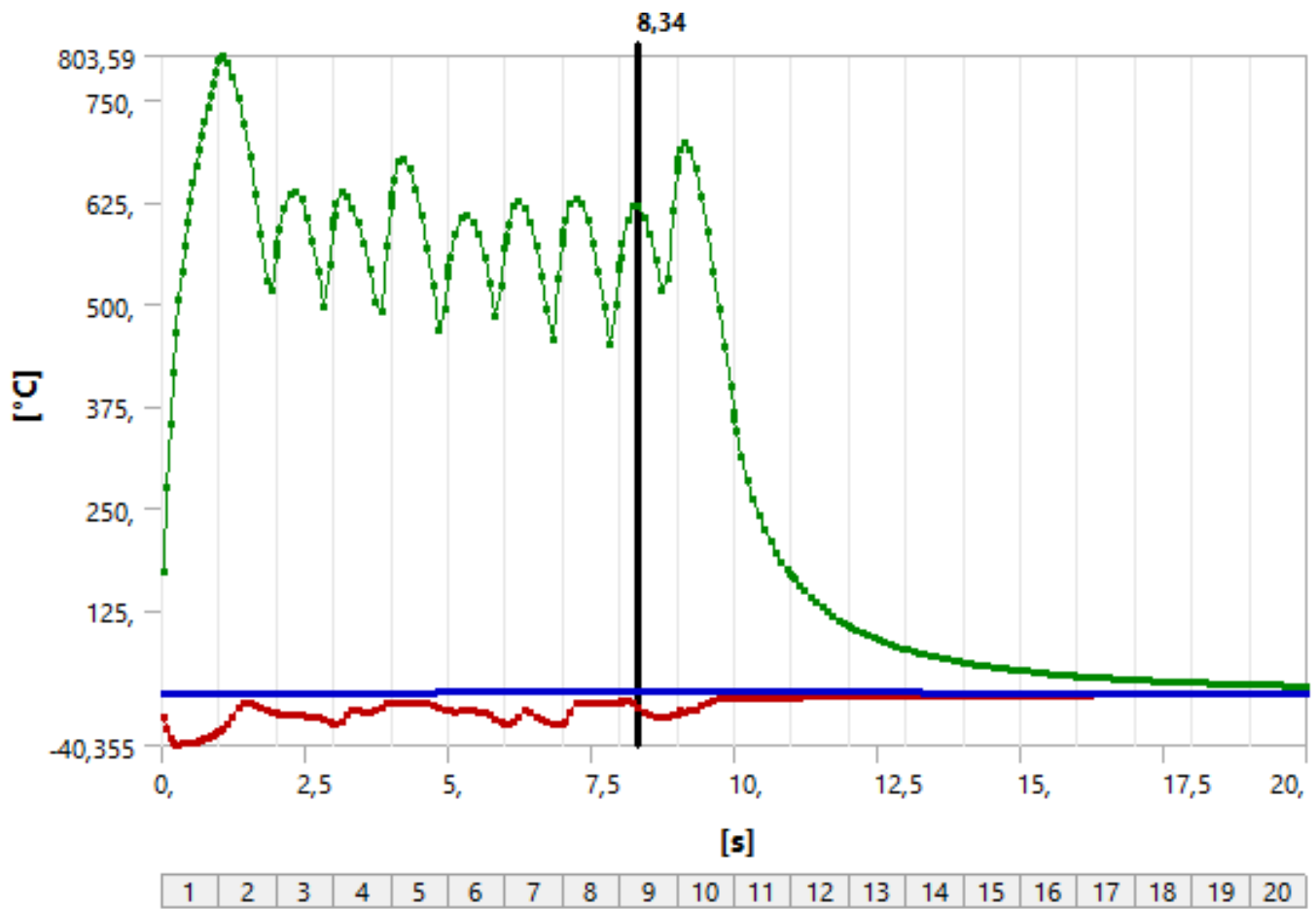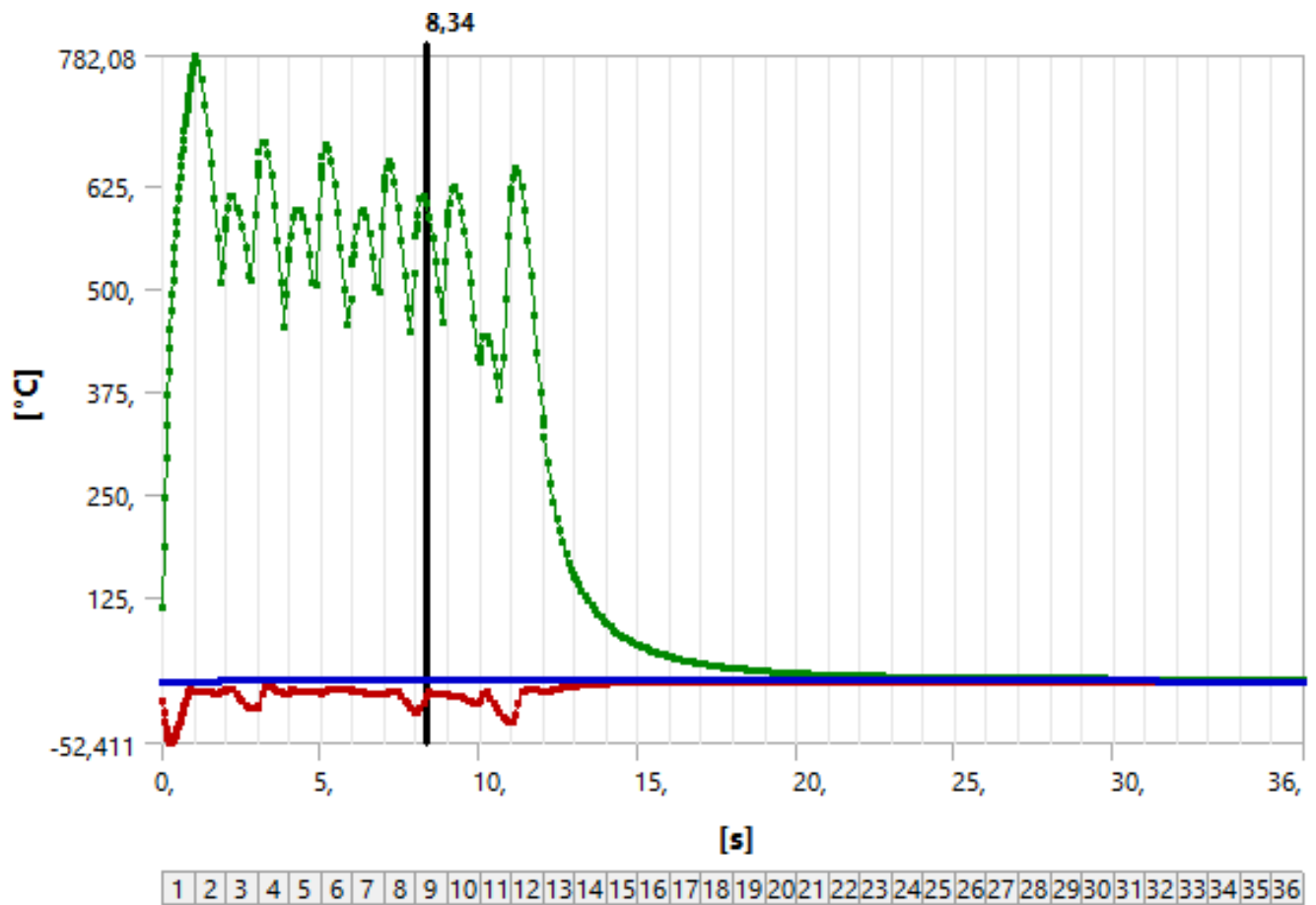## I.14   Temperature - P4D2-BP
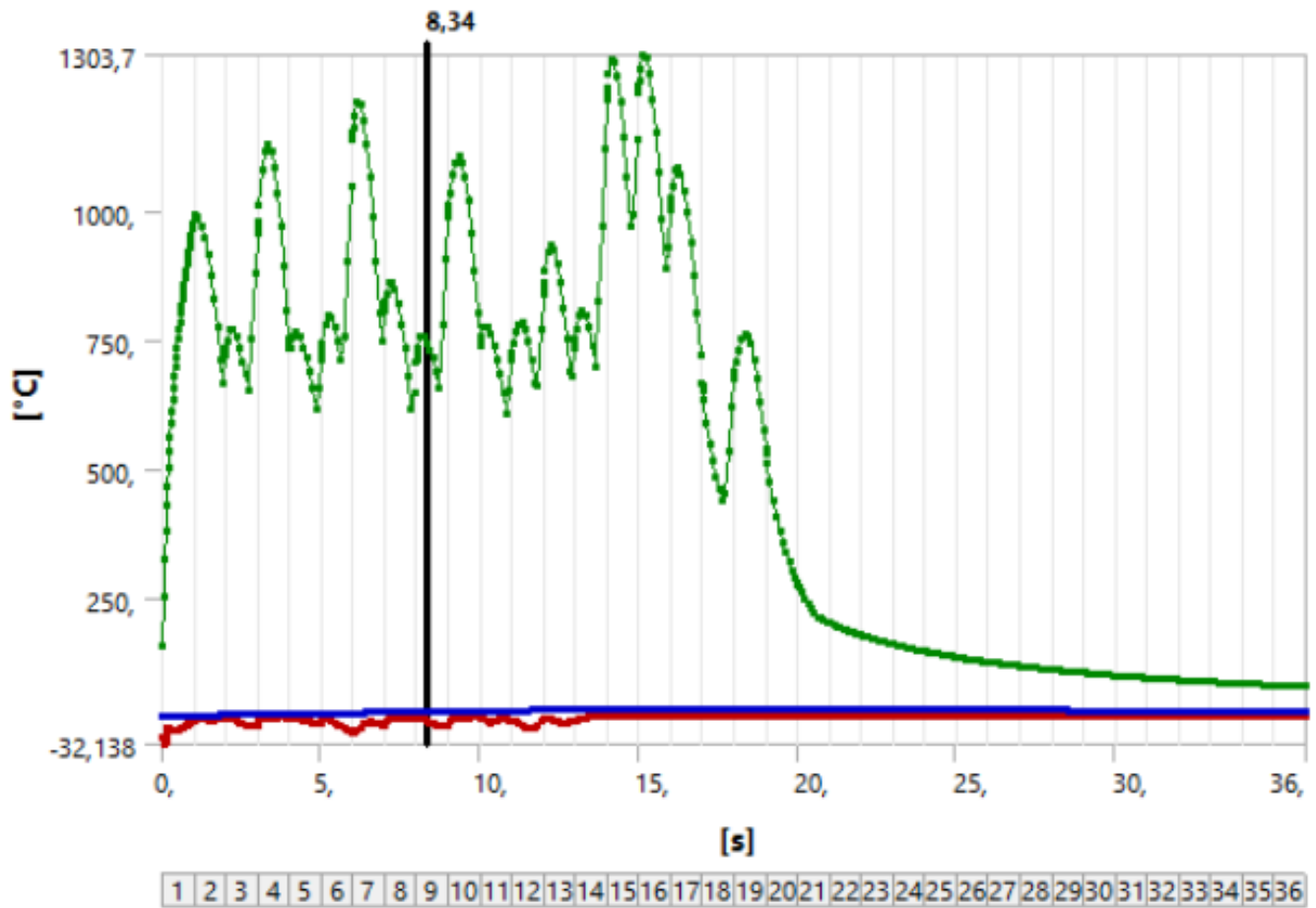
Figure 167: Maximum temperature at 1303°following by a rapid cooling, during a duration in 36 second

I.15   Temperature - P4D3-BP
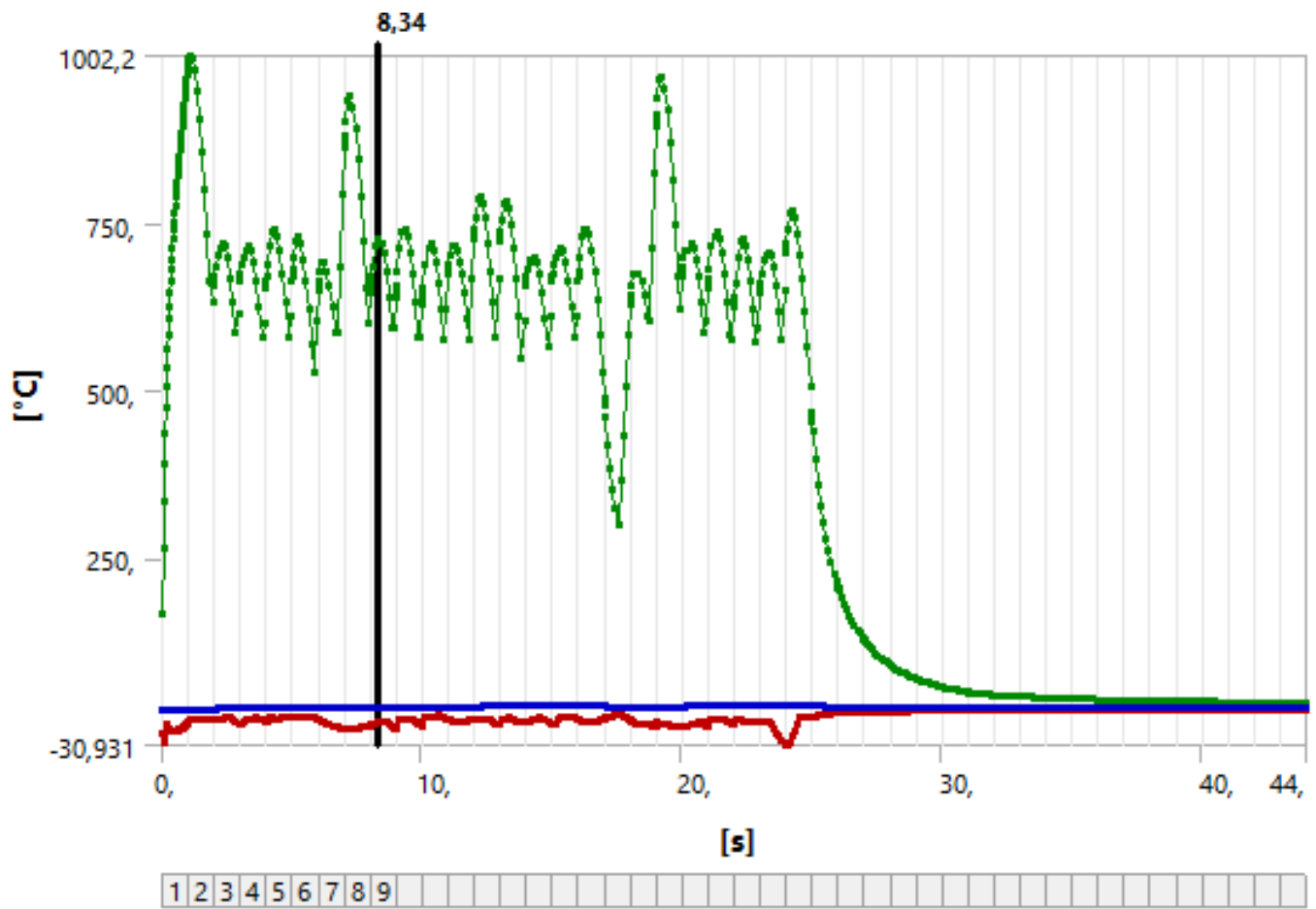
Figure 168: Maximum temperature at 1002°following by a rapid cooling, during a duration in 44 second

J WPQR for each welded thin wall structure

WPQR was developed in purpose to document the procedure of welding the thin wall structures. It was also used to document the layer description in appendix A. WPQR are based on test and fails during the experiment and additionally the technical drawings made in Inventor, which is documented in appendix: K.

J.1   WPQR for P1D1

Welding Procedure Qualification Record (WPAR)				WPQR No: 001 Date: 25.01.2019			
Prod.by: Hans Ivar Arumairasa Project: Thin Wall Structure by Welding				Location: Narvik (UiT) - lab Welding Type Process: GTAW by KUKA-Robot			
Technique:		**Cleaning:**		**Structure:**		Thin Wall Structure	
Movement:	String	Initial cleaning oxide:	Grinding/ machining				
Gas Cup size:	8 [mm]	**Filler metal**					
Single or multipass:	Single	Type:	Bohler CN 13/4				
Process:		Size:	1.2 [mm]				
Polarity:	DC-	**Welding**					
Electrode	3.2 [mm]	Torch Angle	-10 degree				

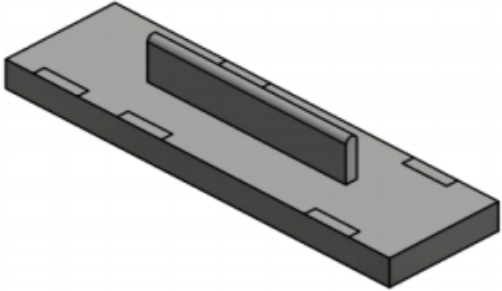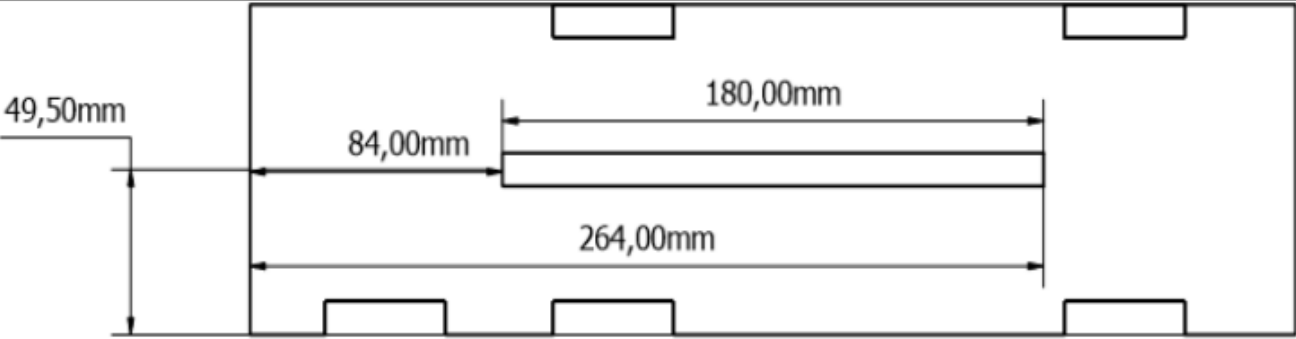| Type:	Automatic	**Position coordinate**			**Heat Treatment:**	**Preheat:**	**PWHT:**
Electrode:	3.2 [mm]	x0 = 170	x1 = 340	x2 = 000	x3 = 000	Type:	Type:
Shielding gas:		y0 = 15	y1 = 15	y2 = 000	y3 = 000	Gas burner	Gas burner
Gas type:	Argon	z0 = 000	z1 = 000	z2 = 000	z3 = 000	Avr.temp in weld:	temp after weld:
Composition	100 %	Layers:	29			36,7°	164,1°

Identification of parent metal:							
Part:	Type:		Thickness	Widt	Length:	Yield Strength	
1	X3CrNiMo13-4		20 [mm]	100 [mm]	350 [mm]	1100 MP	

Identification of filler metal:						
Part:	Type:		Classificaiton	Dia [mm]	Yield Strength	
1	Bohler CN 13/4-IG		EN ISO 14343-A: G 13 4	1,1	950 MP	

Welding Parameters:							
Index:	Heat Input [KJ/mm]	Wire feed speed [mm/sek]	Current [A]:	Voltage [V]:	AVHC	Welding speed [mm/sek]:	Gas [l/min]:
	1,1	2	250	16,4	2.8 [mm]	2.2	12

Welding plan:

49,50mm

84,00mm

180,00mm

264,00mm

Figure 169: WPQR for P1D1

J.2 WPQR for P2D1

Welding Procedure Qualification Record (WPAR)				WPQR No: 002 Date: 26.01.2019				
Prod.by: Hans Ivar Arumairasa Project: Thin Wall Structure by Welding				Location: Narvik (UiT) - lab Welding Type Process: GTAW by KUKA-Robot				
Technique:		**Cleaning:**		**Structure:**		Thin Wall Structure		
Movement:	String	Initial cleaning oxide:	Grinding/ machining					
Gas Cup size:	8 [mm]	**Filler metal**						
Single or multipass:	Single	Type:	Bohler CN 13/4					
Process:		Size:	1.2 [mm]					
Polarity:	DC-	**Welding**						
Electrode	3.2 [mm]	Torch Angle	-10 degree					

Type:	Automatic	**Position coordinate**		**Heat Treatment:**			**Preheat:**	**PWHT:**
Electrode:	3.2 [mm]	x0 = 5	x1 = 175	x2 = 000	x3 = 000		Type:	Type:
Shielding gas:		y0 = 45	y1 = 45	y2 = 000	y3 = 000		Gas burner	Gas burner
Gas type:	Argon	z0 = 000	z1 = 000	z2 = 000	z3 = 000		Avr.temp in weld:	temp after weld:
Composition	100 %	Layers:	31				46.6°	146,1°

Identification of parent metal:								
Part:	Type:			Thickness	Widt	Length:	Yield Strength	
1	X3CrNiMo13-4			20 [mm]	100 [mm]	350 [mm]	1100 MP	

Identification of filler metal:							
Part:	Type:			Classificaiton		Dia [mm]	Yield Strength
1	Bohler CN 13/4-IG			EN ISO 14343-A: G 13 4		1,1	950 MP

Welding Parameters:							
Index:	Heat Input [KJ/mm]	Wire feed speed [mm/sek]	Current [A]:	Voltage [V]:	AVHC	Welding speed [mm/sek]:	Gas [l/min]:
	0.89	1.8	240	14.2	2.8 [mm]	2.3	12

Welding plan:

Figure 170: WPQR for P2D1

J.3   WPQR for P3D1

Welding Procedure Qualification Record (WPAR)				WPQR No: 003 Date: 26.01.2019				
Prod.by: Hans Ivar Arumairasa Project: Thin Wall Structure by Welding				Location: Narvik (UiT) - lab Welding Type Process: GTAW by KUKA-Robot				
Technique:		**Cleaning:**		**Structure:**		Thin Wall Structure		
Movement:	String	Initial cleaning oxide:	Grinding/ machining					
Gas Cup size:	8 [mm]	**Filler metal**						
Single or multipass:	Single	Type:	Bohler CN 13/4					
Process:		Size:	1.2 [mm]					
Polarity:	DC-	**Welding**						
Electrode	3.2 [mm]	Torch Angle	-10 degree					

Type:	Automatic	**Position coordinate**		**Heat Treatment:**		**Preheat:**	**PWHT:**
Electrode:	3.2 [mm]	x0 = 5	x1 = 175	x2 = 000	x3 = 000	Type:	Type:
Shielding gas:		y0 = 10	y1 = 10	y2 = 000	y3 = 000	Gas burner	Gas burner
Gas type:	Argon	z0 = 000	z1 = 000	z2 = 000	z3 = 000	Avr.temp in weld:	temp after weld:
Composition	100 %	Layers:	34			41.7°	169.5°

Identification of parent metal:						
Part:	Type:		Thickness	Widt	Length:	Yield Strength
1	X3CrNiMo13-4		20 [mm]	100 [mm]	350 [mm]	1100 MP

Identification of filler metal:				
Part:	Type:	Classificaiton	Dia [mm]	Yield Strength
1	Bohler CN 13/4-IG	EN ISO 14343-A: G 13 4	1,1	950 MP

Welding Parameters:							
Index:	Heat Input [KJ/mm]	Wire feed speed [mm/sek]	Current [A]:	Voltage [V]:	AVHC	Welding speed [mm/sek]:	Gas [l/min]:
	0.81	1.6	220	13.5	2.7 [mm]	2.2	12
Welding plan:							

Figure 171: WPQR for P3D1

J.4   WPQR for P4D1
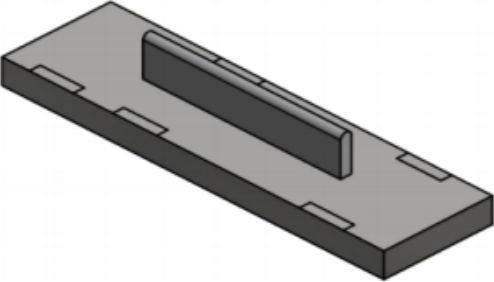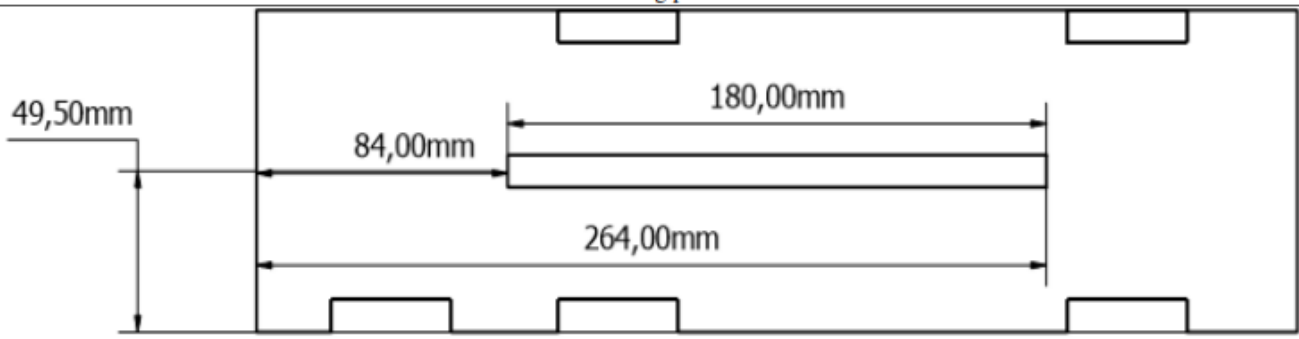
Welding Procedure Qualification Record (WPAR)				WPQR No: 004 Date: 27.01.2019						
Prod.by: Hans Ivar Arumairasa Project: Thin Wall Structure by Welding				Location: Narvik (UiT) - lab Welding Type Process: GTAW by KUKA-Robot						
Technique:		**Cleaning:**		**Structure:**			Thin Wall Structure			
Movement:	String	Initial cleaning oxide:	Grinding/ machining							
Gas Cup size:	8 [mm]	**Filler metal**								
Single or multipass:	Single	Type:	Bohler CN 13/4							
Process:		Size:	1.2 [mm]							
Polarity:	DC-	**Welding**								
Electrode	3.2 [mm]	Torch Angle	-10 degree							
Type:	Automatic	**Position coordinate**		**Heat Treatment:**				**Preheat:**		**PWHT:**
Electrode:	3.2 [mm]	x0 = 40	x1 = 140	x2 = 000	x3 = 000			Type:		Type:
Shielding gas:		y0 = 50	y1 = 50	y2 = 000	y3 = 000			Gas burner		Gas burner
Gas type:	Argon	z0 = 000	z1 = 000	z2 = 000	z3 = 000			Avr.temp in weld:		temp after weld:
Composition	100 %	Layers:	17					-		-

Identification of parent metal:										
Part:	Type:			Thickness	Widt		Length:		Yield Strength	
1	X3CrNiMo13-4			20 [mm]	100 [mm]		350 [mm]		1100 MP	

Identification of filler metal:										
Part:	Type:			Classificaiton			Dia [mm]		Yield Strength	
1	Bohler CN 13/4-IG			EN ISO 14343-A: G 13 4			1,1		950 MP	

Welding Parameters:

Index:	Heat Input [KJ/mm]	Wire feed speed [mm/sek]	Current [A]:	Voltage [V]:	AVHC	Welding speed [mm/sek]:	Gas [l/min]:
	0.73	1.47	220	12.2	2.4 [mm]	2.2	12

Welding plan:

49,50mm

84,00mm

180,00mm

264,00mm

Figure 172: WPQR for P4D1

J.5   WPQR for P5D1
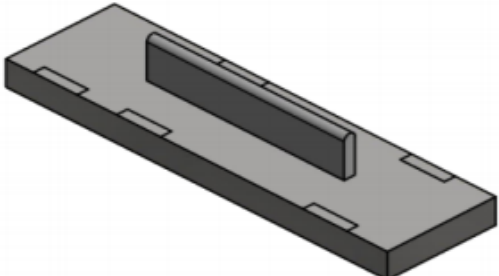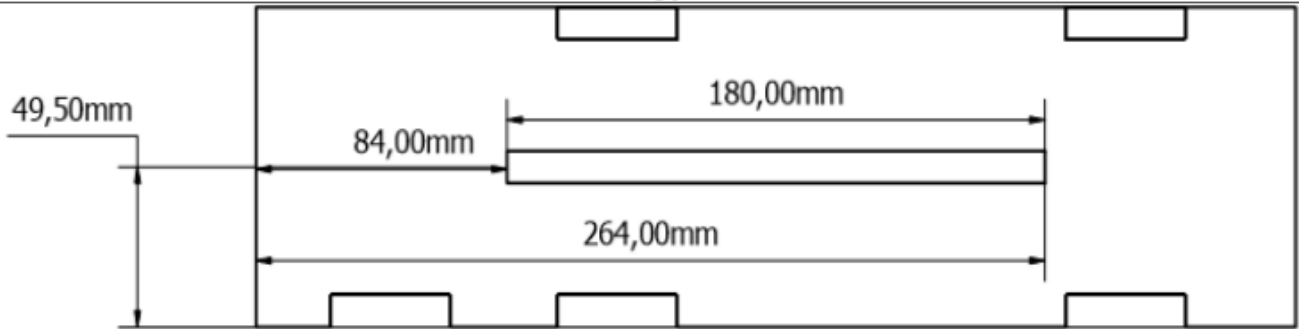
Welding Procedure Qualification Record (WPAR)				WPQR No: 005 Date: 28.01.2019					
Prod.by: Hans Ivar Arumairasa Project: Thin Wall Structure by Welding				Location: Narvik (UiT) - lab Welding Type Process: GTAW by KUKA-Robot					
Technique:		**Cleaning:**		**Structure:**		Thin Wall Structure			
Movement:	String	Initial cleaning oxide:	Grinding/ machining						
Gas Cup size:	8 [mm]	**Filler metal**							
Single or multipass:	Single	Type:	Bohler CN 13/4						
Process:		Size:	1.2 [mm]						
Polarity:	DC-	**Welding**							
Electrode	3.2 [mm]	Torch Angle	-10 degree						
Type:	Automatic	**Position coordinate**		**Heat Treatment:**		**Preheat:**		**PWHT:**	
Electrode:	3.2 [mm]	x0 = 100	x1 = 320	x3 = 0	x4 = 0	Type:		Type:	
Shielding gas:		y0 = 50	y1 = 50	y2 = 0	y3 = 0	Gas burner		Gas burner	
Gas type:	Argon	z0 = 000	z1 = 000	z2 = 000	z3 = 000	Avr.temp in weld:		temp after weld:	
Composition	100 %	Layers:	42			45°		141°	
Identification of parent metal:									
Part:	Type:			Thickness	Widt	Length:	Yield Strength		
1	X3CrNiMo13-4			20 [mm]	100 [mm]	350 [mm]	1100 MP		
Identification of filler metal:									
Part:	Type:			Classificaiton		Dia [mm]	Yield Strength		
1	Bohler CN 13/4-IG			EN ISO 14343-A: G 13 4		1,1	950 MP		

Welding Parameters:

Index:	Heat Input [KJ/mm]	Wire feed speed [mm/sek]	Current [A]:	Voltage [V]:	AVHC	Welding speed [mm/sek]:	Gas [l/min]:
	0.67	0.85	200	12.3	2.4 [mm]	2.2	12

Welding plan:

Figure 173: WPQR for P5D1

J.6   WPQR for P1D2
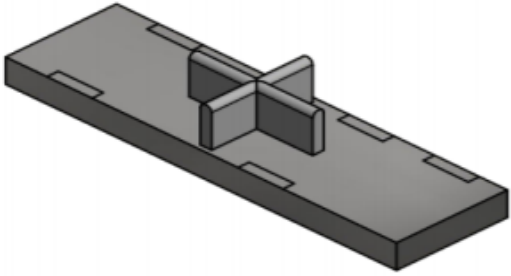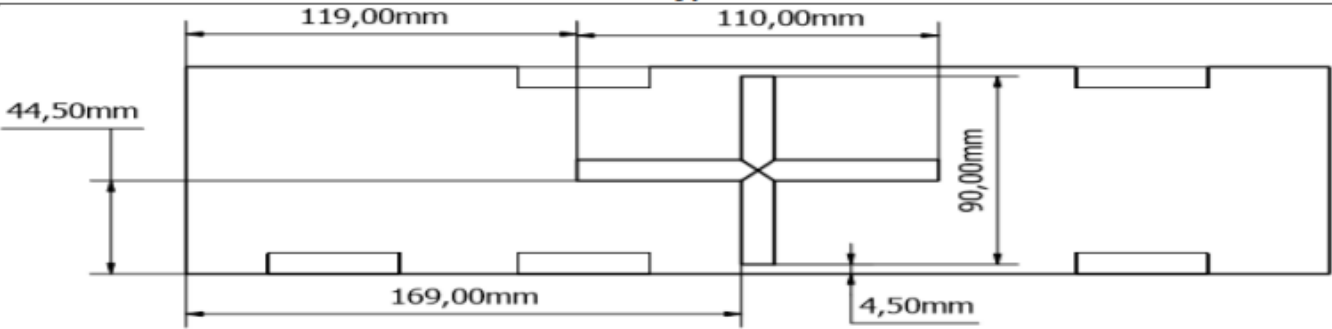
Welding Procedure Qualification Record (WPAR)				WPQR No: 006					
				Date: 29.01.2019					
Prod.by: Hans Ivar Arumairasa				Location: Narvik (UiT) - lab					
Project: Thin Wall Structure by Welding				Welding Type Process: GTAW by KUKA-Robot					
Technique:		**Cleaning:**		**Structure:**		Thin Wall Structure			
Movement:	String	Initial cleaning oxide:	Grinding/ machining						
Gas Cup size:	8 [mm]	**Filler metal**							
Single or multipass:	Single	Type:	Bohler CN 13/4						
Process:		Size:	1.2 [mm]						
Polarity:	DC-	**Welding**							
Electrode	3.2 [mm]	Torch Angle	-10 degree						

Type:	Automatic	**Position coordinate**		**Heat Treatment:**		**Preheat:**	**PWHT:**
Electrode:	3.2 [mm]	x0 = 40	x1 = 140	x3 = 75	x4 = 75	Type:	Type:
Shielding gas:		y0 = 50	y1 = 50	y2 = 85	y3 = 5	Gas burner	Gas burner
Gas type:	Argon	z0 = 000	z1 = 000	z2 = 000	z3 = 000	Avr.temp in weld:	temp after weld:
Composition	100 %	Layers:	11			47°	160°

Identification of parent metal:							
Part:	Type:		Thickness	Widt	Length:	Yield Strength	
1	X3CrNiMo13-4		20 [mm]	100 [mm]	350 [mm]	1100 MP	
Identification of filler metal:							
Part:	Type:		Classificaiton		Dia [mm]	Yield Strength	
1	Bohler CN 13/4-IG		EN ISO 14343-A: G 13 4		1,1	950 MP	

Welding Parameters:							
Index:	Heat Input [KJ/mm]	Wire feed speed [mm/sek]	Current [A]:	Voltage [V]:	AVHC	Welding speed [mm/sek]:	Gas [l/min]:
	1.12	2.0	250	16.4	2.8 [mm]	2.2	12
Welding plan:							

Figure 174: WPQR for P1D2

J.7   WPQR for P2D2
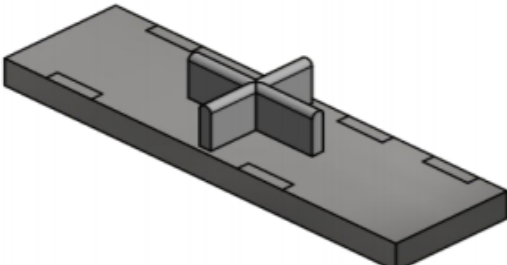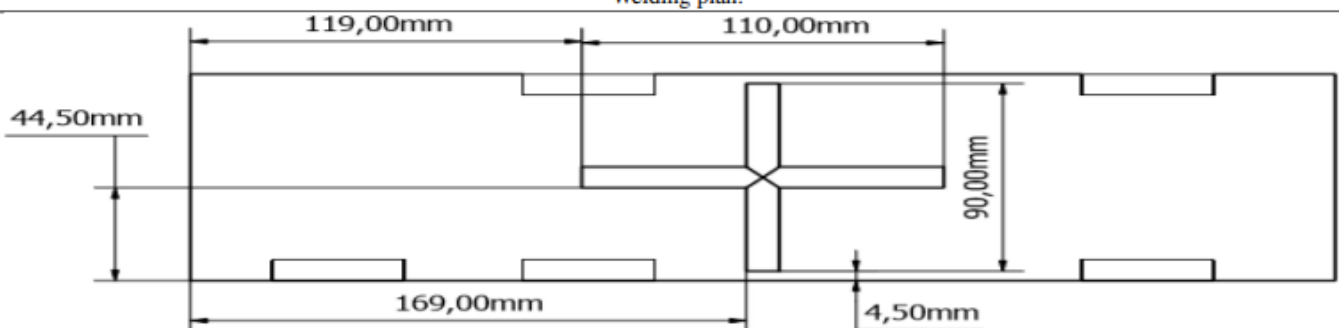
Welding Procedure Qualification Record (WPAR)				WPQR No: 007 Date: 29.01.2019					
Prod.by: Hans Ivar Arumairasa Project: Thin Wall Structure by Welding				Location: Narvik (UiT) - lab Welding Type Process: GTAW by KUKA-Robot					
Technique:		**Cleaning:**		**Structure:**		Thin Wall Structure			
Movement:	String	Initial cleaning oxide:	Grinding/ machining						
Gas Cup size:	8 [mm]	**Filler metal**							
Single or multipass:	Single	Type:	Bohler CN 13/4						
Process:		Size:	1.2 [mm]						
Polarity:	DC-	**Welding**							
Electrode	3.2 [mm]	Torch Angle	-10 degree						
Type:	Automatic	**Position coordinate**		**Heat Treatment:**		**Preheat:**	**PWHT:**		
Electrode:	3.2 [mm]	x0 = 230	x1 = 320	x3 = 270	x4 = 270	Type:	Type:		
Shielding gas:		y0 = 50	y1 = 50	y2 = 85	y3 = 10	Gas burner	Gas burner		
Gas type:	Argon	z0 = 000	z1 = 000	z2 = 000	z3 = 000	Avr.temp in weld:	temp after weld:		
Composition	100 %	Layers:	12			43°	131°		
Identification of parent metal:									
Part:	Type:			Thickness	Widt	Length:	Yield Strength		
1	X3CrNiMo13-4			20 [mm]	100 [mm]	350 [mm]	1100 MP		
Identification of filler metal:									
Part:	Type:			Classificaiton		Dia [mm]	Yield Strength		
1	Bohler CN 13/4-IG			EN ISO 14343-A: G 13 4		1,1	950 MP		
Welding Parameters:									
Index:	Heat Input [KJ/mm]	Wire feed speed [mm/sek]	Current [A]:	Voltage [V]:	AVHC	Welding speed [mm/sek]:	Gas [l/min]:		
	0.89	1.6	240	14.2	2.8 [mm]	2.2	12		
Welding plan:									

Figure 175: WPQR for P2D2

J.8 WPQR for P4D2
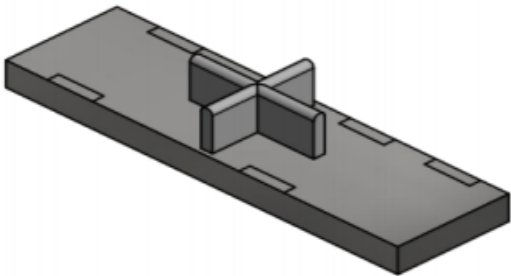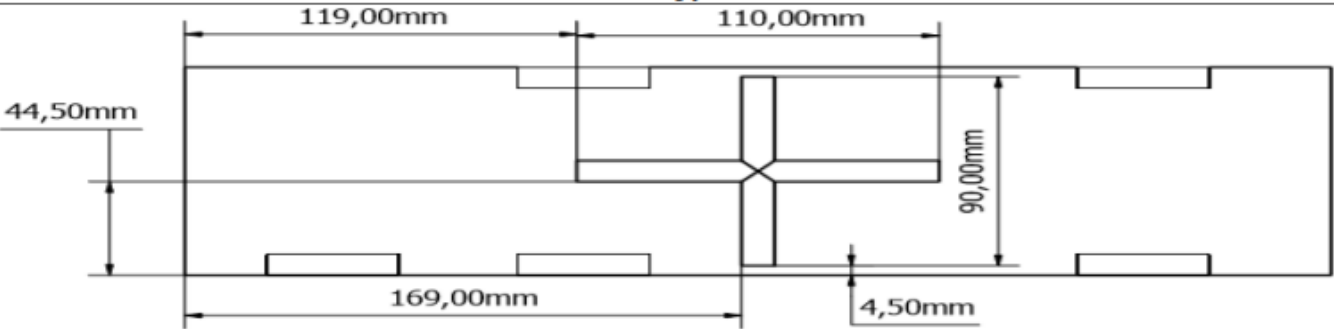
Welding Procedure Qualification Record (WPAR)				WPQR No: 008 Date: 30.01.2019					
Prod.by: Hans Ivar Arumairasa Project: Thin Wall Structure by Welding				Location: Narvik (UiT) - lab Welding Type Process: GTAW by KUKA-Robot					
Technique:		**Cleaning:**		**Structure:**		Thin Wall Structure			
Movement:	String	Initial cleaning oxide:	Grinding/ machining						
Gas Cup size:	8 [mm]	**Filler metal**							
Single or multipass:	Single	Type:	Bohler CN 13/4						
Process:		Size:	1.2 [mm]						
Polarity:	DC-	**Welding**							
Electrode	3.2 [mm]	Torch Angle	-10 degree						
Type:	Automatic	**Position coordinate**		**Heat Treatment:**		**Preheat:**		**PWHT:**	
Electrode:	3.2 [mm]	x0 = 160	x1 = 300	x3 = 222	x4 = 222	Type:		Type:	
Shielding gas:		y0 = 51	y1 = 51	y2 = 95	y3 = 5	Gas burner		Gas burner	
Gas type:	Argon	z0 = 000	z1 = 000	z2 = 000	z3 = 000	Avr.temp in weld:		temp after weld:	
Composition	100 %	Layers:	19			40°		153°	

Identification of parent metal:								
Part:	Type:			Thickness	Widt	Length:	Yield Strength	
1	X3CrNiMo13-4			20 [mm]	100 [mm]	350 [mm]	1100 MP	

Identification of filler metal:						
Part:	Type:		Classificaiton	Dia [mm]	Yield Strength	
1	Bohler CN 13/4-IG		EN ISO 14343-A: G 13 4	1,1	950 MP	

Welding Parameters:

Index:	Heat Input [KJ/mm]	Wire feed speed [mm/sek]	Current [A]:	Voltage [V]:	AVHC	Welding speed [mm/sek]:	Gas [l/min]:
	0.73	1.0	220	12.2	2.4 [mm]	2.2	12

Welding plan:

Figure 176: WPQR for P4D2

J.9   WPQR for P4D3
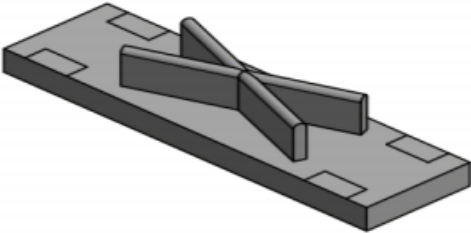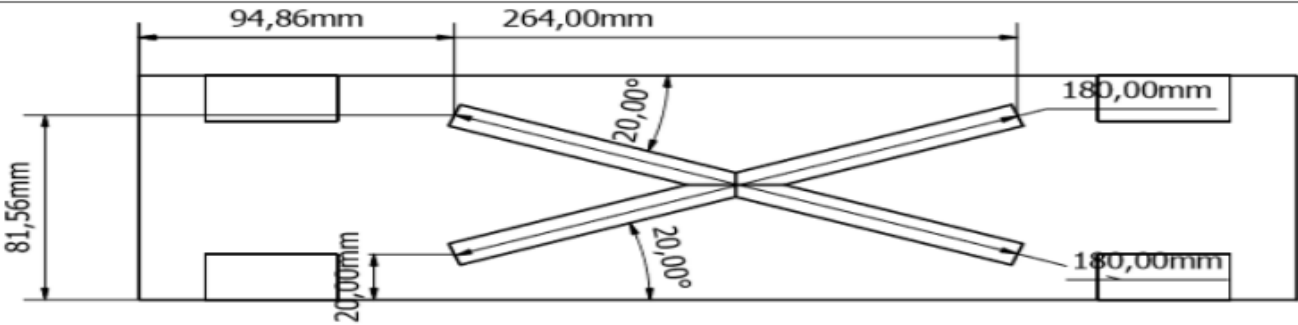
Welding Procedure Qualification Record (WPAR)				WPQR No: 009 Date: 01.02.2019			
Prod.by: Hans Ivar Arumairasa Project: Thin Wall Structure by Welding				Location: Narvik (UiT) - lab Welding Type Process: GTAW by KUKA-Robot			
Technique:		**Cleaning:**		**Structure:**		Thin Wall Structure	
Movement:	String	Initial cleaning oxide:	Grinding/ machining				
Gas Cup size:	8 [mm]	**Filler metal**					
Single or multipass:	Single	Type:	Bohler CN 13/4				
Process:		Size:	1.2 [mm]				
Polarity:	DC-	**Welding**					
Electrode	3.2 [mm]	Torch Angle	-10 degree				
Type:	Automatic	**Position coordinate**		**Heat Treatment:**		**Preheat:**	**PWHT:**
Electrode:	3.2 [mm]	x0 = 230	x1 = 389.3	x3 = 230	x4 = 389.3	Type:	Type:
Shielding gas:		y0 = 20	y1 = 78	y2 = 78	y3 = 20	Gas burner	Gas burner
Gas type:	Argon	z0 = 000	z1 = 000	z2 = 000	z3 = 000	Avr.temp in weld:	temp after weld:
Composition	100 %	Layers:	22			43°	164°

Identification of parent metal:							
Part:	Type:		Thickness	Widt	Length:	Yield Strength	
1	X3CrNiMo13-4		20 [mm]	100 [mm]	350 [mm]	1100 MP	

Identification of filler metal:					
Part:	Type:	Classificaiton	Dia [mm]	Yield Strength	
1	Bohler CN 13/4-IG	EN ISO 14343-A: G 13 4	1,1	950 MP	

Welding Parameters:							
Index:	Heat Input [KJ/mm]	Wire feed speed [mm/sek]	Current [A]:	Voltage [V]:	AVHC	Welding speed [mm/sek]:	Gas [l/min]:
	0.73	1.0	220	12.2	2.4 [mm]	2.2	12
Welding plan:							

Figure 177: WPQR for P4D3

K   Welding plan for welding
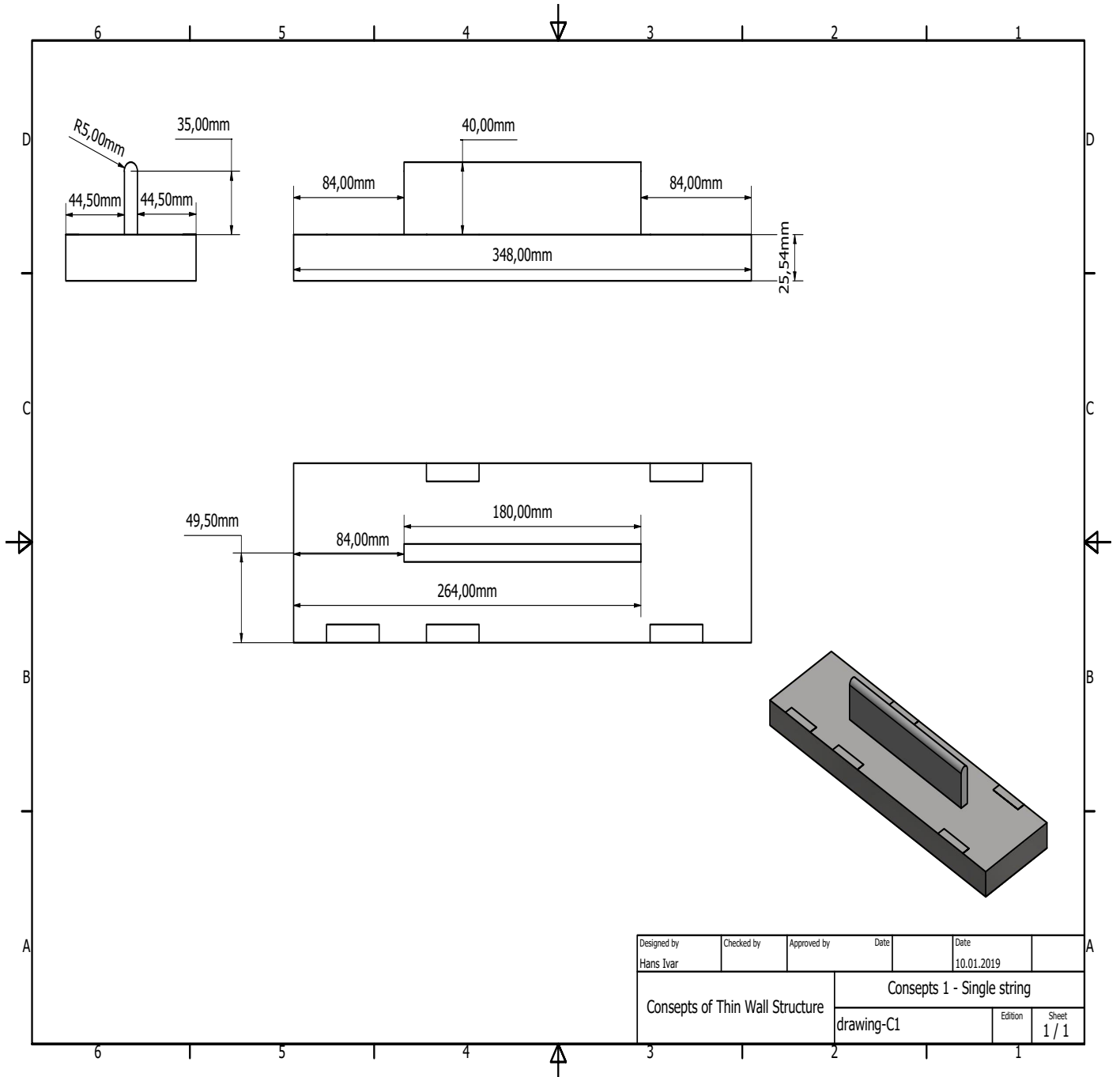
K.1   WP for concept one

Figure 178: WPQR for P4D3

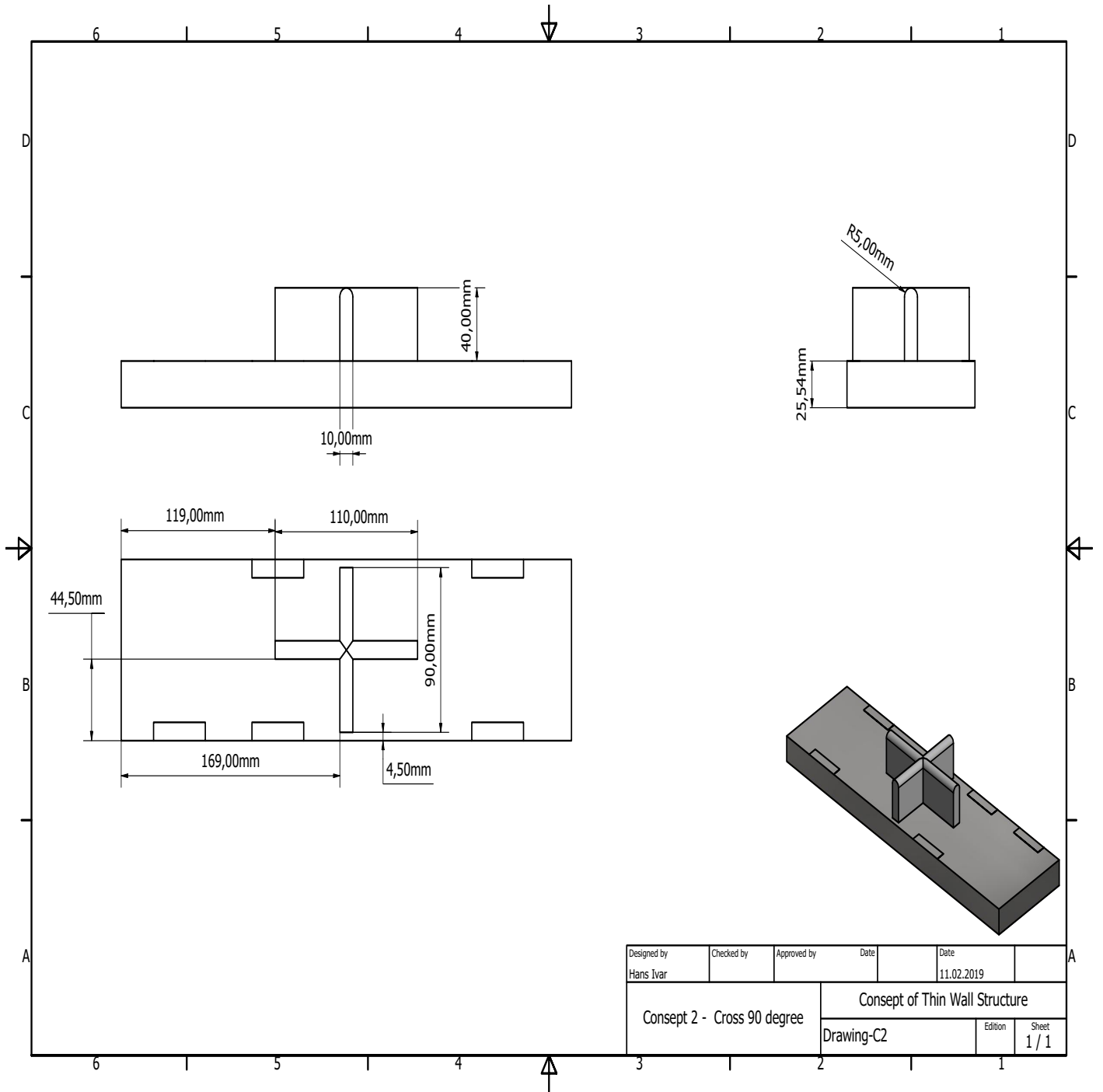## K.2 WP for concept two

Figure 179: WPQR for P4D3

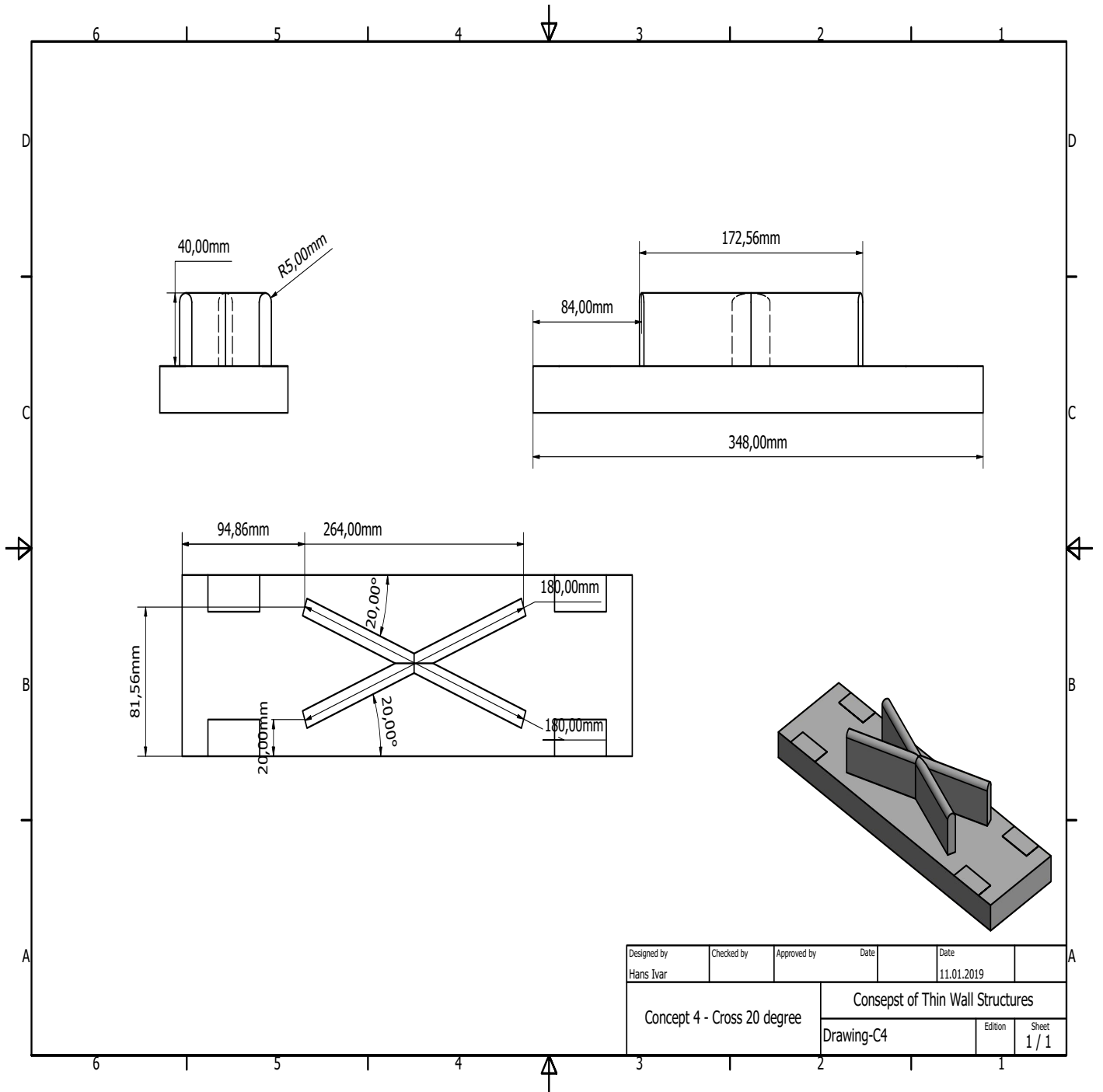## K.3 WP for concept four

Figure 180: WPQR for P4D3

L   Picture from the welded thin wall structures

As a result of the welding process by usage of the KUKA-30 robot and TIG welding, the thin wall structure was made. Totally was 10 samples made where only nine of them was succesfull. The picture below illustrate the sucsessfully onces.

L.1   TWS-P1D1

Figure 181: Result of welding process of P1D1

L.2   TWS-P2D1

Figure 182: Result of welding process of P1D1

L.3   TWS-P3D1

Figure 183: Result of welding process of P3D1

L.4 TWS-P5D1

Figure 184: Result of welding process of P5D1

L.5 TWS-P1D2

L.6 TWS-P2D2

L.7   TWS-P4D2

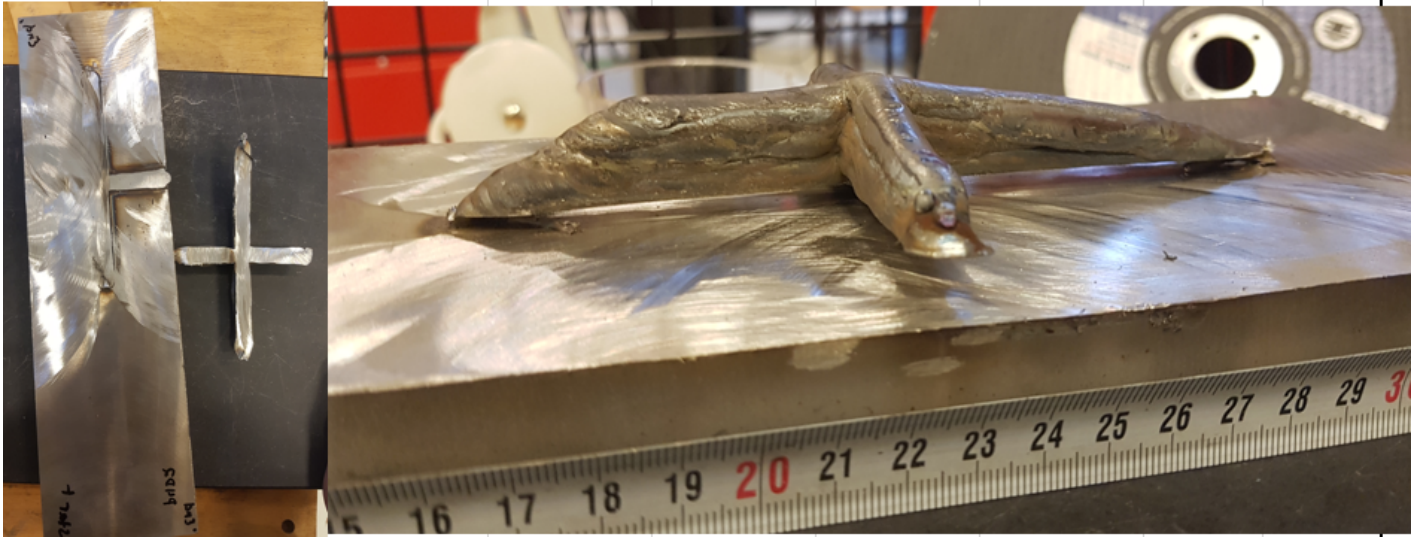Figure 187: Result of welding process of P4D2

L.8   TWS-P4D3

Figure 188: Result of welding process of P4D3